Sedimentology, Ichnology, Sequence Stratigraphy, and Petrography of the Falher F Unit, Wapiti Area, Northwestern Alberta

by

Nabilah Adani

A thesis submitted in partial fulfillment of the requirements for the degree of

Master of Science

Department of Earth and Atmospheric Sciences
University of Alberta

ABSTRACT

The lower Albian (Cretaceous) Falher F submember of the Spirit River Formation in the Wapiti area consists of four stacked coarsening-upward successions of northward prograding strandplain to wave-dominated delta deposits. Routine core analyses revealed that four facies associations can be identified within the study interval, which reflect a shoaling-upward trend from storm-dominated shoreface, wave-dominated shoreface, brackish embayment, to coastal plain settings deposited adjacent to wave-dominated delta. Integration with geophysical well logs enabled the construction of the local paleogeographic evolution of various depositional environments within each parasequence in the study area, which can be explained using a sequence stratigraphic model.

The complexity of the microscale reservoir characteristics within the tight sandstone intervals is largely due to the abundance of chert clasts and grains as well as interstitial allogenic and authigenic components, which contribute to the challenges related to the sandstone drillability and hydrocarbon storability, respectively. In this study, a petrographic approach was primarily employed to understand the relative distribution of the chert content and the diagenetic events within the tight sandstone units. The resulting reservoir characteristics can then be explained in reference to the palaeogeographic framework.

This study shows that changes in the chert-controlled drillability of the Falher F tight sandstone correspond to variations in depositional energy and settings. In terms of hydrocarbon storability, secondary porosities such as dissolution, microfractures, and other micropores that followed the pore-occluding diagenetic events are primarily responsible for retaining the porosity of the unit.

PREFACE

This thesis is an original work by Nabilah Adani. No part of this thesis has been previously published.

We must become ignorant
of what we have been taught,
and be, instead, bewildered.

Run from what is profitable and comfortable.
If you drink those liqueurs, you will spill
the springwater of your real life.

Forget safety.
Live where you fear to live.
Destroy your reputation.
Be notorious.

- *Rumi*

ACKNOWLEDGMENTS

First and foremost, all praise be to God for His endless blessings that have brought me to this point. None of these works would have been possible without His guidance and permission. For what I have achieved, I am eternally grateful.

The Indonesian Endowment Fund for Education has given me not only substantial financial support but also the opportunity for me to experience two extraordinary years of learning, even beyond the scope of geology. May this work inspire future Indonesian young scholars to pursue knowledge wherever it takes.

I especially thank Dr. John-Paul Zonneveld and Dr. Murray K. Gingras who opened a path for me that I did not know I would get a chance to walk along. Thank you, JP, for taking me as a student and for opening the first gate towards many exciting opportunities. Thanks as well for your constant encouragement. Thank you, Murray, for your supervision particularly during JP's sabbatical year, and especially for helping me to surmount an obstacle in my first year. I do not take for granted knowing and working with both of you. Thank you as well, Dr. Sasha Wilson, the chair in my thesis exam committee; for your constructive feedback and being a part of the team that awarded this degree to me.

I am also thankful to have become a part of the Ichnology Research Group. Of all, Carolyn Furlong deserves my highest gratitude for always helping me out with the proofreading that went above and beyond and giving me emotional support when I needed it. Thanks as well to Patricia Gonzaléz, my first friend in the lab, for all the chats and helpful discussions. And to many others who had helped me with everything from how to use the software, microscope, navigate around, and so forth, I wish you all the best for your future endeavours.

There are a lot of other individuals who contributed directly to this work. Many thanks to Raphael Wust (AGAT Laboratories, Calgary) for his assistance that went above and beyond with my thin sections, XRD, and SEM analyses. Big thanks as well to Aaron Richard-Bonks and Emily Vanderstaal (AGAT Lab). Thanks to Martin von Dollen and Mark Labbe (Thin Section Lab, EAS Dept., U of A) and Stephen Cheung (Calgary Rocks and Materials) for creating my thin sections. Thanks to the staff at the Alberta Core Research Centre and EAS, particularly Christiaan Conradie, Igor Jakab, and Lisa Krezanowski for all the assistance. Thank you as well to Dr. Per K. Pedersen and Dennis Meloche for our productive discussions during the 2018 CSPG Core Conference.

Thanks to Dr. Tom Chacko, who had helped me to overcome an obstacle in my first year here. Thanks to Dr. Willem Langenberg for his input during the 2018 ATLAS Symposium. Thanks to Dr. Octavian Catuneanu for the course that will remain very useful for the rest of my career as a geologist. I am also very thankful for the opportunity to have met and learned from Dr. S. G. Pemberton (may he rest in peace) who had passed on his incredible passion in ichnology.

This is all also possible because of the help and support of Prof. Dr. Ir. Yahdi Zaim, Prof. Dr. Ir. Eddy A. Subroto, and Dr. Dasapta Erwin Irawan, S.T., M.T. of my alma mater Bandung Institute of Technology, as well as Mas Himawan Sutanto, S.T., M.Sc. (may he rest in peace) of LEMIGAS. Thank you all for becoming mentors that I looked up to during the years I spent at ITB.

Of all, my parents, Ir. Desmoon and Dra. Srimiati, M.Si, have always been my greatest supporters. Everything I have become thus far was accomplished because of your prayers. Thank you for letting me go halfway around the world to chase my goals. Countless thanks, as well, to my brother Alwan Abdurrahman and my inner circle in the family: Aziz, Bibi, and Om Rudi.

Thank you, Adhi W. Prakoso, S.T, M.Sc., my best friend and partner since 2013. Here’s to successfully acing one shared goal, two continents apart!

To everyone else unlisted here but whose help is engraved in my thoughts, I treasure the opportunity to have crossed paths with all of you. Thanks for becoming a part of something that I am grateful to have accomplished.

Finally, to Canada, my temporary home for the past two years, this work is my memento to you. This journey was so much more than just studying geology or getting a degree; it was also about self-growth and self-compassion in a way that I never knew I needed to understand. Thank you for everything that comes in the package.

TABLE OF CONTENTS

LIST OF TABLES

LIST OF FIGURES

CHAPTER 1

CHAPTER 2

CHAPTER 3

LIST OF SYMBOLS AND ABBREVIATIONS

Chapter II & Appendix I

Lithologies

Conglomerate

Sandstone

Silty sandstone

Siltstone

Claystone/shale

Coal

Physical Sedimentary Structures

Planar bedding
Low angle cross-stratification
Planar cross-stratification
Trough cross-stratification
Hummocky cross-stratification
Swaley cross-stratification
Wave ripple laminae
Current ripple laminae
Wavy bedding
Lenticular bedding
Sediment-filled fracture
Shrinkage/desiccation cracks
Pedogenic slickensides
Stylolite
Load casts
Synaeresis cracks
Soft sediment faulting
Soft sediment deformation

Ichnofossils

root traces
Planolites
Gyrolithes
fugichnia
Cylindrichnus
Asterosoma
Rosselia
Zoophycos
Schaubcylindrichnus
Conichnus/Bergaueria
Glossifungites surface
Macaronichnus
Palaeophycus
Ophiomorpha
Thalassinoides
Diplocraterion
Skolithos
Rhizocorallium
Teichichnus

Extras

Mud clasts
Pebble lag
Shale laminae
Pyrite
Siderite
Carbonaceous matter
Carbonaceous laminae
Wood
Bioclastic debris
Sampled for petrography

Chapter III, Appendix II, & Appendix III

Mineralogy

a	albite
ac	authigenic chlorite
b	biotite
c	chert
ca	calcite cement
cg	calcite grain
cl	chlorite
dc	dolomite cement
dd	dedolomitized
dr	dolomite replacement
fc	ferroan calcite
fdc	ferroan dolomite cement
fdi	ferroan dolomite inclusion
fdr	ferroan dolomite replacement
h	hematite
i	illite
ic	illite coating
k	kaolinite
om	organic matter
m	muscovite mica
p	pyrite
plag	plagioclase
pm	pseudomatrix rock fragment
po	pore
q	quartz grain
qe	quartzite
qo	quartz overgrowth
rf	rock fragment
s	stylolite
si	siderite inclusion

Grain Size

l.v.f.	lower very fine
u.v.f.	upper very fine
l.f	lower fine
u.f.	upper fine
l.m.	lower medium
u.m.	upper medium

Grain Shape

a	angular
r	rounded
sa	subangular
sr	subrounded

Sorting

m	moderately-sorted
w	well-sorted
vw	very well-sorted

Framework

o	open framework
c	closed framework

Depositional Environment

F. Ch.	fluvial channel
Est.	estuarine
BS	backshore
FS	foreshore
Up. S.f.	upper shoreface
Mid. S.f.	middle shoreface
Low. S.f.	lower shoreface

Depositional Time

T	transgressive succession
FP2	parasequence F_p2
FP3	parasequence F_p3

Textural Properties

→	primary porosity
→	secondary porosity
→	overgrowth-nucleus contact
→	long/tangential/concavo-convex contacts
→	sutured contacts
→	mineral name

CHAPTER 1: INTRODUCTION

1.1 PREAMBLE AND RESEARCH BACKGROUND

The lower Albian Spirit River Formation has long been regarded as one of the most prolific gas reservoirs in the Western Canada Sedimentary Basin (Masters, 1979; 1984; Cant, 1983b; 1984; Hayes, 2010; Fockler and McKenzie, 2016; Hirschmiller and Lemke, 2018). The Spirit River Formation is divided into three main members; which, from base to top, are the Wilrich, Falher, and Notikewin members (Alberta Study Group, 1954). The Falher Member is a particularly well-characterized example of marginal to fully marine deposits (e.g. Hobbs, 2003; Armitage, 2004; DesRoches, 2008). The positions of individual Falher shorelines resulted from direct interactions between changes in relative sea level and local rates of sedimentation. The resulting siliciclastic deposits have attracted numerous sedimentological investigations over the past several decades, due to exploration interest in both the largely depleted conventional conglomeratic reservoir and, more recently, tight (unconventional) sandstone reservoir intervals (e.g. Moslow *et al.*, 2017; Newitt, 2017; Zonneveld *et al.*, 2017; Adani *et al.*, 2018; Hirschmiller and Lemke, 2018). This thesis focuses on the sedimentology, ichnology, stratigraphy, and petrography of the Falher F submember.

Masters (1984) recognized as much as 1,750 tcf total gas in place in the west side of the Deep Basin and nearly 3,000 billion barrels of degraded oil in place on the eastern side. However, commercial value of these resources has proven to be a function of available technology, in addition to the economic climate, as it requires horizontal wells and massive hydraulic fracturing to yield the vast majority of these hydrocarbons (Wyman *et al.*, 1980).

With the availability of various drilling technology today such as horizontal wells and multi-stage fracturing, industrial and academic interest have been diverted towards the exploration of the tight sandstone reservoirs (e.g.

Moslow and Ala, 2012; Fockler & McKenzie, 2016; Moslow *et al.*, 2017; Newitt, 2017; Zonneveld *et al.*, 2017; Adani *et al.*, 2018). Nevertheless, drilling into the chert-rich successions using horizontal wells has inevitably resulted in new challenges. A number of key exploration companies have reported low rates of penetration (ROP) and frequent replacement of drilling bit types due to challenges in penetrating detrital chert-dominated intervals in tight sandstone units, particularly in the Falher Member (Zonneveld, pers. comm.). This issue can be addressed by delineating chert distribution trends where possible to identify the varying degree of chert-controlled drillability within the sandstone. This study uses the Falher F submember in the Wapiti Area as a case study. The Falher F in this area is of particular interest as it has proven to be both a conventional and unconventional drilling target over the past few decades (e.g. Masters, 1979; Hayes, 2010; Hirschmiller and Lemke, 2018).

Therefore, in this research, a palaeogeographic framework will be firstly established to provide a robust background on vertical and lateral lithology distributions within the study area. A chert-controlled drillability fairway will be investigated afterwards, with reference to the constructed palaeogeography.

1.2 Study area

The study area lies within the Deep Basin region of northwestern Alberta, specifically in an approximately 1,106 km^2 region, which encompasses portions of Wapiti, Redrock, and Cutbank hydrocarbon fields (Fig. 1.1). It includes townships 65 through 67 and ranges 8 through 11 west of the sixth meridian in western Alberta (Fig. 1.2). More than 300 wells penetrate the Falher F interval in the study area. Among these, 20 wells provide the Falher F conventional diamond core (Table 1.1). These wells are concentrated along a NE-SW trend across T66, R8 to T65, R11 west of the sixth meridian. The studied core intersections range between 7 and 22 m long, totaling approximately 376 m of core that was examined for this research.

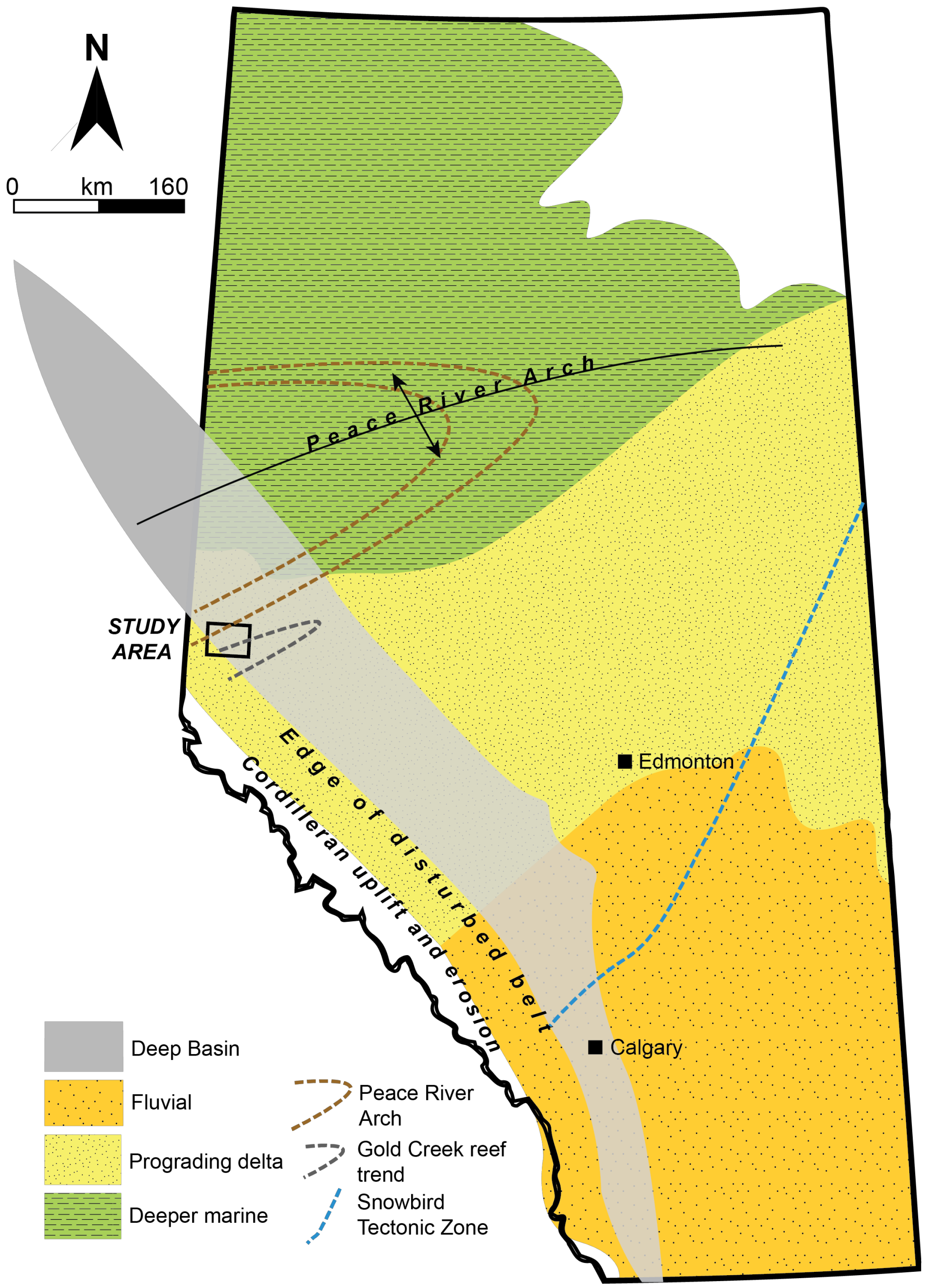

Figure 1.1. Map of Alberta showing the location of the study area. Regional palaeogeographic setting during the Upper Mannville Group deposition, which includes the Spirit River Formation is displayed. The study area was a site for prograding delta with the fluvial source being transported from the south to the deeper marine northward. It is located in the vicinity of Peace River Arch and the Gold Creek reef as a part of a subsiding section, with the edge of the deformed belt indicated. Modified from Jackson (1984), Leckie and Smith (1992), Burwash *et al.* (1994), Switzer *et al.* (1994), Nodwell and Hart (2006).

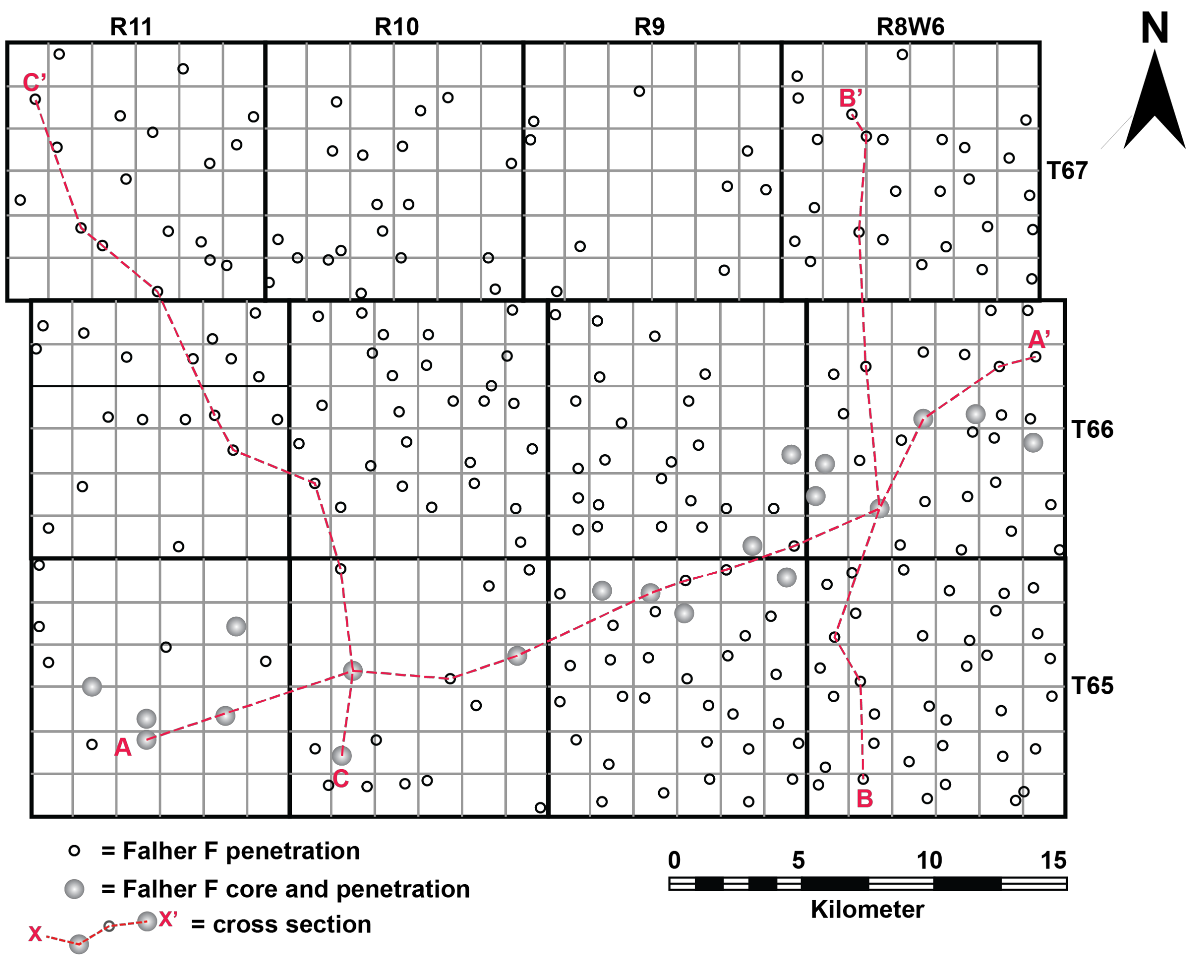

Figure 1.2. The distribution of wells used for this study. The coverage of cross-sections available in Chapter 2 is presented.

Table 1.1. List of wells with the available Falher F cores used in this study.

Well Location				Core Length			Number of Samples		
l.s.d.	Section	Township	Range (W6)	Top (m)	Bottom (m)	Total Recovered	Thin Section	XRD	SEM
3	20	65	11	2844	2854.6	9.2	-	-	-
7	14			3159.4	3177.6	17.5	2		
7	16			3182.4	3200.4	16.8	3		
8	26			2862	2871	9	1		
15	9			3008	3019	9.4	1		
6	8		10	2955	2969.41	10	3		
6	20			2905.6	2923.8	18.2	4	1	
14	24			2760.4	2778.4	17.7	2	1	
3	33		9	2723	2741.1	18.1	2		
5	32			2902.4	2918.4	16	3	1	1
10	36			2643	2652.4	9	2		
13	27			2634	2652	17.75	4		
7	13	66	9	2513.8	2532	18.2	4	1	
8	2			2562.5	2580	17.8	5	1	
1	8		8	2572	2590	18	2		1
2	21			2505	2520	15	2	1	
3	18			2466	2484	17.75	4	2	1
5	7			2535	2544	9	1		
8	22			2575	2590.8	13.35	4		
11	13			2556	2564	7.84	1		

1.3 OBJECTIVES

The study presented in the first part of this research (Chapter 2) was carried out in order to attain the following objectives:

1. Differentiating the Falher F cored intervals into several sedimentary facies according to changes in lithology, physical and biogenic structures, as well as additional sedimentary features.
2. Categorizing the sedimentary facies into several facies associations according to their associated architectural elements.

3. Establishing a fifth order sequence stratigraphic framework, which includes vertically stacked stratigraphic units, corresponding bounding surfaces, and their horizontal variability.
4. Illustrating palaeogeographic maps and the compatible depositional model, which is based on changes in relative sea level and rates of sedimentation across different stages of depositional timings.

The subsequent study (Chapter 3) was conducted to accomplish the objectives as follows:

1. Classifying the type of the Falher F sandstone based on textural and compositional attributes with respect to maturity.
2. Differentiating the textural and compositional properties of the sandstone, which includes the grain size, grain shape, framework, sorting, and types of detrital framework grains, matrix, and interstitial diagenetic cements.
3. Categorizing the sandstone into several petrofacies according to the textural and compositional attributes as well as identical diagenetic evolution.
4. Delineating possible controls of changes in the mineralogical suites (i.e. relative abundance of chert) across the depositional strike and dip direction, which contribute to the sandstone drillability.
5. Characterizing diagenetic events that are responsible for changes in sandstone reservoir quality, with respect to sandstone porosity.

1.4 METHODOLOGY

Selected Falher F cores were logged and analyzed at the Alberta Core Research Center (Alberta Energy Regulator) in Calgary, Alberta. These cores were available for public viewing as per June 2017. They were described with attention paid to sedimentary fabric, physical sedimentary structures, biogenic sedimentary structures, and stratal packaging as well as identification of stratigraphically significant surfaces.

Sedimentological examination included identification of lithological characteristics, sedimentary structures, accessory sedimentary features, stacking patterns, and types of contacts. Ichnological examination included identification of ichnogenera present, their relative abundances, intensity of bioturbation, diversity of ichnogenera, distribution of bioturbation, designation of ichnofacies, and ethological interpretations. Sequence stratigraphic examination included identification of vertical successions, bounding surfaces, and genetically related intervals. Based upon these observations, lithofacies and lithofacies associations were assigned, depositional environments were interpreted, and sequence stratigraphic units and surfaces were identified.

Petrophysical well logs were obtained through the GeoScout database. The primary logs utilized herein were gamma ray, sonic, density-neutron, and resistivity logs. Core observations were tied and calibrated to the corresponding logs and used to recognize the geophysical well log patterns. Wells without available Falher F cores were interpreted through extrapolation of data from cored wells. Cross-sections that are oriented roughly parallel and perpendicular to depositional strike or palaeoshoreline were constructed based on these extrapolations. These cross-sections illustrate the sequence stratigraphic intervals across the study area.

Isopach maps and formation top maps were computer-generated using the kriging and inverse distance algorithm, respectively, which are available in GeoScout modules. Based on comparisons of results produced by other available methods, these methods appear to be the most visually suitable for each type of maps.

Sixty-eight thin section samples were acquired from the sandstone intervals of available core. A minimum of one and up to five thin sections in every Falher F core were collected, except in well 100/03-20-065-11W6/00, where core intervals only exhibit sandy mudstone that is currently not a lithology of interest. Thin sections were impregnated with blue epoxy and subsequently half-dyed with either double-carbonate stains or feldspar stains. Conventional petrographic analyses were employed to qualify the textural characteristics, which included grain size, grain roundedness, sorting, framework openness, and grain contacts. Traditional point counting method was performed to quantify the mineralogical compositions, which included detrital framework grains, matrix, and intergranular authigenic cement. As many as 300 points were counted on 50 samples representing all Falher F sandstone sampling points, by utilizing computer-generated recursive grid method available in JMicroVision software. These thin sections also represented all sandstone lithofacies within the Falher F. Eight very fine-grained sandstone samples were further analyzed by X-Ray Diffraction technique and three of them by Scanning Electron Microscope at the AGAT Laboratories in Calgary, Alberta. The staff at AGAT provided the resulting images, curves, and mineral quantifications.

1.5 Stratigraphy

The Spirit River Formation of the Fort St. John Group in northwestern Alberta consists of a 350 m thick clastic wedge, which prograded into an epeiric seaway in present-day Alberta and British Columbia during the lower Albian (Cant, 1984). It consists of generally coarsening-upward successions, which include, from oldest to youngest, the Wilrich, Falher, and Notikewin members (Fig. 1.3; 1.4). Authors have differing opinions on the exact number of successions within the Spirit River Formation, particularly due to the varying opinions on the definition of the base of Falher and the top of Wilrich. This has resulted in overlapping sequences being assigned to both Wilrich and Falher G, H, and so forth (e.g. Zonneveld and Moslow, 2004; Newitt; 2017). Authors also have contrasting opinions regarding whether to include or disregard the Falher E as a succession, as it is most frequently reported as a thick succession of coal (~4 m) (Leckie, 1986b) instead of typical Falher coarsening-upward shoreface deposits. This “fourth coal” (Leckie, 1986b) may generally be used as a datum reference to correlate the Falher submembers above and below. Other workers such as Jackson (1984), however, assigned sandstone bodies in the Deep Basin to the Falher E.

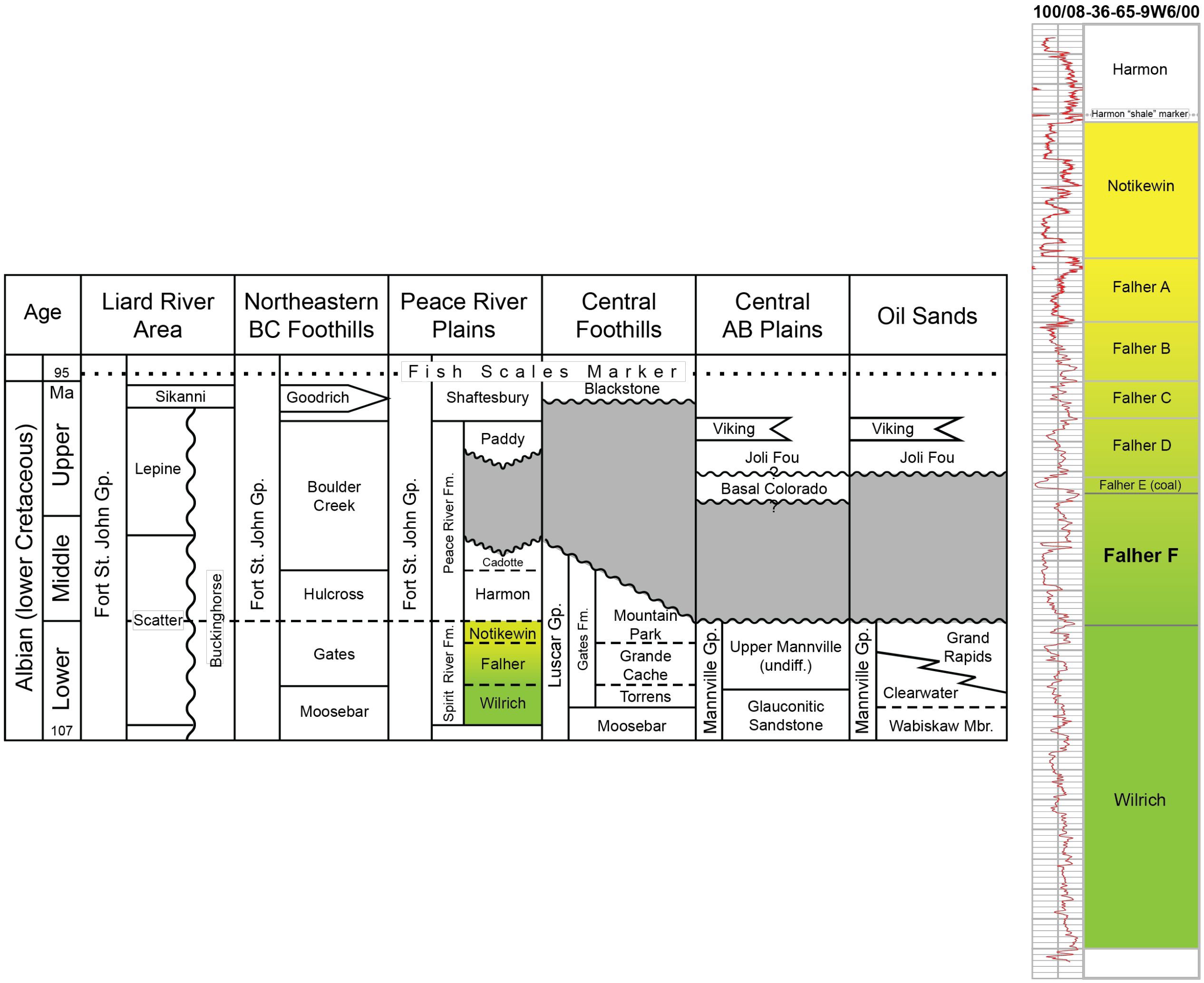

Figure 1.3. Lithostratigraphic nomenclature for Albian (lower Cretaceous) units in Alberta and northeastern British Columbia (modified from Smith *et al.*, 1984).

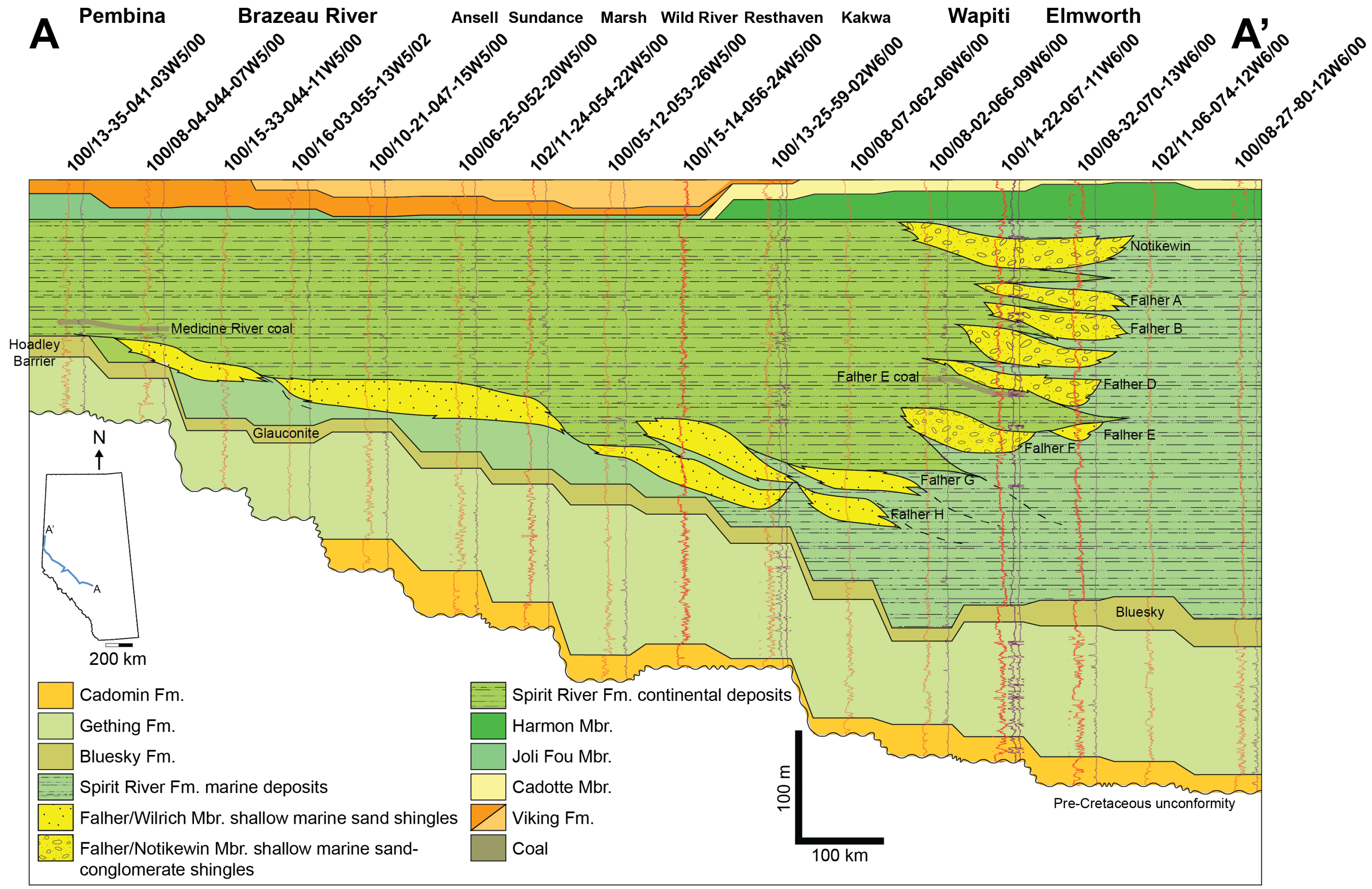

Figure 1.4. Regional cross-section of the west-central Alberta showing producing fields of the Spirit River Formation. The study area is represented by the Wapiti Field.

In the western outcrop belt (western Alberta and northeastern British Columbia) the Spirit River Formation is stratigraphically equivalent with the Moosebar and Gates formations (Stott, 1968; 1982; Leckie and Walker, 1982; Leckie, 1983). Northward, the offshore deposits of Spirit River Formation pinch out and transition into the marine shale of the Clearwater Formation (Jackson, 1984) or the Buckinghorse Formation (Stott, 1982). Southward, the terrestrial equivalent of the Spirit River is the Beaver Mines Formation of the Blairmore Group in the central and southern foothills of Alberta (McLean and Wall, 1981).

1.6 Depositional history

The Falher Member of the Spirit River Formation lies within the Deep Basin of the Western Canada Sedimentary Basin. The Western Canada Sedimentary Basin was formed as a product of collision during early Mesozoic, during which allochthonous terrains accreted onto the western margin of the North American continent (Porter *et al.*, 1982; Monger, 1989; Leckie and Smith, 1992). Stratigraphically, this period marked a significant basin configuration change, as evidenced by the formation of first-order sequence stratigraphic surface, which separated the older passive margin underneath and the newly formed foreland basin above (Leckie and Smith, 1992). The over-thrusting of accretionary deposits in an eastward direction during late Jurassic was interpreted to result in loading of the lithosphere, and in turn, the erosion of the Cordilleran foreland thrusts. Consequently, the clastic sediment began to accumulate in the Deep Basin, which constitutes the deepest region in the Alberta syncline and its extension in British Columbia (Porter *et al.*, 1982). This region consists of westward-thickening Mesozoic rocks that reaches over 4,570 m (15,000 ft) depth at its contact with the Foothills overthrusts (Masters, 1979).

The Cordilleran uplift and accretion continued to trigger subsidence in the foreland basin throughout the Cretaceous. This resulted in the development of a shallow epicratonic sea, which eventually formed the site of deposition for the Spirit River Formation. By the Aptian, and continuing through the Albian, marine transgression had inundated the continental deposits of the interior basin from the Boreal Seaway in the north and the Gulf Coast in the south (Smith *et al.*, 1984). This was interpreted to result from the combination of eustatic sea level rise and basinal tectonic subsidence (Hancock and Kauffman, 1979). In the early Albian, most of Alberta was characterized by fully marine to marginal marine conditions. The seaway expanded to its southward limit in present-day Montana of USA (Stelck, 1975) coincident with the deposition of the lower Spirit River Formation. This marine incursion resulted in a thick accumulation of marine shale of the Wilrich Member in the north, which is progressively replaced by marginal and shallow marine deposits of the Falher and Notikewin members towards the south (Stelck, 1975).

During the late early Albian, the initiation of the Laramide Orogeny triggered the thrusting and uplift on the Cordilleran foreland thrust belt. A period of rapid progradation commenced, allowing the accumulation of multiple cycles of northward prograding clastic wedges (Williams and Stelck, 1975; Smith *et al.*, 1984). The progradation was possibly intensified with the simultaneous accretion of the Insular Superterrane (Monger, 1989; 1999; Monger and Price, 2002). The Falher marine deposits prograded into the Boreal Sea as an overall regressive cycle with pulses of higher frequency regressive-transgressive cycles. This was evidenced by the presence of thicker marine clastic successions being separated by thinner terrestrial coal deposits. The thickest intervals of Falher marginal marine clastics are found in Township 64 to 78, west of the sixth meridian. This occurrence divided the Falher offshore deposits to the north and the Falher terrestrial deposits to the south (Cant, 1995; Casas and Walker, 1997).

Following the cessation of Falher progradation, the Notikewin Member prograded into the Boreal Sea. In total, the Falher and Notikewin members prograded more than 480 km into the Clearwater marine shale basin (Jackson, 1984; Smith *et al.*, 1984). The northward depositional limit of these two youngest members of the Spirit River Formation was estimated to be at the Peace River Arch, possibly due to rapid structural subsidence (Cant, 1988; Pate, 1988).

1.7 PREVIOUS WORKS ON THE STRATIGRAPHY OF THE FALHER MEMBER AND EQUIVALENTS

Stott (1968) presented an outcrop-based study of the Gates Formation (Spirit River-equivalent) in northeastern British Columbia. Among his works were the production of regional palaeogeographic maps for lower Cretaceous deposits in the study area and assigning the conglomerate and sandstone deposits of the Bullmoose Mountain as alluvial and shallow marine deposits, respectively. Stott (1982) later reassessed those deposits as deltaic facies. His observation also led to the recognition of four large-scale transgressive-regressive cycles, the first (oldest) to which he assigned the Moosebar and Gates formations.

McLean (1979) observed the correlation between the outcrops of the Gates Formation in northeastern British Columbia and subsurface data of the Falher and Notikewin members in the Elmworth Field of west-central Alberta. He proposed that the conglomerate bodies observed in the study area were of tidal channel and distributary channel deposits. Armstrong (1979), however, argued that most of the conglomerate bodies present in the Elmworth Field were beach deposits. Leckie and Walker (1982) similarly interpreted the depositional environments of Falher and Wilrich members in the Deep Basin through the field observation of Moosebar and Gates formations outcrop in northeastern British Columbia. However, they interpreted the conglomerate outcrops to have been deposited as fluvial, beach, offshore graded storm, and offshore bar deposits.

Leckie (1986b) interpreted that the transgressive-regressive cyclicity within the Gates Formation of northeastern British Columbia represented fourth-order cycles. These were interpreted to have been a product of tectonic subsidence in the Peace River Arch. MacDonald (1988) correlated six cycles of Moosebar and Gates outcrops in the deformed western section of the Deep Basin with the Falher and Wilrich cycles subsurface data in the eastern section. They interpreted these cycles to be the product of interactions between overall second order eustatic sea level rise of early Albian, somewhat constant rate of sedimentation, and minor fluctuations in the local subsidence of the Deep Basin.

The Alberta Study Group (1954) provided the original definition of the Falher Member with Imperial Falher No. 1 well (UWI 100/12-23-077-21W5/00) as the type locality for the unit. Cant (1984) proposed eight stratigraphic cycles within the Spirit River Formation. He assigned five of them into the Falher Member (A to E), in which he interpreted each sequence to consist of shoreface deposits overlain by coastal plain deposits. A subsequent regional study by Jackson (1984) divided the Falher Member up to eight members (A to H). He also provided several palaeogeographic maps during Aptian to middle Albian Mannville Group deposition throughout Alberta and British Columbia, indicating that the Falher Member had approximately east to west-oriented palaeoshorelines. Smith *et al.* (1984) also presented the palaeogeography of the Lower Cretaceous strata surrounding the Elmworth field. Unlike Jackson (1984), he divided the Falher Member into five units (A to E). Carmichael (1988) studied the Falher A- and Notikewin-equivalent conglomerate bodies in northeastern British Columbia. He suggested that these conglomeratic lobes were developed during marine transgression in estuarine settings.

Following these earliest works, studies regarding the sequence stratigraphy of particular submembers within the Falher emerged in the 1990's and onwards.

Cant (1995) investigated the Falher A and B submembers and proposed that the conglomerate bodies in the Falher A were deposited as transgressive barrier islands, resting on top of a ravinement surface. Rouble and Walker (1997) proposed an alternative hypothesis, postulating that the conglomerate units were parts of prograding shoreface deposits. Their studies of Falher A and B submembers suggested the presence of marine flooding surfaces and regressive surfaces of marine erosion between each allomember within the two units. Hobbs (2003) in his MSc thesis recognized two maximum flooding surfaces associated with the upper and lower limit of the Falher A.

Arnott (1993) studied the Falher D submember by employing subsurface data in the Wapiti and Elmworth fields of west-central Alberta. He proposed four stratigraphic intervals within the Falher D, which are bounded by marine flooding surfaces and a "sequence boundary." Casas and Walker (1997) later recommended different surfaces for the Falher D and C in an overlapping, but larger study area. They suggested that bounding surfaces between each Falher C and D stratigraphic cycle are transgressive surfaces of marine erosion, with a sequence in the Falher C that is bounded by a regressive surface of marine erosion. Armitage *et al.* (2004) also investigated the Falher C, which were assigned four internal parasequences. Their idea was that the conglomerate lobes were deposited during the relative sea level fall, therefore the base is a regressive surface of marine erosion. Field studies of the Falher C submember by Caddel and Moslow (2004) in northeastern British Columbia are in agreement with this interpretation. Hoffman (2008) in his MSc thesis divided the Falher D into two parasequences bounded by transgressive surfaces of erosion, similar to Casas and Walker's (1997) interpretation that differed with Arnott's (1993).

Nodwell and Hart (2006) presented the first publication on the Falher F member in Elmworth and Wapiti fields. They suggested that the conglomerate succession within the Falher F was deposited due to the structural control underneath the Falher F palaeoshoreline, specifically the Devonian Gold Creek Reef trend. This observation is based on the absence of evidence for relative sea level fall, as opposed to the interpretation of Falher C (Armitage *et al.*, 2004; Caddel and Moslow, 2004). DesRoches (2008) in his thesis proposed similar sequence stratigraphic surfaces for the Falher F and added an additional parasequence below the parasequence F1 of Nodwell and Hart (2006).

Zonneveld and Moslow (2004) provided the only outcrop-based study on the Falher G submember (Wilrich-equivalent) to date. They discovered the first conglomerate shoreface assigned to the Falher G, southward of the palaeoshoreline of younger Falher in northeastern British Columbia. Newitt (2017) in his MSc thesis investigated the newly emerging play of Wilrich Member, which is equivalent to his interpretation of the basal Falher up to O. His study proposed that the Wilrich-equivalent strata comprise a highly progradational sequence, in contrast to the middle and upper Falher submembers

(F through A), which possess considerable aggrading components in a general prograding manner.

1.8 Previous work on the reservoir characteristics of Falher Member and equivalents

Available studies regarding the petrographic properties of the Falher tight sandstone are limited. The most comprehensive studies were provided by Leckie (1986a), Youn (1981), Cant (1983), Cant and Ethier (1984), Tilley and Longstaffe (1989), and recently a thesis research by Newitt (2017).

Leckie (1986a) examined the provenance of the Gates Formation outcrops (Falher Member-equivalent) in northeastern British Columbia and suggested that the sediments were probably sourced from as far as the western section Omineca Crystalline Belt and eastern section of Intermontane Belt. He also found that the predominant sandstone type in Falher-equivalent successions is litharenite, with predominant rock fragments ranging from chert to dolomite clasts towards the west.

Youn (1981) and Cant (1983) interpreted porosity loss within Falher sandstone units to be largely controlled by diagenetic factors. Subsequently, Cant and Ethier (1984) provided the first detailed petrographic study on the Falher conglomerate and sandstone units, particularly, with respect to the presence of sandstone as the matrix of the conglomerate. They elaborated similar interpretations of Cant (1983) and recognized that the low porosity and permeability within the Falher sandstone is primarily due to the formation of quartz overgrowth, mechanical compaction on argillaceous rock fragments, and cementation by carbonate and clay minerals. This observation was also supported by Harris (2014), who added that the primary porosity in Falher sandstone is commonly retained in the quartz-rich sandstone, while chert-rich sandstone relies on the secondary porosity.

Tilley and Longstaffe (1989) provided a thorough explanation of the diagenesis and pore water evolution in the Deep Basin by using samples from various Falher submembers. They identified several authigenic stages within the Falher Member, which were associated with different stages from early burial to the generation of methane. Among the most important diagenetic minerals that they observed were quartz overgrowths, dolomite cement, illite, dickite, ankerite, hematite, and calcite cement.

Most recently, Newitt (2017) conducted a petrographic study on samples from the Wilrich interval (approximately Falher K, N, and O-equivalent). Newitt (2017) commented on the abundance of volcanic rock fragments within the basal Falher unit. He proposed that this was likely to have been affected by the shifting volcanic activities in the southern portion of Cordillera and that the detritus of volcanic rock fragments may be increasing to the northwest due to the added distance of axial drainage (Mellon, 1967). In conjunction with his stratigraphic interpretation of the Falher O being highly progradational with negligible aggrading components, he also proposed that such configuration had resulted in a specific paragenetic sequence that was affected by the early influx of meteoric water.

1.9 SUMMARY

Based on the existing knowledge on the Falher F sedimentology, stratigraphy, and reservoir characteristics, further studies are still required to better understand the properties as well as spatial and temporal variability in the interest of tight sandstone exploration. Therefore, this study aims to establish a palaeogeographic framework for the Falher F in the Wapiti area and employ such model to explain the microscale heterogeneity within the Falher F unit. This research may also serve as a reference for future works on many of its analogous units in the Western Canada Sedimentary Basin.

CHAPTER 2: SEDIMENTOLOGY, ICHNOLOGY, STRATIGRAPHY, AND PALAEOGEOGRAPHY OF THE FALHER F UNIT, WAPITI AREA, NORTHWESTERN ALBERTA

INTRODUCTION

When exploration in the Deep Basin of the Western Canada Sedimentary Basin (WCSB) commenced during the 1970's (Masters, 1978; 1979), the lower Albian Spirit River Formation proved to be a horizon of particular interest, which remains so to this day. Initially, conglomeratic units within the Falher Member served as the principal producing unit within the formation (Cant, 1983a; Cant and Ethier, 1984; Smith, 1984). These gravelly units that occur between the underlying sandy shoreface and overlying muddy coastal plain succession possess high permeability and porosity (~0.5 to 5000 md; up to ~20% porosity) (Cant, 1983a). The highest quality reservoirs are preserved within well-sorted, unimodal to bimodal, clast-supported, pebbly conglomerate beds. They were predominantly deposited as proximal upper shoreface and foreshore conglomerate (Cant and Ethier, 1984; Smith, 1984; Arnott, 1993; VanSickle, 1995; Casas and Walker, 1997; Rouble and Walker, 1997; Armitage *et al.*, 2004; Caddel and Moslow, 2004; Zonneveld and Moslow, 2004; Nodwell and Hart, 2006). Despite their excellent permeability and porosity, these pebble-rich reservoirs comprise only a minor proportion of individual Falher units. The larger proportion consists of tight sandstone reservoirs with comparably low permeability and porosity (~0.01 to 0.5 md permeability; <1 to 7% porosity) (Cant, 1983b). Both of these types of reservoir share similarly high gas storage (Moslow *et al.*, 2017).

Recent interest has focused towards regionally and volumetrically extensive sandstone on basin-centered hydrocarbon systems (Zaitlin and Moslow, 2006). In the Deep Basin of Western Canada Sedimentary Basin, interbedded High Permeability Basin-Centered Gas System (HP-BCGS) and Low Permeability Basin-Centered Gas System (LP-BCGS) is hosted within conglomerate and tight sandstone lithologies (Zaitlin and Moslow, 2006; Moslow and Zaitlin, 2008). Due to low permeabilities in the latter intervals, horizontal wells coupled with multi-stage fracs are required to reach the equal deliverability that conventional conglomeratic intervals once provided (Zaitlin and Moslow, 2006; Newitt and Pedersen, 2015; Moslow *et al.*, 2017; Zonneveld *et al.*, 2017).

In addition to low permeability and moderate porosity, challenges in tight sandstone exploration may include low rates of penetration (ROP) and frequent bit replacement, due to cements or lithological heterogeneities such as chert pebble or granule layers (Zonneveld *et al.*, 2017). In the Falher submembers, some sandstone intervals may have a high percentage of chert, whereas other beds can be highly quartz-dominated (Jackson, 1984; Cant and Ethier, 1984; Harris, 2014). Therefore, this study is divided into two parts; the first provides a depositional model for the Falher F at Wapiti and reconstructs the local palaeogeography of individual parasequences, which will serve as the background for the subsequent study on the tight sandstone characterization.

REGIONAL PALAEOGEOGRAPHY AND PREVIOUS STUDIES

The Western Canada Sedimentary Basin (WCSB) is an asymmetrical foreland basin that thickens to the west towards the Cordillera, where it is bounded by the Rocky Mountain Front Ranges thrust belt (Porter *et al.*, 1982; Monger, 1989; Leckie and Smith, 1992; Cant, 1983b; Monger and Price, 2002). The Deep Basin flanks to the western portion of WCSB and comprises the thickest segment of the Spirit River Formation (Cant, 1983b; Jackson, 1984; Masters, 1984; Smith *et al.*, 1984). During the Albian (lower Cretaceous), the Spirit River Formation was deposited in a shallow epeiric sea, as a series of overall progradational parasequence sets following the southward transgression of the Clearwater (Boreal) Sea (Williams and Stelck, 1975). By the time of the Falher Member progradation, the Clearwater (Boreal) Sea had occupied most of northeastern British Columbia as well as northern and central Alberta (McLearn, 1944). Fluvial systems primarily flowed from the west and southwest from the tectonically active Cordilleran region (McLean, 1979). Macdonald *et al.* (1988) suggested that the Spirit River Formation was deposited during an overall second order eustatic sea-level rise of early Albian age when the rates of local subsidence in the Deep Basin underwent only minor changes. Moslow *et al.* (2017) interpreted the Deep Basin to be an underfilled foreland basin during the deposition of the Spirit River Formation.

Within the Spirit River Formation, the Falher Member is conformably underlain and overlain by the Wilrich and Notikewin members, respectively (Fig. 2.1). These three members each comprise multiple coarsening-upward successions. In the Falher Member, these parasequence sets are informally named Falher A (younger) to Falher F (older). Apart from these six units, many authors have also assigned lower Falher submembers from G up to O beneath the Falher F (Jackson, 1984; Smith *et al.*, 1984; Macdonald *et al.*, 1988; Zonneveld and Moslow, 2004; Newitt, 2017; Zonneveld *et al.*, 2017). In spite of their lithologic resemblance to the younger Falher submembers, widespread consensus on their status has not been achieved and some authors or industry groups include these units in the Wilrich play. Regardless of their inclusion in the Wilrich Member or Falher Member, these submembers represent individual northward prograding shoreface successions that gradually coarsen upward from heterolithic proximal offshore mudstone to foreshore sandstone and/or pebbly conglomerate. These prograding deposits are capped, at least at their landward limit, by coastal plain mudstone successions.

The earliest detailed studies of the Falher Member focused on its palaeogeographic reconstruction (Leckie and Walker, 1982; Cant, 1984; Jackson, 1984; Smith *et al.*, 1984) and conglomerate petrology (Cant, 1983a; b; Cant and Ethier, 1984; Leckie, 1986b). Conglomerate depositional environments were among the most frequently debated, which included settings ranging from fluvial,

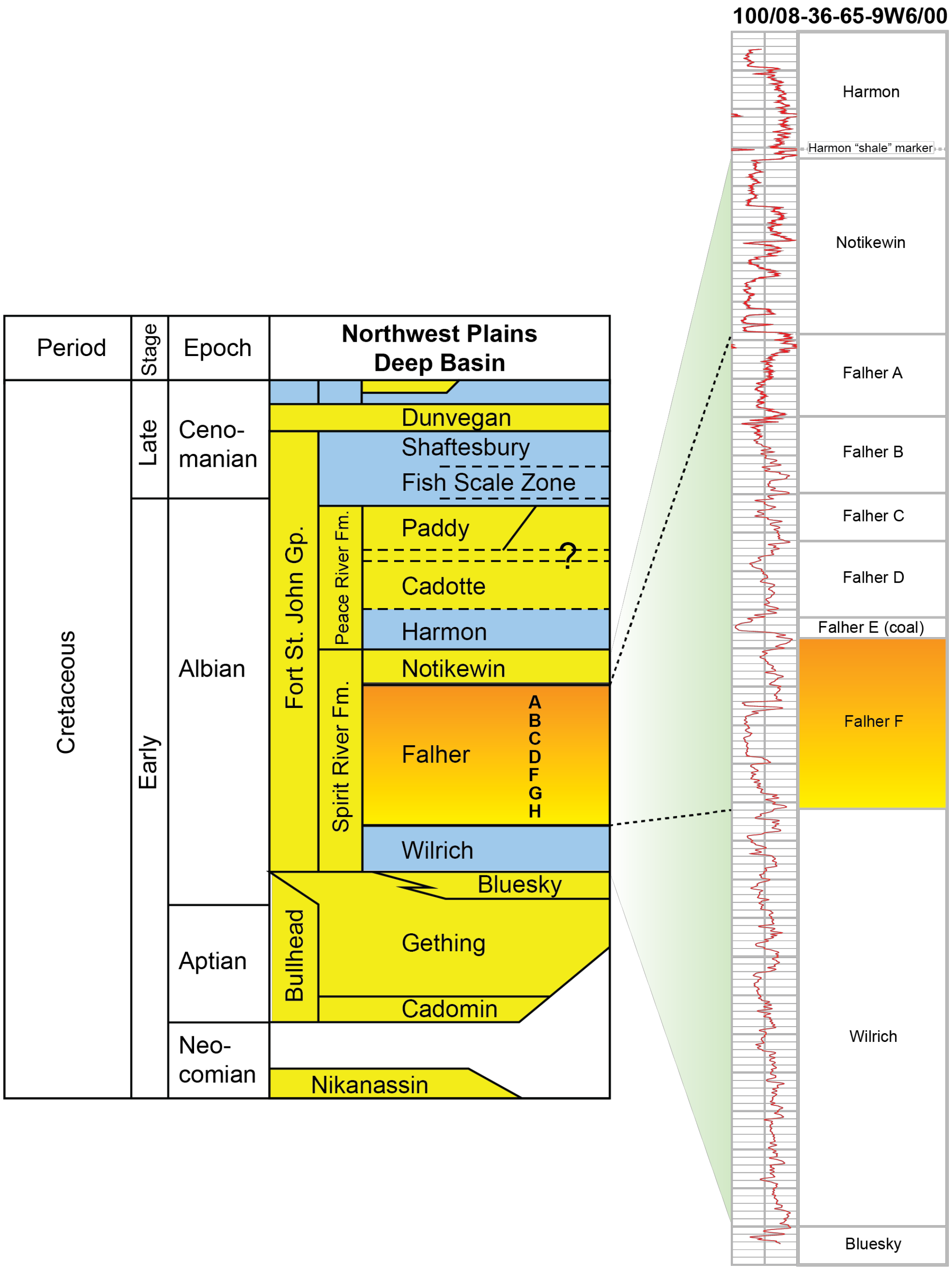

Figure 2.1. Lithostratigraphic nomenclature for Cretaceous units in the northwestern portion of the Deep Basin, Alberta (modified from Zaitlin and Moslow, 2006). An example of gamma ray log response on the Spirit River Formation exhibits an overall coarsening-upward trend.

tidal, to distributary channel and transgressive barrier island for the Falher A and B in Elmworth Field (McLean, 1979; Cant, 1984; Cant, 1995) as well as beach, braided river, and offshore in northeastern British Columbia outcrops of Falher- and Wilrich-equivalent Moosebar Formation (Leckie and Walker, 1982). Subsequently, more works have been conducted on the sequence stratigraphy of each Falher submember, which recorded evolving basin configurations and relative sea level patterns. Detailed studies are available for the Falher A and B (Rouble, 1996; Rouble and Walker, 1997; Hobbs and MacEachern, 2002; 2003; Hobbs, 2003), Falher C (Casas, 1996; Casas and Walker, 1997; Caddel, 2000; Armitage, 2002; Armitage *et al.*, 2004; Caddel and Moslow, 2004), Falher D (Arnott, 1993; Casas, 1996; Casas and Walker, 1997; Hoffman, 2006), Falher F (DesRoches, 2008; Nodwell, 2004; Nodwell and Hart, 2006), Falher G (Zonneveld and Moslow, 2004), up to Falher O (Newitt, 2017). Contrary to the initial studies, the most recent works generally agree that most of the conglomerate bodies in the Elmworth and Wapiti areas were deposited in upper shoreface to foreshore settings. Other studies include reservoir characterization (VanSickle, 1995; Moslow and Ala, 2012; Bann and Ross, 2014a; b; Fawcett, 2014; Newitt and Pedersen, 2016; Moslow *et al.*, 2017) and coastal plain stratigraphy (Wadsworth *et al.*, 2003).

To date, available studies restricted to the Falher F unit have resulted in conglomerate depositional mechanism and reservoir property frameworks. Nodwell and Hart (2006) suggested that the conglomeratic body of the Falher F was deposited under the influence of the Gold Creek reef trend below the palaeoshoreline. Attempts also have been made to separate facies deposited under strandplain and wave-dominated deltaic settings (DesRoches *et al.*, 2007; 2008), which may influence reservoir quality variations along depositional strike (e.g. Bann and Ross, 2014a; b). The latest study on the lower Falher (Wilrich-equivalent) in the Wapiti-Kakwa area indicated that there are mineralogical variations that change stratigraphically and with the proximity to their fluvial sources (Zonneveld *et al.*, 2017). This study complements the existing investigations by providing the local palaeogeographic evolutions of the Falher F in the Wapiti area.

DATABASE AND METHODS

This study was conducted using Falher F core and wells from predominantly the Wapiti Field and other adjacent fields (T65-67, R8-11W6M) within the Deep Basin of northwestern Alberta (Fig. 2.2). Sedimentological and stratigraphic observations were made on core from 20 wells totalling 376 m in total length. Attention was paid to sedimentary and biogenic structures, grain size, stratigraphic stacking patterns, and petrographic aspects. Cores were calibrated with the geophysical well logs and correlated with >300 uncored wells penetrating the Falher F unit in the study area. Cores chosen were those that were publicly available during June 2017 (Fig. 2.3). Gamma ray and sonic logs were the primary wireline logs used to identify changes in lithology; although neutron porosity, neutron density, resistivity, and caliper logs were also utilized to help identify lithological characteristics. Isopach maps and three cross-sections, both strike-oriented and dip-oriented, were constructed to map marine conglomerate and sandstone bodies as well as visualize the distribution of the Falher F deposits in the study area.

FACIES ASSOCIATIONS AND DEPOSITIONAL ENVIRONMENTS

The Falher F succession in the Wapiti area can be divided into thirteen lithofacies (Table 2.1). These lithofacies can be further grouped into four facies associations (Table 2.2), which is elaborated below.

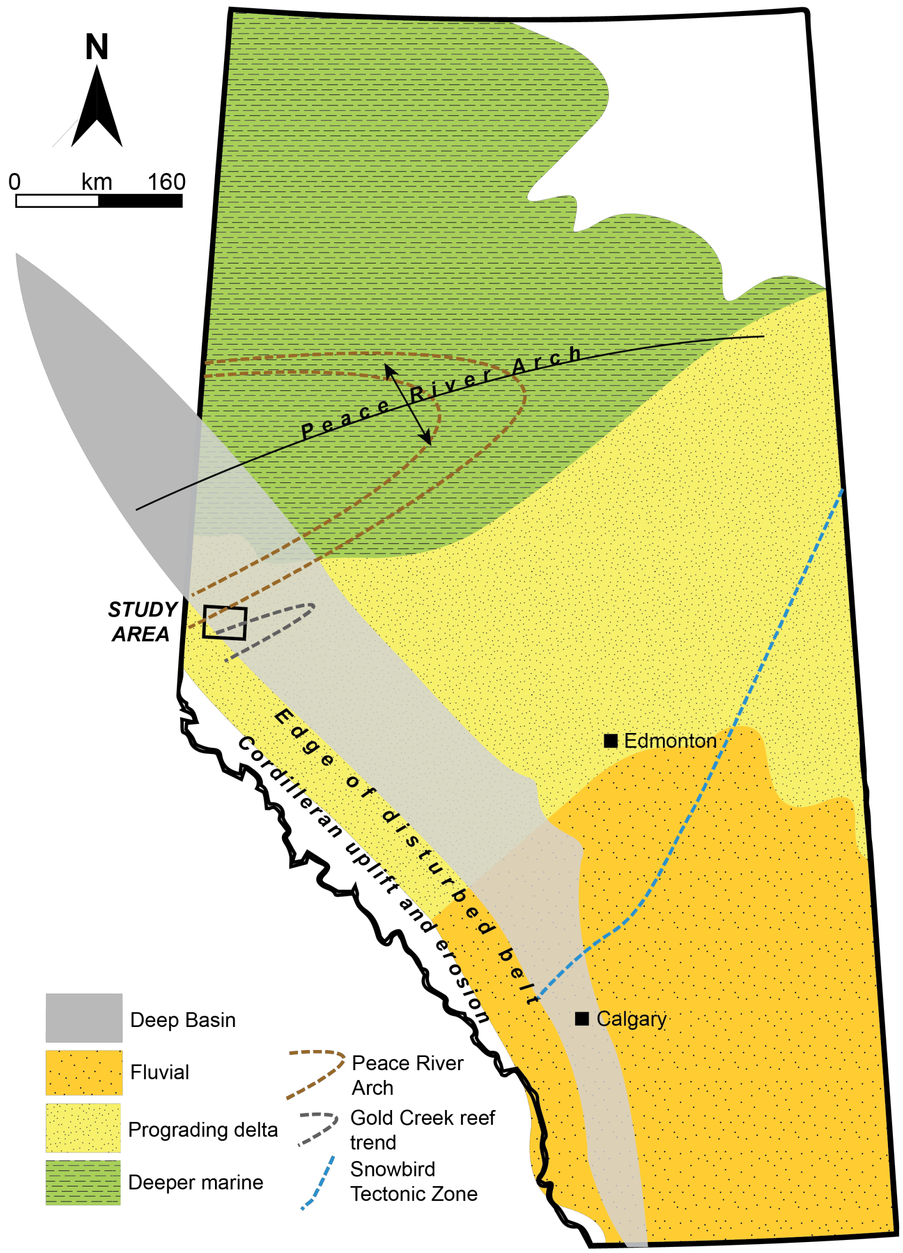

Figure 2.2. Map of Alberta showing the location of the study area. Regional palaeogeographic setting during the Upper Mannville Group deposition, which includes the Spirit River Formation is displayed. The study area was a site for prograding delta with the fluvial source being transported from the south to the deeper marine northward. It is located in the vicinity of Peace River Arch and the Gold Creek reef as a part of a subsiding section, with the edge of the deformed belt indicated. Modified from Jackson (1984), Leckie and Smith (1992), Burwash *et al.* (1994), Switzer *et al.* (1994), Nodwell and Hart (2006).

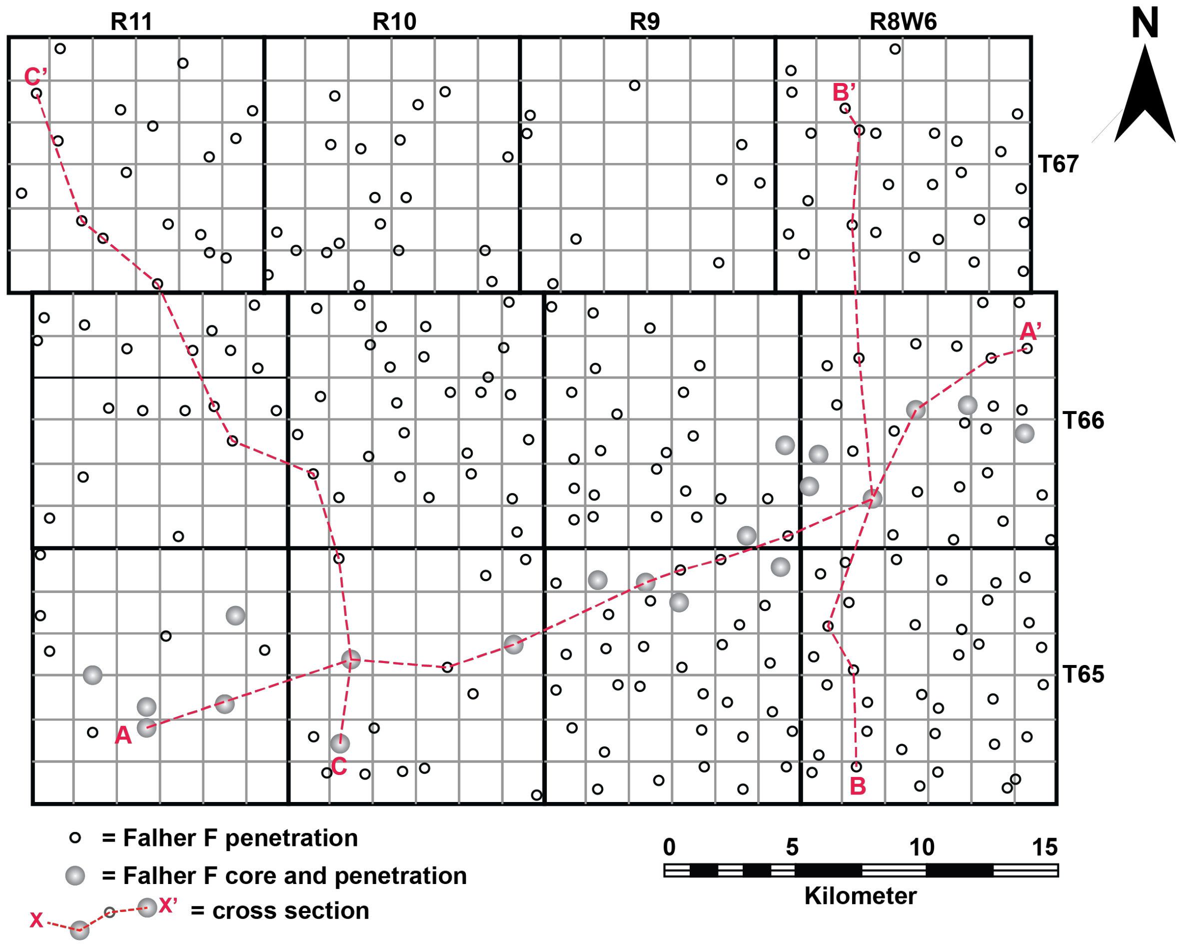

Figure 2.3. The distribution of wells used for this study. The coverage of cross-sections is presented.

Table 2.1. Lithofacies identified within the study interval.

Facies	Lithology	Structures			BI	Ichnofossil Assemblages	Depositional Environment	Facies Assoc.	Thickness
		Sedimentary	Other Features	Biogenic					
1	Heterolithic sandy mudstone	Micro-HCS, current ripple laminae, lenticular beddings	Common speckles of pyrite grains within thin sandy lenses, very rare carbonaceous matters	Abundant *Planolites, Palaeophycus;* common *Asterosoma, Ophiomorpa;* rare *Zoophycos, Teichichnus,* fugichnia	2 to 5	Archetypal *Cruziana* Ichnofacies	Offshore transition, proximal prodelta	FA1	0.5 – 2 m
2	Argillaceous lower very fine- to lower fine-grained sandstone	HCS	Rare carbonaceous drapes, intercalation of very thin shale beds (<10 cm), mud clasts (3-30 mm), spherulitic siderite, locally pebbly	Abundant *Palaeophycus*, *Schaubcylindrichnus*, *Ophiomorpa*, *Rosselia*; common *Thalassinoides*, *Planolites*, *Asterosoma*; rare *Cylindrichnus*	0 to 5	Archetypal *Cruziana* Ichnofacies	Lower shoreface, distal delta front	FA1	0.5 – 4.5 m
3	Lower very fine to lower fine-grained sandstone	HCS, SCS, current ripple laminae	Rare carbonaceous drapes, intercalation of very thin shale beds (<10 cm), mud clasts (3-30 mm), spherulitic siderite, soft sedimentary deformation, locally pebbly	Abundant *Rosselia*, *Teichichnus*, *Ophiomorpa*, *Macaronichnus*, *Palaeophycus*, *Schaubcylindrichnus*, *Planolites*, fugichnia; common *Cylindrichnus*, *Conichnus*, *Diplocraterion*; rare *Skolithos*, navichnia	0 to 5	Archetypal *Skolithos* to proximal *Cruziana* Ichnofacies	Lower to middle shoreface, upper to lower distal delta front	FA1	0.5 – 7 m

4	Lower very fine- to lower fine-grained sandstone	Trough cross-beddings, parallel laminae, wave and current ripple laminae	Common carbonaceous matter, rare wood fossils, white calcareous lenses, locally pebbly	Abundant *Palaeophycus*, *Planolites*, *Macaronichnus*; common *Thalassinoides*; rare *Bergaueria*, *Ophiomorpa*, *Rosselia*, *Schaubcylindrichnus*	0 to 4	Archetypal *Skolithos* Ichnofacies	Upper shoreface, proximal delta front	FA2	0.5 – 9 m
5	Upper very fine- to upper fine-grained sandstone	Massive to very poorly defined planar to low-angle parallel laminae, swash zone cross-stratifications	Rare carbonaceous debris, wood fossils, locally pebbly	Cryptic bioturbation, monospecific assemblages of *Macaronichnus*	0 or 6	N/A	Upper shoreface to foreshore, lower delta plain to proximal delta front	FA2	1.5 – 6.5 m
6	Lower medium- to upper very coarse-grained sandstone	Planar to low-angle parallel beddings, planar cross-stratifications, trough cross-stratifications	Locally pebbly	N/A	0	N/A	Lower shoreface to foreshore, proximal delta front to lower delta plain	FA1, FA2	0.1 – 0.4 m
7	Polymodal poorly-sorted matrix-supported conglomerate	Massive to trough cross stratifications, high angle cross stratifications, planar beddings	Clasts size up to >16 mm, matrix is upper fine to coarse sandstone, clasts are generally chert, quartz, and other rock fragments. Abundant carbonaceous matter, rare wood fossils.	N/A	0	N/A	Distributary channel (proximal delta front)	FA2	0.2 – 1 m

8	Bimodal poorly to moderately well sorted conglomerate	Massive to planar beddings, tabular cross-beddings, trough cross-beddings	Clasts size up to >16 mm, matrix is upper fine to coarse sandstone, clasts are chert, quartz, and other rock fragments	N/A	0	N/A	Upper shoreface	FA2	1.5 – 9 m
9	Unimodal well sorted clast-supported conglomerate	Massive to planar to low-angle parallel beddings, tabular cross-beddings, trough cross-beddings	Clasts size up to 8 mm, matrix is lower very fine- to lower fine-grained sandstone, clasts are predominantly chert	N/A	0	N/A	Foreshore	FA2	0.5 – 4 m
10	Upper very fine- to upper fine-grained sandstone	Massive to low angle planar beddings	Carbonaceous debris	Abundant rootlets	0	N/A	Backshore	FA2, FA3	0.5 – 1.5 m
11	Interbedded sandy mudstone and argillaceous very fine-grained sandstone	Combined flow ripples, wave ripples, current ripples, planar parallel laminae, wavy to lenticular beddings, climbing ripples, tabular to trough cross laminae	Soft sediment deformation, mud clasts, synaeresis cracks, siderite nodules and mottles, secondary calcite veins, shale laminae	Abundant *Planolites*, *Palaeophycus*, *Cylindrichnus*, *Skolithos*, *Asterosoma*, *Ophiomorpha*, *Rosselia, Thalassinoides*, rootlets, navichnia; common *fugichnia, Teichichnus, Diplocraterion, Gyrolithes, Bergaueria, Rhizocorallium*	0 to 5	Mixed *Skolithos-Cruziana* Ichnofacies	Estuary (flood tidal delta, central basin, bayhead delta), lagoon, washover sand, intertidal flat, marsh	FA3	0.5 – 5.5 m

12	Interbedded massive mudstone and coal	Mudstone is predominantly massive, but very rarely and locally parallel laminated	Soft sedimentary deformation, carbonaceous matter, wood fossils, pedogenic slickensides, bivalve clasts, siderite nodules and mottles, siderite- filled shrinkage cracks, calcite veins	Common rootlets	0 to 3	N/A	Lagoon, marsh, swamp, flood plain	FA3, FA4	0.5 – 1.5 m
13	Lower very fine-grained sandstone	Planar beddings, climbing ripples	Abundant intraformational mud clasts (up to boulder size), soft sedimentary faulting, spherulitic siderite	N/A	0	N/A	Fluvial channel, crevasse splay	FA4	9 m

Table 2.2. Facies associations identified within the study interval.

Facies Association		Summary	Ichnofacies Expression	Depositional Settings
FA1	Storm-dominated shoreface and distal deltaic complex	Coarsening-upward succession of interstratified sandy mudstone gradually or abruptly changes upwards into hummocky- to swaley-cross stratified very fine-grained sandstone.	Moderately diverse archetypal *Cruziana* Ichnofacies	Above storm-weather wave base, below fair-weather wave base (i.e. offshore transition to middle shoreface in strandplain and wave-dominated delta settings)
FA2	Wave-dominated shoreface and proximal deltaic complex	Coarsening-upward succession of planar laminated to cross stratified fine-grained sandstone interbedded and interfingers with, as well as gradually or abruptly changes upwards into, massive to stratified conglomerate. Matrix-rich to matrix-supported, poorly-sorted, polymodal, organic-rich conglomerate gradually shifts upwards into clast-supported, well-sorted, bimodal to unimodal, chert-dominated conglomerate.	Moderately diverse proximal *Cruziana* to archetypal *Skolithos* Ichnofacies; *Macaronichnus segregatis* suite	Above fair-weather wave base, below high tide remarks (i.e. upper shoreface to foreshore in strandplain and wave-dominated delta settings)
FA3	Back barrier/brackish embayment and lower delta plain complex	Fining upward succession of massive to low angle-laminated, organic-rich sandstone abruptly overlain by interbedded massive to organic-rich mudstone, heterolithic sandy mudstone, and coal.	Diminutive *Skolithos* and *Cruziana* Ichnofacies	Intertidal zone (i.e. backshore, estuarine or brackish bay, lagoon)
FA4	Coastal plain and upper delta plain complex	Interbedded mudstone and coal. Fining-upward succession of unburrowed planar-laminated sandstone.	N/A	Supratidal zone (i.e. lacustrine, marsh, swamp, fluvial channel, crevasse splay)

Facies Association (FA) 1: Storm-influenced Shoreface and Distal Deltaic Complex

Discussion

Facies association FA1 shows gamma ray log signature of a funnel-shaped pattern that goes from relatively high to moderate gamma ray values (Fig. 2.4). The complete succession of facies association FA1 consists of bioturbated, very dark grey, sandy mudstone (Figs. 2.5; 2.6A, B) which shifts upwards into low angle to planar parallel laminated sandstone (Figs. 2.5; 2.6E, F), with the latter being infrequently argillaceous (Figs. 2.6C, D). Changes between the two contrasting lithologies may either be gradational or sharp.

At the lowest proportion of the sandstone, low angle to planar parallel laminae frequently terminate against low-angle erosive contacts. This feature is interpreted as hummocky cross-stratification (HCS) (Fig. 2.6E). Towards the younger beds, the HCS may shift into steepening-upwards low angle laminae, often more clearly-defined. These laminae may also display concave-up foresets that tend to gradually converge upwards (Fig. 2.6F). In addition, they may have well-defined sharp, erosive, tangential contacts, which intersect the underlying sets of laminae (Fig. 2.6F). These laminae are interpreted to be swaley cross-stratification (SCS) following HCS termination. Towards the top of FA1, symmetrical, rather poorly-defined, cm- to dm-scale asymmetrical current ripple laminae are occasionally interbedded with the recurring parallel laminae.

Biogenic structures within FA1 are moderately diverse (12 ichnotaxa). The lowermost mudstone unit records the most thorough bioturbation within the Falher F succession, with intensity ranging from moderately low to very high (BI = 2 – 5). The remaining sandstone facies mainly preserve none to moderate bioturbation, although infrequently thoroughly bioturbated (BI = 0 – 5).

Trace fossil suites of FA1 exhibit a shift from predominantly deposit-feeding structures at the base to predominantly dwelling structures of inferred suspension-feeders and passive carnivores towards the top. These include

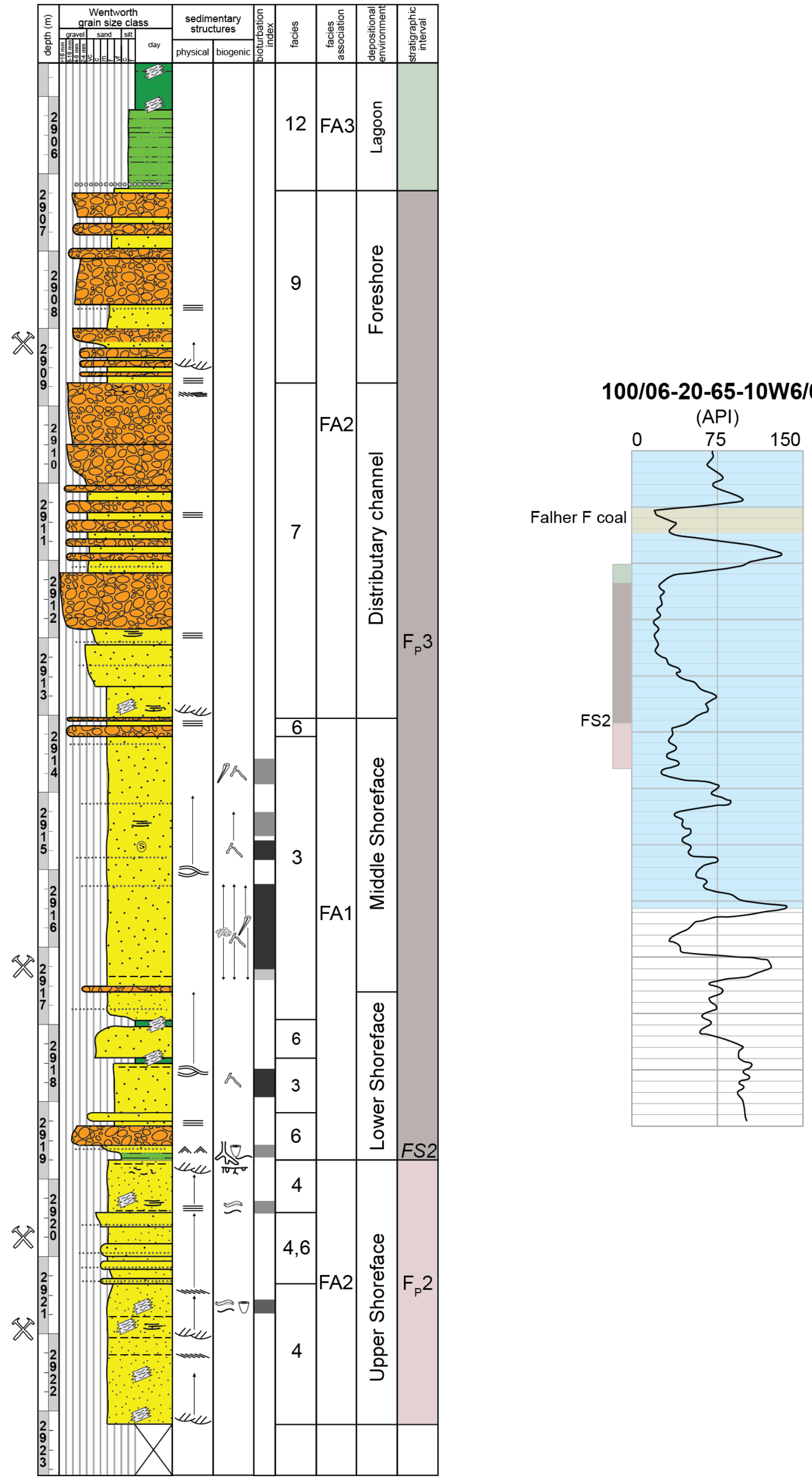

Figure 2.4. Calibrated core interval and gamma-ray log for well 100/06-20-065-10W6/00.

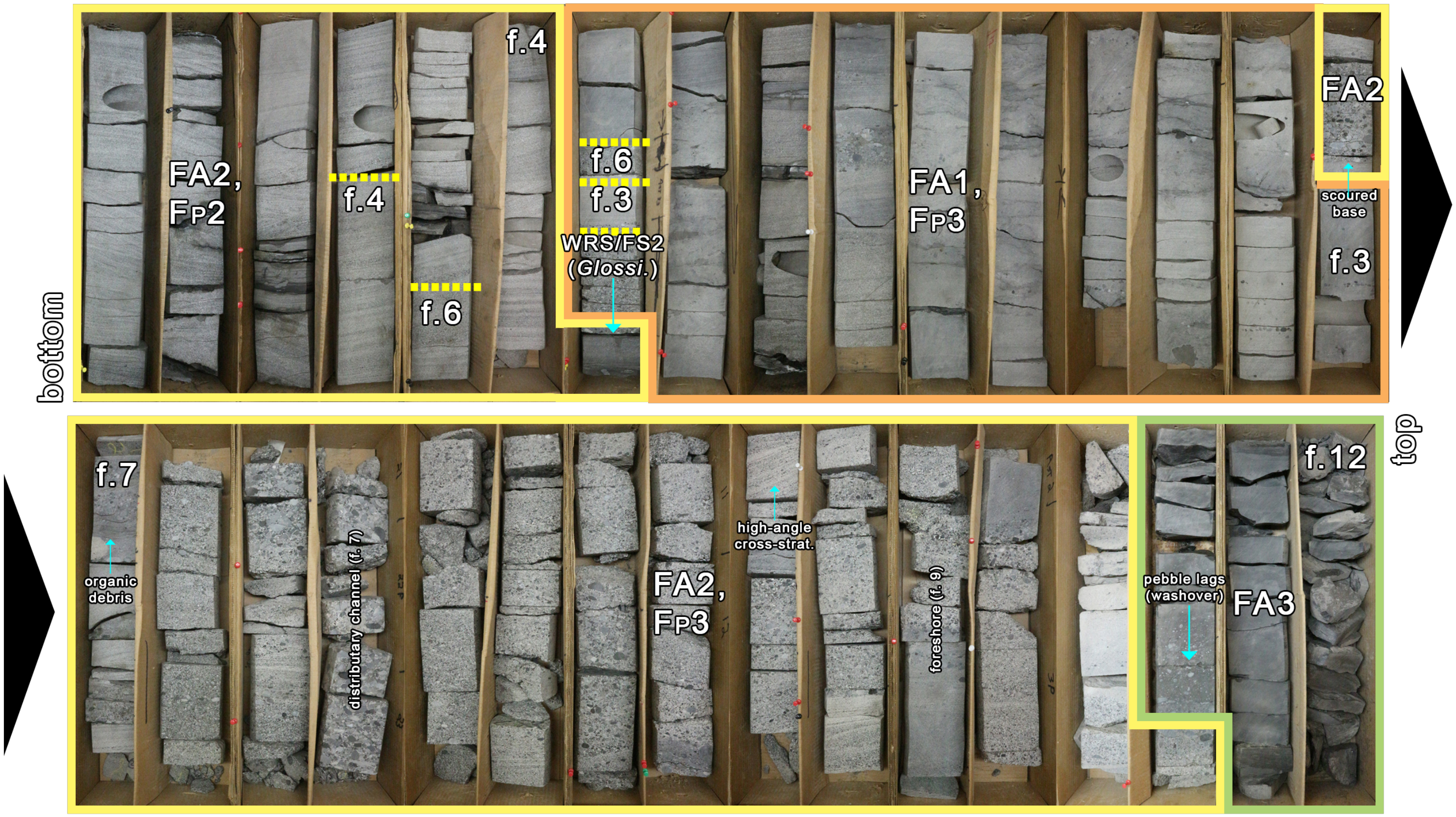

Figure 2.5. Diamond core box shot of well 100/06-20-065-10W6/00 displayed in Figure 2.4. Note the *Glossifungites* surface marking the wave ravinement surface separates the underlying FA2 and overlying FA1. Note also the juxtaposition of two conglomeratic facies interpreted as distributary channel and foreshore in FA2.

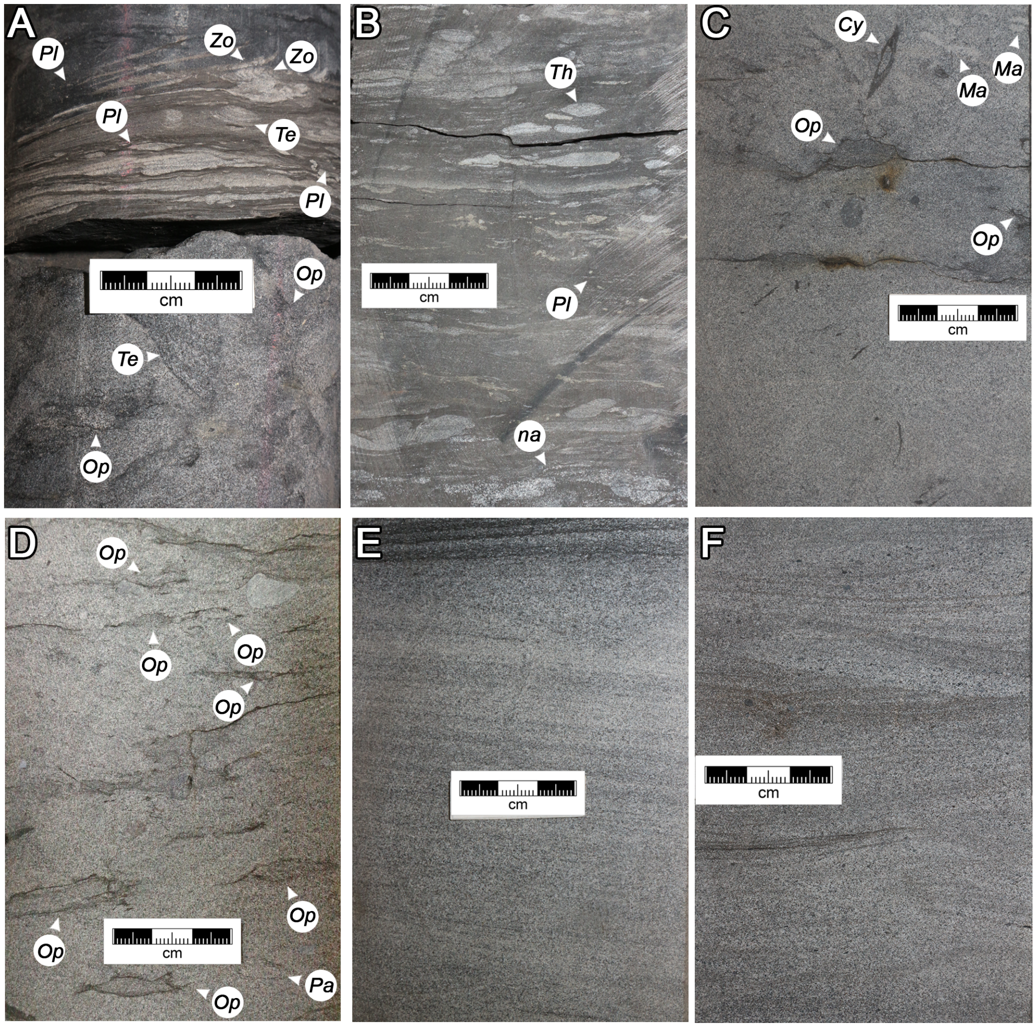

Figure 2.6. Core photographs of facies 1 through 3. **A)** Facies 1, pervasively burrowed heterolithic mudstone (upper offshore) (well 100/05-32-065-9W6/00, 2913.4 m); **B)** Facies 1, lenticular-bedded heterolithic mudstone (upper offshore) (well 100/05-32-065-09W6/00, 2913.5 m); **C)** Facies 2, moderately burrowed silty very fine-grained sandstone (lower shoreface) (well 100/06-20-065-11W6/00, 2916.9 m); **D)** Facies 3, moderately burrowed very fine-grained sandstone with monotypic assemblage of *Ophiomorpha* (lower shoreface) (well 100/13-27-065-09W6/00, 2645.9 m); **E)** Facies 3, scarcely bioturbated very fine-grained sandstone with low-angle planar parallel laminae interpreted as HCS (lower shoreface) (well 100/01-08-066-08W6/00, 2581.1 m); **F)** Facies 3, SCS-bedded very fine-grained sandstone (middle shoreface) (well 100/03-18-066-8W6/00, 2470.5 m). Abbreviations: *Pl = Planolites, Zo = Zoophycos, Te = Teichichnus, Op = Ophiomorpha, Cy = Cylindrichnus, Ma = Macaronichnus, Th = Thalassinoides, na* = navichnia.

abundant *Planolites*, *Palaeophycus*, *Schaubcylindrichnus*, *Ophiomorpha*, *Rosselia*, and *Teichichnus* as well as common *Thalassinoides*, *Cylindrichnus*, *Conichnus*, and *Diplocraterion* (Figs. 2.6A, B, C, D). Additionally, in the lowermost mudstone interval, there are rare occurrences of very low density populations of *Zoophycos* (Fig. 2.6A), whereas rare occurrences of unlined *Skolithos* are restricted to the uppermost sandstone strata. Rare fugichnia and navichnia (cf. Gingras *et al.*, 2007) are observed within several discrete beds throughout the interval. Bioturbated strata are also frequently enriched with a monospecific assemblage. This is mostly the case with *Ophiomorpha*, *Schaubcylindrichnus*, *Palaeophycus*, and *Teichichnus* (Fig. 2.6D).

Interpretation

Facies association FA1 represents the stratigraphically deepest shoaling-upward succession of the Falher F unit in the study area, deposited between fair-weather wave base and slightly above apparent storm-weather wave base in a coastal setting. This corresponds to offshore transition to middle shoreface settings (Johnson and Baldwin, 1996; Davis and Fitzgerald, 2004). Mudstone and silty sandstone reflect deposition through predominantly suspension settling that is typical of a low energy environment (Hsü and Jenkyns, 1974; Jenkyns, 1978). Concurrently, episodic storm activities transported sandy materials from shallower successions and deposited micro-HCS sandstone in more distal settings (Dott and Bourgeois, 1982; Krassay, 1994). It is also evident in the rare lenticular bedded mudstone, which preserves evidence of an occasional shift to higher energy deposition (Reineck and Wunderlich, 1968; Krassay, 1994) (Fig. 2.6A). The abundant presence of speckles of pyrite, a mineral that does not commonly occur in abundance in the proximity of freshwater influences (Berner, 1984), is also consistent with deposition in the offshore transition and below.

The occurrences of HCS and SCS are attributed to the product of storm-enhanced combined flows and are typically confined to the region between fair-weather wave base and storm-weather wave base (Harms *et al.*, 1975; Duke *et al.*, 1991; Dumas and Arnott, 2006). At the seaward limit of the storm-driven currents, tractive sheet-like flows may also have been responsible for the preservation of planar parallel laminated beds that interstratifies with the HCS beds (Swift *et al.*, 1983).

The coarser lithologies, as well as locally developed pebble lags, were likely introduced into this facies associations during the peak of storm activity (Plint and Norris, 1991; Krassay, 1994). Storm-induced rip-currents may have scoured and reworked sediment from the foreshore to upper shoreface and transport those coarser materials further basinward (Reading and Collinson, 1996). During the end stages of storm waning flow, suspension settling may have occurred as well and deposited thin shale beds up to 3 cm.

The trace fossil assemblage reflects the switch from archetypal *Cruziana* Ichnofacies into archetypal *Skolithos* Ichnofacies, supporting the changes of environment from offshore transition into middle shoreface, respectively (Crimes, 1975; Frey *et al.*, 1990; MacEachern and Pemberton, 1992). Additionally, the common presence of fugichnia, which is indicative of rapid sedimentation or mixed erosion and sedimentation, suggest dynamic sedimentary environments (Frey, 1973; Ekdale *et al.*, 1984).

Discerning between storm-dominated strandplain successions and laterally equivalent storm-dominated distal deltaic complexes in the Falher F is challenging as the two environmental settings retain many features in common. In particular, both settings were influenced by storm reworking between depositional events, leaving few features to indicate fluvial input to the coast (cf. DesRoches *et al.*, 2007). This is common in wave-dominated deltaic succesions where wave and storm effects are pronounced, and evidences of fluvial input in deltaic source areas are overprinted (Bhattacharya and Walker, 1992; Bhattacharya and Giosan, 2003). The paucity of core through facies deposited below storm-weather base in the Falher F core also impedes the possible separation based on their ichnofossil profiles (cf. DesRoches, 2008).

Facies Association (FA) 2: Wave-dominated Shoreface and Proximal Deltaic Complex

Discussion

Stratigraphically on top of FA1, FA2 is the most commonly cored interval through the Falher F succession. This owes to the fact that this interval preserves both prolific, conventional conglomeratic reservoirs and unconventional tight sandstone reservoirs. On gamma ray log, this lithofacies shows the continuation of funnel-shaped pattern of the underlying FA1 that goes into the lowest gamma ray values in a single parasequence (Fig. 2.4).

The typical succession consists of laminated to bioturbated lower very fine- to lower fine-grained sandstone (Figs. 2.7A, B, C), which interfingers with, and may shift upward into, its laterally equivalent massive to laminated conglomerate beds (Figs. 2.8A, B, C, D). These two lithologies are often intercalated with well-segregated upper fine- to upper medium-grained sandstone beds.

The lowermost sandstone exhibits cross-stratification in which laminae angles steepen upwards, with typically sharp, erosive upper contacts that the underlying steeply-inclined foresets terminate against (Fig. 2.7A). Sandstone with these laminae characteristics indicate trough cross-stratified beds. Towards the younger intervals, sandstone may appear to be more massive or characterized by very poorly-defined planar to low angle parallel laminae. These laminae are distinguishable with the HCS and SCS of FA1 (Fig. 2.7C), owing to the absence of reactivation surfaces and the pairings of laminae.

Although the laterally equivalent conglomeratic strata share many similarities in terms of the frameworks between each conglomeratic facies (i.e. predominantly clast-supported, moderately well-sorted with very well-rounded and low-sphericity chert-dominant grains), they are distinguishable primarily based on their grade of sorting and clast composition. The complete succession of the conglomeratic counterpart may exhibit gradual changes from the underlying matrix-rich or matrix supported, poorly-sorted, polymodal to bimodal conglomerate (Figs. 2.8A, B, C) to the uppermost clast-supported, well-sorted, unimodal conglomerate (Fig. 2.8D). These changes are typically accompanied by the notable decrease of sandstone intercalations and terrestrially-derived organic matter. Conglomerate clasts also shift from boulder- to cobble-rich into granule-dominated beds, with lithologies switching from chert- and rock fragment-rich into strictly chert-dominated. Throughout the conglomeratic intervals that are frequently massive, planar beddings, tabular cross-beddings, and trough cross-beddings are occasionally present (Fig. 2.9). The matrix-rich intervals may also display high-angle cross-stratifications. The presence of these structures in conglomerate units is most readily recognized where sandy matrix or thin laminae of sandstone fill the contact between each conglomerate bed. Where the conglomerate is highly clast-supported, the recognition relies more on the imbrication trend of the clasts (Fig. 2.9).

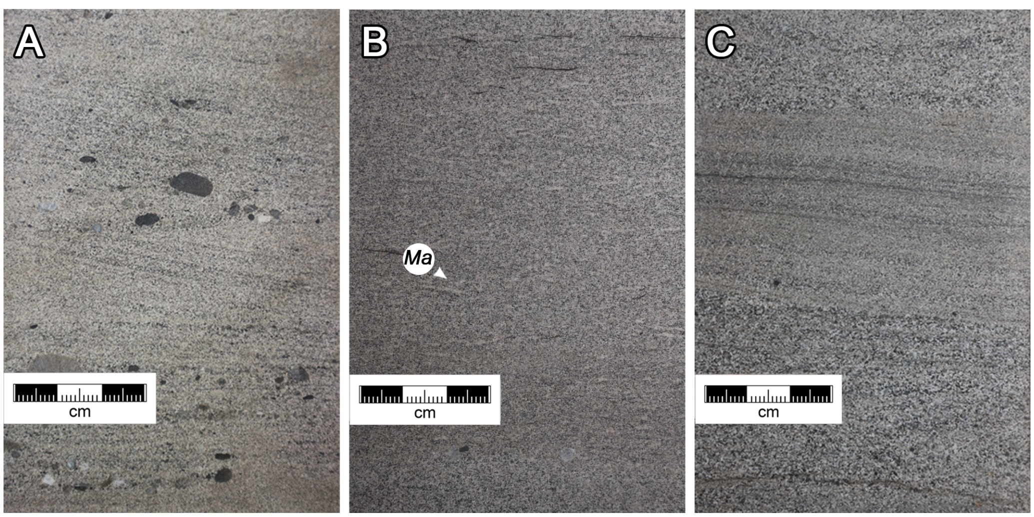

Figure 2.7. Core photographs of facies 4 through 6. **A)** Facies 4, laminated pebbly upper fine-grained sandstone with cross-beddings that steepen upwards, indicating trough cross-stratifications (upper shoreface) (well 100/01-08-066-08W6/00, 2578.1 m); **B)** Facies 5, thoroughly bioturbated very fine-grained sandstone with monotypic assemblage of *Macaronichnus segregatis* (foreshore) (well 100/03-18-066-08W6/00, 2468.7 m); **C)** Facies 6, very well-segregated fine- and medium-grained sandstone (upper shoreface) (well 100/03-18-066-08W6/00, 2482.3 m).

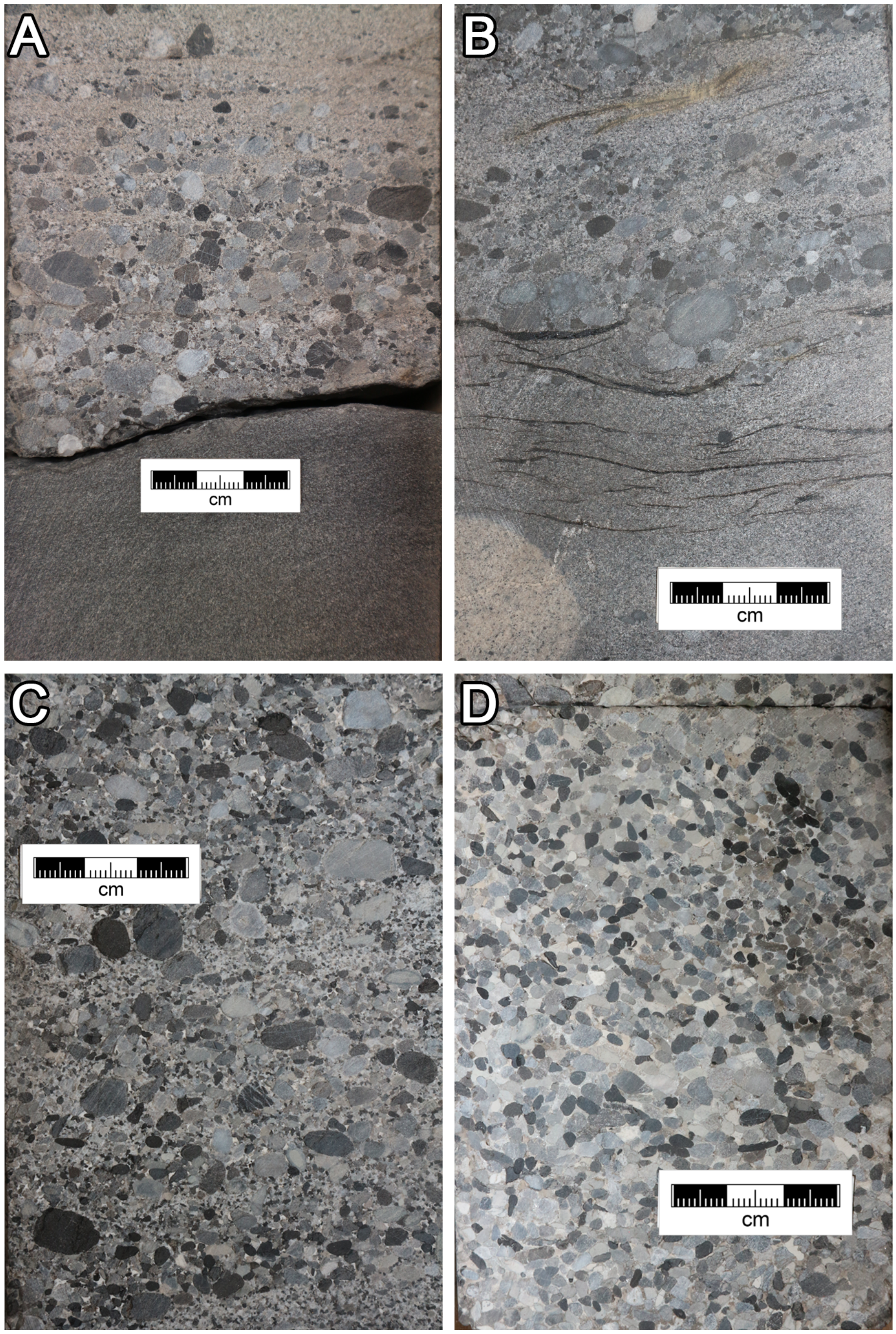

Figure 2.8. Core photographs of the conglomeratic units. **A)** Transgressive lags separating the underlying FA1 and overlying FA2 (well 100/01-08-066-08W6/00, 2583.2 m); **B)** Facies 7; matrix-supported, poorly-sorted, organic-rich polymodal conglomerate (distributary channel) (well 100/06-20-065-10W6/00, 2913.6 m); **C)** Facies 8; matrix-rich, moderately-sorted bimodal conglomerate (upper shoreface) (well 100/14-24-065-11W6/00, 2769 m); **D)** Facies 9; clast-supported, well-sorted unimodal conglomerate (foreshore) (well 100/10-36-065-09W6/00, 2643.9 m).

Figure 2.9. Diamond core box shot from well 100/07-14-065-11W6/02 (3165 – 3177 m). Poorly-sorted conglomerate interpreted as distributary channel deposit (facies 7) scoured over transgressive coal deposited in coastal plain (facies 12).

Trace fossil suites within this facies association are restricted to beds consisting of fine-grained or finer sandstone. Infrequent occurrences of trace fossils in conglomeratic units have been reported (e.g. MacEachern and Hobbs, 2004; Dashtgard, 2006), however, such occurrences were not encountered in the Falher F.

Facies association FA2 preserves moderately diverse biogenic structures (nine ichnotaxa). They are sporadically distributed among discrete intervals, with the vast majority of the sandstone strata being unburrowed. Similar to FA1, trace fossils occur as high density and low diversity population. Their intensity ranges from moderately low to high (BI = 2 – 4) but can be exceptionally very high where monospecific assemblage of *Macaronichnus* occurs (BI = 6) (Fig. 2.7C). Cryptic bioturbation is also interpreted to be present in strata with poorly-defined laminae or massive appearance (Pemberton *et al.*, 2012). The ichnotaxa include primarily dwelling structures of inferred suspension feeders and passive carnivores, followed by common dwelling structures of inferred deposit feeders. They include abundant *Palaeophycus*, *Planolites*, and *Macaronichnus;* common *Thalassinoides*; as well as rare *Bergaueria*, *Ophiomorpha*, *Rosselia*, and *Schaubcylindrichnus*. A *Glossifungites* surface is infrequently present, separating the contact between FA2 and the overlying FA1 of younger parasequence (Fig. 2.5; 2.4). As opposed to FA1, vertically-oriented trace fossil suites predominate over horizontal burrows.

Interpretation

Typically overlying FA1, FA2 is interpreted to reflect deposition within the foreshore to upper shoreface in both strandplain and wave-dominated proximal delta front setting. The bidirectional trough cross-stratified beds, which are typically attributed to the prevalent bidirectional translation waves and longshore currents actively working in the surf zone (Hunter *et al.*, 1979), are a particularly prominent characteristic of this facies association.

The scoured-based, poorly-sorted, organic-rich conglomerate beds are interpreted to be gravelly distributary channels, primarily due to their high-angle stratification, open framework, and poorly-sorted appearance (Figs. 2.8A, B; 2.9), which are in contrast with the upper shoreface and foreshore conglomerate (Nemec and Steel, 1984; Massari and Parea, 1988; Hart and Plint, 2003; MacEachern and Hobbs, 2004) (Figs. 2.8C, D; 2.10). The abundance of terrestrial-derived organic debris also implies rapid sedimentation and minimal winnowing effects during deposition (McLean, 1979) (Fig. 2.8B). Similar occurrences of gravel-rich distributary channel conglomerates with matrix-rich to matrix-supported framework, massive to cross-bedded, and coarsest size of pebble clasts among other conglomeratic units have also been reported in many ancient successions (e.g. Arnott, 1991; 1994; 2003; Yin *et al.*, 2016). Schmidt and Pemberton (2004) interpreted a similar depositional unit in the Notikewin Member as upper shoreface, but that was due, in part, to the presence of trace fossils (*Macaronichnus* and *Conichnus*) that were not observed in the study interval. In well 100/07-14-065-11W6/02, a unit contact of poorly-sorted, high angle stratified conglomerate scouring into an underlying thin coal bed occurs (Fig. 2.9). This probably suggests the erosional nature of individual distributary channels, similar to the observations of McLean (1979) and Rouble and Walker (1997) in an upper Falher conglomerate interval in the Elmworth Field. In modern gravelly river deltas, for instance the Copper River fan-delta in Alaska, internal medium- to large-scale cross beddings are also observed, as well as plant debris and occasional thin muddy intervals (Figs. 2.5; 2.9) (Galloway, 1976).

Due to the recurring cycles of deposition and entrainment of the sediment inherent to the nearshore, the sediments are well-winnowed and resulting in textural and compositional maturity (Folk, 1951; Pettijohn, 1975). When assessing various Falher F sandstone units from different depositional settings in the palaeobasin, there is an increase in the degree of sorting, grain roundedness, and grain sphericity, as well as changes in framework relationship and

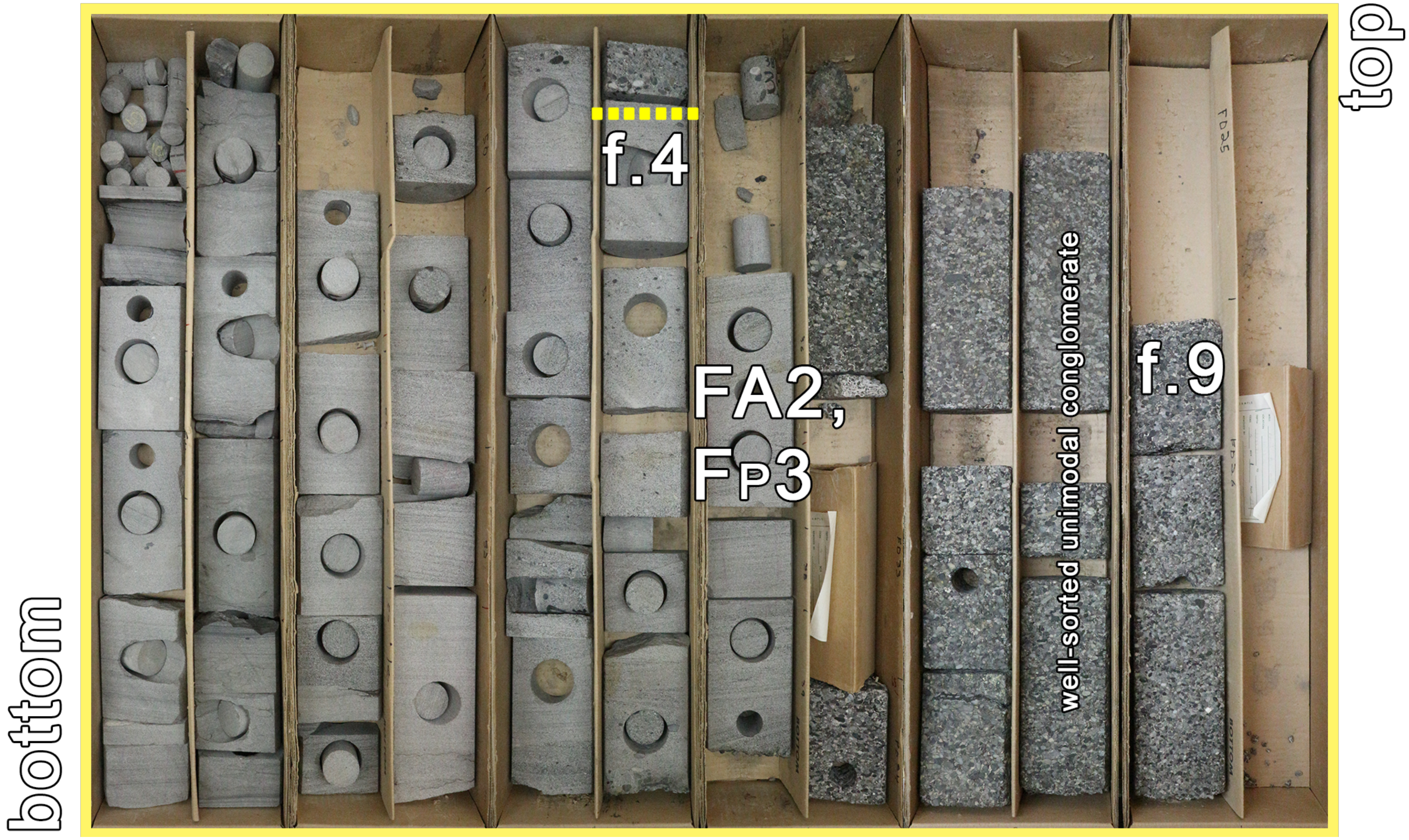

Figure 2.10. Diamond core box shot from well 100/11-13-066-8W6/00. Note the well-sorted, closed framework conglomerate, interpreted as beach deposits (facies 9) that is in contrast with the distributary channel conglomerate in Figure 2.9.

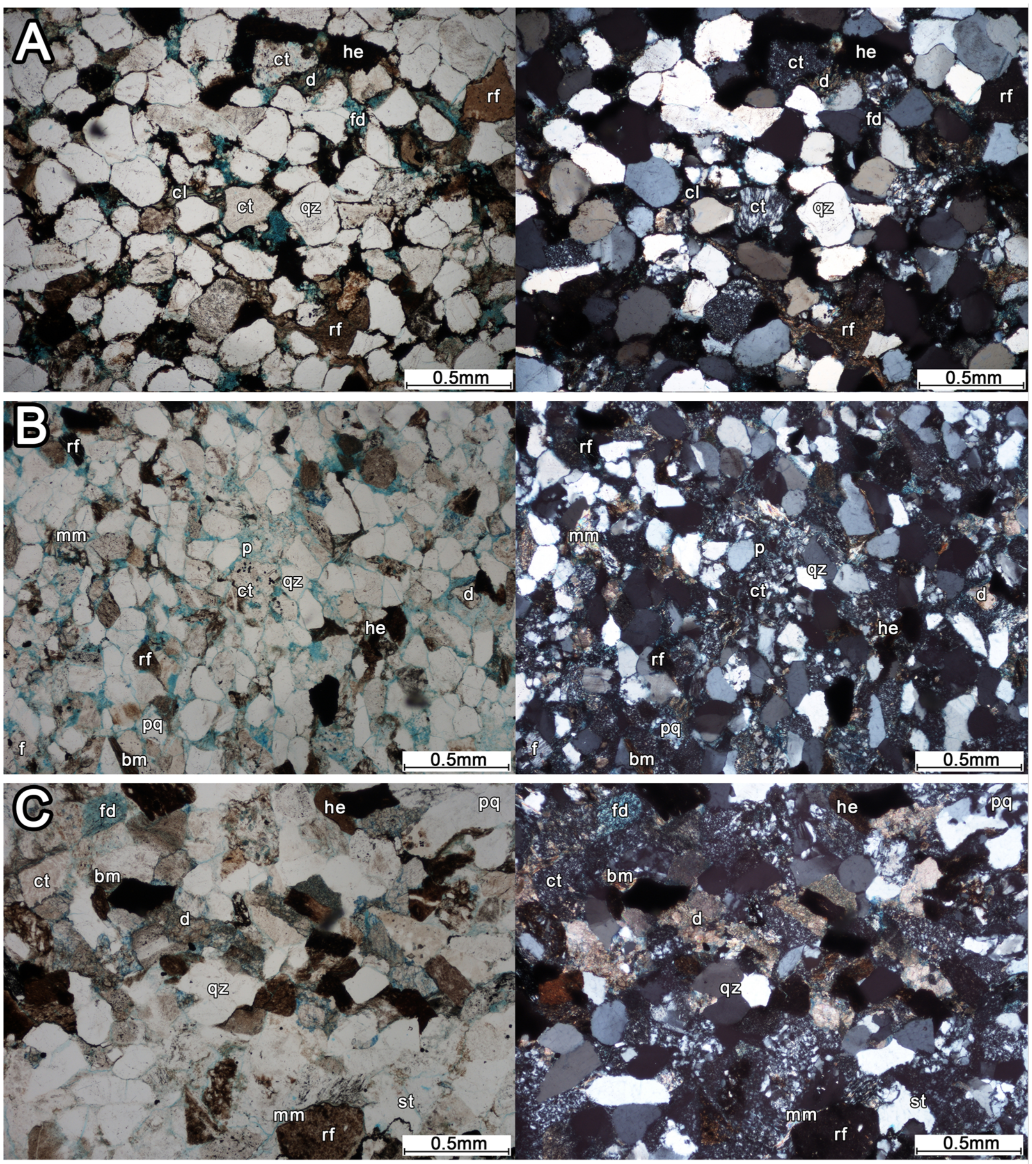

Figure 2.11. Petrographic images displaying deepening successions from A to C. Note that as the facies changes from shoreface (C) to foreshore (A), the sandstone undergoes an increase in both textural and compositional maturity, as indicated by the enhanced proportion of quartz, ratio of clasts vs. matrix, and the higher degree of clast sphericity and roundedness. **A)** Foreshore sandstone (well 100/07-14-065-11W6/02, 3168.3 m); **B)** Upper shoreface sandstone (well 100/11-13-066-08W6/00, 2563 m); **C)** Middle shoreface sandstone (well 100/05-32-065-09W6/00, 2917.7 m).

mineralogical composition towards the foreshore (Figs. 2.11A, B, C). The sandstone shows a tendency towards quartz-rich litharenite in the shoaling upward trend (Fig. 2.11A), with unstable mineral components more common in the deeper successions (Fig. 2.11C). Thus, wave-winnowing is reflected in the primary bulk porosity and permeability that rendered FA2 to be the principal producer (Hart and Plint, 2003). The common accumulation of gravels in a sand-dominated shoreline succession may indicate proximity to a fluvial point source (Kirk, 1980).

The sandstone trace fossil association in FA2 includes low-diversity and high-density assemblages of traces constructed by opportunistic colonizers, similar to those of FA1, albeit with much fewer deposit feeding traces. The consistently predominant dwelling structures of suspension feeders and passive carnivores from FA2 is consistent with the archetypal *Skolithos* Ichnofacies. Traces were generated by organisms that flourished in harsh settings, characterized by frequently shifting sand substrates with unpredictable rates of sedimentation (Pemberton *et al.*, 1992). The presence of discrete monospecific assemblage of *Macaronichnus* has also been regarded to be a reliable indicator of intertidal to shallow subtidal deposits (Clifton and Thompson, 1978; Saunders and Pemberton, 1990). This is a typical attribute of upper shoreface and beachface in both strandplain and wave-dominated proximal delta front, consistent with the sedimentological observation (MacEachern and Pemberton, 1992; Pemberton *et al.*, 1992).

FACIES ASSOCIATION (FA) 3: BRACKISH EMBAYMENT

Discussion

This succession either caps or interfingers with previously mentioned facies associations in landward direction. It consists of various types of finer-grained lithologies with minor sandstone, resulting in relatively high gamma ray expression on the geophysical well log (Fig. 2.12). An exception occurs when coals are encountered, which results in a sharp gamma ray deflection leftward. The complete succession of FA3 includes laminated to bioturbated

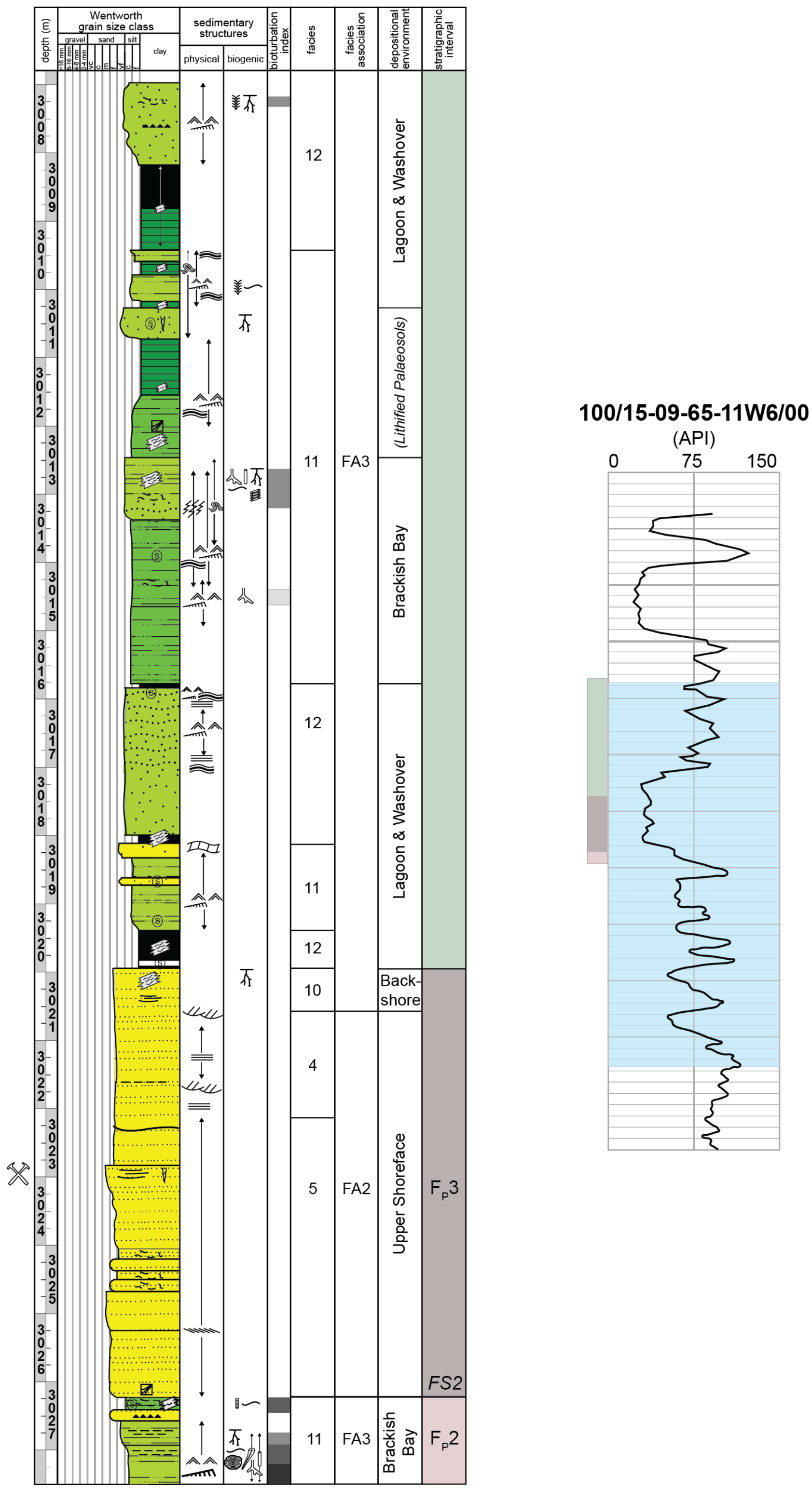

Figure 2.12. Calibrated core interval and gamma-ray log for well 100/15-09-065-11W6/00, showing all facies within FA3 succession.

sandstone with heightened abundance of rootlets towards the top (Fig. 2.14A), capped by interbedded massive to carbonaceous mudstone and coal as well as interstratified sandy mudstone and bioturbated argillaceous sandstone (Figs. 2.14B, C).

The underlying coarser-grained strata exhibit changes from bidirectional cross-bedded sandstone into predominantly massive to low-angle planar parallel bedded sandstone upwards. The overlying finer-grained strata are significantly darker, and where sand content is elevated shows interstratification of predominantly wavy beddings, planar laminae, cross ripples, combined flow ripples, and other minor physical structures (Table 2.1; Figs. 2.12; 2.13; 2.14C).

Similar to FA2, the ichnotaxa are sporadically distributed and restricted to the sand-dominant intervals or sandy-silty interface. The biogenic structures are diverse (16 ichnotaxa) with bioturbation intensity ranging from predominantly none to moderately high (BI = 0 – 4). Other ichnotaxa include: diminutive, yet abundant, *Planolites, Palaeophycus, Cylindrichnus, Skolithos, Asterosoma, Ophiomorpha, Thalassinoides, Rosselia*, navichnia; common *Teichichnus,* fugichnia; as well as rare *Gyrolithes, Bergaueria, Diplocraterion,* and *Rhizocorallium*. They generally occur as low-diversity, high-density trace fossils association throughout discrete, isolated beds.

Interpretation

Facies association FA3 records the deposition in a back-barrier complex with backshore and estuary bayhead delta at the most seaward and landward position, respectively. The abundance of rootlets on backshore deposits reflects intervals of subaerial exposure which allowed colonization by plants (Davis, 1978). The gently inclined parallel laminae indicate possible landward-oriented inclination upon receiving sediments from the eroded beach seaward, typical of backshore (Johnson and Baldwin, 1996).

Overlying backshore deposits are lagoonal to estuarine successions.

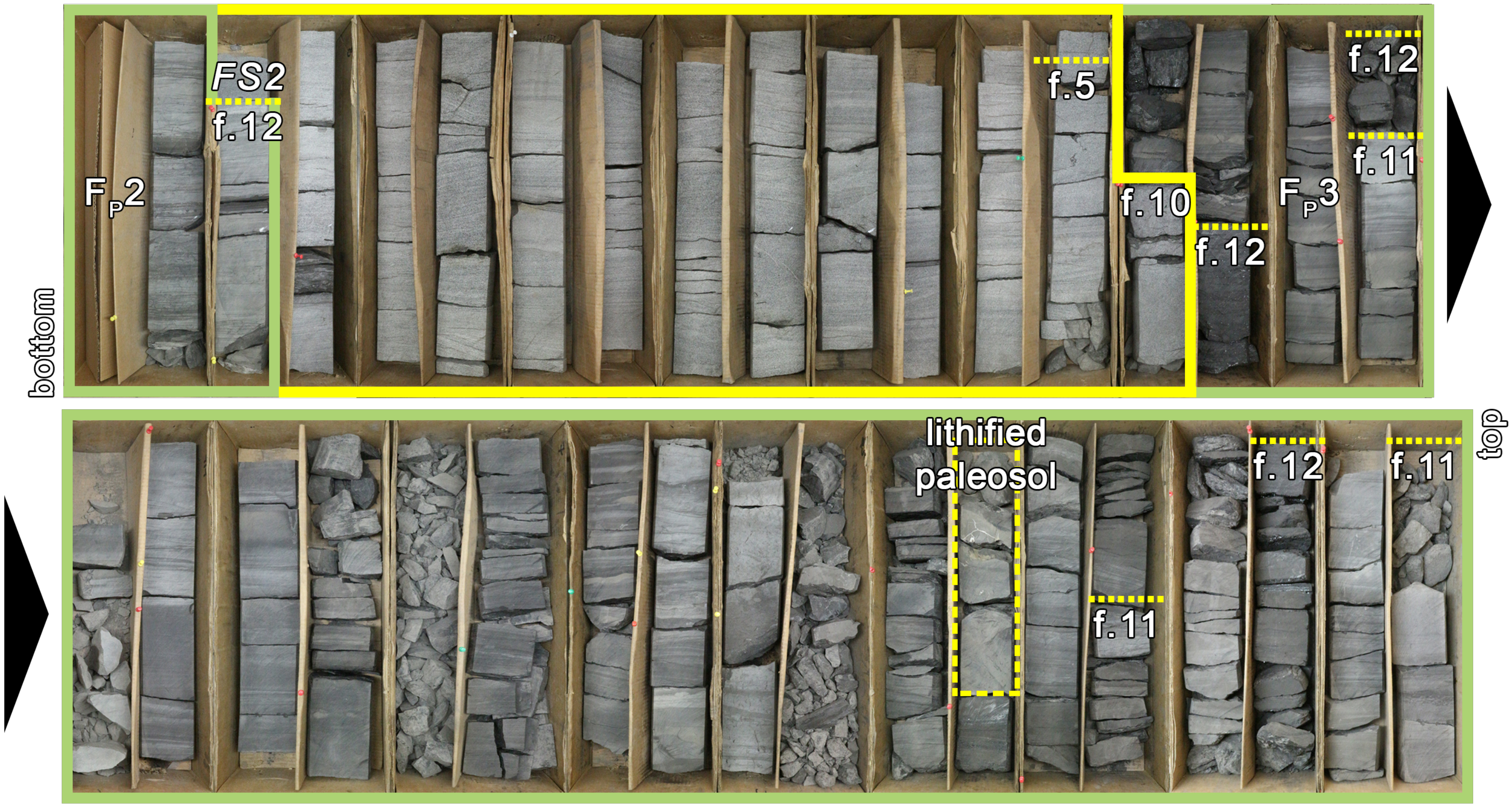

Figure 2.13. Diamond core box shot from well 100/15-09-065-11W6/00 displayed in Figure 2.12. The lithified palaeosol at depth 3011.2 - 3011.7 m may indicate a subaerial unconformity during the deposition of F_P4 forced regressive shoreface.

Massive to organic-rich mudstone is interpreted to reflect deposition in a quiet water with restricted circulations, typical of lagoonal settings (Boyd *et al.*, 1992; Reading and Collinson, 1996). Where sand content is elevated and shows low-angle dipping stratifications, it is interpreted to reflect washover events into the lagoon (Boyd *et al.*, 1992; Reading and Collinson, 1996).

Pattison and Walker (1994) reported a similar occurrence of interstratified sandy mudstone with planar laminae, current ripples, discrete sandstone stringers, and planar to trough cross-stratifications in the late Albian Viking wave-dominated estuary of Alberta. The presence of synaeresis cracks attests to fluctuating salinity levels which implies the presence of direct fluvial input (Plummet and Gostin, 1981). The abundance of soft sedimentary structures, while not diagnostic of a specific environment, supports the occurrence of these beds in an aqueous environment with episodically high sedimentation rates (Allen, 1982).

The grey mudstone with rootlets, siderite mottles, secondary calcite veins, and siderite- filled desiccation cracks tapering vertically down the beds is interpreted to represent moderately mature palaeosols (Fig. 2.14D) (Wright, 1986; 1992; Bown and Kraus, 1987; Kraus, 1999). The desiccation cracks on the palaeosols reflect drier intervals (Tanner, 2003). The marked absence of carbonaceous materials is consistent with periodic drying and consequent oxidation of carbonaceous materials (Wadsworth *et al.*, 2003). Siderite fillings may have resulted from periodically high-water table saturating the soils, or eluviation from higher soil profile that brings iron into them (Leckie *et al.*, 1989). Another lithified paleosol is observed on siltstone with pedogenic slickensides, which is interpreted to have been resulted from "gravitational compaction or shrink-swell forces" generating the alignment of clay, thus their "polished, finely-grooved surfaces with a waxy lustre" (Leckie *et al.*, 1989; p. 316).

The trace fossil suites of facies association FA3 reflect emplacement in a brackish setting in that it is characterized by diminutive, high-density, and low-diversity populations (Pemberton *et al.*, 1982). It represents an impoverished *Cruziana* Ichnofacies restricted to sandier strata. They primarily consist of "facies-crossing" forms that reflect rapid harvesting of food (*Planolites* and *Thalassinoides*) as well as deposit feeding and/or subordinate suspension feeding (*Skolithos, Gyrolithes,* and *Cylindrichnus*) typical of brackish environment (Gingras *et al.*, 2012; MacEachern *et al.*, 2012). Similar trace fossil assemblages of wave-dominated estuarine succession were also found in the Albian Viking Formation of Alberta, albeit with more discernible occurrences and larger morphologic scale (MacEachern and Gingras, 2007; MacEachern and Pemberton, 1994).

FACIES ASSOCIATION (FA) 4: COASTAL PLAIN

Discussion

This facies association constitutes the most landward succession of the Falher F in the study interval. Its gamma ray signature may either be similar to FA3 back-barrier complex or possess a bell- to serrated-shaped pattern. Core availability, however, does not provide observable contacts between the facies present. In some cores, FA4 is characterized by interbedded massive to organic-rich mudstone and coal, whereas one core exhibits fining-upward, laminated very fine-grained sandstone beds (Fig. 2.14D). The former overlaps with strata that are also included within the previously mentioned FA3 brackish embayment succession. Therefore, the differentiation of such strata that alternatively belong to either the FA3 brackish embayment or the FA4 coastal plain succession is dependent upon their stratal relationship with the adjacent environment above and below. The sandstone is largely planar parallel-bedded, with preserved minor climbing ripples at the uppermost interval. None of these deposits exhibits any presence of biogenic structures.

Interpretation

This succession records the deposition in a shore-proximal coastal plain

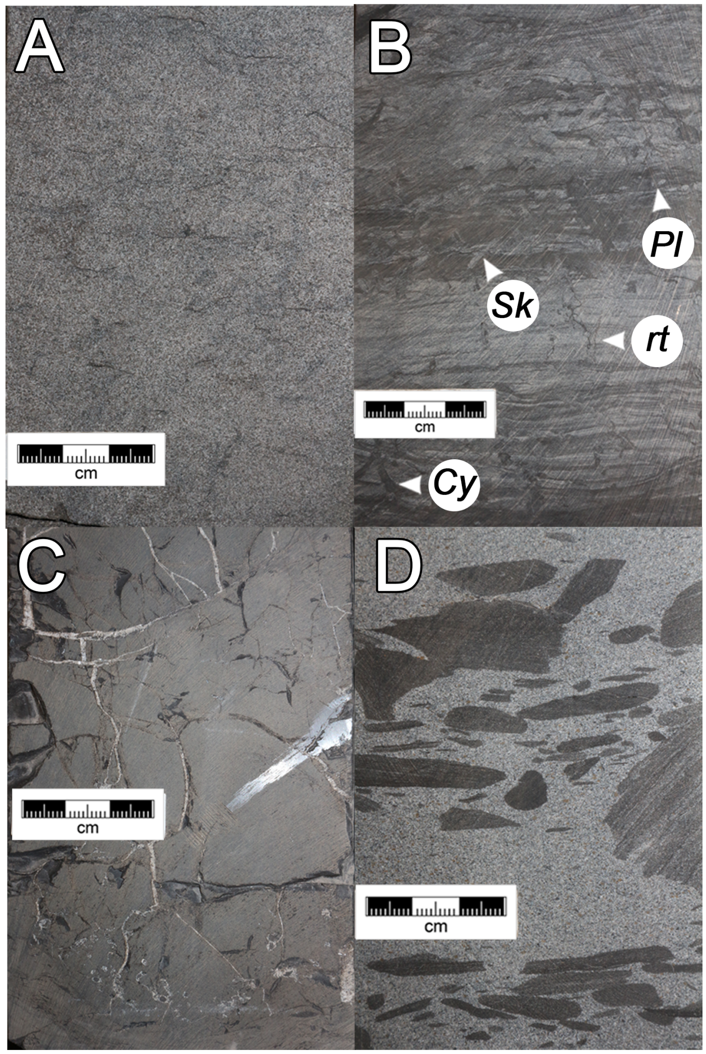

Figure 2.14. Core photographs of facies 10 through 13. **A)** Facies 10; very fine-grained sandstone with no apparent primary structures as the result of pervasive rootlets (backshore) (well 100/03-18-066-8W6/00, 2466.6 m); **B)** Facies 11; bioturbated heterolithic sandy mudstone. Note the impoverished suite with moderate diversity, implying a setting with reduced salinity (brackish bay) (well 100/15-09-065-11W6, 3028.2 m); **D)** Facies 11; lithified palaeosol with secondary calcite veins, siderite-filled shrinkage cracks, siderite mottles, and rootlets (well 100/03-20-065-11W6/00, 2854.2 m); **E)** Facies 13; laminated very fine-grained sandstone with abundant rip-up clasts (fluvial channel) (well 100/08-26-065-11W6/00, 2870.4 m). Abbreviations: *Ma = Macaronichnus, Sk = Skolithos, Pl = Planolites, Cy = Cylindrichnus, rt* = root traces.

setting, with subenvironments including marsh, swamp, and fluvial channel (Figs. 2.13; 2.12). The basinward limit of this facies association coincides with the less marine-influenced elements of FA3, which normally lies at the uppermost portion of the Falher F succession. More proximal successions occur to the south of the present study area and are rarely cored.

The unburrowed planar-laminated sandstone represents fluvial channel deposits in terrestrial settings without the evidence of tidal or brackish water influence. The strikingly abundant mud clasts and erosional intraclasts were likely derived from cutbank collapse, and incorporation of flood plain mudstone intraclasts into the channel (Nichols, 2009) (Fig. 2.14D). In the uppermost part, where small climbing ripples are sandwiched between parallel laminae, increasingly rapid deposition is indicated, such as when a crevasse splay is deposited on top of the former channel (e.g. van Gelder *et al.*, 1994) or perhaps during a seasonal increase in flow.

CONSTRAINTS ON DEPOSITIONAL ENVIRONMENTS

While primary sedimentary features provide the principal basis on interpreting depositional settings in this study, trace fossils associations are no less significant indicators to place those environments into a depositional framework where ecological constraints are taken into account. In general, the marine successions of the Falher F (FA1 and FA2) exhibit impoverished trace fossil suites with low bioturbation intensity, particularly in comparison to other wave- and storm-dominated shoreface successions in the Western Interior Seaway (MacEachern and Pemberton, 1992) such as the Albian Bluesky Formation in west-central Alberta (Male, 1992), Albian Viking/Bow Island Formation in south-central Alberta (Raychauduri *et al.*, 1992; Raychauduri and Pemberton, 1992), Albian Cadotte Member of the Peace River Formation in west-central Alberta (MacEachern *et al.*, 1994), and Turonian Cardium Formation in west-central Alberta (Vossler and Pemberton, 1988). This indicates that the basin may have been exposed to various physico-chemical stresses thus making the environment too hostile for tracemakers (Gingras *et al.*, 2011).

In the Falher F, the relatively diminutive ichnotaxa present are dominated by opportunistic tracemakers such as *Planolites*, *Thalassinoides*, *Cylindrichnus*, and *Skolithos* rather than a diverse suite of traces representing multiple behavioural types and including fully forms such as *Zoophycos*. The diminutive size of the traces and the restriction of ethological categories support the interpretation of reduced salinity in the study area during the Falher F deposition (Pemberton and Wightman, 1992; MacEachern *et al.*, 2005). During the Falher F deposition, the Boreal Seaway in the Wapiti area was shallow (Cant, 1984) and probably characterized by numerous fluvial feeders in the form of small to moderate scale deltas. Similar to several modern seaways such as the Baltic Sea where river run-offs are among the factors that reduce the marine salinity, and consequently, the ecological varieties (Hänninen, 2015), the southern limit of the basin was likely characterized by salinities below normal marine conditions. The rare occurrence of fully marine trace signatures typical of the *Zoophycos* or *Nereites* Ichnofacies in the offshore mudstone of Falher F in the study area also indicates the relatively shallow overall palaeobathymetry of the Boreal Sea. Bann and Fawcett (2016) also observed profound deltaic signatures in the ichnofossil assemblages of the Wilrich member, which is interpreted to have been a result of progradation of a delta into a low-accommodation shallow sea southward of the Wapiti area. It is probable that such conditions persisted during the deposition of lower Falher submembers.

The preferential occurrence of traces with moderate to thick sediment linings such as *Conichnus*, *Diplocraterion*, *Rhizocorallium*, *Rosselia*, and *Teichichnus* suggests rapid sedimentation and colonization of loose, shifting substrates (MacEachern *et al.*, 2007). Most of these traces are equilibrichnia, consistent with tracemakers that respond well to sudden erosion or sedimentation (Pemberton and MacEachern, 1997; Pemberton and MacEachern, 2005). This interpretation is supported by the general trend of low bioturbation, which is also consistent with persistently high rates of sedimentation, possibly linked to the proximity of direct supplies of sediment from the neighboring distributary channel of deltaic system (MacEachern *et al.*, 2007). The predominance of probable opportunistic (r-selected) tracemakers over those of equilibrium (K-selected) assemblages also suggests the perpetual notable contribution of storm-induced rapid emplacement of sediments (Ekdale, 1985; Droser and Bottjer, 1989; MacEachern and Pemberton, 1992). In the study interval, this occurs as densely packed, low diversity trace assemblages which overlap through adjacent environmental settings, such as *Ophiomorpha, Schaubcylindrichnus, Palaeophycus*, and *Teichichnus*.

The Clearwater (Boreal) Sea during lower Albian time was a very narrow seaway within an embayment created by uplift of the western Canadian Cordillera and surrounded on all sides except the narrow northern opening by continental landmasses (e.g. palaeogeographic maps of Blakey, 2016). This restricted morphology likely contributed to a persistent brackish state during many intervals due to restricted circulation and numerous deltas arriving from the mountains to the west and from the lowlands to the east and south. Core-based foraminiferal studies from the Upper Mannville succession support the hypothesis of widespread brackish conditions in the WCSB during the late Albian time (e.g. Holmden *et al.*, 1997; Mattison and Wall, 1993; Stritch and Schröder-Adams, 2000).

STRATIGRAPHIC FRAMEWORK

The Falher F unit in the Wapiti area consists of four coarsening-upward parasequences of coarser-grained shoreface deposits followed by a thinner succession of silty to shaly coastal plain deposits. These parasequences are informally assigned here as F_P1 through F_P4 (Figs. 2.15, 2.16, 2.17). Parasequence F_P1, F_P2, and F_P4 are sand-bearing deposits, whereas parasequence F_P3 is locally enriched by conglomerate. In the Wapiti area, these parasequences are dominated by facies association FA1 and FA2, which interfinger to the south

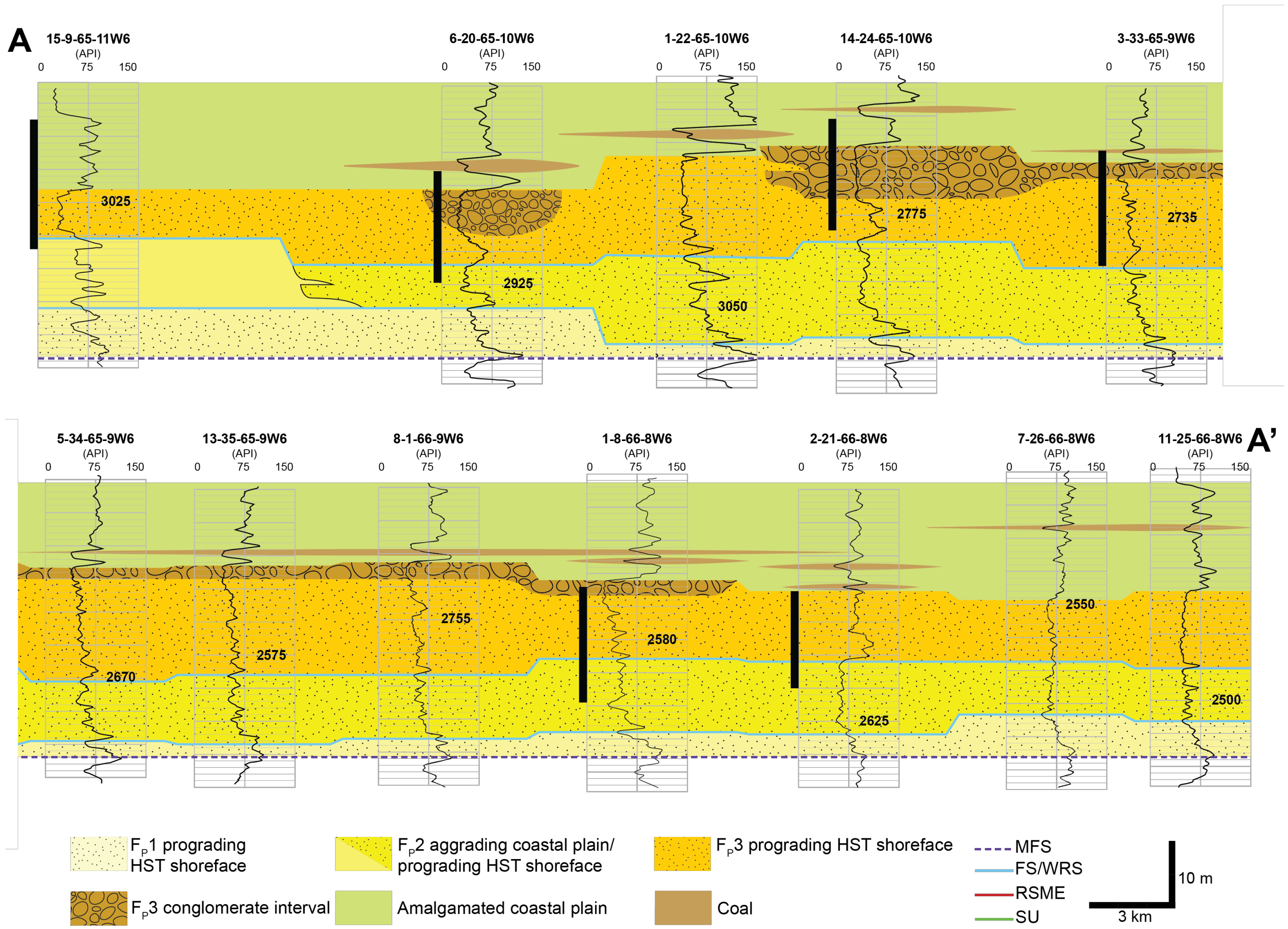

Figure 2.15. Strike-oriented gamma ray cross-sections: A-A'. Location of wells can be seen in Figure 2.3.

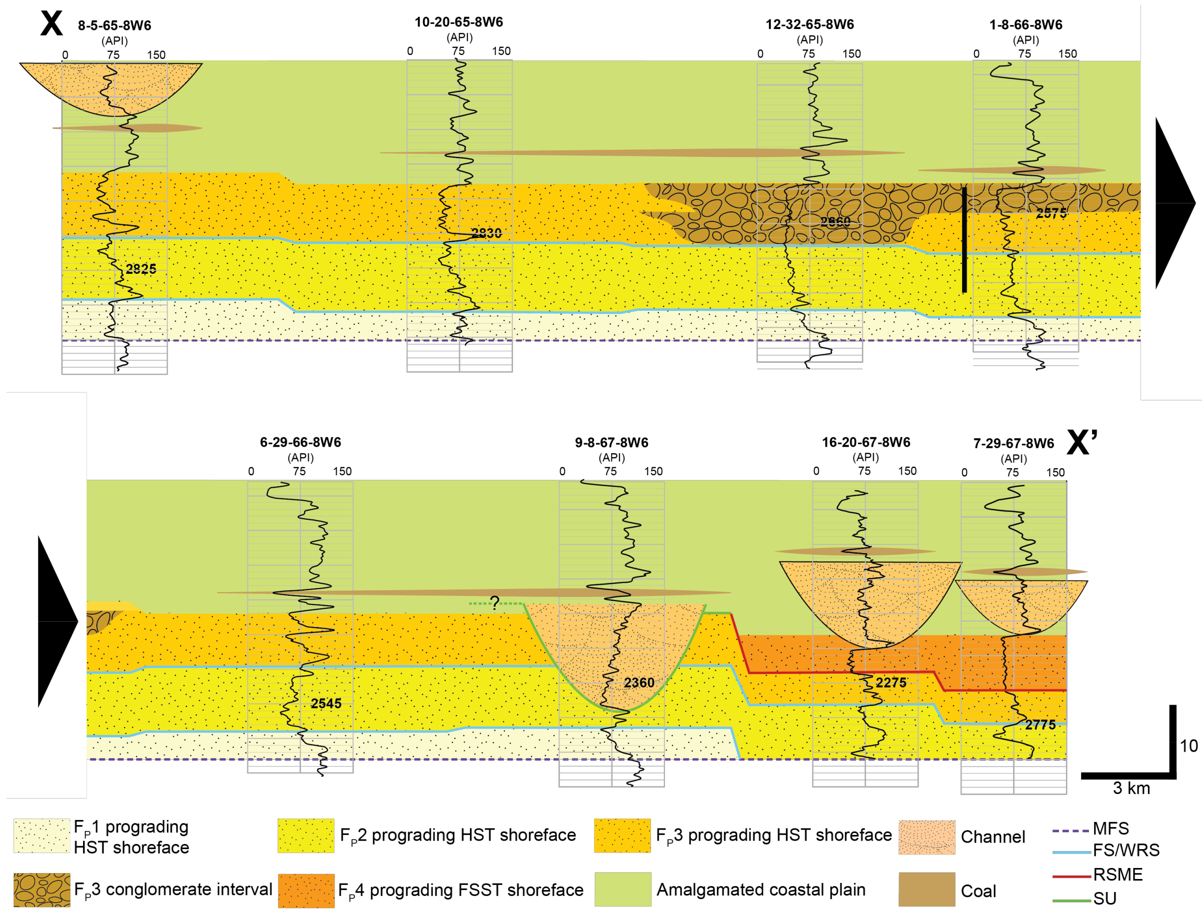

Figure 2.16. Dip-oriented gamma ray cross-sections: B-B'. Wells are located in the eastern portion of the study area (see Figure 2.3). Note the fluvial onlap between well 100/09-08-067-8W6/00 and 100/16-20-067-08W6/00.

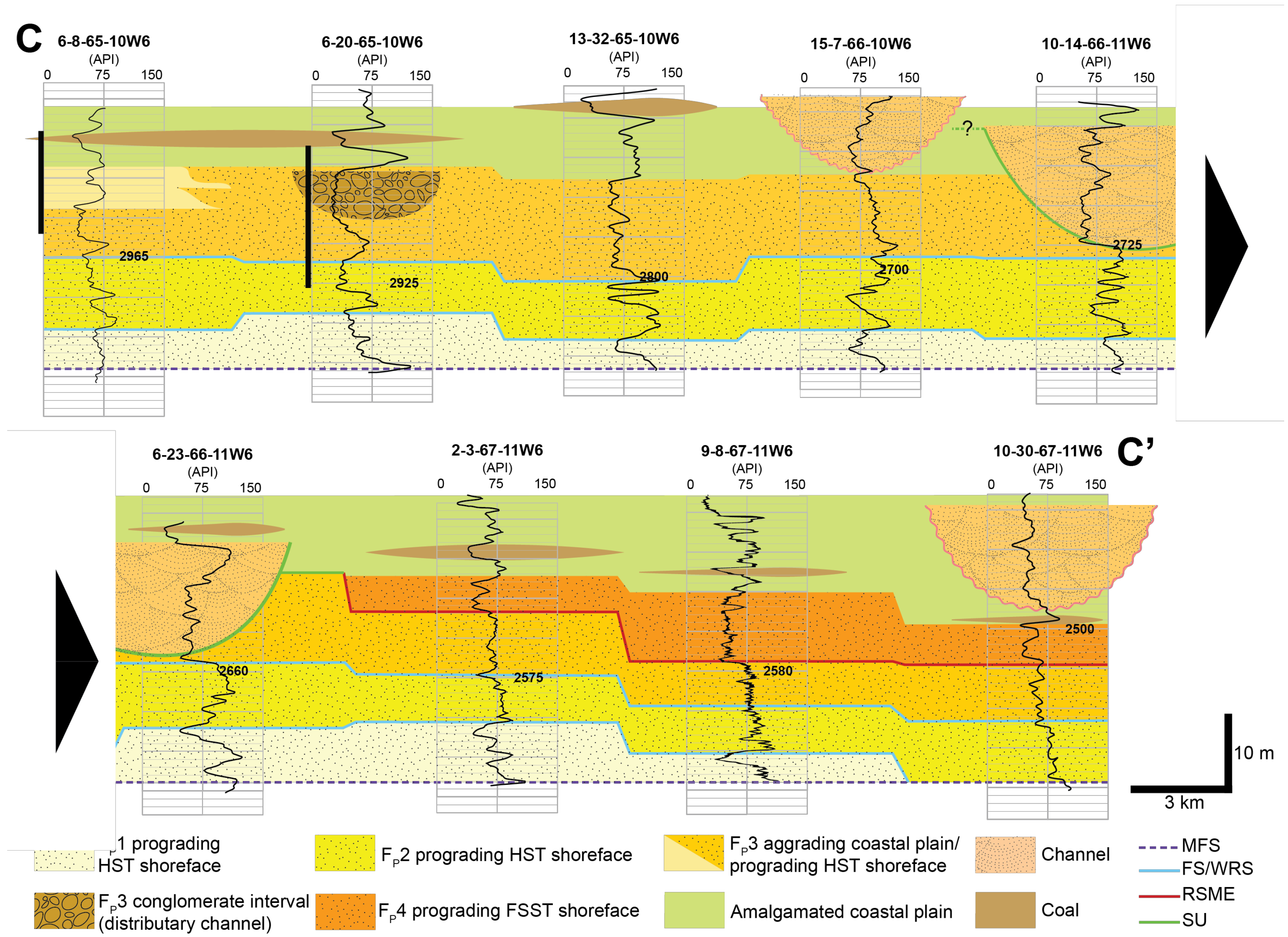

Figure 2.17. Dip-oriented gamma ray cross-sections: C-C'. Wells are located in the western portion of the study area (see Figure 2.3).

with FA3 and FA4 (Figs. 2.15, 2.17). These progradational deposits are capped by a succession of aggradational to retrogradational non-marine deposits. Northward progradation of each parasequence is indicated through the isopach maps of shoreface bodies associated with each parasequence (Figs. 2.18A, B, C), which shows northward shifting depocentre. An isopach map of the conglomerate concentration during parasequence F_P3 reveals an ENE-WSW trend (approximately 265°) (Fig. 2.19).

The base of the Falher F is interpreted to be a maximum flooding surface (MFS) (Figs. 2.15, 2.16, 2.17). This interpretation is based on the consistent gamma ray log signature that marks the end of rightward deflection below the base of Falher F. Above this peak of highest radioactivity, the log pattern begins to deflect leftward, indicating the shift towards the progradation of parasequence F_P1. Therefore, this surface is interpreted to mark the end of transgression during the Falher G deposition in the study area. The top of the Falher F is more challenging to trace, due to the amalgamation of Falher F and E coal-bearing non-marine successions that possess no distinctive expression on the geophysical well logs. This top is interpreted to be a flooding surface (FS).

Each prograding succession of F_P1 through F_P3 is separated by a marine flooding surface that represents a short-lived back-step of the shoreline positions (Fig. 2.15A). This is typically recorded by thin offshore transition mudstone units (facies 1, FA1) (Figs. 2.6A, B) directly overlying shoreface sandstone beds (facies 2 to 6, FA2) (Figs. 2.6C, D, E, F; 2.7A, B, C). These brief transgressions are of higher frequency (fifth order) compared to the final transgression (fourth order) that marks the end of Falher F deposition. The base of the mudstone or storm deposits marks an abrupt deepening at the top of each parasequence and is regarded as co-planar marine flooding surface (FS) and wave ravinement surface (WRS) (Figs. 2.15; 2.16; 2.17). The latter is most apparent where transgression-induced scouring or *Glossifungites* surfaces are evident (Fig. 2.5). Poorly-sorted pebble lags infrequently occur on this surface, providing an evidence of ravinement (Fig. 2.5). Where mudstone is absent, the abrupt deepening occurs as HCS- or SCS-bedded sandstone (facies 2 and 3 of FA1, respectively) overlying

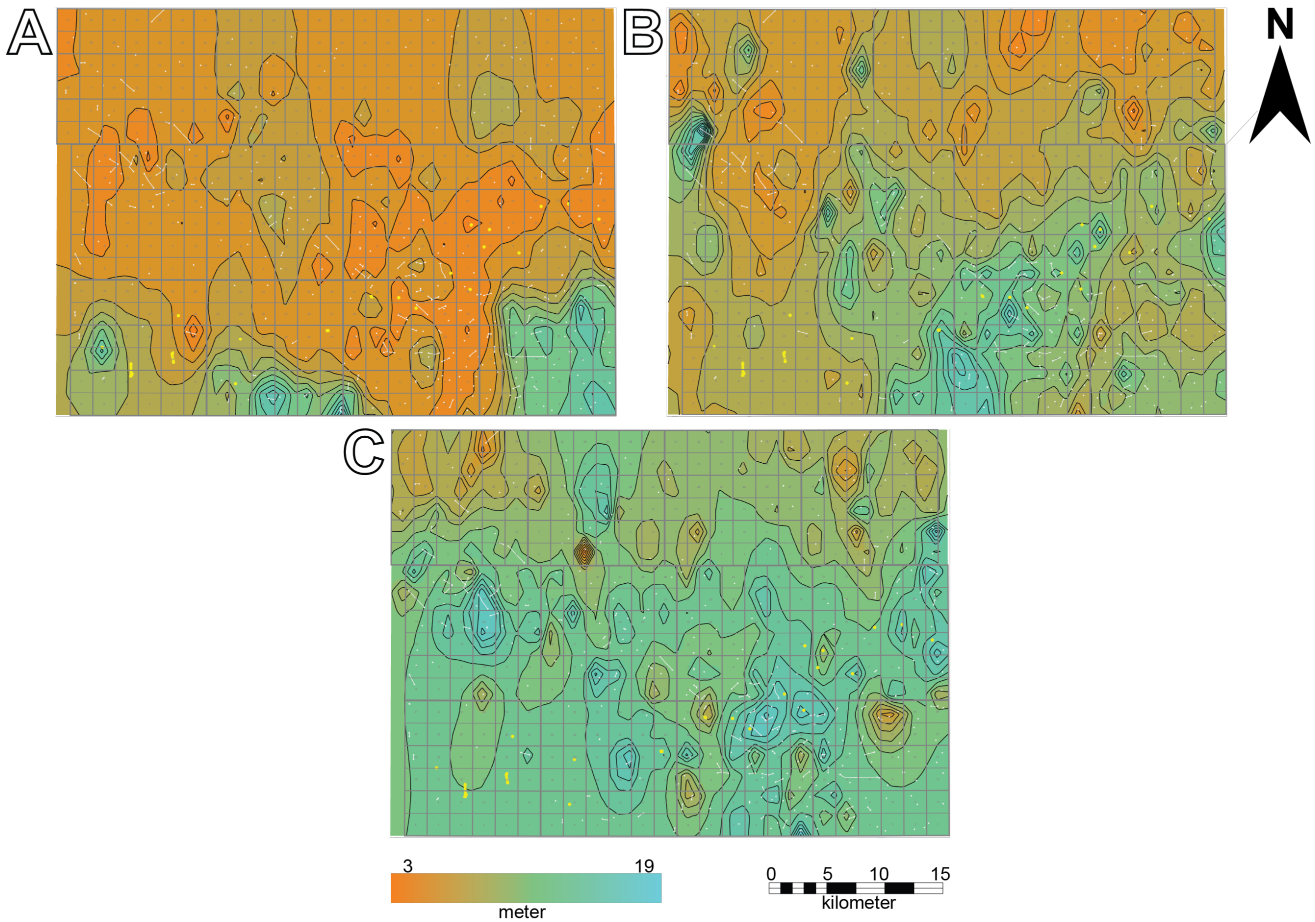

Figure 2.18. Isopach maps of the Falher F shoreface bodies deposited during parasequence: **A)** F_P1, **B)** F_P2, and **C)** F_P3 time.

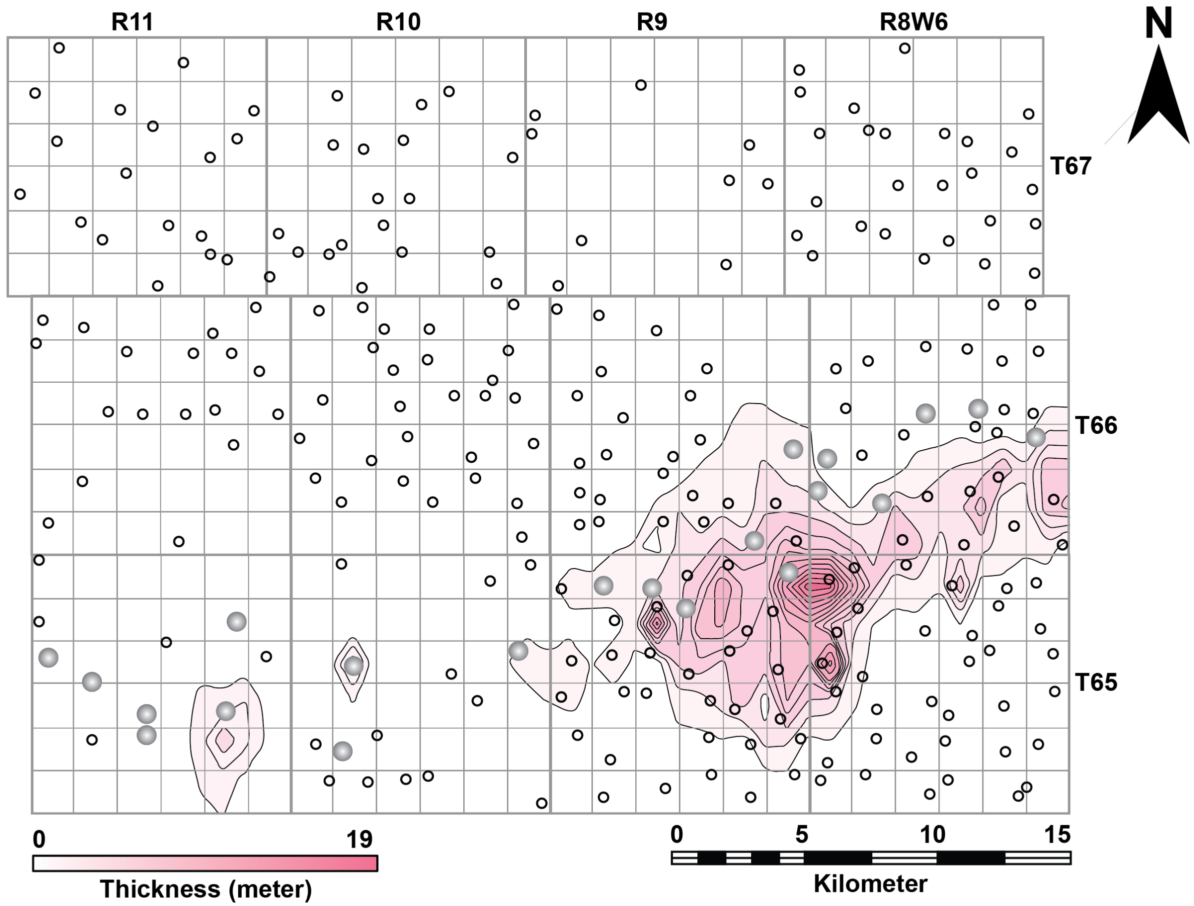

Figure 2.19. Isopach map of conglomerate bodies in parasequence F_P3. The orientation shows a WSW-ENE trend approximately N75ºE. Note the separate depocentres in the western and eastern area.

cross-bedded or crypto-bioturbated sandstone (facies 4 and 5 of FA2, respectively) (Figs. 2.4; 2.5), which was also observed by Nodwell and Hart (2006). When the Falher F is characterized by amalgamated non-marine components (FA3 and FA4) in palaeolandward direction, the tracing of the FS/WRS is uncertain (van Wagoner *et al.*, 1990).

In contrast with several other Falher submembers where the contact between the conglomerate-rich parasequence (F_P3) and the underlying sand-rich parasequence (F_P2) is characterized by regressive surface of marine erosion (RSME) (e.g. Armitage *et al.*, 2004; Caddel and Moslow, 2004), the base of Falher F conglomeratic parasequence is not characterized by a RSME. The F_P3/F_P2 contact is typified by an abrupt deepening thus marked as FS/WRS, as opposed to abrupt shallowing. However, an RSME appears at the base of sand-rich parasequence of F_P4 based on the geophysical well log appearance that shows sharp-based shoreface succession (Figs. 2.16; 2.17). Due to the absence of core for F_P4, however, this interpretation solely relies on the wireline log responses.

The landward equivalent of the RSME is a subaerial unconformity (SU) on top of parasequence F_P3. On wireline logs, this surface does not have distinguishable signatures. However, its presence is indicated in core by the presence of lithified palaeosols (well 100/03-20-065-11W6/00, Fig. 2.14C; well 100/15-09-065-11W6/00, Figs. 2.13, 2.12) (Wright and Marriott, 1993; Kraus, 1999).

Three cross-sections, which parallel the approximate depositional strike and dip during conglomerate deposition, are presented as Figure 2.15 through Figure 2.17. For this study, the MFS separating Falher F and the underlying Falher G was chosen as the datum. Picking the appropriate stratigraphic datum for the Falher F however requires careful attention, as there does not seem to be an ideal surface that fulfills every criterion of being synchronously flat, conformable, and easily traced on the geophysical well logs. This surface, chosen as it is interpreted to be a conformable, reasonably planar surface, is close to the study interval and thus eliminates issues associated with differential compaction and erosional condensation.

PALAEOGEOGRAPHIC RECONSTRUCTION

FP1 PROGRADATION: HIGHSTAND NORMAL REGRESSION FOLLOWING MAJOR TRANSGRESSION

Prior to the southward transgression that marked the onset of termination of Falher G, the study area was entirely characterized by fluvial aggradation and expansion of the coastal plain. This can be observed on gamma ray and sonic logs from several wells that display thin (<1 m) coal beds below the MFS contact between the Falher F and G. With continuing rise of relative sea level that outpaced sediment input, the study area was subaqueously inundated.

The earliest progradation of the Falher F had its onset when the rate of sedimentation surpassed the relative sea level rise. When the palaeoshoreline reached its southernmost position prior to that progradation, the MFS was recorded. The initial palaeoshoreline, where FP1 was first deposited, may have occurred outside the study area, as indicated by the geophysical log patterns of FP1 in southernmost positions of T65. In eastern locations, the initial deposit of Falher F is represented by funnel-shaped geometries of relatively low gamma ray API, indicating possible coarsening-upward sandstone strata (well 100/06-08-065-10W6/00, Fig. 2.17). This pattern is continuous throughout the entire southern limit of study area, in spite of changes into higher gamma ray API towards the westernmost area (well 100/08-05-065-08W6/00, Fig. 2.16; well 100/15-09-065-11W6/00, Fig. 2.15). However, the funnel trend is maintained. This implies that the eastern portion of the study area records deposition of probable sand-rich, mud-poor units (i.e. facies 3 to 5, FA2) while the western portion was likely characterized by more argillaceous units (i.e. facies 1 to 2, FA1), possibly due to the deeper palaeobathymetry at that time (Fig. 2.20A). Shoreface deposits of FP1 is interpreted to have prograded until approximately

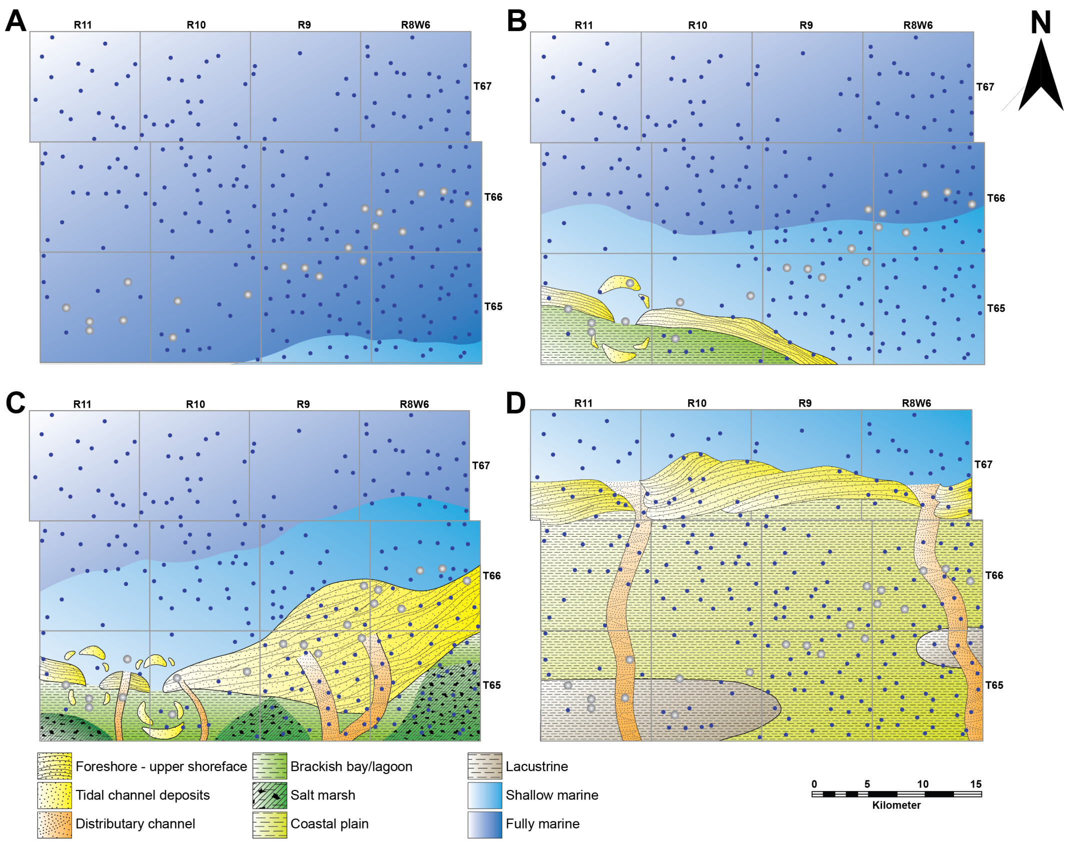

Figure 2.20. Palaeogeographic reconstruction during F_P1 through F_P4 time. **A)** During the F_P1 progradation, the study area records only the F_P1 fully marine succession. **B)** During the F_P2 progradation, a barrier configuration protecting an embayment was formed. This embayment may have been connected with a fluvial source southward as the trace fossils found in the deposits exhibit salinity-induced physico-chemical stress. An inlet was formed, connecting the bay with the fully marine realm. **C)** A re-orientation of palaeoshoreline during the F_P3 deposition occurred, likely propelled by the major fluvial sources to the east. The barrier configuration is maintained. The advent of palaeoshoreline to T66 where a topographic feature existed had triggered the deceleration of progradation, enabling gravels to accumulate (Nodwell and Hart, 2006). **D)** Base level fall during early F_P4 occurred following the highstand, and major fluvial channels were incising into the previous shoreline of F_P3.

the northern limit of T66, indicating a progradation of minimum 20 km in the study area.

FP2 PROGRADATION: TRANSGRESSION FOLLOWED BY CONTINUATION OF NORMAL REGRESSION

At the culmination of F_P1 progradation, sediment input that was exceeded by the rise of relative sea level resulted in a marine transgression and landward shift in the position of the shoreline. The final position of the palaeoshoreline during this transgression occurred at approximately T65, R11W6 and further southward. Wireline logs responses indicate notable rightward kicks of the gamma ray profiles on top of F_P1, which indicate the presence of transgressive shale of initial F_P2 deposits. Flooding surface (FS1) was recorded at the base of the transgressive unit.

Depositional strike of the F_P2 palaeoshoreline was oriented approximately WNW-ESE (Fig. 2.20B), as indicated by F_P2 core in southwestern study area and wireline log responses where cores are absent. Core from well 100/15-09-065-11W6/00 (Figs. 2.14, 2.13) and 100/07-16-065-11W6/02 (Appendix I) preserve the uppermost interval of F_P2, which indicate brackish bay setting (facies 11, FA3). During this interval, a barrier configuration had emerged and separated the enclosed brackish body of water from the fully marine realm. The possible presence of the associated inlet that acted as a conduit for sediment into the bay, is illustrated by high-angle cross-bedded, minimally bioturbated sandstone in core 100/07-14-065-11W6/02 (Fig. 2.9).

The formation of a barrier system during regional progradational conditions suggests abundant sediment supply, coupled with the possibly slow rise or stillstand of relative sea level in a wave-dominated setting. Such barriers may have formed due to several possible mechanisms. Firstly, there may have been an embayed coastline wherein longshore sediment transport formed a spit due to a reduction in wave energy in the more protected embayment (Davis and Fitzgerald, 2004). If sediment supply was not reduced, the spit would have grown across the embayment resulting in a barrier coast. Secondly, the abundant sediment supply remained high resulting in a series of prograding beach ridges that developed as the landward margin subsided (Davis and Fitzgerald, 2004). Any mechanism was possible, and sediments were sourced from both the young cordillera to the west and the North American main to the east through both fluvial systems and longshore drift via wave- and storm-induced currents.

The FP2 shoreline prograded at least as far north as the central part of T66 as evidenced from core in well 100/02-21-066-8W6/00 that preserved the furthest north FP2 upper shoreface succession observed in this study (Appendix I). Deeper shoreface deposits (FA1) occurred further north outside of the study area (Figs. 2.18B; 2.16, 2.17).

FP3 PROGRADATION: TRANSGRESSION FOLLOWED BY CONTINUATION OF NORMAL REGRESSION AND ACCUMULATION OF CONGLOMERATE BEDS

Similar to the onset of FP2 accumulation, another series of transgression had put the previous progradation to stop and FS2 was recorded at the limit of regression. This abrupt deepening which superimposed on parasequence FP2 is observed on core as units of FA1 capping those of FA2 (e.g. well 100/03-33-065-09W6/00, 100/05-32-065-09W6, 100/06-20-065-10W6/00, 100/08-02-066-09W6/00, 100/14-24-065-11W6/00; Figs. 2.4; 2.5; Appendix I) which belong to FP2 and FP3, respectively. Upon gradual return to normal regression as the sedimentation rate outpaced the relative rise of sea level, coarser materials began to fill out the basin.

As mentioned earlier, parasequence FP3 is characterized by conglomerate-bearing strata that grade laterally into their sandstone-dominated successions (Fig. 2.15). Those conglomerate beds accumulated following an ENE-WSW trend that is primarily constrained along T65-66, R8-9W6 in the study area (Fig. 2.19; 2.20C). The isopach map of FP3 conglomerate bodies suggests that there are three discrete sites where conglomerate beds accumulated (Fig. 2.19). Generally, they diminished along strike to the southwest, where the two isolated depocentres occur. These depocentres, both of which are cored (wells 100/06-20-065-10W6/00 and 100/07-14-065-11W6/02; Figs. 2.5 and 2.9) display more poorly sorted conglomerate than the thickest conglomerate accumulation in the east (e.g. well 100/10-36-065-09W6/00; Fig. 2.10). These lithologies are typical of distributary channels (facies 7, FA2), whereas the major conglomerate depocentre exhibits the evidence of predominant shoreface and foreshore conglomerate (facies 8 and 9, FA2) (Fig. 2.10). Conglomerate beds attributed to distributary channels are also encountered in well 100/13-27-065-09W6/00 (Appendix I). This implies that each discrete conglomerate body is associated with its own direct landward source and that longshore transport sourced from point source mouthbar deposits was limited in local reworking and transport. Based on the size and thickness, it is suggested that the distributary channels on the western side of the study area were relatively of lower energy compared with the main conduit on the eastern side.

Many previous Falher workers have linked the accumulation of gravels in single parasequences to changes primarily in sourcing and transport mechanism (Arnott, 1993; Rouble and Walker, 1997; Armitage *et al.*, 2004; Caddel and Moslow, 2004). However, Clifton (2003) also suggested that the seafloor geometry influenced the concentration of shallow marine pebbles. In light of this mechanism, the trapping of nearshore conglomerate bodies in the Falher F was interpreted by Nodwell and Hart (2006) to have been largely due to the presence of a "topographic step" that extends into the T65-T66, R11-R10W6 where the thickest conglomerate beds are lying on. According to their observation, the Falher F palaeoshoreline did not reach this position until the parasequence F_P3 depositional time; thus, the gravels were accumulated only above this higher-gradient structure as compared to the surrounding palaeoseafloor.

A differing argument was brought by Meloche (2011) who proposed that the conglomerate accumulation was due to the tectonic tilting across the Snowbird Tectonic Zone, southeast of the study area (Fig. 2.1), which was responsible for the headward erosion and more extensive chert gravels incorporation at the fluvial source points during highstand. Plint and Walker

(1987) also preferred the tectonic warping and uplift to the west of this study area to have been the major control for shoreface conglomerate concentration of the Cardium Formation in Kakwa Area. Regardless of the different approaches, these workers agreed that the relative sea-level fall was not accountable for the thick gravel emplacement.

Besides the absence of abrupt shallowing between the top of sand-rich parasequence FP2 and conglomerate-rich FP3, the disfavor of interpreting FP3 conglomerate-rich interval as a forced regressive succession is also based on the similarities on pebble sizes and composition on FP3 and pebbly localities of the underlying FP2. This was also considered by Schmidt and Pemberton (2004) in their analyses of the Notikewin conglomerate unit that incorporates this study area. This compositional resemblance between conglomerate-rich parasequence FP3 and sand-rich parasequence FP2 suggests that the fluvial source or transport did not become anomalously gravel-enriched during FP3 deposition, since the gravels had been introduced into the basin during the previous progradational cycle of FP2. Therefore, base level lowering likely did not occur during FP3 time. The presence of fluvial incisions prior to or during FP3 deposition that otherwise would have existed as the result of relative sea level fall is also not observed in the study area.

South of the FP3 shoreline, core indicating brackish bay (FA3) are present (e.g. well 100/03-20-065-11W6/00, 100/07-16-065-11W6/02, and 100/15-09-065-11W6/00; Appendix I). This suggests that the conglomeratic bodies had possibly acted as a barrier that protected the embayment, maintaining the barrier configuration of FP2.

FP4 PROGRADATION: BASE LEVEL FALL (FALLING STAGE SYSTEMS TRACT) FOLLOWED BY BASE LEVEL RISE (LOWSTAND SYSTEMS TRACT)

The FP3 progradation in the study area was terminated by a rapid drop in relative sea level that resulted in an abrupt shift of the shoreline to the southern portion of T67 (Fig. 2.20D). Due to the lowering of relative sea level and thus a northern shift of fair-weather wave base, the uppermost deposits of FP3 were eroded into as sediments of F_P4 were deposited. This erosive base of F_P4 is interpreted as a regressive surface of marine erosion (RSME) (van Wagoner *et al.*, 1990), where a sharp-based shoreface is deposited erosionally on older shoreface units. On the cross-sections, this is observed as a notable kick of lower gamma ray values right above this surface on individual well logs (Figs. 2.16, 2.17). This erosional contact resulted in the juxtaposition of sediments deposited in a proximal, sand-bearing shoreface environment directly on top of sediments deposited in a more distal, mud-dominated offshore environments.

During this falling stage systems tract, the fluvial system landward of the palaeoshoreline was perhaps subjected to fluvial incision instead of fluvial bypass, which can be attributed to the base level drop below the "topographic step" of parasequence F_P3 palaeoshoreline (Nodwell and Hart, 2006) and the resulting gradient adjustment of downstream valley. The recognition of either fluvial bypass or incision solely based on well log data is quite challenging. However, assuming that exposed segments of former seascapes were steeper than the fluvial graded profile, fluvial incision would have occurred at the downstream termination of the steep exposure and propagates upstream (Schumm, 1993; Posamentier, 2001; Catuneanu, 2006). This is reasonable, given that the basinward limit of F_P3 conglomerate beds lies at the end of major topographic break attributed to the structural reef of Gold Creek reef trend (Nodwell and Hart, 2006). This is also supported by the well log responses (Fig. 2.17) where the inferred incised channel fills in well 100/10-14-066-11W6/00 and 100/06-23-066-11W6/00 exhibit no similarities with adjacent surrounding wells; thus, being unrelated to juxtaposed facies (Posamentier and Allen, 1999).

Additionally, in areas where two adjacent thick conglomerate wells seem to be separated by anomalously very thin to none conglomerate strata in between (Fig. 2.19), it may be due to post-depositional erosion of the pre-existing conglomerate bodies by a younger (F_P4-equivalent) channel. This is particularly applicable to mud-filled channels, which are characterized by high radioactivity values, which may have filled during the subsequent transgression. An example of this occurs in the well 100/09-08-067-08W6/00 (Fig. 2.16) which is bounded laterally by sand-bearing coarsening-upward F_P3 succession, but exhibits a series of mud-dominated fining-upwards units, implying a channel fill.

Regions where brackish bays had previously developed became non-depositional or erosional site and an unconformity was formed due to this sedimentary bypass. Thus, a subaerial unconformity (SU) was developed landward of the earliest F_P4 palaeoshoreline. This interval of non-deposition allowed the formation of the palaeosols, which were cored in wells 100/15-09-065-11W6/00 (Fig. 2.13) and 100/03-20-065-11W6/00 (Fig. 2.14C), at a level that was not recovered in any other core in the study area. Of note, no substrate-controlled ichnofacies were observed at the contact on the uppermost portion of the F_P3.

At the later stage of F_P4, base level likely rose again; thus, the rise in relative sea level returned the progradation back into normal regression. This process was likely accompanied by the onlap of newly-deposited non-marine deposits onto the region affected by the subaerial unconformity (i.e. fluvial onlap; Mitchum Jr., 1977) starting at the shoreline position and continuing upstream. The upper limit of this lowstand systems tract is interpreted to be the <1 m coal seam landward of F_P4, which developed rather poorly, possibly due to the high rates of clastic influx and low rates of space creation typical of lowstand system (Catuneanu, 2006). The formation of coal possibly terminated as the increase in accommodation space outpaced peat accumulation rates and the brackish bay drowned the peat marsh (e.g. Wadsworth *et al.*, 2003).

CONCLUSION

The lower Albian Falher F submember of the Spirit River Formation in the Wapiti area of the Deep Basin was deposited as a series of prograding sand- and conglomerate-bearing shoreface overlain by marginal- to non-marine mud-dominated deposits. Along the depositional strike, the strandplain morphs into their wave-dominated deltaic equivalents. Thirteen facies are recognized and grouped into four facies associations, which reflect fully marine or distal delta front to proximal prodelta (FA1), shallow marine or proximal delta front (FA2), marginal marine or lower delta plain (FA3), and terrestrial or upper delta plain (FA4) environment.

The palaeogeographic reconstruction of the Falher F presented here was built upon sequence stratigraphic framework that enabled the division of the Falher F into four parasequences in the study area, assigned F_P1 through F_P4 informally. The base of Falher F is a maximum flooding surface (MFS) that marked the southernmost transgression of the underlying Falher G and onset of progradation of F_P1. The base level was rising during the deposition of F_P1 to F_P3, and each of these deposits was deposited as a normal regressive highstand systems tract. Each of those parasequences was bounded by designated flooding surface/transgressive surface of erosion (FS1/WRS1 and FS2/WRS2) where abrupt deepening of the next parasequence occurred right above the older unit. Following the F_P3 progradation, the base level began to fall during F_P4 deposition, causing F_P4 to prograde in a forced regressive manner (falling-stage systems tract). A regressive surface of marine erosion (RSME) was emplaced between F_P4 and F_P3 clinoform, and there is a disconformity observed as an abrupt shallowing between the youngest F_P3 strata and the overlying F_P4 deposit. Landward of the RSME, a subaerial conformity (SU) was developed concurrently. Following the outpace of sediment supplies by the resulted accommodation, the base level rose again. Thus, the later stage of F_P4 emerged as a normal regressive lowstand systems tract.

The depositional model and palaeogeographic reconstruction of the Falher F will be required to further explain variations in mineral occurrences within the tight sandstone units. Spatial and temporal changes in depositional style as the fluvial profile undergoes perpetual adjustment throughout different systems tract will likely determine the compositional and textural discrepancies between different sand bodies in the palaeobasin. Thereby, this study will present the fundamental to which the further study on the Falher F microscale properties is based on.

CHAPTER 3: DETAILED PETROGRAPHY OF THE FALHER F TIGHT SANDSTONE: INSIGHTS ON THE CHERT-CONTROLLED DRILLABILITY FAIRWAY AND HYDROCARBON STORABILITY

INTRODUCTION

The Western Canada Foreland Basin has actively been the site where extensive studies on tight sandstone reservoirs are taking place, particularly in the Deep Basin of west-central Alberta (Moslow and Zaitlin, 2008; Hayes, 2010; Fockler and McKenzie, 2016). The Deep Basin also hosts ample highly porous and permeable coarse-grained units, which were previously explored and exploited as vertically-drilled conventional targets (e.g. the Albian Cadotte Member, Albian Viking Formation, and Barremian Cadomin Formation; Zaitlin and Moslow, 2006). These lucrative targets, however, have experienced progressive hydrocarbon depletion over the past few decades. With new drilling and exploitation technology, those units currently have new economic potential in previously untapped tighter unconventional intervals. Among units that are still actively explored today is the lower Albian Spirit River Formation, particularly sandstone horizons in the Wilrich and Falher members.

Exploration and exploitation of tight reservoirs have resulted in new challenges that likely have not been encountered before in the conventional reservoirs. Important challenges include moderate porosity and low permeability. Within the sandstone of the Falher Member, porosity commonly ranges from 0 to less than 10%, whereas permeability ranges from 0.001 to 0.5 md (Cant and Ethier, 1984). Several causes have been briefly reported (Youn, 1981; Cant, 1983b; Cant and Ethier, 1984; Harris, 2014; Newitt, 2017), all of which correspond to its textural and compositional variety. In this study, a detailed examination of factors affecting the porosity of Falher will be presented.

Another challenge that is particularly significant for the Falher Member is the horizontal drillability (i.e. ease of horizontal penetration) of the sandstone (Zonneveld, pers. comm.). Drillability or penetrability can be defined as the resistance of rocks to penetration by drilling technique, as measured by the rate of penetration. Among many factors that may be involved, one that gives the most direct impact is the petrographic property. Within the Falher sandstone, detrital chert is a major detrital component, apart from quartz. It has been widely reported that chert regularly causes drilling problems due to its ultra-durability that is higher than regular, monocrystalline quartz (Mensa-Wilmot *et al.*, 1999; Mensa-Wilmot and Fear, 2001; Olson *et al.*, 2008). This issue especially persists when horizontal wells are used to penetrate the low-permeability beds of tight reservoirs. The varying degree of sandstone penetrability across relatively small lateral extent requires frequent changes of drilling bits, which are very unfavourable both cost- and time-wise. Therefore, it is important to understand how compositional changes develop both laterally and vertically.

Chapter 2 addressed the sedimentology, stratigraphy, ichnology, and palaeogeography of the Falher F in the Wapiti area. The current chapter constitutes a petrographic study that provides a micro-scale evaluation of the Falher F tight sandstone and an assessment of the usefulness of petrography in assessing reservoir attributes, based on the framework provided in the previous chapter. This includes compositionally controlled sandstone drillability and hydrocarbon storability in the Falher F sandstone intervals. This study may thus serve as a reference for future exploration in the Falher tight gas reservoir, or its analogues that are widespread across Western Canada Foreland Basin.

GEOLOGICAL SETTING AND PREVIOUS STUDIES

The lower Albian Spirit River Formation in the Deep Basin of west-central Alberta was the initial, and one of the most prolific conglomeratic reservoirs in the Deep Basin during the 1990's and 2000's. The Deep Basin preserves a westward-thickening foredeep within the Western Canada Sedimentary Basin (WCSB) foreland basin in the deepest part in the Alberta syncline, east of the Foothills overthrust belt (Masters, 1979; 1984). Up until the late 20th century, studies were focused primarily on high-permeability conglomerate reservoirs hosted within the younger members of the Spirit River, which are the Notikewin and Falher members. When multistage hydraulic fracturing and horizontal wells became commercially viable during the 2000's, companies gradually shifted their interest into the more widely distributed, conglomerate-encasing tight sandstone intervals. This brings further exploration to low-permeability sandstone units in both the Notikewin and Falher members, as well as the older, fine-grained sandstone units in the Wilrich Member (the Falher G up to O of Zonneveld and Moslow, 2004 as well as Newitt, 2017). The focus of this study is the Falher F submember (Fig. 3.1).

The lower Albian Falher Member was deposited as prograding deltaic to shoreface deposits, northward to the Boreal Sea (Cretaceous Epeiric Seaway) following the period of marine retreat upon termination of the underlying marine Wilrich Member deposition (Smith *et al.*, 1984). Each cycle of Falher submembers consists of coarsening upward sandstone and conglomerate shoreface deposits followed by muddier deposits of a more terrestrial origin. Detailed studies related to each submember have been focused on their sedimentology and stratigraphy (Arnott, 1993; Casas and Walker, 1997; Rouble and Walker, 1997; Armitage *et al.*, 2004; Caddel and Moslow, 2004; Zonneveld and Moslow, 2004; Nodwell and Hart, 2006; Hoffman, 2006; DesRoches, 2008; Newitt, 2017), whereas detailed microscale works are available in limited studies (Cant and Ethier, 1984; Tilley and Longstaffe, 1989; Newitt, 2017). This study attempts to fill this knowledge gap by investigating compositional attributes of the Falher F that contribute to its porosity and chert-controlled drillability.

Petrographic descriptions of the Falher unit were first made available by Youn (1981) and Cant (1983b) on coarser sand units resembling the conglomerate bodies. In general, these authors agreed upon several key points, which are the presence of quartz overgrowths, carbonate cements, and authigenic clays, all of which disrupt the porosity. Cant and Ethier (1984) further recognized the impact

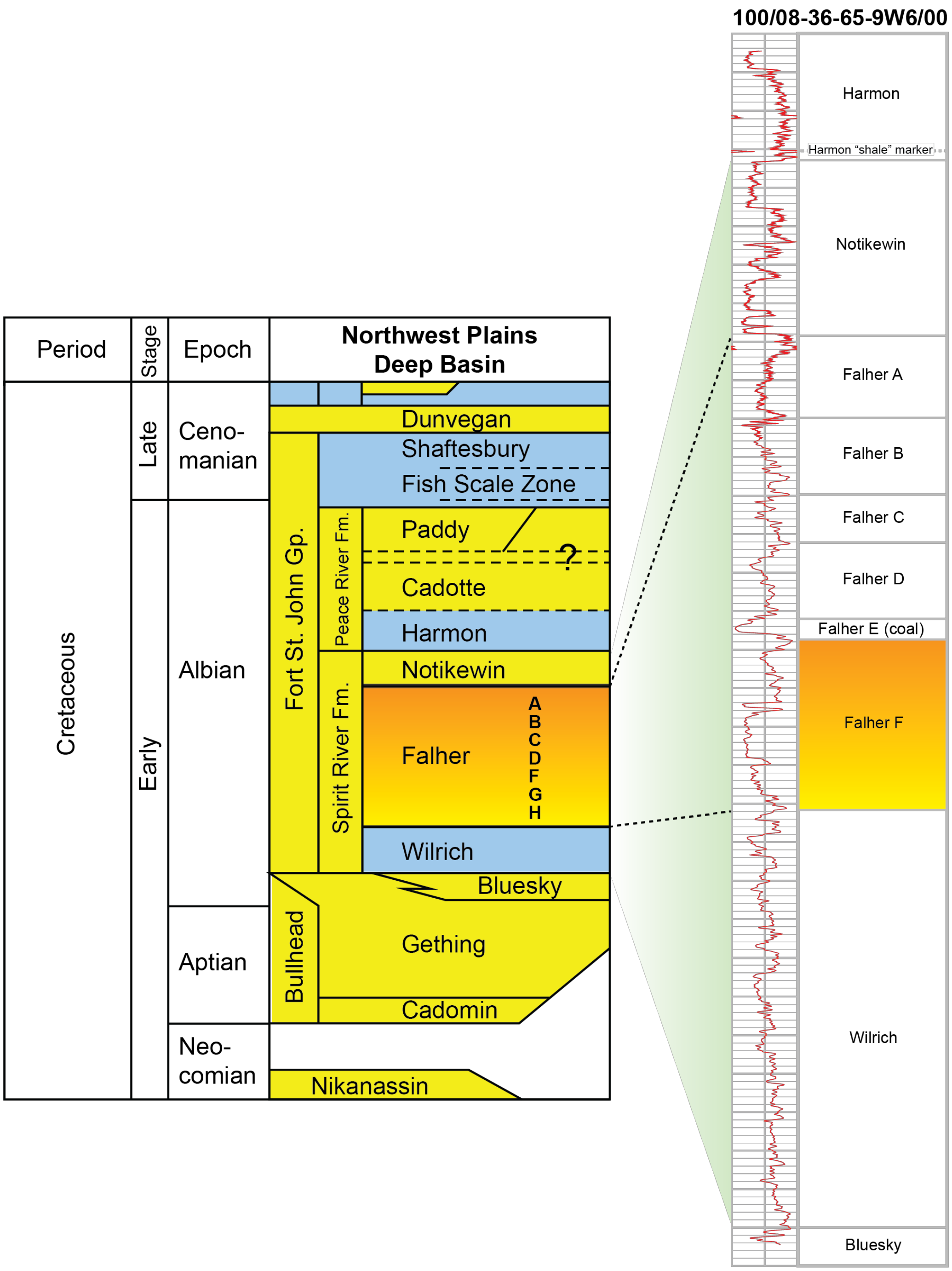

Figure 3.1. Lithostratigraphic nomenclature for Cretaceous units in the northwestern Deep Basin, Alberta (modified from Zaitlin and Moslow, 2006). An example of gamma ray log response on the Spirit River Formation exhibits an overall coarsening-upward trend.

of rock fragment pseudomatrix to the reduced porosity. In his regional palaeogeographic reconstruction, Jackson (1984) interpreted the presence of chert within the Falher Member as implying western provenance from the Cordillera. Leckie (1986a) studied the Gates Formation (Spirit River-equivalent) in northeast British Columbia and found that most sandstone is chert arenite, with some feldspathic arenite. Tilley and Longstaffe (1989) utilized isotope analyses to define the paragenetic sequence within the Falher Member in a regional scale that included this study area.

Decades later, studies focused on sandstone petrography of the Spirit River Formation emerged. Moslow and Zonneveld (2012) reported the predominance of feldspathic litharenite to lithic arkose in the outcrop of the Falher G (Wilrich-equivalent), which is quite unique compared to other Falher units. Harris (2014) found that the primary porosity is preserved better in the Falher quartz arenite, whereas Falher litharenite has a better developed secondary porosity due to the leaching of abundant chert. Newitt and Pedersen (2016) interpreted that the highly progradational versus aggradational stacking pattern in the basal Falher (Wilrich-equivalent) and middle Falher (F to C), respectively, has contributed much in the diagenetic evolution of sandstone from both types. Corresponding work by Newitt (2017) interpreted that the former may have caused the formation of early ferroan dolomite cement, which prevented the compaction of potential pseudomatrix in a lower Spirit River sandstone unit he referred to as the Falher O.

Continuing prior studies, this work emphasizes the relationships of the detrital framework grains and authigenic minerals within the Falher F that may affect its reservoir quality. The diagenetic evolution within the unit is discussed here to help explain the differences between various Falher F sandstone units in the study area.

Chapter 2 provided the framework on the Falher F stratigraphy, focusing in the Wapiti area. The Falher F has been interpreted to consist of four facies associations (FA1 to FA4) deposited in four parasequences (F_P1 to F_P4). Preserved depositional environments range from lower shoreface to fluvial channel and all environments in between. The palaeogeographic framework of the Falher F is also presented in Chapter 2, highlighting palaeoshoreline positions and the lateral distribution of depositional environments within each parasequence. Therefore, the petrographic approach herein is based on interpretations provided in the previous chapter.

DATABASE AND METHODS

This study is conducted in the portion of the Wapiti area (T65-67, R8-11W6M) within the Deep Basin of northwestern Alberta (Fig. 3.2). Sixty-eight thin sections representing 50 sampling points from cores of 20 wells penetrating the Falher F submember have been collected and studied. The depth of these samples ranges from 2,460 to 3,200 m (Table 3.1). Based on observations in Chapter 2, they represent Falher F parasequence F_P2 through F_P3 and the transgressive succession, which were deposited in lower shoreface to fluvial channel (Table 3.2).

All slides of thin sections were impregnated with blue epoxy. Fifty thin sections, each represent all 50 data points, were half-stained using the "double carbonate stain" composed of alizarin red S and potassium ferrocyanide. The remaining 18 slides were also half-stained using the "K-feldspar stain" composed of sodium cobaltinitrite.

The 50 double carbonate-stained thin sections were analyzed using the traditional point counting method. JMicroVision software was used to point-count all samples. As many as 300 points from each sample generated using the recursive grid method were labeled according to whether they were detrital framework grains, matrix (if any), or interstitial cement. To ensure even distribution of visible minerals during the point counting, samples that are lower very fine sand- to lower fine sand-sized were studied under 40x magnification,

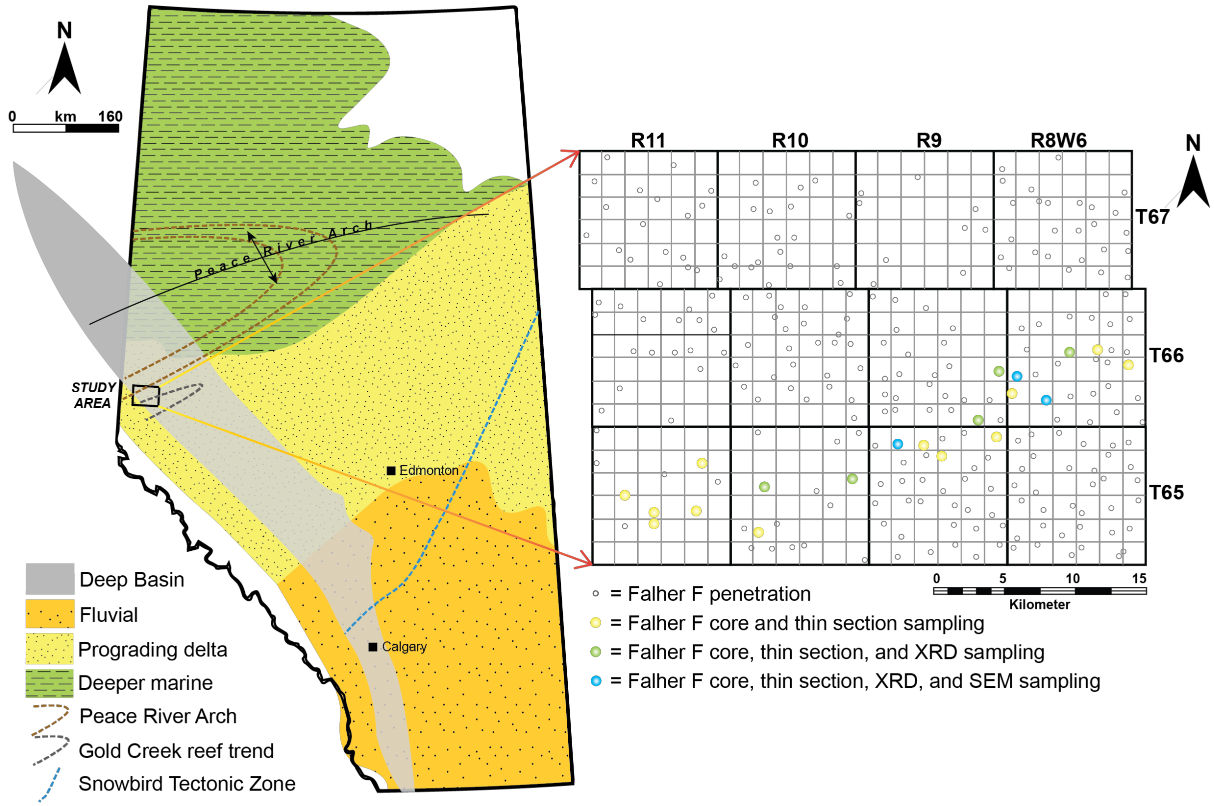

Figure 3.2. Map of Alberta showing the location of the study area and the distribution of wells used for this study. Regional palaeogeographic setting during the Upper Mannville Group deposition, which includes the Spirit River Formation is displayed. The study area was a site for prograding delta with the fluvial source being transported from the south to the deeper marine northward. It is located in the vicinity of Peace River Arch and the Gold Creek reef as a part of a subsiding section, with the edge of the deformed belt indicated. Modified from Jackson (1984), Leckie and Smith (1992), Burwash *et al.* (1994), Switzer *et al.* (1994), Nodwell and Hart (2006).

Table 3.1. Summary of the petrographic analysis results of the studied tight sandstone. Core analyses are taken from publicly available data in GeoScout database as per June 2018. For abbreviations, refer to List of Abbreviations.

**Q = monocrystalline quartz, polycrystalline quartz, and chalcedony; C = chert and quartzite; RF = rock fragments including dolomite clasts*

Well	Depth	Texture				(see Chapter 2 for details)		Composition (raw)			Composition (normalized)			Core Analysis	
		Grain Size	Grain Shape	Sorting	Framework	Depositional Environment	Stratigraphic Succession	Q*	C*	RF*	Q*	C*	RF*	Permeability (Kmax) (md)	Porosity (frac)
1-8-66-8W6	2579.4	u. f. - u. m.	a - sr	w	o	Up. S.f.	FP3	41.01	46.33	6.67	43.62	49.28	7.09	0.86	5.4%
1-8-66-8W6	2585.2	l. - u. v. f.	a - sr	m	o	Mid. S.f.	FP2	21.34	24.34	27.99	28.97	33.04	37.99	0.04	3.2%
10-36-65-9W6	2647.0	l. m.	a - r	w	c	FS	FP3	37.67	43.33	8.33	42.17	48.51	9.32	8.67	8.6%
10-36-65-9W6	2652.3	l. - u. f.	a - sa	w	c	Up. S.f.	FP3	38.66	34.67	15.67	43.44	38.96	17.61	2.13	7.0%
11-13-66-8W6	2563.0	l. f.	a - sr	w	c	Up. S.f.	FP3	46.00	31.99	12.66	50.74	35.29	13.97	n/a	n/a
13-27-65-9W6	2645.6	u. v. f.	a - sr	w	c	Up. S.f.	FP3	33.34	30.00	21.00	39.53	35.57	24.90	0.87	1.6%
13-27-65-9W6	2646.0	l. f.	sa - sr	w	o	Up. S.f.	FP3	23.00	27.00	20.33	32.70	38.39	28.91	0.87	1.6%
13-27-65-9W6	2647.5	l. f.	a - sa	w	c	Up. S.f.	FP3	38.67	21.67	22.00	46.96	26.32	26.72	0.87	1.6%
13-27-65-9W6	2650.8	u. f.	a - sr	w	c	Up. S.f.	FP3	41.33	34.67	20.67	42.75	35.86	21.38	0.20	2.1%
14-24-65-10W6	2776.5	u. v. f.	a - sr	w	c	Low. S.f.	FP3	35.33	32.66	20.00	40.15	37.12	22.73	0.04	2.4%
14-24-65-10W6	2777.5	u. v. f.	a - sr	w	c	Low. S.f.	FP3	26.00	33.66	27.66	29.78	38.55	31.68	0.36	2.2%
15-9-65-11W6	3024.0	u. v. f. - l. f.	a - sr	w	c	Up. S.f.	FP3	39.00	32.67	11.00	47.18	39.52	13.31	n/a	n/a
2-21-66-8W6	2513.8	u. v. f. - l. f.	a - sr	w	c	Est.	T	36.34	41.34	15.33	39.07	44.45	16.48	0.06	3.1%
2-21-66-8W6	2514.6	u. v. f. - l. f.	a - sr	w	c	Est.	T	34.00	37.66	7.34	43.04	47.67	9.29	0.09	6.8%

3-18-66-8W6	2468.6	u. v. f.	sa - r	w	c	Up. S.f.	FP3	38.00	43.67	8.00	42.38	48.70	8.92	0.07	2.8%
3-18-66-8W6	2480.4	u. f.	sa - sr	m	c	Mid. S.f.	FP2	28.33	35.33	7.67	39.72	49.53	10.75	0.94	4.3%
3-18-66-8W6	2481.6	u. v. f.	a - sa	w	c	Mid. S.f.	FP2	35.67	39.00	22.67	36.64	40.07	23.29	0.14	4.7%
3-18-66-8W6	2483.5	u. v. f. - u. f.	a - sa	m	c	Low. S.f.	FP2	38.01	31.34	9.33	48.31	39.83	11.86	n/a	n/a
3-33-65-9W6	2734.3	u. v. f.	a - sr	w	c	Mid. S.f.	FP3	29.00	29.67	29.00	33.08	33.84	33.08	0.06	3.3%
3-33-65-9W6	2740.4	l. - u. v. f.	a - sr	w	c	Up. S.f.	FP2	36.66	32.67	16.67	42.63	37.99	19.38	0.04	2.8%
5-32-65-9W6	2908.1	u. v. f. - u. f.	a - sr	w	c	Up. S.f.	FP3	28.67	37.33	26.66	30.94	40.29	28.77	0.06	3.3%
5-32-65-9W6	2911.3	l. f.	sa - sr	w	c	Up. S.f.	FP3	42.67	21.66	12.00	55.90	28.38	15.72	0.13	6.8%
5-32-65-9W6	2914.1	u. v. f.	a - sr	w	c	Low. S.f.	FP3	42.67	28.00	21.34	46.38	30.43	23.19	0.05	4.2%
5-7-66-8W6	2535.1	u. v. f. - u. f.	a - sr	m	c	Up. S.f.	FP3	39.33	45.00	9.00	42.14	48.22	9.64	0.60	4.3%
6-20-65-10W6	2909.4	u. f.	sa - sr	w	c	FS	FP3	46.67	22.67	2.67	64.81	31.48	3.71	0.72	5.2%
6-20-65-10W6	2917.3	l. f.	a - sr	w	c	Low. S.f.	FP3	22.00	38.34	19.00	27.73	48.32	23.95	n/a	1.4%
6-20-65-10W6	2920.7	l. - u. f.	sa - sr	w	c	Up. S.f.	FP2	34.67	34.33	24.34	37.14	36.78	26.08	0.27	3.1%
6-20-65-10W6	2922.0	u. f.	a - sa	w	c	Up. S.f.	FP2	38.00	33.33	14.66	44.19	38.76	17.05	0.87	5.3%
6-8-65-10W6	2961.6	u. v. f. - u. f.	a - r	m	o	Est.	T	17.00	15.00	27.00	28.81	25.42	45.76	n/a	0.8%
6-8-65-10W6	2963.3	l. v. f.	a - sa	m	o	Est.	T	27.00	9.67	36.67	36.81	13.19	50.00	n/a	n/a
6-8-65-10W6	2963.9	u. f.	a - sr	v.w.	c	FS	FP3	56.00	20.34	7.67	66.66	24.21	9.13	0.51	7.3%
7-13-66-9W6	2517.5	l. f.	a - r	m	c	Up. S.f.	FP3	42.67	29.00	13.32	50.21	34.12	15.67	0.06	2.8%
7-13-66-9W6	2521.6	u. v. f.	a - sr	m	c	Mid. S.f.	FP2	33.00	36.00	16.33	38.67	42.19	19.14	0.01	4.7%
7-13-66-9W6	2524.1	l. f.	a - sa	m	c	Mid. S.f.	FP3	36.66	36.67	11.01	43.47	43.48	13.05	0.01	3.1%
7-13-66-9W6	2531.3	u. v. f. - u. f.	a - -r	p	c	Up. S.f.	FP2	35.34	25.33	21.67	42.92	30.76	26.32	0.05	4.7%
7-14-65-11W6	3168.3	l. f.	sa - r	w	c	FS	FP2	51.33	9.33	13.00	69.69	12.67	17.65	n/a	n/a
7-14-65-11W6	3175.9	u. f.	a - sr	w	c	Up. S.f.	FP2	52.34	12.33	13.00	67.39	15.87	16.74	n/a	n/a
7-16-65-11W6	3188.9	l. - u. f.	a - sr	w	o	Est.	T	19.34	33.00	11.33	30.38	51.83	17.79	n/a	n/a
7-16-65-11W6	3195.5	l. f.	a - sr	w	c	Up. S.f.	FP3	30.00	40.66	14.67	35.16	47.65	17.19	n/a	n/a

7-16-65-11W6	3199.1	u. v. f.	a - sr	w	c	Low. S.f.	F_P3	41.00	30.66	20.68	44.40	33.20	22.40	n/a	n/a
8-2-66-9W6	2568.5	l. v. f.	a - sr	m	c	Est.	T	23.00	25.33	10.00	39.43	43.43	17.14	0.23	6.7%
8-2-66-9W6	2571.0	u. f.	sr - r	v.w.	c	FS	F_P3	42.67	39.33	7.34	47.76	44.02	8.22	0.94	5.7%
8-2-66-9W6	2575.8	u. v. f. - l. f.	a - sr	w	c	Low. S.f.	F_P3	39.00	37.01	11.99	44.32	42.06	13.63	0.36	4.2%
8-2-66-9W6	2579.6	u. v. f.	a - sr	w	c	Up. S.f.	F_P2	42.00	26.34	19.33	47.91	30.04	22.05	0.09	5.2%
8-2-66-9W6	2579.8	l. f.	sa - sr	w	o	Up. S.f.	F_P2	32.66	34.00	17.67	38.73	40.32	20.95	0.21	7.0%
8-22-66-8W6	2575.8	u. f.	a - sr	p	o	Est.	T	25.67	23.33	31.66	31.82	28.92	39.25	n/a	n/a
8-22-66-8W6	2578.7	u. f.	a - -r	p	o	Est.	T	27.00	16.00	21.33	41.97	24.87	33.16	n/a	n/a
8-22-66-8W6	2581.5	l. f.	a - sr	w	c	Est.	T	16.66	48.33	16.67	20.40	59.18	20.41	n/a	n/a
8-22-66-8W6	2585.4	l. - u. v. f.	sa - -r	m	o	Est.	T	31.00	9.67	12.33	58.49	18.25	23.26	n/a	n/a
8-26-65-11W6	2884.7	l. - u. v. f.	a - sa	w	c	Fl. Ch.	T	25.67	42.33	13.99	31.31	51.63	17.06	n/a	n/a
Average								**35**	**31**	**17**	**42**	**37**	**20**	**0.63**	**4.1%**
Minimum								17	9	3	20	13	4	0.01	0.8%
Maximum								56	48	37	70	59	50	8.67	8.6%

Table 3.2. Facies associations identified within the study interval. Further details are available in Chapter 2.

Facies Association		Summary	Ichnofacies Expression	Depositional Settings
FA1	Storm-dominated shoreface and distal deltaic complex	Coarsening-upward succession of interstratified sandy mudstone gradually or abruptly changes upwards into hummocky- to swaley-cross stratified very fine-grained sandstone.	Moderately diverse archetypal *Cruziana* Ichnofacies	Above storm-weather wave base, below fair-weather wave base (i.e. offshore transition to middle shoreface in strandplain and wave-dominated delta settings)
FA2	Wave-dominated shoreface and proximal deltaic complex	Coarsening-upward succession of planar laminated to cross stratified fine-grained sandstone interbedded and interfingers with, as well as gradually or abruptly changes upwards into, massive to stratified conglomerate. Matrix-rich to matrix-supported, poorly-sorted, polymodal, organic-rich conglomerate gradually shifts upwards into clast-supported, well-sorted, bimodal to unimodal, chert-dominated conglomerate.	Moderately diverse proximal *Cruziana* to archetypal *Skolithos* Ichnofacies; *Macaronichnus segregatis* suite	Above fair-weather wave base, below high tide remarks (i.e. upper shoreface to foreshore in strandplain and wave-dominated delta settings)
FA3	Back barrier/brackish embayment and lower delta plain complex	Fining upward succession of massive to low angle-laminated, organic-rich sandstone abruptly overlain by interbedded massive to organic-rich mudstone, heterolithic sandy mudstone, and coal.	Impoverished suite of *Skolithos* and *Cruziana* Ichnofacies	Intertidal zone (i.e. backshore, estuarine or brackish bay, lagoon)
FA4	Coastal plain and upper delta plain complex	Interbedded mudstone and coal. Fining-upward succession of unburrowed planar-laminated sandstone.	N/A	Supratidal zone (i.e. lacustrine, marsh, swamp, fluvial channel, crevasse splay)

whereas samples that are up to upper fine sand-sized were observed under 20x magnification.

Additionally, X-ray Diffraction was performed on selected eight samples from seven wells (Table 3.3). Scanning Electron Microscope analysis was also carried out on two samples from two wells. Core porosity and permeability data were gathered from the GeoScout database that is available for public viewing as per June 2018.

GENERAL PETROGRAPHIC RESULTS

Petrography shows that the Falher F tight sandstone interval in the study area is composed of mature to submature, lower very fine- to upper fine-grained sandstone with minor localized thin beds of coarser grains. Sandstone samples were found to range between poorly and very well-sorted, although moderate- to well-sorted samples are the most common (Fig. 3.3A, B). All grains from angular to rounded occur. However, sub-angular to sub-rounded grains predominate among samples (Fig. 3.3C). They have open to closed framework, with the former usually due to the presence of authigenic overgrowth or other intergranular cements among the detrital framework (Fig. 3.3C; D). In sandstone with closed framework, grain contacts are mainly long and concavo-convex (Fig. 3.3E). Only in very few poorly- to moderately-sorted samples were the tangential contacts observed; whereas sutured contacts are quite uncommon (Fig. 3.3F). Stylolitization of the sutured contacts is most common where granule-sized chert grains are tightly jammed among finer, yet equally competent grains, such as quartz or another chert. In very fine-grained sandstone, stylolitization and sutured contacts were very infrequently observed. The complete summary of all samples with their corresponding depositional environments and parasequences as interpreted in Chapter 2 is shown in Table 3.1 and Appendix II. Figure 3.4 shows an example of typical Falher F tight sandstone core log with its associated thin section samples.

Table 3.3. Summary of the mineral abundance in samples analyzed using X-Ray Diffraction technique.

Well	Depth	% Minerals											
		Silica	Albite	Carbonate Minerals				Clay Minerals				Pyrite	Apatite
				Calcite	Dolomite	Fe-dolomite	Siderite	Illite/Mica	Smectites	Kaolinite	Chlorite		
Petrofacies II													
8-2-66-9W6	2579.6	59.2	4.6		3.9	3.3	0.4	14.5		11.1	2.6	0.3	0.1
Petrofacies III													
3-18-66-8W6	2468.6	39.1	14.3	1.7		1.3		29.5		11.2	2.6	0.2	
Petrofacies IV													
14-24-65-10W6	2777.5	44.6	5.7		8.5	11.2		15.6		13	0.9	0.4	
2-21-66-8W6	2514.6	50	4.2		15.2	9.8	1.1	8.2		7.4	3	0.4	0.6
3-18-66-8W6	2483.5	62.4	4.4		14	7	0.3	8.5		1.6	1	0.1	
6-20-65-10W6	2917.3	44.8	9.2		6.5	1.9		24.2		11.9	1.2	0.3	0.1
5-32-65-9W6	2917.7	47.9	6.1		1.4	1.8		8.3	12.9	19.7	1.7	0.3	
Petrofacies V													
7-13-66-9W6	2521.6	36.5	24	4.3	1	1.7		21.3		8.9	2.3		

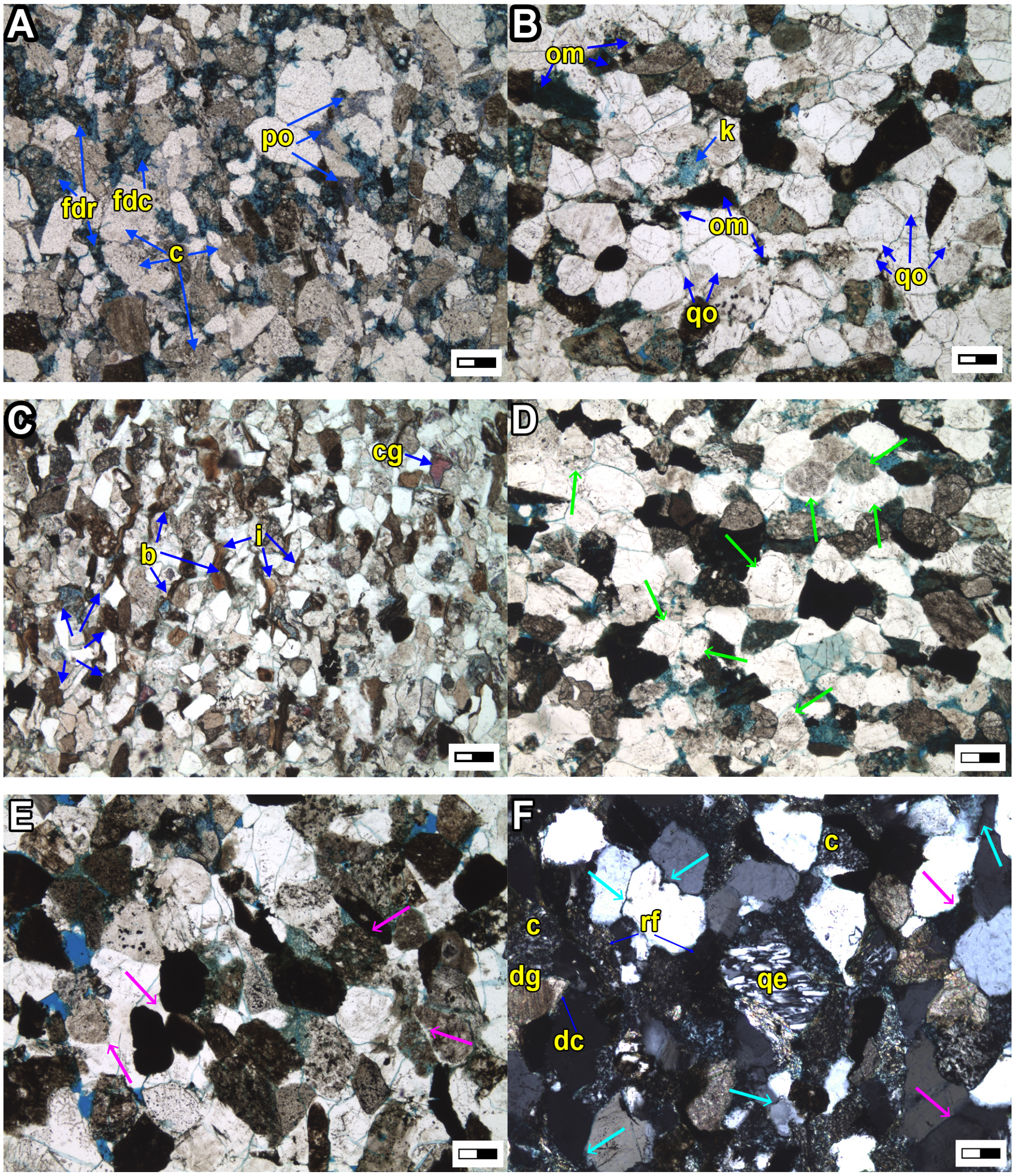

Figure 3.3. Petrographic images showing textural variations within the studied tight sandstone. Scale is 0.2 mm. **A)** Moderately sorted mature sandstone. Ferroan dolomite is dark teal-coloured due to staining. (Well 100/03-18-066-08W6/00; 2480.4 m; PPL) **B)** Very well-sorted mature sandstone. Pores are visibly blue, but with different shade. (Well 100/06-08-065-10W6/00; 2963.9 m; PPL) **C)** Subangular- to subrounded-grained sandstone, very well-sorted. (Well 100/07-13-066-09W6/00; 2524.1 m; PPL) **D)** Subangular to rounded grains. Note that quartz grains that are originally well-rounded may appear angular due to the enclosing overgrowth. (Well 100/07-14-065-11W6/02; 3175.9 m; PPL) **E)** Sandstone dominated by concavo-convex contacts. (Well 100/06-20-065-10W6/00; 2922 m; PPL) **F)** Sandstone with sutured contacts, and more abundantly, long contacts. (Well 100/11-13-066-8W6/00; 2563 m; XPL)

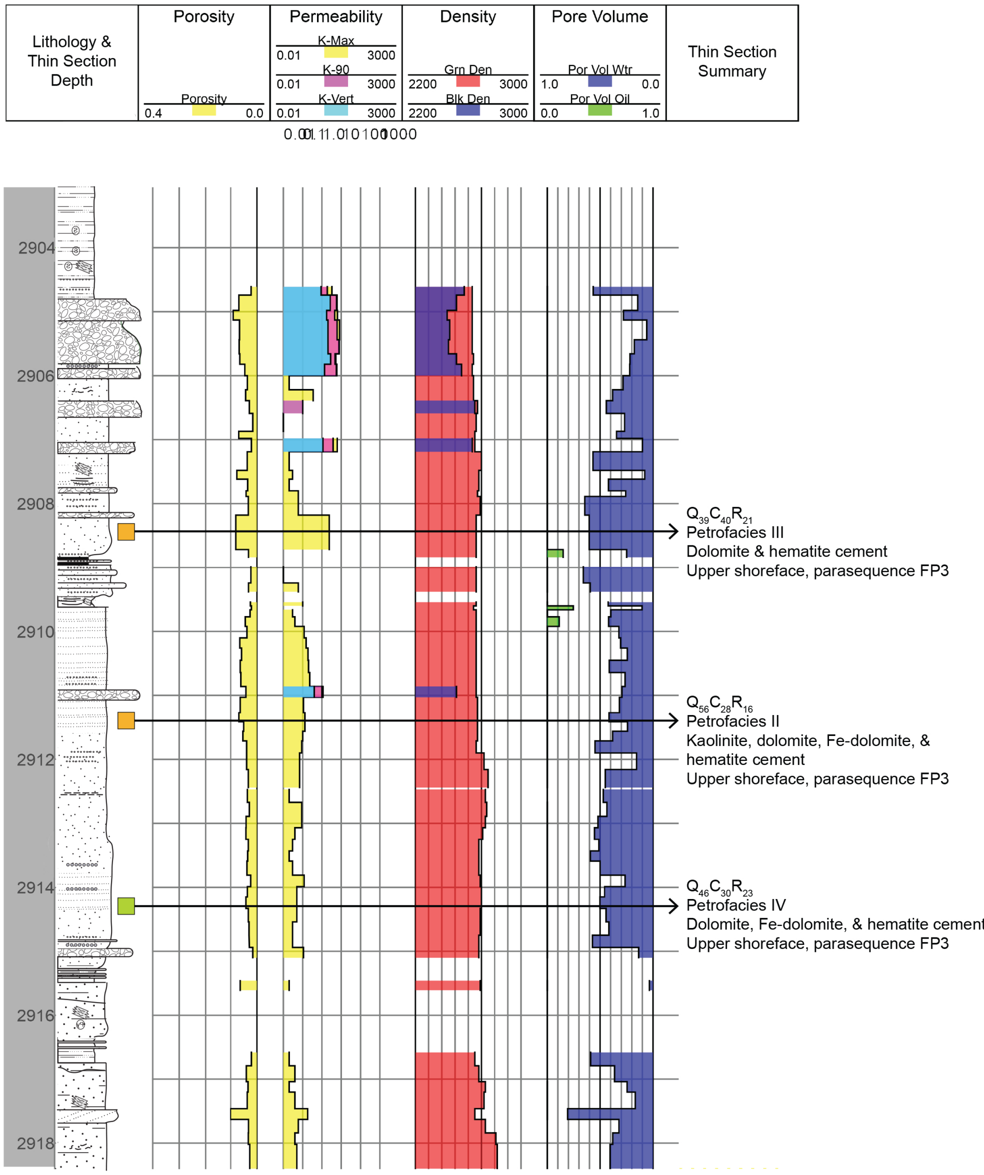

Figure 3.4. Calibrated core interval, core analyses, and petrographic analysis results for well 100/05-32-065-09W6/00. An example of a typical succession of the Falher F in the study area is shown, exhibiting coarsening-upward sandstone capped with conglomerate interval, and overlain by coastal plain mudstone. Corresponding porosity, permeability, density, and pore volume data were gathered from GeoSCOUT (publicly available; accessed on June 2018).

Point counting shows that the Falher F sandstone consists mainly of quartz, chert, and sedimentary rock fragments (Table 3.1). In 20% of the samples, dolomite grains are also markedly abundant (Table 3.4). All of the sandstone samples are depleted in feldspars. Therefore, the Falher F sandstone can be exclusively grouped into submature to mature chert arenite (Folk, 1974). This classification is equivalent to “quartzite” of Pettijohn (1949), “quartzose” of Dapples *et al.* (1953), “orthoquartzite” of Folk (1954), and “quartzarenite” of McBride (1963), all of which lump quartz and chert together into a single endmember in the triangular plot. Folk’s (1974) classification is chosen to: 1) avoid the perception of quartz being the most dominant mineral grain in all samples, and 2) emphasize the amount and importance of detrital chert as a separate endmember. Within the sample population, 26% are chert-dominated, 24% have an equivalent proportion of quartz versus chert, and the remaining are quartz-dominated, albeit to a proportion that does not exclude them from chert arenite (Table 3.4).

There is very little to none exhibited relationship between the grain size and detrital or mineralogical composition in the tight sandstone. Nonetheless, in coarser sandstone, grains that are coarser than lower medium sand are predominantly chert and, less commonly, sedimentary rock fragments. Due to the similarity of porosity and permeability of these sandstone intervals with the conventional conglomeratic reservoir, these coarser sandstone units are therefore not considered relevant for this study.

The most commonly found detrital framework components and authigenic minerals are discussed below, in descending order of abundance.

DETRITAL FRAMEWORK GRAINS

Detrital framework composition determines the mechanical and chemical stability of a lithology. Within the Falher F chert arenite, average grain composition according to the commonly used standard plot by Dott (1964) is $Qt_{79}F_1RF_{20}$; where Qt is quartz and chert, F is feldspar, and RF is rock fragments.

Considering the particular interest in drillability as measured with the relative abundance of chert, which is known as one of the most mechanically durable detritus (Abbott and Peterson, 1978; Harrell and Blatt, 1978; McBride and Picard, 1987; Yagishita and Ohkubo, 2007), a modified plot (Q-C-RF) is used instead for this study. The first endmember (Q) consists of mono- and polycrystalline quartz, both of which have the relatively moderate to low mechanical durability among silicate minerals, albeit being mechanically and chemically stable (Harrell and Blatt, 1978). The second endmember I is composed of ultra-durable silicate group clasts (Abbott and Peterson, 1978), which are chert and quartzite. The last endmember (RF) consists of rock fragments of any type, including dolomite grains, which, in general, are less stable than quartz or chert (Dott, 1964; Pittman and Larese, 1991; Garzanti *et al.*, 2015). When transitions occur among silica variants, typically between chert or quartzite and polycrystalline quartz, decision of grouping is made by the proportion of cryptocrystalline quartz (<5 μm) and the possible presence of fibrous chalcedonic texture. On the absence or very minor proportion of those parameters, grains are regarded as polycrystalline quartz instead. Based on this classification, the average composition of the Falher F chert arenite samples is $Q_{43}C_{37}RF_{20}$.

Quartz occurs as mono- and polycrystalline types. Together, they vary from 16.7 to 56% per sample with an average of 34%. The monocrystalline quartz may contain chlorite or heavy minerals inclusion, such as zircon. They predominantly have undulatory extinction. Blatt and Christie (1963) interpreted that generally, undulous quartz grains are less mechanically stable as opposed to the non-undulous grains due to their provenance and transport history. Undulatory extinction in quartz is the first deformation stage following their response to stress (Young, 1976) and the amount of such quartz is affected by diagenesis, folding, and faulting (Conolly, 1965). Therefore, this may attest to the possible transport history of the sandstone, which may affect subsequent interpretations regarding its durability.

Detrital chert ranges from 8.3 to 48%, with an average of 30.4%. Under the PPL view, the detrital chert may appear to have colourless radiolarian, diatom, or sponge spicules that are commonly referred to as "circular ghosts." This emphasizes their major provenance as biogenic silica precipitates rather than diagenetic or replacement chert (Shanmugam and Higgins, 1988). They may have authigenic inclusions, predominantly of dolomite and ferroan dolomite, and less commonly siderite. Less commonly, they may be cut by veins of drusy quartz. However, without stable isotope or fluid incision analyses, it is difficult to interpret whether such features are allogenic or syndepositional. The latter, however, may contain useful information regarding the extent of local mechanical compaction when interpreted correctly.

It has been reported that the presence of clay mineral or mica inclusions within chert reduces its durability (Harrell and Blatt, 1978). However, due to the very low percentages in the Falher F sandstone (generally less than five points per 300 points counted per sample), their effect is considered minimal to negligible. Nonetheless, where the amount of such inclusions is significant within a chert clast, as shown by the reduced competence of the clast, the chert is regarded as a miscellaneous rock fragment instead.

Miscellaneous rock fragments (RF), with chert and quartzite being excluded, range from 2.7 to 30.3% with an average of 12.3%. RF predominantly consists of sedimentary rock fragments, followed by iron-stained rock fragments with unknown origin, low- to medium-grade metamorphic rock fragments, and a trace amount of volcanic rock fragments. This contrasts with the observation in the basal Falher (Wilrich-equivalent) by Newitt (2017) where volcanic rock fragments predominated the rock fragment portion. When compared with Leckie's (1986a) study in the Gates Formation (Falher-equivalent), the descending percentage of each rock fragment type is similar, although Leckie (1986a) reported a relatively higher proportion of volcanic rock fragments.

Sedimentary rock fragments generally consist of argillaceous rock fragments, limestone, and carbonaceous rock fragments. Due to the ductility, softer rock fragments such as shale and claystone often undergo plastic deformation, causing them to occur as pseudomatrix (Dickinson, 1970). When point-counted petrographically, however, they are regarded as detrital framework grains.

Metamorphic rock fragments, excluding schistose quartzite, commonly occur as slaty shale. Its recognition may be confused with highly deformed claystone pseudomatrix because both of them have a preferential orientation of clay minerals within. However, because provenance is not the primary goal of this study, this problem can be neglected but should be addressed in future studies in which the exact origin of sandstone grains is desired.

Volcanic rock fragments observed herein are characterized by a glassy matrix with extremely fine feldspathic laths. There is also a considerable amount of reddish dark brown to nearly opaque, iron oxide-stained rock fragments with that may originate as volcanic rock fragments. Such iron oxide stains are commonly formed due to the alteration of ferromagnesian minerals (i.e. olivine, pyroxene, amphiboles, micas) (McBride, 1985), all of which are the most common lithic grains constituting volcanic rock fragments.

In some cases, shale and chert clasts have also been partially obscured by similar oxide stains. In chert, the original clast shape commonly survives, implying its higher competency than other rock fragments. Thus, in a closed framework sandstone, it is commonly surrounded by concavo-convex contacts. In contrast, other rock fragments may deform plastically and exhibit wisps of iron-stained lithic fragments that fill the interstices between more rigid grains. These behaviors may thus help differentiating between iron oxide-stained chert and other rock fragments (Dickinson, 1970). Therefore, not all of these iron-stained lithic grains are of volcanic precursors.

Detrital dolomite also occurs in considerable amount, reaching up to 24% with an average of 4.1% where present. In 20% of samples, they are of significant importance due to their abundance that is similar to, or higher than, at least one of the Q-C-RF (excluding detrital dolomite) endmembers. Even though dolomite grains may appear similar to some of the euhedral-shaped authigenic dolomite cement, they can be distinguished by their grain shape and textural relationship. The detrital dolomite may show more even, well-defined boundaries due to having been transported in the past, and usually have similar grain size with other detrital components. Dolomite grains also tend to be dirtier and dustier, implying an older age than the subsequently formed cement.

Quartzite also regularly occurs across most samples, reaching up to 3% with an average of 0.9% where present. Schistose quartzite is distinguished from polycrystalline quartz by their predominantly aligned orientation of sutured sub-crystals, indicating pressured conditions typical of metamorphic regions. They may also contain interspersed flakes of illite or mica.

Micas are also dispersed in most samples, reaching up to 4% in micaceous sandstone with an average of 0.8% where present. Biotite is the most common type, followed by muscovite and chlorite. Their generally splayed and kinked appearances are good indicators that significant mechanical compaction had occurred.

Other detrital grains in descending abundance include chalcedony, calcite, albitized feldspars, and heavy minerals (i.e. zircon and tourmaline). Each of these minerals generally occurs less than 1% per sample, although in very rare cases, calcite and albite are found to be as much as 4.7 and 2.3%, respectively. Albite is the only feldspar variant that is encountered in the Falher F sandstone.

AUTHIGENIC INTERSTITIAL MINERALS

While sandstone drillability is heavily dependent on the detrital framework composition, porosity is strongly controlled by intergranular

Table 3.4. Summarized point-counting results of the studied tight sandstone. Raw point counting data is shown in Appendix II. For abbreviations, refer to List of Symbols and Abbreviations for Chapter 3 and Appendix II.

**Q = monocrystalline quartz, polycrystalline quartz, and chalcedony; C = chert and quartzite; RF = rock fragments including dolomite clasts*

Well	Depth	Detrial Quartz	Chert, Quartzite	Rock Fragments				Authigenic Cement						Thin Section Porosity	Core Analysis		Composition (normalized)			Texture				(See Chapter 2 for details)	
				Iron-stained RF	Metamorphic RF	Sedimentary RF	Dolomite	Kaolinite	Illite/smectite	Dolomite	Fe-dolomite	Calcite & Fe-calcite	Iron Oxide		Permeability, Kmax (md)	Porosity (frac)	Q*	C*	RF*	Grain Size	Grain Shape	Sorting	Framework	Depositional Environment	Stratigraphic Succession
Petrofacies I																									
1-8-66-8W6	2579.4	41.0	46.3	3.0		3.7							0.3	5.3	0.9	5.4	43.6	49.3	7.1	u.f. – u.m.	sa – r	w.	o.	Up. S.f.	F_P3
13-27-65-9W6	2650.8	41.3	34.7	6.7		7.0	7.0						1.0	2.3	0.2	2.1	42.8	35.9	21.4	u.f.	sa – r	w.	c.	Up. S.f.	F_P3
3-18-66-8W6	2481.6	35.7	39.0	5.3	1.0	5.7	10.7						2.0	0.3	0.1	4.7	36.6	40.1	23.3	u.v.f.	sa – sr	w.	c.	Mid. S.f.	F_P2
6-20-65-10W6	2920.7	34.7	34.3	9.7		10.3	4.3						3.3	3.0	0.3	3.1	37.1	36.8	26.1	l. – u.f.	sa – sr	w.	c.	Up. S.f.	F_P2
																Mean	**40.0**	**40.5**	**19.5**						
Petrofacies II																									
10-36-65-9W6	2647.0	37.7	43.3	5.3		3.0		2.3						8.3	8.7	8.6	42.2	48.5	9.3	l. m.	a – r	w.	c.	FS	F_P3
10-36-65-9W6	2652.3	38.7	34.7	14.7		0.7	0.3	4.0			0.3			6.7	2.1	7.0	43.4	39.0	17.6	l. – u.f.	a – sa	w.	c.	Up. S.f.	F_P3
11-13-66-8W6	2563.0	46.0	32.0	5.7		4.7	2.0	1.3		1.0	1.0		0.7	5.0			50.7	35.3	14.0	l.f.	a – sr	w.	c.	Up. S.f.	F_P3
5-32-65-9W6	2911.3	42.7	21.7	3.3		6.7	2.0	4.7		4.3	0.7		1.3	12.3	0.1	6.8	55.9	28.4	15.7	l.f.	sa – sr	w.	c.	Up. S.f.	F_P3
6-20-65-10W6	2909.4	46.7	22.7	2.0		0.7		2.7	0.3	0.7	5.7		0.7	17.3	0.7	5.2	64.8	31.5	3.7	u.f.	sa – sr	w.	c.	FS	F_P3
6-20-65-10W6	2922.0	38.0	33.3	9.3		5.0	0.3	3.3		1.3	1.7		2.7	5.0	0.9	5.3	44.2	38.8	17.0	u.f.	a – sa	w.	c.	Up. S.f.	F_P2
6-8-65-10W6	2963.9	56.0	20.3	5.0		2.7		2.3					4.7	7.3	0.5	7.3	66.7	24.2	9.1	u.f.	a – sr	v.w.	c.	FS	F_P3
7-14-65-11W6	3168.3	51.0	9.3	5.3		7.7		8.3					9.7	7.7			69.7	12.7	17.6	l.f.	sa – r	w.	c.	FS	F_P2
7-14-65-11W6	3175.9	52.3	12.3	7.3		4.0	1.7	5.7		4.7	0.7		0.3	11.0			67.4	15.9	16.7	u.f.	a – sr	w.	c.	Up. S.f.	F_P2
8-2-66-9W6	2571.0	42.7	39.3	6.7		0.7		4.0						5.7	0.9	5.7	47.8	44.0	8.2	u.f.	sr – r	v.w.	c.	FS	F_P3
8-2-66-9W6	2579.6	42.0	26.3	7.0	0.3	3.7	8.3	2.7			2.7		0.3	5.3	9.0	5.2	47.9	30.0	22.0	u.v.f.	a – sr	w.	c.	Up. S.f.	F_P2
8-2-66-9W6	2579.8	32.7	34.0	7.3		5.0	5.0	3.0	0.7	0.7	5.7		3.3	2.0	0.2	7.0	38.7	40.3	21.0	l.v.f. – l.f.	sa – r	w.	o.	Up. S.f.	F_P2
																Mean	**54.6**	**31.7**	**13.7**						

Petrofacies III																									
3-18-66-8W6	2468.6	38.0	43.7	1.7	0.7	4.3			1.3	0.3	2.7		4.7		7.0	2.8	42.4	48.7	8.9	u.v.f.	sa – sr	w.	c.	Up. S.f.	$F_{p}3$
5-32-65-9W6	2908.1	28.3	37.3	11.3		15.3				0.7			4.0	2.7	6.0	3.3	30.9	40.3	28.8	u.v.f. – u.f.	a – sr	w.	c.	Up. S.f.	$F_{p}3$
5-7-66-8W6	2535.1	39.3	45.0	2.3	1.0	5.7			2.0	0.7	0.3		1.7		0.6	4.3	42.1	48.2	9.6	u.v.f. – u.f.	a – sr	m.	c.	Up. S.f.	$F_{p}3$
2-21-66-8W6	2513.8	36.3	41.3	2.0		11.3	2.0		0.7	0.3	1.3		3.3		6.0	3.1	39.1	44.4	16.5	u.v.f. – l.f.	a – sr	w.	c.	Est.	T
8-22-66-8W6	2581.5	16.7	48.3	8.7	0.7	6.7	0.3		3.0		3.0		6.7				20.4	59.2	20.4	l.f.	a – sr	w.	c.	Est.	T
8-26-65-11W6	2884.7	25.7	42.3	2.7	0.3	11.0				0.7	6.0		10.7				31.3	51.6	17.1	l. – u.v.f.	a – sa	w.	c.	Fl. Ch.	T
																Mean	**34.4**	**48.7**	**16.9**						
Petrofacies IV																									
1-8-66-8W6	2585.2	21.0	24.3	5.0		7.3	15.3			1.0	24.7		0.3	0.3	4.0	3.2	29.0	33.0	38.0	l. – u.v.f.	a – sr	m.	o.	Mid. S.f.	$F_{p}2$
13-27-65-9W6	2645.6	33.3	30.0	2.7	0.7	16.0	1.3		0.3	1.0	13.0		0.7		0.9	1.6	39.5	35.6	24.9	u.v.f.	a – sr	w.	c.	Up. S.f.	$F_{p}3$
13-27-65-9W6	2646.0	23.0	27.0	2.7		7.7	9.7			1.0	26.7		1.0		0.9	1.6	32.7	38.4	28.9	l.v.f. – l.f.	sa – sr	m.	o.	Up. S.f.	$F_{p}3$
13-27-65-9W6	2647.5	38.7	21.7	2.3	0.3	9.3	10.0			1.3	14.0		1.0		0.9	1.6	47.0	26.3	26.7	l.f.	a – r	w.	c.	Up. S.f.	$F_{p}3$
14-24-65-10W6	2776.5	35.3	32.7	3.7	1.3	1.0	13.0			4.7	1.3		2.0	1.0	4.0	2.4	40.2	37.1	22.7	u.v.f.	a – sr	w.	c.	Low. S.f.	$F_{p}3$
14-24-65-10W6	2777.5	26.0	33.7	2.3		0.3	24.0		1.7	7.7	1.3		1.0	0.3	0.4	2.2	29.8	38.5	31.7	u.v.f.	a – sr	w.	c.	Low. S.f.	$F_{p}3$
15-9-65-11W6	3024.0	39.0	32.7	4.3	1.0	4.7	1.0		1.3	2.0	12.3		1.7				47.2	39.5	13.3	u.v.f. – l.f.	a – sr	w.	c.	Up. S.f.	$F_{p}3$
2-21-66-8W6	2514.6	34.0	37.7	0.7	0.3	2.7	3.7		1.3	0.3	13.7		1.0	4.0	9.0	6.8	43.0	47.7	9.3	u.v.f. – l.f.	a – sr	w.	c.	Est.	T
3-18-66-8W6	2480.4	28.3	35.3		0.7	3.7	3.3			5.7	15.3		1.0	6.7	0.9	4.3	39.7	49.5	10.8	u.f.	sa – sr	m.	c.	Mid. S.f.	$F_{p}2$
3-18-66-8W6	2483.5	38.0	31.3	3.0	0.3	3.0	3.0		1.0	3.3	11.3		2.3	3.0			48.3	39.8	11.9	u.v.f. – u.f.	a – sa	m.	c.	Mid. S.f.	$F_{p}2$
3-33-65-9W6	2740.4	36.7	32.7	8.7	0.3	5.7	2.0			6.3			2.3	2.7	4.0	2.8	42.6	38.0	19.4	l. – u.v.f.	a – sr	w.	c.	Up. S.f.	$F_{p}2$
3-33-65-9W6	2734.3	29.0	29.7	7.3		14.3	7.0		0.3	0.7	10.0		0.3	0.3	6.0	3.3	33.1	33.8	33.1	u.v.f.	a – r	w.	c.	Mid. S.f.	$F_{p}3$
5-32-65-9W6	2914.1	42.7	28.0	2.7		5.0	13.0			2.0	0.3		1.7	3.0	5.0	4.2	46.4	30.4	23.2	u.v.f.	a – sr	w.	c.	Low. S.f.	$F_{p}3$
6-20-65-10W6	2917.3	22.0	38.3	7.7	1.0	7.0	3.0		1.0	4.3	4.0		9.3	0.3		1.4	27.7	48.3	23.9	l.f.	a – sr	w.	c.	Mid. S.f.	$F_{p}3$
6-8-65-10W6	2963.3	27.0	9.7	9.0		20.0	7.7			9.3	10.7		6.7				36.8	13.2	50.0	l.v.f.	a – sa	m.	o.	Est.	T
7-16-65-11W6	3188.9	18.3	33.0	3.0	1.3	4.3	2.0		1.0	13.0	17.3		3.3				30.4	51.8	17.8	l. – u.f.	a – sr	w.	o.	Est.	T
7-16-65-11W6	3195.5	30.0	40.7	8.3		4.3	2.0		2.0	6.0	4.0		1.7	0.7			35.2	47.7	17.2	l.f.	a – sr	w.	c.	Up. S.f.	$F_{p}3$
7-16-65-11W6	3199.1	41.0	30.7	7.7	1.0	2.3	9.7			1.3	3.3		2.7				44.4	33.2	22.4	u.v.f.	a – sr	w.	c.	Low. S.f.	$F_{p}3$
8-2-66-9W6	2568.5	23.0	25.3	5.0		3.7	1.3		4.0	6.3	22.0		7.0		0.2	6.7	39.4	43.4	17.1	l.v.f.	a – sr	m.	c.	Est.	T
																Mean	**38.5**	**38.2**	**23.3**						
Petrofacies V																									
6-8-65-10W6	2961.6	17.0	15.0	12.7		7.7	6.7			12.0	11.7	10.3	5.7			0.8	28.8	25.4	45.8	u.v.f. – u.f.	a – r	m.	o.	Est.	T
7-13-66-9W6	2517.5	42.7	29.0	8.7		2.3	1.3		0.7		1.7	5.7	0.7	2.3	6.0	2.8	50.2	34.1	15.7	l.f.	a – r	m.	c.	Up. S.f.	$F_{p}3$
7-13-66-9W6	2521.6	33.0	36.0	6.0		8.0			0.7	1.0	2.0	2.0	0.3	3.7	1.0	4.7	38.7	42.2	19.1	u.v.f.	a – sr	m.	c.	Mid. S.f.	$F_{p}2$
7-13-66-9W6	2524.1	36.7	36.7	2.7	0.3	4.0	3.7		4.0	3.0	4.3	1.0	0.3	0.3	1.0	3.1	43.5	43.5	13.1	l.f.	a – sa	m.	c.	Mid. S.f.	$F_{p}3$
7-13-66-9W6	2531.3	35.3	25.3	4.3		11.3	6.0	2.3		9.3	0.7		1.3	3.7	5.0	4.7	42.9	30.8	26.3	u.v.f. – u.f.	a – r	p.	c.	Up. S.f.	$F_{p}2$
8-2-66-9W6	2575.8	39.0	37.0	3.3	1.0	6.7	1.0			1.7	2.0	1.0		4.0	0.4	4.2	44.3	42.1	13.6	u.v.f. – l.f.	a – sr	w.	c.	Low. S.f.	$F_{p}3$
8-22-66-8W6	2575.8	25.7	23.3	11.0	0.3	19.0	1.3			3.7	4.0	7.3	4.0				31.8	28.9	39.3	u.f.	a – sr	p.	o.	Est.	T
8-22-66-8W6	2578.7	27.0	16.0	5.3	0.3	14.0	1.7			9.7	13.7	6.3	1.3				42.0	24.9	33.2	u.f.	a – r	p.	o.	Est.	T
8-22-66-8W6	2585.4	31.0	9.7	3.3		4.3	4.7		0.3	20.3	4.0	12.3	5.3				58.5	18.2	23.3	l. – u.v.f.	sa – r	m.	o.	Est.	T
																Mean	**42.3**	**32.2**	**25.5**						

cementing materials and other interstitial components. Several important interstitial minerals are present within the Falher F sandstone, with each of them contributing to varying impacts towards the porosity.

Quartz overgrowths are a major cement component within the Falher Member. All samples exhibit quartz overgrowths, but the percentage was not quantifiable with point counting method used, largely due to the placing of JmicroVision-generated grids and crosshairs that mostly offsets the width of the overgrowth. Most of the grains also lack outer vacuoles, thus complicating the identification of the actual boundaries between the grains and overgrowths. The overgrowths generally occur as syntaxial to euhedral-shaped, with the former being more predominant. In most samples, the lack of a visible dust line at the end of the quartz nuclei and the beginning of overgrowth may make the grains appear to be angular (Fig. 3.5A). This commonly occurs where the welding of quartz overgrowth forms compound grains composed of interlocking crystalline aggregates in mature sandstone units. Due to the abundance of quartz overgrowths, point contacts between quartz are commonly difficult to observe. Where point contacts are observed, they commonly only show very little evidence of pressure solution.

Dolomite cement is also very widely spread in most samples. Total authigenic dolomite can be up to 20.3% with an average of 3.2%. It generally occurs as pore-occluding, patchy, subhedral blocky spars (Fig. 3.5B). Compared with detrital dolomite, dolomite cement appears to consist more of isolated crystals that generally incorporate the rims of surrounding grains. Thus, their authigenic origin can be deduced. In some cases, the cement appears as equant rhombs, strengthening evidence of never having been transported (Ulmer-Scholle *et al.*, 2015).

Authigenic dolomite may also occur as euhedral, rhombic inclusions or patchy replacement. Both the replacement and inclusions are most often associated with detrital chert or rock fragments, although the replacement is also found on albite.

Ferroan dolomite cement is commonly associated with its non-ferroan counterpart. It may reach up to 26.7% with an average of 7%. It may appear as enclosing rims or rhombohedral overgrowths outside the dolomite detrital grain and cement (Fig. 3.5B), or pore-filling material evenly distributed within intergranular pore spaces. It may also appear as poikilotopic cement (Fig. 3.5C).

Ferroan dolomite replacement is more sparsely distributed than dolomite replacement cements. However, it is common as inclusions and usually associated with the dolomite inclusions. The rhombic, euhedral ferroan dolomite inclusions are most commonly encountered on chert.

Kaolinite acts as an important cement in the more visibly porous intervals. The observed kaolinite in thin sections can be up to 8.3% with an average of 3.8%. Additionally, XRD results point out that very rarely, it can be up to 19.7% (Table 3.3). It is observed as pore-filling booklets that partially occlude oversized voids, which have been sites of former dissolution (Fig. 3.5D).

Iron oxide cements, which generally consist of possibly hematite and other minerals, are observed in all samples. It ranges from 0.3 to 10.7% with an average of 2.8%. In some examples, the iron oxide cements alter detrital organic matter (Fig. 3.5D). Generally, iron oxide is dispersed as specks around framework grains (Fig. 3.5D) that completely infills intergranular pore spaces (Fig. 3.5E) or the stylolitized contacts (Fig. 3.5F). Reddish to nearly opaque hematite may occur as pore-lining cement that evenly encloses the contacts between syntaxial quartz overgrowth. In that case, its lack of presence on the rims that separate detrital quartz and quartz overgrowths may indicate its later formation that postdated the quartz overgrowths.

In several samples, iron oxide-stained rock fragments that have been deformed as pore-occluding pseudomatrix may appear very similar to authigenic iron oxide cement. In cases where the opaque materials perfectly fit the interstices without rims that overlap onto the surrounding detrital grains, it is a good indication that it is merely pseudomatrix and not true iron oxide cement (Fig. 3.6E).

Calcite cement is restricted to a few samples, and their localized presence seems to be highly related to intercalated beds or laminae of calcareous fossil debris. It reaches up to 12.3% with an average of 5.1%. The occurrence may be as sporadic, void-filling crystals or as poikilotopic cement up to 0.5 mm in size. It is generally associated with dolomite and ferroan dolomite cements that share similar textures and crystal shapes (Fig. 3.5G). Its ferroan counterpart is present infrequently and generally mixed within the calcite.

Calcite replacement commonly corrodes chert, albite, and rock fragments. Dedolomitization is also often observed, either as partial or complete leaching of dolomite grains.

Illite/smectite mixed layer is not frequently easy to be spotted in thin sections, and point counting only shows a 1.4% average. Based on XRD and SEM results, however, their percentage is much higher. X-ray diffraction analyses indicate up to 29.5%, although some of this are likely other types of mica that have overlapping peaks with illite/smectite on XRD patterns (Lanson and Velde, 1992). The absence of readily distinguishable features such as meshwork illite often confuses the petrographic observation. Illite is commonly found as very thin and fine strands, often coat the quartz overgrowths or any detrital framework. Where rock fragments or chert clasts have been pushed together to form pseudomatrix, flakes of illite may also fill the point contact (Fig. 3.5H). This may prevent pressure solution on chert grains and aids to define the pseudomatrix boundaries, and in turn, the detrital origin of the pseudomatrix.

POROSITY TYPES

As expected for typical tight sandstone, porosity in the Falher F is almost exclusively of secondary origin. Exceptions may occur in quartz-dominated sandstone that grade into conglomerate bodies, where primary porosity may be retained. Except in these units, detrital grain dissolution was the major

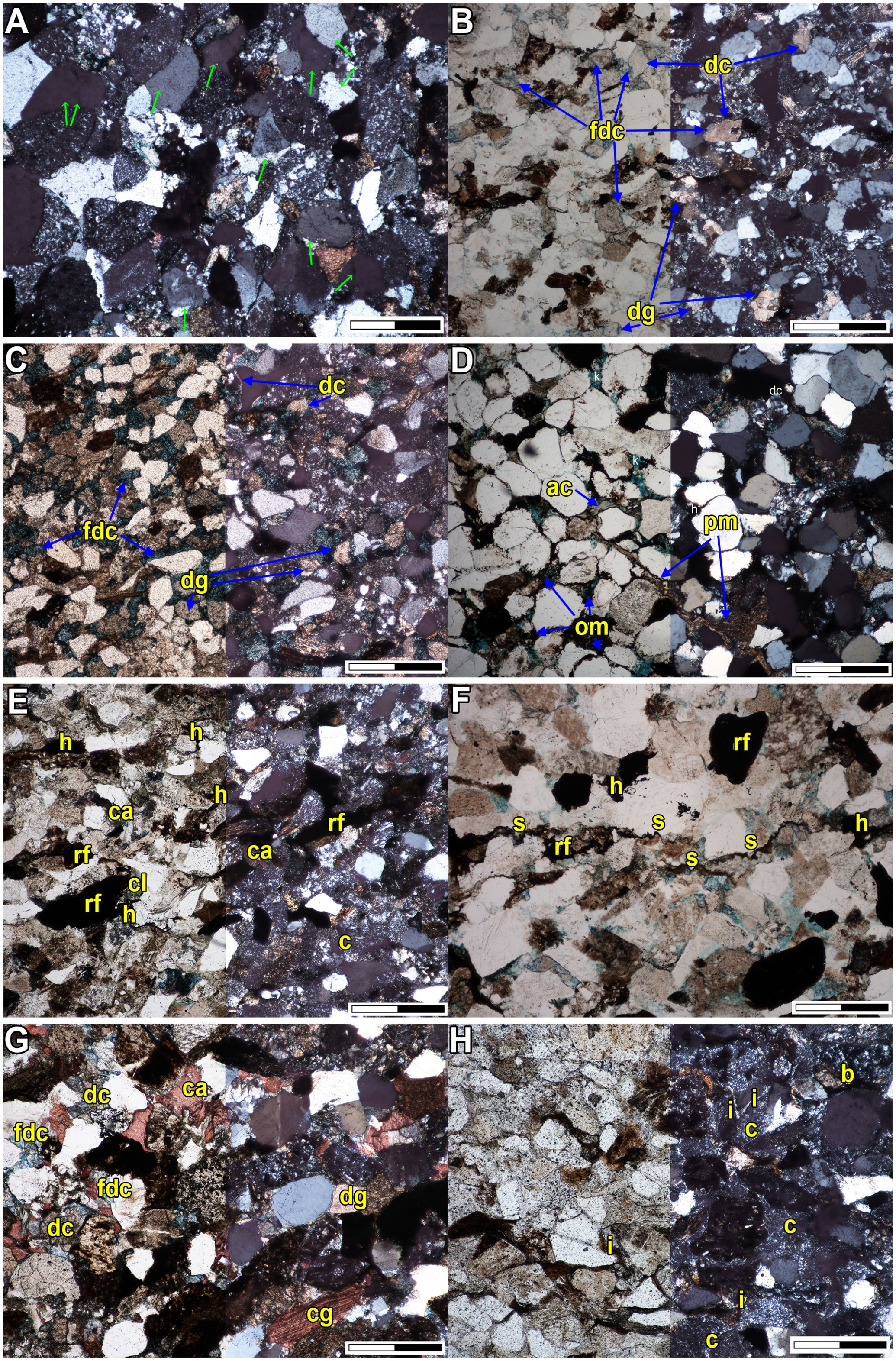
A
B
dc
fdc
dg
C
dc
fdc
dg
D
ac
pm
om
E
h
h
h
ca
rf
ca
rf
cl
rf
h
c
F
rf
h
s
s
rf
s
s
h
G
dc
ca
fdc
fdc
dg
dc
cg
H
b
i
i
c
c
i
i
c

Figure 3.5. Petrographic images showing various cements in the studied tight sandstone. Scale is 0.5 mm. **A)** The lack of visible vacuoles between quartz grains and their overgrowths may make grains appear to be more angular than its original roundedness. (Well 100/03-18-066-08W6/00; 2481.6 m; PPL | XPL) **B)** Authigenic dolomite cement occurring as patchy euhedral-shaped cement with ferroan rims. (Well 100/07-16-065-11W6/02; 3199.1 m; PPL | XPL) **C)** Poikilotopic ferroan dolomite cement appearing to be dark teal due to staining. (Well 100/13-27-065-09W6/00; 2646.0 m; PPL | XPL) **D)** Sites of feldspar dissolution and subsequent kaolinite precipitation may appear to be empty dissolution pores with blue epoxy still visibly clear. (Well 100/07-14-065-11W6/02; 3168.3 m; PPL | XPL) **E)** Sporadic distribution of opaque minerals, possibly a mix of hematite and organic matter, may appear similar to iron-rich argillaceous pseudomatrix. Note a chlorite grain being compacted onto adjacent grain. (Well 100/08-22-066-08W6/00; 2581.5 m; PPL | XPL) **F)** Iron oxide filling stylolitized point contacts. Note that the extending stylolite is a product of amalgamation of at least three smaller stylolites. (Well 100/07-16-065-11W6/02; 3195.5 m; PPL) **G)** Calcite, dolomite, and ferroan dolomite cement are present simultaneously. Note the generally similar patchy, granulous texture of all cements. (Well 100/08-22-066-08W6/00; 2575.8 m; PPL | XPL); **H)** Chert-dominated arenite with abundant illite/smectite and biotite that are squeezed along the point contacts of more rigid grains. (Well 100/05-07-066-8W6/00; 2535.1 m; PPL | XPL)

mechanism of porosity creation. Chert and rock fragments are the most commonly dissolved grains (Fig. 3.6A). Chert that is more prone to dissolution tends to have more impurities, as observed in the remaining portion of partially dissolved grains, and may also have initial micropores as well (Cochran, 1991). Partial dissolution appears to be a lot more common than complete dissolution. Commonly observed dissolution along the boundaries of point contacts between quartz overgrowth may also indicate dissolution of quartz cement, which may form locally extensive networks (Ghosh, 1991).

Microfracturing is also common, particularly along grain contacts and less commonly along crystal planes. Rather uncommonly, channels or tubes up to 20 μm wide are also formed, which were probably resulted from the pressure release during subsequent uplift. These channels may form along grain point contacts in a closed-framework sandstone, or surrounding granules that are present among sand grains (Fig. 3.6B). It is important to distinguish this channel-type pore with channel artifacts that may be caused during sample handling, by observing the presence of any pore-filling cement in such channels.

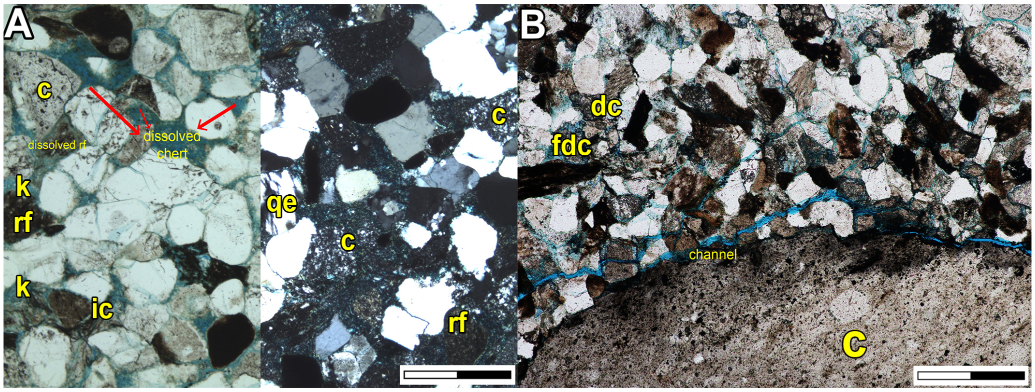

Figure 3.6. Petrographic images showing the porosity types in the studied tight sandstone. Scale is 0.5 mm. **A)** Dissolved chert and rock fragments were recognized based on the available remnants. Note how the resulting network of oversized secondary pores may resemble primary porosity. (Well 100/08-02-066-09W6/00; 2571 m; PPL | XPL) **B)** Channel between chert granule and sand grains in this image is not an artifact, as shown by the presence of granular iron oxide cement within the channel. This sample also has abundant dissolution pores of chert, rock fragments, and possibly quartz overgrowths. Well 100/05-32-065-09W6/00; 2914.1; PPL)

PETROFACIES AND DIAGENETIC VARIATIONS IN THE FALHER F

Within the Falher F chert arenite, local variations exist due to the differences in textural and compositional maturity. Authigenic porosity-affecting minerals also vary among samples. These differences allow the chert arenite to be further sub-grouped into different petrofacies. Each of these petrofacies corresponds to different diagenetic history and results in different reservoir quality, particularly with respect to the porosity.

Texturally, these petrofacies are evaluated based on their degree of winnowing, sorting, and rounding (following Folk, 1974). Compositionally, these petrofacies are classified based on their detrital framework and cementing agents. There are five petrofacies that are elaborated below, in descending degree of maturity and with increasing diagenetic complexity from petrofacies I to V.

The summary and detailed list of samples can be observed in Table 3.5 and 3.4, respectively. There may be overlapping features between these petrofacies. In cases where such overlapping features are regarded to have been of less significance as compared with other more conspicuous features, the petrofacies is assigned based on the latter.

PETROFACIES I: MATURE, QUARTZ-CEMENTED CHERT ARENITE

Petrographic Results

The most petrographically mature sandstone within the Falher F is found primarily towards higher stratigraphic positions within each parasequence and within the Falher F as a whole, which is in the upper shoreface. There is, however, also a sample from a middle shoreface succession that exhibits similar maturity (Fig. 3.7A), possibly deposited very close to the middle-upper shoreface boundary in the fair-weather wave base (Aigner, 1985; Johnson and Baldwin, 1996). This petrofacies is composed of well-sorted, upper very fine- to upper medium-grained sandstone with sub-angular to rounded grains. The average composition of the sandstone is $Q_{39}C_{40}RF_{21}$.

Within this cleanest sandstone of the Falher F chert arenite, syntaxial quartz overgrowth is the only major interstice cement. Ferroan dolomite is present in samples from well 100/03-18-066-08W6/00 and 100/06-20-065-10W6/00 as dolomite grain-coating rims not thicker than 50 μm and inclusions (Fig. 3.7A), but their presence does not alter the pores that are predominantly occluded by silica cement. In some samples, the grains are also coated by iron oxide, up to 100 μm thick. The iron oxide, however, acts not as grain coatings that otherwise could have prevented extensive silica overgrowth, but simply as an enclosing layer between overgrowth layers. The iron oxide may also occur along the contacts of other tightly compacted detrital grains or

Table 3.5. Petrofacies identified within the tight sandstone of the study interval.

Petrofacies		Sorting	Grain Size	Grain Shape	Avg. Clast Composition	Other Clast Present	Major Pore-occluding Materials	Minor Pore-occluding Materials	Depositional Environments
I	Mature, silica-cemented chert arenite	Well sorted	Upper very fine – upper medium	Subangular to rounded	$Q_{40}C_{41}RF_{19}$	Zircon, tourmaline	Quartz overgrowth	Hematite, ferroan oxide coatings	Upper shoreface
II	Mature, silica- and kaolinite-cemented chert arenite	Well to very well sorted	Upper very fine – lower medium	Subangular to rounded	$Q_{55}C_{32}RF_{14}$	Zircon, tourmaline	Quartz overgrowth, kaolinite	Hematite, ferroan oxide coatings, ferroan dolomite	Upper shoreface, foreshore, backshore
III	Submature-mature, tightly-compacted chert arenite	Moderate to well sorted	Upper very fine – upper fine	Angular to subrounded	$Q_{34}C_{49}RF_{17}$	Illite, micas, feldspars	Argillaceous pseudomatrix, welded chert, quartz overgrowth, smectite/illite	Hematite, ferroan oxide coatings	Upper shoreface, foreshore, estuarine, fluvial channel

IV	Submature-mature, tightly-compacted, dolomite- and silica-cemented chert arenite	Moderate to well sorted	Lower very fine – lower fine	Angular to subrounded	$Q_{39}C_{38}RF_{23}$	Illite, micas, feldspars	Ferroan dolomite, dolomite, quartz overgrowth	Argillaceous pseudomatrix, welded chert, smectite/illite, hematite, ferroan oxide coatings	Lower shoreface, middle shoreface, upper shoreface, tidal channel, estuarine
V	Submature-mature, tightly-compacted, silica-, calcite- and dolomite-cemented chert arenite	Poor to well sorted	Lower very fine – upper fine	Angular to rounded	$Q_{42}C_{32}RF_{25}$	Calcite, illite, micas, feldspars	Calcite, ferroan dolomite, dolomite, quartz overgrowth	Argillaceous pseudomatrix, welded chert smectite/illite, hematite, ferroan oxide coatings, ferroan calcite	Lower shoreface, middle shoreface, upper shoreface, estuarine

diminish where such compaction occurs. This implies that the coatings were emplaced before, during, and also after the burial compaction.

Porosity estimates derived from thin section observation in all samples are similar to the results of core analyses, yielding values ranging from 2.1 to 5.4%. Partial quartz overgrowth dissolution can be observed, albeit rarely (Fig. 3.7B). Primary intergranular voids are still preserved in sample 100/01-08-066-08W6/00 (2579.4 m) (Figs. 3.8A, B). Others have secondary porosities in the forms of partially to completely dissolved chert and rock fragments that form a visible network in thin sections as well as microfractures that are typically quite subtle in thin sections.

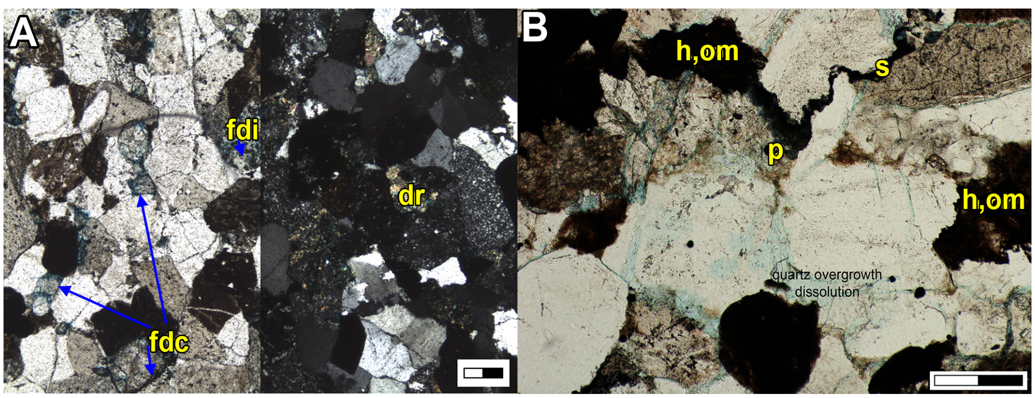

Figure 3.7. Samples representing petrofacies I. Scale is 0.2 mm. **A)** A middle shoreface sample exhibiting textural and compositional maturity, as shown by the lack of interstitial matrix. Dolomite occurs as inclusion and partial replacement on chert. (Well 100/03-18-066-08W6; 2481.6 m; PPL | XPL) **B)** Secondary porosity occurring as partial dissolution of quartz overgrowths. (Well 100/06-20-065-10W6/00; 2920.7 m; PPL)

PETROFACIES II: MATURE, KAOLINITE- AND SILICA-CEMENTED CHERT ARENITE

Petrographic Results

Another mature sandstone type from successions interpreted as upper shoreface and foreshore is included in petrofacies II. It consists of well- to very

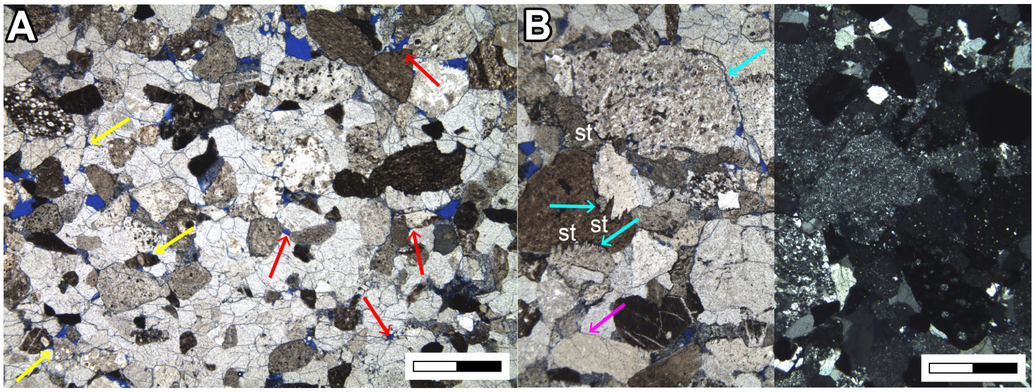

Figure 3.8. Porosity types preserved in petrofacies I. Scale is 0.2 mm. **A)** Sandstone with minor primary pores. However, larger secondary grains can be mistaken as primary pores due to their intergranular relationship that is restricted among grain contacts. With careful observation, remnants of older, dissolved grains may be observed. (Well 100/01-08-066-08W6; 2579.4; PPL) **B)** Stylolites, long, and concavo-convex contacts in granules that are dispersed among finer grains. Image taken from the same sample with image A. (Well 100/01-08-066-08W6; 2579.4 m; PPL | XPL)

well-sorted, upper very fine- to upper fine-grained sandstone with sub-angular to rounded grains. The average composition is $Q_{55}C_{32}RF_{14}$. Unlike petrofacies I, which is a mix of quartz- and chert-dominated sandstone, this petrofacies consists almost exclusively of quartz-dominated chert arenite.

The major authigenic cements in this petrofacies are quartz overgrowth and vermicular-shaped kaolinite. A few samples are also cemented by patchy ferroan dolomite (Fig. 3.9A). In most samples, intermixed iron oxide (e.g. hematite) and organic matter are also present, and can be very abundant in certain samples. For instance, in sample 100/07-14-065-11W6/02 (3168.3 m), they coat most grains and quartz overgrowth as well as occlude interstitial pore spaces (Fig. 3.9B). The presence of grain-coating hematite cement has been reported to drastically reduce reservoir permeability, resulting in similar impacts to illite. Ali *et al.* (2012) reported that 3% hematite-lining cement is sufficient to completely block pore connections, even though the main factor lies in the presence of the grain-lining hematite itself, regardless of the amount. This issue is probably of concern in localized Falher F succession as it may be responsible for local reservoir compartmentalization.

The most readily noticeable feature within this petrofacies is its common oversized pores. These pores, which are mostly secondary in origin, may form a network that can be mistaken as primary intergranular porosity (Figs. 3.9A; C). At the depths of which these samples were collected (>2400 m), the sandstone is very unlikely to have preserved significant primary porosity, unless exceptional geological conditions, such as overpressure, have occurred (e.g. Bjørlykke *et al.*, 1979). Of note, porosity quantified from point counting in Falher F samples that have outsized pore spaces can exceed the porosity gathered via core analyses by up to 300%. This occurs commonly in thin sections with channel-type pores, in which most voids appear to be cement-free in thin section. Thin section porosity that is higher than the core analyses may indicate the presence of micro-cements that are not detected at microscope scale, or extensive pores that are localized at the bed- to lamina-scale.

Core porosity in this petrofacies ranges from 5.2 to 8.6%, which is higher than the average Falher F tight sandstone porosity. While a very minor proportion comes from preserved primary pores, the majority is resulted mainly from extensive grain dissolution. Remnant materials from dissolved frameworks in otherwise completely empty pores may help to define their secondary origin. Microfractures are also a common feature.

X-Ray Diffraction Results

Analyses of XRD performed on sample 100/08-02-066-09W6/00 (2580.0 m) revealed a higher amount of kaolinite than thin section observation, as much as 11.1% (Table 3.3). Poorly structured illite/smectite was also detected, up to 14.5%. Since XRD does not differentiate clay minerals that occur as lithic grains within rock fragment material from pore-filling clay, it is hypothesized that this unusually high percentage of clay may indicate an atypically high proportion of

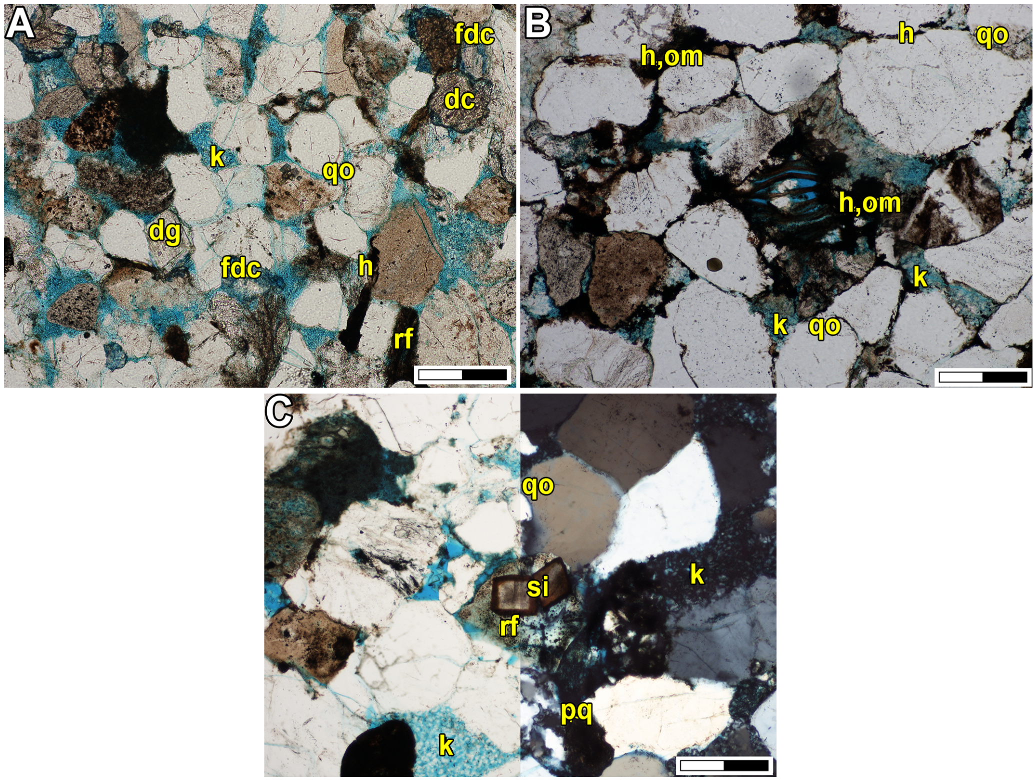

Figure 3.9. Samples representing petrofacies II. Scale is 0.2 mm. **A)** Sandstone with kaolinite, quartz overgrowths, patchy dolomite and ferroan dolomite cements, and minor iron oxide cements. (Well 100/05-32-065-09W6/00; 2911.3 m; PPL) **B)** Hematite and organic matter are unusually high in this sample. Note that iron oxide occurs as coatings between quartz grains and its overgrowth, and outside the overgrowth, indicating its early and prolonged authigenesis with respect to quartz cementation. (Well 100/07-14-065-11W6/02; 3168.3 m; PPL) **C)** Oversized pores may be clogged by kaolinite, iron oxide, or completely cement-free. (Well 100/06-08-065-10W6/00; 2963.9 m; PPL | XPL)

the former, although it is also acknowledged that some of this disparity may result from misinterpretation of other micas as smectite/illite due to the same peak on XRD patterns. Regardless, it is necessary to note that in certain cases in the Falher F, clay minerals may complicate the diagenetic effects to the reservoir quality. Further laboratory analyses are necessary to further test the impact of clay minerals within this unit.

PETROFACIES III: SUBMATURE-MATURE, TIGHTLY-COMPACTED CHERT ARENITE

Petrographic Results

The submature to mature, tightly compacted chert arenite petrofacies occurs in samples interpreted as upper shoreface, estuarine, and fluvial channel. It consists of moderate- to well-sorted, lower very fine- to upper fine-grained sandstone with angular to subrounded grains. The average composition is $Q_{34}C_{49}RF_{17}$, with all samples being chert-dominated. This petrofacies contains a higher proportion of less stable framework minerals, such as detrital micas and argillaceous rock fragments (Fig. 3.10A). Tangential arrangement of some of the clay minerals with adjacent grain is also indicative of detrital clay origin (e.g. Walker *et al.*, 1978).

It has been reported that chert-dominant sandstone may serve as a more stable reservoir in comparison with quartz-dominated sandstone due to a lesser likelihood of quartz overgrowth formation (e.g. Melvin and Knight, 1986; Bloch, 1994; Landers *et al.*, 2008). However, Larese and Hall (2003) reported that chert percentages higher than 40% may lead to significant compactional welding, and in turn, permanent porosity loss. In this petrofacies, for example, chert grains can often be observed as being tightly welded with surrounding chert grains due to their abundance (Fig. 3.10A). Where it occurs, no visible porosity is observed, unless subsequent dissolution followed. However, the degree of compaction observed in this unit is such that compaction did not necessarily lead to pressure solution among sand-sized grains. This is evidenced by the common absence of sutured contacts, which was possibly affected by common grain-lining illite, biotite, or iron oxide cement.

The abundance of chert has also promoted extensive rock fragment pseudomatrix due to mechanical compaction of malleable rock fragments versus more competent chert clasts (Dickinson, 1970). Rock fragment pseudomatrix is thus one of the most important interstitial components in this petrofacies, due to its ductile deformity (Fig. 3.10B). Illite-rich chert also tends to behave in the similar way to pseudomatrix (Marinai, 1987). Therefore, where illite-bearing chert is present, it is regarded as an unstable rock fragment rather than a chert grain.

Quartz overgrowth is present, albeit in much lesser quantities than in other petrofacies. Iron oxide cement and organic matter, particularly as coatings, also occur in all samples, up to 10.67% in the fluvial channel sandstone. Detrital illite also occurs as a pore-filling clay mineral. A minor amount of authigenic ferroan dolomite occurs in all samples, albeit as a replacement mineral rather than pore-filling cement.

In thin section, this petrofacies appears to be devoid, or nearly devoid, of porosities. However, core porosity shows moderate porosity values, ranging from 2.8 to 4.3%. This implies the presence of microporosity, particularly those that may be associated with point contacts along competent grains, such as chert-to-chert or chert-to-quartz, and also within clay minerals. Very rarely, microfractures and very subtle partial leaching of rock fragment are observed in thin sections (Fig. 3.10C).

X-Ray Diffraction Results

Similar to petrofacies II, analyses performed on sample 100/03-18-066-08W6/00 (2468.6 m) revealed an extremely high proportion of clay minerals (up to 29.5% for poorly structured mixed layer of illite/mica and 11.2% for kaolinite; Table 3.3). The partially dissolved framework grains may have been sites where micro-kaolinite precipitated, although this is not visible in thin section. Albite also comprises a high percentage of this petrofacies (up to 14.3%). While these results confirm a lesser degree of maturity relative to other petrofacies, they also indicate a limit of the utility of petrography in the analysis of complex, clay-rich lithologies.

Scanning Electron Microscope Results

Analyses of SEM conducted on sample 100/03-18-066-08W6/00 (2468.6 m) reveal the presence of plagioclase feldspar (possibly albite as revealed by XRD) that is dissolved, thus creating intragranular porosity (Fig. 3.10D). Such porosities may help explain the core porosity values that cannot be proven by thin sections. There are also well-defined concavo-convex boundaries between quartz grains, possibly indicating the absence of overgrowths (Fig. 3.10E). The lack of observed sutured contacts within such tightly compacted sandstone is compelling as is the presence of booklet-shaped micro-kaolinite that is not observed in thin sections (Fig. 3.10F).

PETROFACIES IV: SUBMATURE-MATURE, DOLOMITE- AND QUARTZ-CEMENTED CHERT ARENITE

Petrographic Results

This petrofacies predominates among the Falher F sandstone in the study area. It is represented in nearly all Falher F depositional environments (i.e. lower shoreface, middle shoreface, upper shoreface, and estuarine). This submature to mature sandstone consists of moderately- to very well-sorted, lower very fine- to upper fine-grained sandstone with angular to subrounded grains. The average composition is $Q_{39}C_{38}RF_{23}$. A very few samples were observed to be rock fragment-dominated, a characteristic that is not observed in previously mentioned petrofacies. Similar to petrofacies III, the detrital micas and argillaceous rock fragments are abundant.

As is typical of all Falher F petrofacies, quartz overgrowths are present. However, ferroan dolomite and dolomite cement compose the most distinguishable intergranular fills (Fig. 3.11A). In the case of sample 100/01-08-066-08W6/00 (2585.2 m), the sandstone appears to be matrix-supported due to the overwhelming proportion of poikilotopic ferroan dolomite cement in a

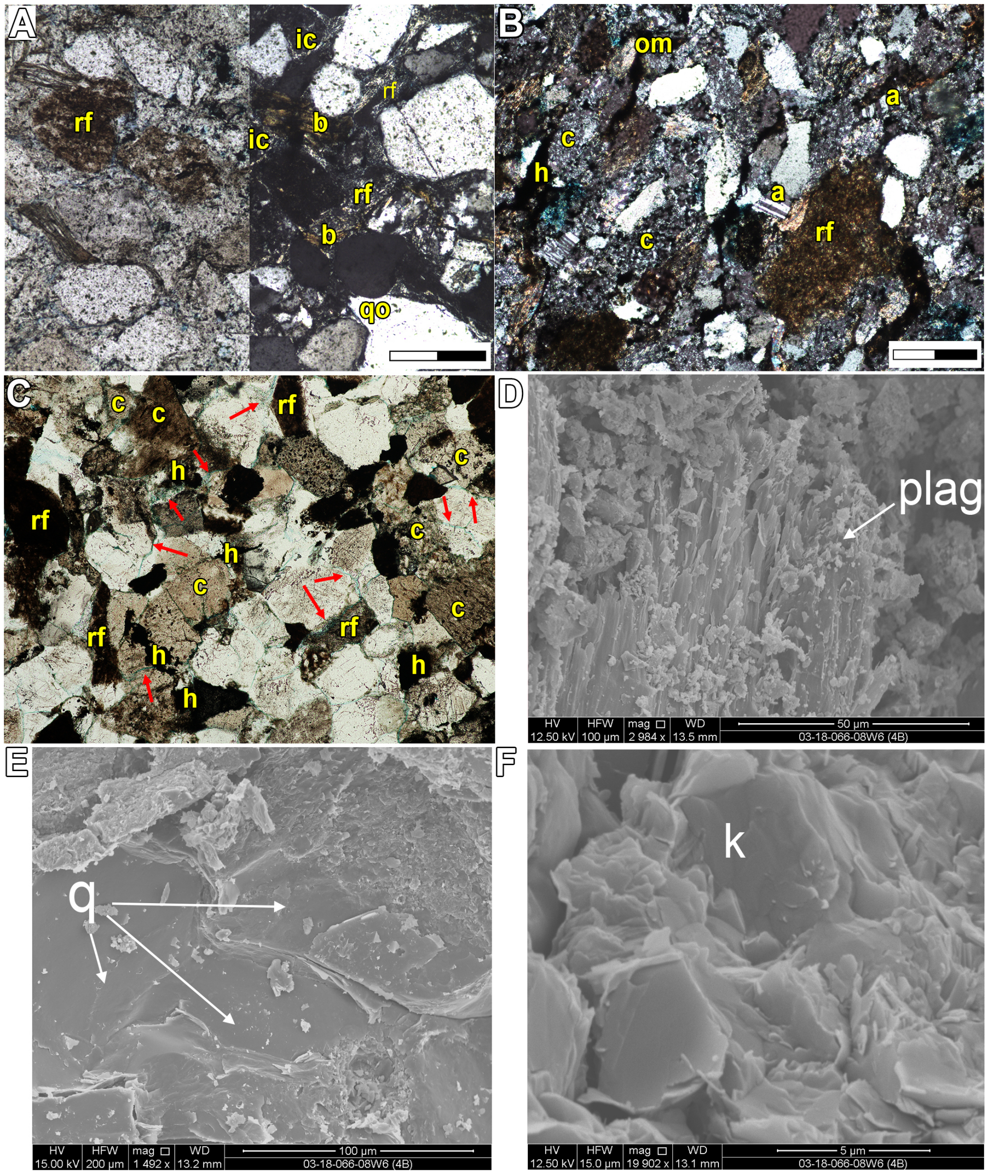

Figure 3.10. Samples representing petrofacies III. Scale for thin sections is 0.1 mm. **A)** Sample enriched with biotite and possibly authigenic clay minerals (illite). Grain-coating illite is markedly abundant and may be confused with biotite without careful considerations. (Well 100/05-07-066-08W6/00; 2535.1 m; PPL | XPL) **B)** Shale clast as pseudomatrix is present among chert-dominated sandstone. (Well 100/08-26-065-11W6/00; 2884.7 m; XPL) **C)** Microfractures and partial leaching of grains are common to abundant. (Well 100/05-32-065-09W6/00; 2908.1 m; PPL) **D)** A SEM image of micropores created due to partial dissolution of plagioclase feldspar. (Well 100/03-18-066-08W6; 2468.6 m) **D)** A SEM image of quartz grains being tightly compacted together without sutured contacts, only concavo-convex contacts. (Well 100/03-18-066-08W6; 2468.6 m) **E)** A SEM image of kaolinite cements present in considerable amount yet undetected during routine petrography. (Well 100/03-18-066-08W6; 2468.6 m)

well-sorted sandstone (Fig. 3.11B). This relatively anomalous sandstone compared to other Falher F chert arenite may be easily mistaken as a wacke if one misinterprets the ferroan dolomite cement as epimatrix. Iron oxide cement is also present throughout all samples (Fig. 3.11C).

Dolomite replacement appears on the rims of quartz as well as the outer boundaries of chert and rock fragments (Fig. 3.11B). The latter feature, however, was restricted to only a few samples. Goldstein and Rossi (2002) reported that earlier overgrowth zones may be unstable, thus allowing more stable quartz overgrowth to result from recrystallization of the less stable phase. In the Falher F, the presence of dolomite as the rims of quartz grains may indicate that initial, unstable quartz overgrowth was replaced by the dolomite before more stable quartz overgrowths could nucleate.

Thin section porosities are generally lower than porosities obtained from core analyses where poorly-defined pores occur, which range from 1.4 to 6.8%. Dissolution of chert and rock fragments is the main mechanism by which secondary porosity developed. Thus, even though chert and rock fragments compactional interactions are responsible for nearly all of the porosity loss, they may compensate a few percent of the loss through the succeeding dissolution (Harris, 2014). The ratio as to how much primary porosity loss was caused by pseudomatrix versus how much secondary porosity was gained through subsequent leaching is questionable, but the resulting porosity percentage suggests that the presence of chert and rock fragment pseudomatrix may not compromise the porosity to an extreme degree.

X-Ray Diffraction Results

Similar with other petrofacies, analyses performed on four samples resulted in a higher amount of albite, smectite/illite, and kaolinite than what point counting suggested (Table 3.3). There is an observed tendency for kaolinite to show marked abundance where samples have common partially dissolved framework grains. Poorly defined laths of a high birefringence mineral typical of illite are also scattered in those pore spaces. It is possible that clay-sized minerals accumulated in those restricted spaces but were failed to be detected during the thin section analysis.

Scanning Electron Microscope Results

SEM analyses performed on sample 100/01-08-066-08W6/00 (2585.2 m) shows an abundance of ferroan dolomite. Figure 3.11D display the simultaneous occurrence of quartz overgrowths and associated ferroan dolomite cement. There is also rare intercrystalline porosity within ferroan dolomite grains (Fig. 3.11E). These features occur below the level of resolution of conventional thin section petrography, indicating that the presence of pores is likely more extensive than what can be observed in thin sections.

PETROFACIES V: SUBMATURE-MATURE, CALCITE-, DOLOMITE-, AND QUARTZ-CEMENTED CHERT ARENITE

Petrographic Results

This petrofacies occurs within lithologies interpreted to represent a wide range of depositional environments, from lower, middle, and upper shoreface to estuarine. This submature to mature sandstone consists of poorly- to moderately-sorted, lower very fine- to upper fine-grained sandstone with angular to rounded grains. The average composition is $Q_{40}C_{35}RF_{25}$. Within this petrofacies, the sandstone may be quartz-, chert-, or rock fragment-dominated.

The combination of authigenic cement and replacement in this petrofacies is also the most complex among the Falher F sandstone. Apart from quartz overgrowth, ferroan dolomite, and dolomite, pervasive cementation by calcite is also observed (Fig. 3.12A). Very rarely, ferroan calcite cement is also mixed with calcite cement with no distinctive boundaries or transition. Non-ferroan calcite and dolomite also occur as replacement minerals. Iron oxide cement is commonly

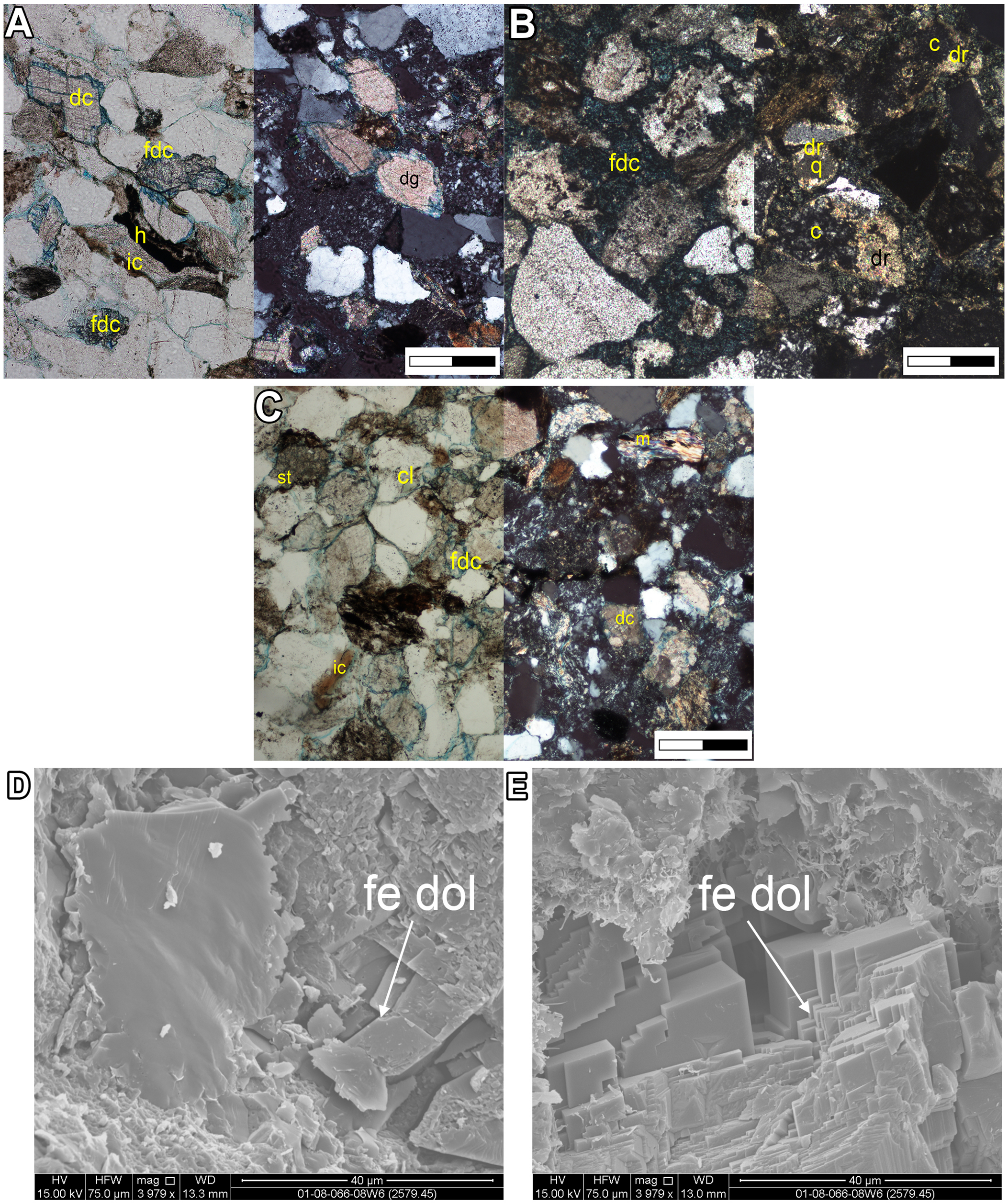

Figure 3.11. Samples representing petrofacies IV. Scale for thin sections is 0.1 mm. **A)** Dolomite grains and cements are both enclosed by ferroan dolomite rims. The cleaner, euhedral-shaped dolomite with uniform grain size is indicative of allogenic attribute. Note the present of dusty rims on dolomite grain labelled "dg", strengthening the evidence of grains due to the presence of cement overgrowth and subsequent ferroan dolomite rims. (Well 100/05-32-065-09W6; 2914.1 m; PPL | XPL) **B)** Sample with an anomalous feature of ferroan dolomite. The major cement is texturally early ferroan dolomite, based on the observation that the cement being accumulated in an extensive intergranular primary porosity. Dolomite cement has also corroded the outer rims of quartz grains, chert, and other rock fragments. (Well 100/01-08-066-08W6/00; 2585.2

m; PPL | XPL) **C)** Thin iron oxide lining occurs among grains, most visible on the left slide closer to the stylolite. (Well 100/14-24-065-10W6/00; 2777.5 m; PPL | XPL) **D)** Quartz grains with visible overgrowths among ferroan dolomite cement, indicating that both of the overgrowths and ferroan dolomite probably occur simultaneously. **E)** Intragranular microporosity is present in a feldspar grain. Similar feature may be present in many samples but is failed to be noticed under regular thin section observation.

Present at a considerable amount. In very few samples where secondary porosity is prevalent, for instance in well 100/07-13-066-09W6/00 (2531.3 m), kaolinite also fills the spaces (Fig. 3.12B). Rock fragment pseudomatrix appears to be common, even though the prevalent carbonate cement commonly interferes with its recognition.

Thin section porosity and core porosity generally yield similar amounts, ranging from 0.8 to 4.7%. Dissolution along point contacts is most commonly observed, with lesser abundance of framework grain dissolution. These secondary pores may form a well-defined network.

X-Ray Diffraction Results

Consistent with other petrofacies, analyses performed on sample 100/07-13-066-09W6/00 (2521.6 m) exhibit a higher percentage of albite, smectite/illite, and kaolinite than thin-section analyses indicate (Table 3.3). Similar textures are noted between this sample and XRD samples for petrofacies III, indicating that textures may complicate observation in thin sections to the point wherein much of the proportion of clay-sized components is not able to be considered significant.

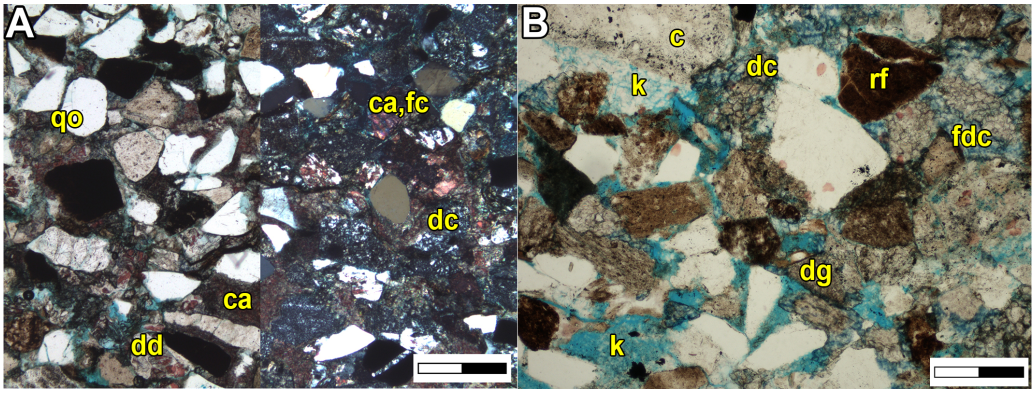

Figure 3.12. Samples representing petrofacies V. Scale is 0.2 mm. **A)** All types of carbonate cement are present. Note that dissolution is pervasive (bottom left) where dolomite is also pervasive, possibly indicating dolomitization that generated subsequent pores. (Well 100/07-13-066-09W6/00; 2517.5 m; PPL | XPL) **B)** Outsized pores with kaolinite filling, similar to samples of petrofacies II, locally occur. (Well 100/07-13-066-09W6/00; 2531.3 m; PPL)

COMPOSITIONAL VARIATIONS AND DISTRIBUTIONS

Petrographic results have shown that there is very minor readily observed relationship between petrofacies and ratios of detrital compositions. The relationship between assigned petrofacies and detrital compositions is generally limited to the division of rock fragment-rich (i.e. petrofacies III to V) and rock fragment-depleted (i.e. petrofacies I and II), as well as an exemplary case in petrofacies II and III that consists of entirely quartz- and chert-dominated sandstone, respectively. No apparent trend on quartz versus chert ratio is observed. Thus, the relative abundance of chert to define the sandstone drillability is analyzed using triangular plots of Q, C, and RF values instead. For this plot, data points are colour-coded based on their interpreted depositional environments or facies associations and shape-coded based on their occurrence in the depositional succession (see also Table 3.1; 3.2). Corresponding petrofacies are not reflected on data points, due to reasons stated earlier.

Trends are discussed based on comparisons of samples across different depositional environments, parasequences, and palaeogeographic context, all of which are based on observations in Chapter 2. To summarize, samples were collected from parasequence FP2, FP3, and subsequent transgression. Isopach maps of all parasequences and conglomerate accumulation, including FP1 and FP4 that are unrepresented in core, reveal northward progradation with palaeoshoreline evolutions trending ENE-WSW to E-W (Figs. 3.13A, B, C, D; 3.14). Conglomerate bodies of older, depleted conventional reservoirs accumulate only in the FP3 palaeoshoreline, resulting in two separate accumulations that thin westward (Fig. 3.14). The conglomerate accumulation was proposed by Nodwell and Hart (2006) and Meloche (2011) to have been a product of a palaeotopographic step associated with the Devonian Gold Creek reef trend (Nodwell and Hart, 2006) or tectonic-induced (Meloche, 2011), rather than due to relative sea level fall. Chapter 2 supported this idea due to the absence of evidence for a regressive surface of marine erosion below the conglomeratic parasequence and similar compositions between conglomerate-rich parasequence and the underlying normal regressive succession. The isopach map of the conglomerate bodies indicates the local presence of distributary channels contemporaneous with conglomerate deposition (Fig. 3.14). Formation top maps of parasequence FP2 and FP3 are also presented to display the lateral continuity of marine deposits from each succession (Figs. 3.15A, B). All data points available are presented in Figure 3.16A.

DEPOSITIONAL ENVIRONMENT-DEPENDENT TREND

Twenty-four samples were collected from shallow marine depositional units, and 12 were taken from fully marine units. A nicely divided trend can be established for samples deposited in each environment (Figs. 3.16B, C). Sandstone deposited in upper shoreface to foreshore (beach) settings is

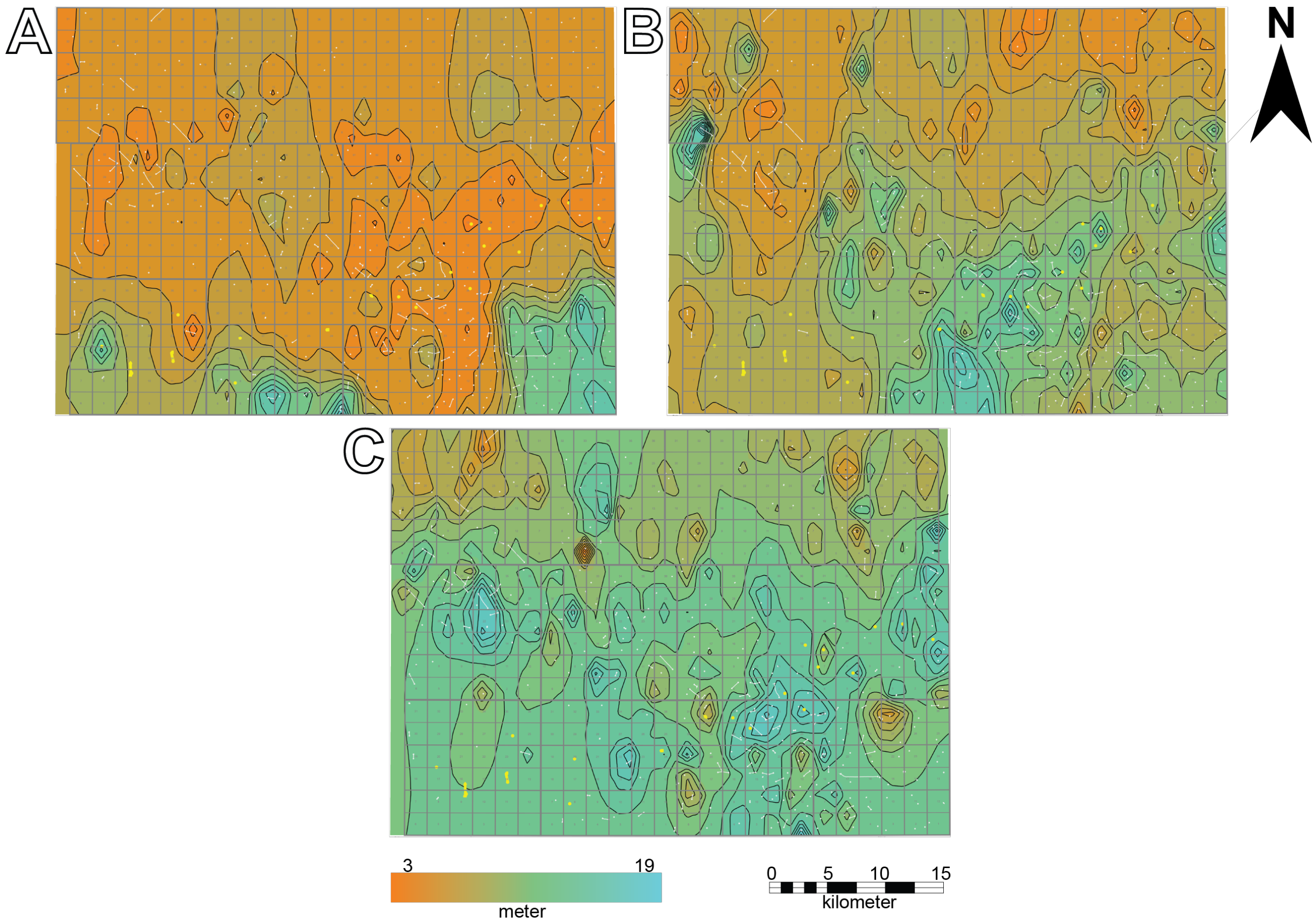

Figure 3.13. Isopach maps of the Falher F shoreface bodies deposited during parasequence: **A)** F_P1, **B)** F_P2, and **C)** F_P3 time.

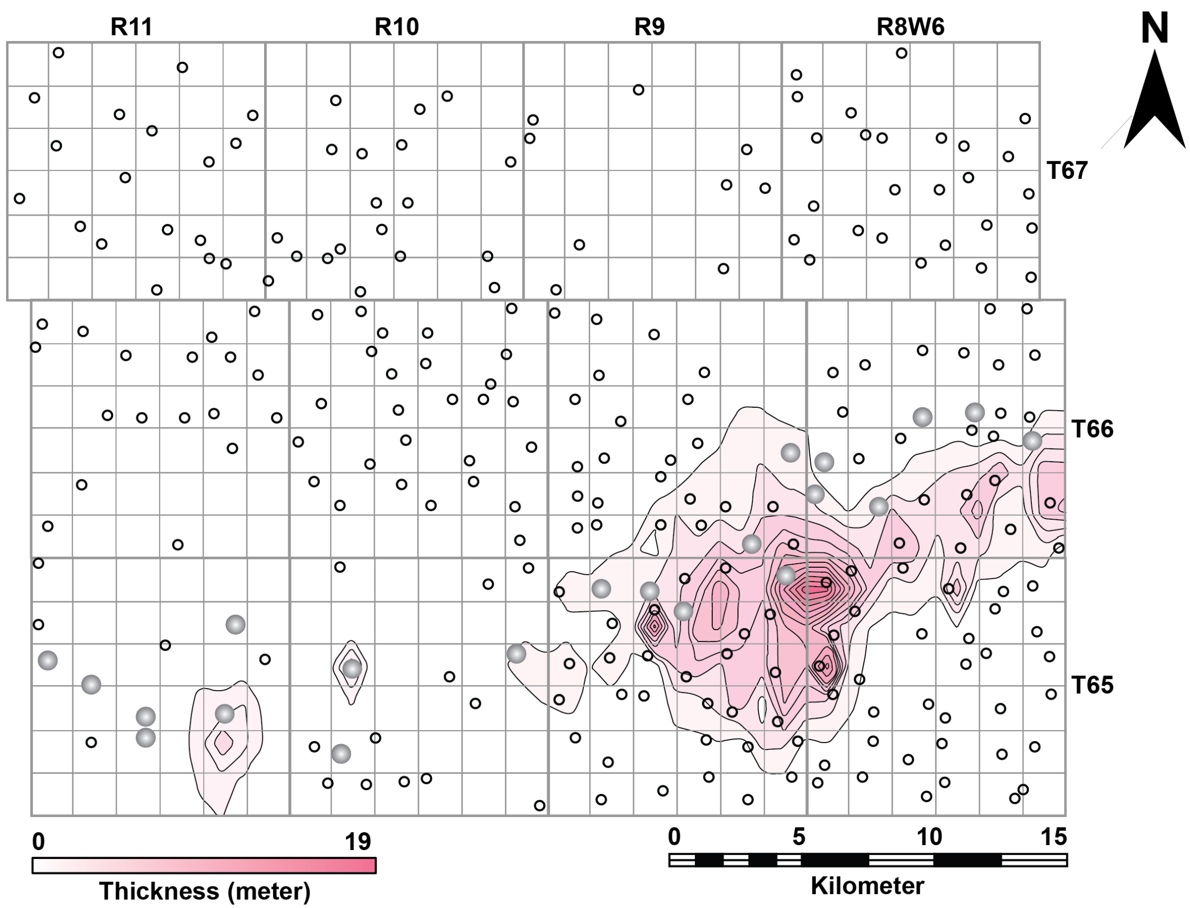

Figure 3.14. Isopach map of conglomerate bodies in parasequence F_P3. The orientation shows a WSW-ENE trend approximately N75ºE. Note the separate depocentres in the western and eastern area.

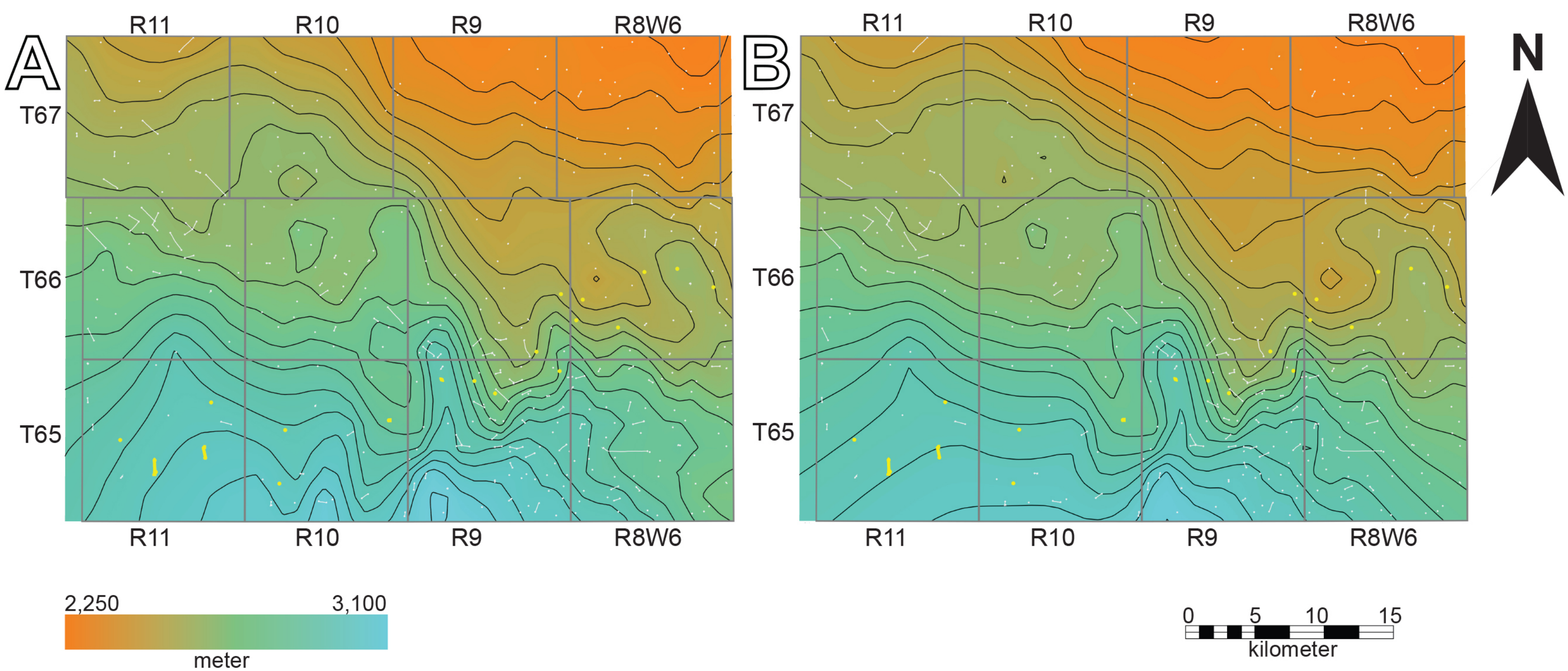

Figure 3.15. Formation top maps of parasequences: **A)** F_P2 and **B)** F_P3.

dominated by quartz or the combination of quartz and chert, typical of products of intense, continuous winnowing and sorting by wave actions (Pettijohn, 1975). On the other hand, sandstone deposited in the more seaward settings is dominated by sand-sized detrital chert. Even though minor variations exist, the general trend is strong and coherent. Plint and Norris (1991) as well as Krassay (1994) found that where shoreface gradients are low, storm energy is capable of eroding the sea floor as well as transporting chert basinwards, regardless of the relative sea level condition. The shallow depth reported from the Cretaceous epeiric seaway of WCSB (Cant, 1984) thus may support a similar mechanism for chert- and quartzite-rich sandstone accumulation basinward.

In the transgressive succession, the sandstone appears to have a much more diverse composition (Figs. 3.16B, C). Samples range from quartz-dominated, chert-dominated, to rock fragment-dominated. This may be controlled by the more complicated energy system, which is the mixed results of fluvial, tidal, and wave energy.

PARASEQUENCE-DEPENDENT TREND

Where samples that are deposited in similar depositional environments have contrasting Q:C ratios, they may have been deposited during different temporal intervals (i.e. different parasequences), record different distances from fluvial point sources, or record subtly different energy levels. Relatively anomalous middle to lower shoreface sandstone units where Q:C > 1 (quartz-dominated) are restricted to a population taken from parasequence F_P3 (Fig. 3.16B), as are upper shoreface to foreshore sandstone units with Q:C < 1 (chert-dominated) (Fig. 3.16C). An exception occurs in a shallow marine sample from well 100/08-02-066-09W6/00 (2579.8 m) taken from parasequence F_P2 (Fig. 3.16C), but due to the very subtle difference (Q:C ~1), this anomaly is considered to be insignificant.

Other samples from parasequence FP3 follow the general trend (Fig. 3.16E), as do all samples from parasequence FP2 (Fig. 3.16D). This likely indicates a change in dispersal mechanism from parasequence FP2 to FP3.

In general, parasequence FP3 is also dominated by samples that have overlapping compositions with one another (Fig. 3.16E), regardless of the depositional settings, whereas parasequence FP2 exhibit cleaner separation between samples of contrasting depositional environments (Fig. 3.16D). The most evident change across the two parasequences is the presence of conglomerate bodies in the younger parasequence. Therefore, further comparison involving the conglomerate-associated control is discussed below.

PALAEOGEOGRAPHY-DEPENDENT TREND

Core studies presented in Chapter 2 indicated the possible locations for distributary channels that provided sediments to the Falher F deltaic shoreface during deposition of parasequence FP3 (Figs. 3.16F, G). Samples from this stratigraphic time that are deposited adjacent to the distributary channel have more variable Q:C ratios than samples deposited away from the channel (Figs. 3.16F, G, respectively). The latter shows a more closely linked compositional distribution, as opposed to the former in which samples are more scattered on the plot. This suggests that proximity to a fluvial point source may have been an important control on sediment composition. Thus, the predictability of detrital composition is complicated as wave energy, proximity to a fluvial point source, and the nature of the fluvial system (i.e. overall energy and corresponding ability to erode and deliver clasts from chert bedrock) simultaneously affected mineralogical compositions in local settings.

According to the palaeogeographic framework, there are two distinct river mouth-associated depocentres in the study area. When samples from the east (Fig. 3.16H) are compared with the west (Fig. 3.16I), the western datasets

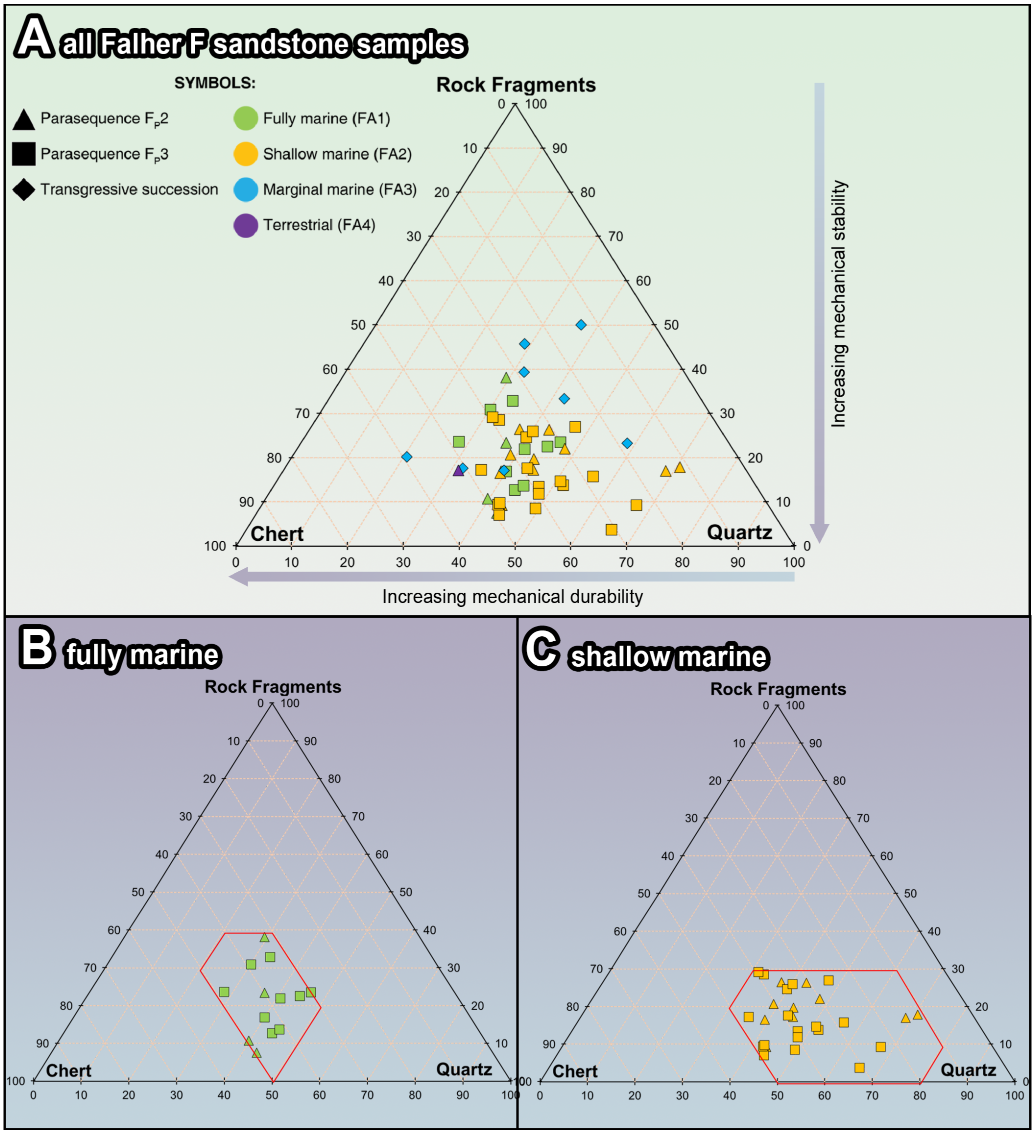

Figure 3.16. Ternary diagrams showing relative proportion of quartz, chert, and rock fragments in the studied tight sandstone. Data points are colour- and shape-coded according to their depositional environments and parasequences. **A)** Data points from all samples are presented. Note that samples show an increasing mechanical stability from the more terrestrially-influenced to marine-influenced sandstone. **B)** Plot for samples deposited in the most distal position (i.e. storm-dominated shoreface and distal delta front). Note that nearly all samples are chert-dominated, and samples that are more quartz-rich are restricted to samples from parasequence F_P3. **C)** Plot for samples deposited in the proximal portion of the basin (i.e. wave-dominated shoreface and proximal delta front). Note that nearly all samples are quartz-dominated, and samples that are more chert-dominated are restricted to samples from parasequence F_P3, similar to (B).

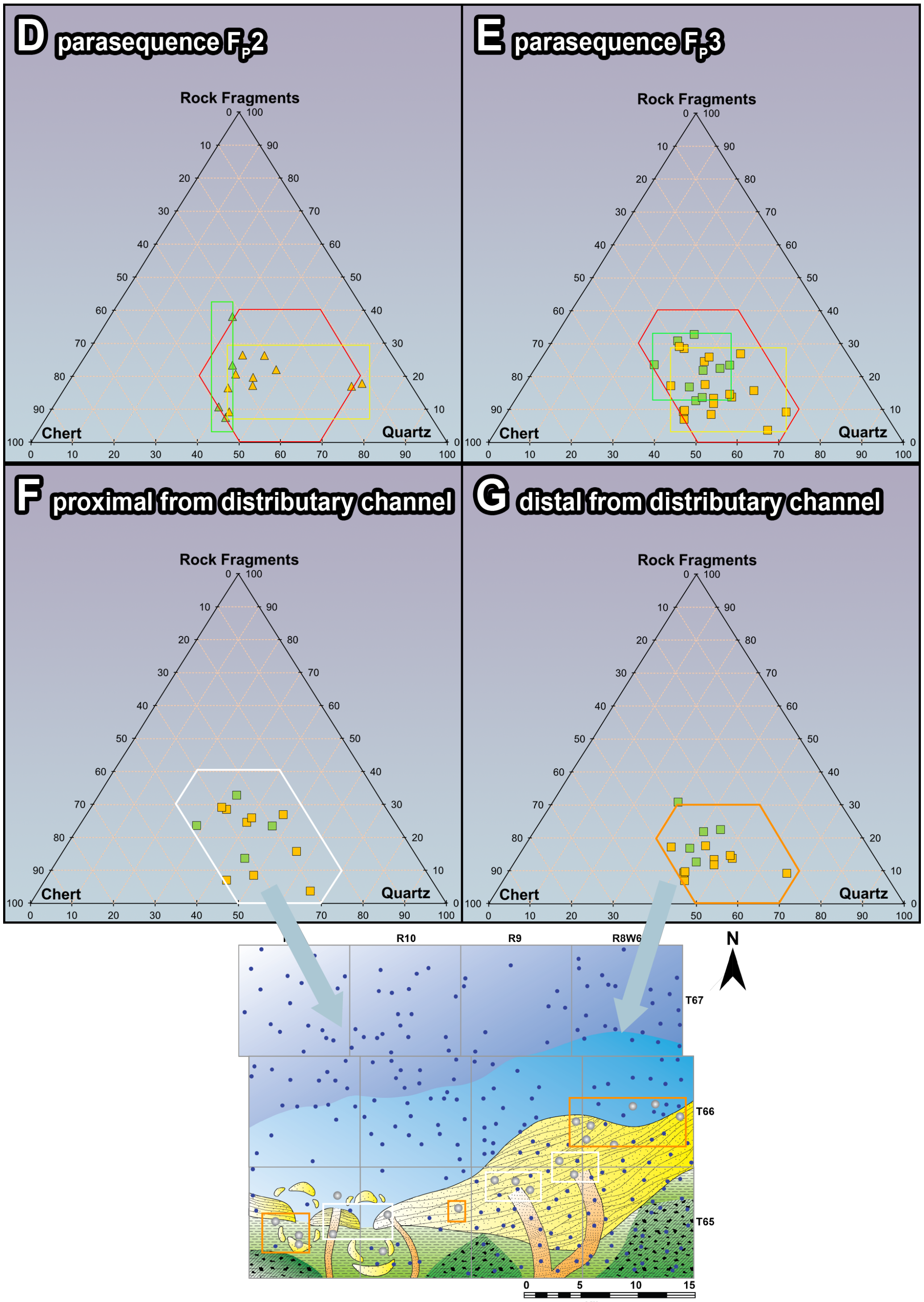

(cont.) **Figure 3.16. D)** Plot for samples deposited during parasequence F_P2 time, with available samples from fully marine and shallow marine samples only. **E)** Plot for samples deposited during parasequence F_P3 time, with available samples from marine samples only. **F)** Plot for samples deposited adjacent to distributary channel. Note that although there are similarities between compositional ratios of different samples, they generally exhibit more variable compositions than the (G) plot. **G)** Plot for samples deposited adjacent to distributary channel. Note that samples tend to share closely similar compositions as opposed to the (F) plot.

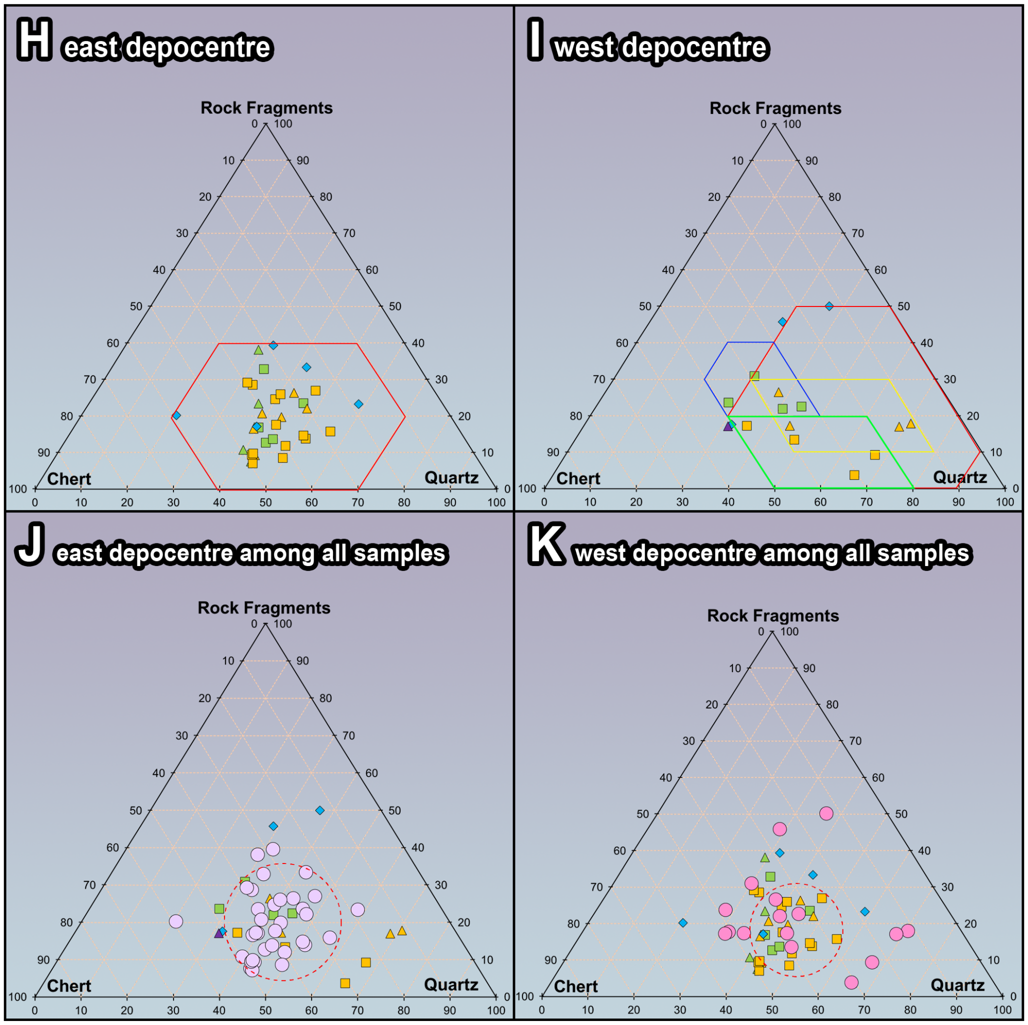

(cont.) **Figure 3.16. H)** Plot for samples deposited in the eastern depocentre. Note that compositions tend to overlap with each other with a very little separation. **I)** Plot for samples deposited in the western depocentre. Note that samples from different depositional environments generally have contrasting compositions. **J)** Distribution of samples from the eastern depocentre as compared to all samples used for this study. Most samples tend to be inside of the circle of reference. **K)** Distribution of samples from the western depocentre as compared to all samples used for this study. Most samples tend to be outside of the circle of reference.

samples exhibit more contrast in the Q:C ratio of proximal versus distal samples. On the other hand, eastern datasets tend to be considerably more uniform and coherent, with very minimum to almost no contrast across different depositional environments. This implies that channel type perhaps differs between the two regions, which is also indicated by two separate conglomerate bodies that occur in the two areas. c *et al.* (1993) postulated that meandering rivers have a more distinctive signature once arriving in deltaic settings than braided rivers do, even though subsequent marine reworking typically overprints much of the original deposits. However, considering the relatively small extent of the study area, it is questionable whether or not two different river systems can be present side-by-side. Regardless, the controls may be of similar concepts, where one downstream end has a persistently higher source of energy as compared to the other.

DISCUSSION

CHERT ABUNDANCE FAIRWAY

In the Wapiti area, Falher F conglomeratic deposits occur in two discrete depocentres in the west and east direction (Fig. 3.14). However, samples from both areas constitute similar petrofacies and lithofacies (Chapter 2), implying considerable relationship within a likely same river system. Sandstone samples from the two depocentres only differ primarily in the Q:C ratio. The variance in plots of sandstone composition suggests that two related but distinct fluvial delivery systems (i.e. similar source but distinct channel type and corresponding transport distance) were responsible for changes in compositional ratios across the study area.

Samples from western areas consistently exhibit compositional ratios that are dominated by one endmember. Regardless of the stratigraphic interval, all distal and proximal samples from the western wells are chert- and quartz-dominated, respectively (Fig. 3.16I). Moreover, data points from this area are commonly located closest to each endmember among all Falher F samples, indicating the most distinctive and contrasting compositions (Fig. 3.16K).

On the contrary, data points from the eastern area do not normally show extreme adjacency to any single endmember (Fig. 3.16H). Their composition appears to be more uniform, with Q:C ratios that are rather similar for both proximal and distal samples. When all distal and proximal samples are plotted together, their compositions strongly overlap with each other (Fig. 3.16J).

It can be deduced that in the western point source, fluvial energy was likely lower than in the eastern point source. It was probably not strong enough to transport relatively more abundant coarse chert to the basin, as evidenced by less laterally extensive chert-rich conglomerate accumulations. This also implies that sand-sized chert in the basin had perhaps been the results of primarily reworked coarser chert clasts (Harrell and Blatt, 1978; McBride and Picard, 1987; Yagishita and Ohkubo, 2007). As well, the low energy of the western channel was likely inadequate to dominate the depositional signature, and therefore, marine forces predominated and resulted in a strongly wave-reworked succession. This is the opposite of the trend observed at the mouth of the eastern fluvial system. Wave reworking sorted shoreface sand bodies in the west more effectively than those in the east, leaving sandstone beds that are strongly quartz-dominated in the foreshore and upper shoreface. Basinward, in storm-dominated settings, the sandstone is strongly chert-dominated due to rapid transport out of the zone of daily wave reworking. Therefore, the fluvial channel in the west may have meandered more, undergone longer travel distance, or comprised a smaller branch of the main channel in the east.

In contrast, the fluvial energy in the eastern channel was likely strong enough to be able to deposit sediments of identical compositional ratios from proximal to distal areas. The channel may have been a more braided type, had a shorter transport distance from source to sink, or comprised the major feeder channel in the region. Thus, evidence of wave reworking is less pronounced relative to the western region, although still significant.

Due to the local scale of the study area, it is thus less likely that the area possesses two different river systems across relatively narrow distance (approximately 10 km). Present-day wave dominated deltas such as Brazos River in Texas (Rodriguez *et al.*, 2000), Costa de Nayarit in Mexico (Curray *et al.*, 1969), and Grijalva Delta in Mexico (Psuty, 1967) are among the many examples in which across 20 km or less distance, there are only channels sourced from a single river system. However, minor trunks may branch out from the major feeder channels in those deltas. Therefore, it is interpreted here that based on present-day examples, the eastern channel may have acted as the primary conduit, whereas the western fluvial feeder was bifurcated from that older channel, regardless of the river system type.

This interpretation also helps to explain the presence of two distinct conglomerate bodies in the Wapiti area, with the western lobe being more laterally limited than the eastern. Regardless of Nodwell and Hart's (2006) interpretation that conglomerate accumulations in the study area resulted from structural control, distinct differences in fluvial feeder channel type may also explain the geometry of the deposits and their separation into two distinct lobes.

This suggests that, across Wapiti area, controls on the distribution of chert versus quartz is related to the nature of local fluvial systems and marine depositional processes. Additionally, regardless of the channel type, chert should be more dominant across depositional dip basinward. Based on these, the Falher F sandstone in the study area can be grouped into four categories of different relative proportion of chert versus quartz, which corresponds to specific depositional area (Table 3.6). The mineralogically least drillable sandstone with the highest relative proportion of chert can be found in the fully marine sandstone. The order towards the mineralogically most drillable sandstone is followed by shallow marine sandstone in eastern depocentre that is proximal from distributary channel, shallow marine sandstone in eastern depocentre that is distal from distributary channel, and shallow marine deposits in western depocentre, respectively (Table 3.6; Fig. 3.17).

Based on this distribution, the replacement of drilling bit when performing horizontal drillings are expected to be reduced when horizontal wells are directed landward to the south, or along strike westward towards the minor trunk, or away from any of the fluvial feeders or deltaic positions (approximately T65 9W6 and T65 10W6) along strike towards the more strandplain locations (Fig. 3.17); as the wells go towards or along sandstone deposits that are compositionally more favourable from the penetrability standpoint. Formation tops of parasequence F_P2 and F_P3, where major tight sand reservoirs of the Falher F occur, also reveal that the areas parallel to the depositional strike westwards from the major trunk in T65 R9W6 have laterally extensive Falher F sandstone units across a consistent depth (Figs. 3.15A, B). Therefore, horizontal wells are more likely to penetrate the same depositional lithofacies from the same parasequence, which likely to have more homogenous mineralogical properties and thus drillability.

Table 3.6. Index of relative proportion of chert within the studied tight sandstone. It is recommended here that drilling bit replacement and/or low rate of penetration that are controlled by chert abundance may be minimized when drilling along intervals with the same relative abundance of chert, or from higher to lower abundance.

Relative Proportion of Chert	Quartz vs. Chert Ratio	Palaeogeographic Distribution
Low	Avg. 2.5	Shallow marine deposits in western depocentre
Moderately high	Avg. 1.4	Shallow marine deposits in eastern depocentre, distal from distributary channel
Moderately high	Avg. 1.1	Shallow marine deposits in eastern depocentre, proximal from distributary channel
High	Avg. 0.9	Fully marine deposits

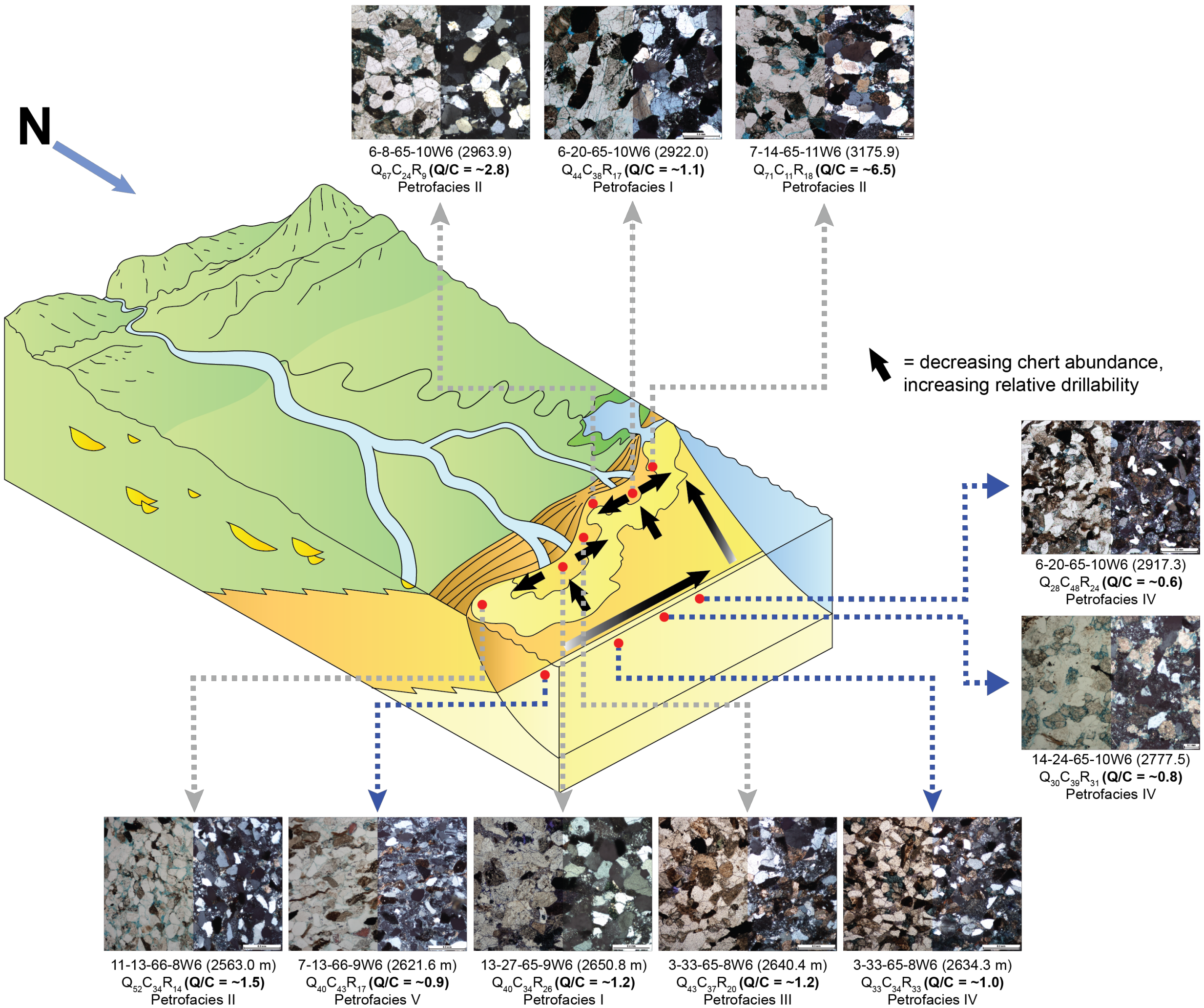

Figure 3.17. Block diagram showing the distribution of various sandstone samples with various relative abundance of chert clasts. Petrographic images of representative samples are displayed. Note that chert content increases basinward, and along palaeoshoreline towards settings with higher energy.

DIAGENETIC HISTORY

It is important to understand the evolution of pore-reducing and pore-enhancing mechanisms of the sandstone bodies. Tilley and Longstaffe (1989) utilized stable isotope analyses as an aid in developing a diagenetic evolution model of the Falher Member in the Deep Basin. Although these analyses provide a robust basis to explain changes that occurred throughout the authigenic processes on a relatively regional scale, local variations occur in the Falher F submember of the Wapiti area and are addressed below.

Here, the terms eodiagenesis and mesodiagenesis are used for the paragenetic sequence interpretation. These terms were first introduced by Choquette and Pray (1970) for sedimentary carbonates but has been adapted by siliciclastic workers accordingly. Schmidt and Macdonald (1979b, p. 177) defined eodiagenesis as "the regime at or near the surface of sedimentation where the chemistry of the interstitial water is mainly controlled by the surface environment prior to effective burial," and mesodiagenesis as "the subsurface regime during effective burial." The paragenetic sequence is summarized in Fig. 3.17, and interpretation provided here is mainly based on the observed textural relationship between each authigenic mineral. The complete series of diagenetic evolution below are only expressed in petrofacies V, which preserves all types of cement, but can be implemented accordingly to petrofacies I through IV by disregarding authigenic minerals that are not present within the concerning petrofacies.

Eodiagenesis

Marine waters during the earliest stage of deposition were likely already in a reducing state due to the abundance of organic matter associated with deltaic deposition. This promoted the early precipitation of chlorite in petrofacies I to V, as observed from the incorporation of chlorite by subsequent quartz overgrowth and dolomite cement (Fig. 3.5E). This observation contrasts Tilley and Longstaffe (1989) who discovered significant amount of chlorite north of T71 and siderite in the opposite direction, as the Falher F in the study area typically lacks siderite.

Anoxic pore waters also supported the subsequent early formation of pyrite, possibly at the expense of chlorite and detrital ferromagnesian minerals such as biotite. The minor amount of pyrite observed, which is restricted to petrofacies III and IV likely indicates relatively high sedimentation rates during deposition, based on its requirement of long period of exposure to the seawater to produce iron sulphide (Bjørlykke, 1983). This is consistent with regressive conditions along a deltaic setting.

Quartz overgrowth is assessed as one of the earliest cements throughout petrofacies I to V. The absence of inclusion of any authigenic minerals in the overgrowths and common syntaxial textures, which occupied most of the primary pores in petrofacies I, supports this interpretation (Fig. 3.6A). This suggests that the silica was precipitated before other authigenic materials had been emplaced and before mechanical compaction had significantly reduced pore spaces. The rare sutured and stylolitized contacts precludes the likelihood that burial-induced pressure solution was the primary source of silica, although it is acknowledged that these processes may be significant on a local scale. Dissolution of biogenic silica from detrital chert (McBride, 1983; Bjørlykke and Egeberg, 1993), silica byproducts from early kaolinization of feldspars (Keller, 1978; Worden and Morad, 2003), and later, dissolution of quartz from increasing pH due to the almost parallel formation of early carbonate cement (Siever, 1962) are more likely sources of the silica requisite for early quartz overgrowths.

Based on the evidence of kaolinite booklets being incorporated into its surrounding dolomite and ferroan dolomite cement (Fig. 3.9A), the breakdown of plagioclase-type feldspar likely occurred very early. These minerals provided loci in which kaolinite subsequently precipitated throughout petrofacies II to V (McBride, 1985) (Fig. 3.12B). This reaction may also produce smectites (Hower *et al.*, 1976), as observed in an XRD sample (Table 3.3; well 100/05-32-065-09W6/00, 2917.7 m).

Early ferroan dolomite cement was observed in only a single sample as a rather exceptional case among other Falher F sandstone (Fig. 3.11B). Meyer (2003) interpreted early ferroan dolomite cement to be controlled by the mixing of freshwater and saline water in a prograding storm-dominated shoreface associated with an estuarine system. The very localized occurrence of this cement in the Falher F may indicate anomalous conditions wherein similar mechanisms temporarily occurred.

Mesodiagenesis

With increasing temperature during burial, minerals with strong hydrous properties, such as smectites and kaolinite, may become unstable and generate less hydrous mineral phases (Bjørlykke, 1983). Dewatering from these reactions may trigger dissolution of other minerals, creating secondary porosity or promoting mineral replacement. Increasing temperature also promoted chemically unstable minerals, most commonly ferromagnesian minerals (i.e. lithic grains from volcanic rock fragments and micas), to become more prone to dissolution. The resulting Mg and Fe ions became more readily available to enter new mineral phases, due to the decreasing hydration effects on those ions that commonly occur at the surface temperature (Usdowski, 1968). The increasing abundance of Mg and Fe encouraged the formation of dolomite as early burial cement in petrofacies IV through V (Morad, 1998). Authigenic dolomite may also replace unstable silica phases nucleating on quartz grains and create overgrowths similar in appearance to quartz overgrowths but composed of dolomite rims instead (Goldstein and Rossi, 2002) (Fig. 3.11B). Later, with enhanced reducing conditions with depth, the absence of sulphide minerals facilitated the incorporation of dissolved Fe ions into ferroan dolomite in petrofacies II through V.

The dissolution of carbonate detritus and carbonaceous debris provided Ca and C ions to produce calcite cements (Blatt, 1979). The localized and discrete accumulation of calcite among Falher F sandstone in the study area, which is limited to petrofacies V only, probably confirms the lack of Ca-rich feldspars in the Falher F. Therefore, the source of Ca and C ions relied solely on the scattered presence of calcareous and carbonaceous matters (i.e. bioclasts, plant debris, and so forth). The onset of calcite precipitation probably overlapped with the formation of dolomite and ferroan dolomite cement, as is indicated by the three carbonate cements incorporating each other into their occupying pores (Fig. 3.12A). Calcite and ferroan calcite were possibly the last to precipitate among other carbonate minerals. At some point, when the pore waters became saturated with respect to Ca, Mg ions were removed and thus dedolomitization took place (Fig. 3.12A). During these processes of carbonate cementation and simultaneous replacement on chert and other grains, the silica source was constantly replenished and provided prolonged stages of quartz overgrowth formation (Dapples, 1959; Schmidt and MacDonald, 1979a).

Illite is observed to occur over quartz overgrowths and, more commonly, squeezed between compacted grains in petrofacies II through V (Figs. 3.11A, C). Therefore, it was likely to form via illitization of smectites following the extensive formation of quartz overgrowths, but prior to significant mechanical compaction. Metallic ions requisite for illite formation were likely sourced internally from the abundance of argillaceous rock fragments (Blatt, 1979). This was aided with degradation processes of feldspars and ferromagnesian minerals as discussed above.

With burial, mechanical compaction became significant in chert- and malleable rock fragment-rich units, and was responsible for the formation of pseudomatrix that caused primary intergranular porosity loss in petrofacies III through V. The impacts of pseudomatrix are not pronounced in petrofacies I and II, as they are generally depleted in rock fragments. Thus, the primary intergranular porosity is still retained in petrofacies I and II, albeit to a minor extent. With the subsequent maturity of kerogen, dissolution was intensified by decarboxylation of the organic matter during bitumen maturation (McBride, 1979), creating secondary porosities across all petrofacies. This leaching particularly affected chert and rock fragments, therefore compensating the impacts of intergranular porosity loss promoted by the preceding formation of pseudomatrix. Tilley and Longstaffe (1989) suggested that following the maximum burial, the Falher units underwent large-scale uplift that promoted influx of meteoric water. Flushing of meteoric water thus may also contribute to the further creation of secondary porosities (Morad *et al.*, 2010). Based on the widespread and common occurrence of secondary porosities in the study interval, these processes were likely to have occurred at a large scale and thus provided the Falher F tight sandstone with well-defined network of porosities, either as pores that are visible in thin sections or micropores that are only detectable by SEM analysis.

Table 3.7. Paragenetic sequence of the studied tight sandstone. Interpretation is based on textural relationships among various diagenetic events.

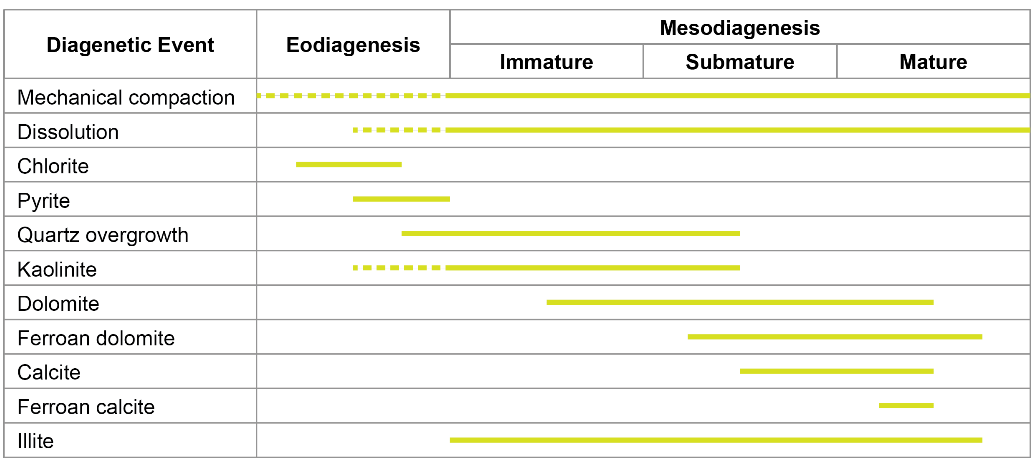

CONCLUSIONS

Within the lower Albian Falher F chert arenite in the Wapiti area, the following attributes can be concluded:

1. There are five petrofacies in the Falher F chert arenite, with each one exhibiting an increased degree of complexity in terms of its paragenetic sequence and decreasing maturity from petrofacies I to V. In the cleanest quartz-dominated sandstone, quartz overgrowth is the only interstitial cement. In the dirtier sandstone, porosity is significantly reduced by any

combination of quartz overgrowth, kaolinite, dolomite, ferroan dolomite, calcite, ferroan calcite, iron oxide, illite, pseudomatrix from rock fragments, or welded chert clasts.

2. In regard to the chert-controlled sandstone drillability, there is very minimum direct relationship observed between each petrofacies and quartz to chert ratio. This is due to the combination of sandstone from various depositional environments within each petrofacies, which is proven to be the most dominant control of chert distributions. Exceptions apply in petrofacies II and III, where quartz and chert each predominates the petrofacies, respectively.

In terms of determining the chert-controlled drillability fairway of a wave-dominated delta and shoreface, with examples from the lower Albian Falher F chert arenite, the followings can be pointed out:

1. The petrographic approach is a low-cost, yet valuable tool as an initial approach to evaluate sandstone drillability. Although applicable to all sandstone-hosted reservoir units, it is most readily applied to successions that are subject to relatively homogenous energy type (i.e. shoreface, wave-dominated delta, or fluvial channel) similar to those discussed in this study. It should be expected that within environments exposed to the mixings of various fluvial, marine, tidal, and/or other forces such as aeolian and glacial processes, changes may be significantly more complicated and challenging to interpret.
2. In the Falher F, the contrasting Q:C ratio is predominantly controlled by: 1) depositional environments (i.e. wave-dominated versus storm-dominated setting); 2) proximity to the shoreline (i.e. changes in a dip-direction), 3) the nature of fluvial feeder systems (i.e. local fluvial channel type), and 4) proximity to distributary channels.
3. In light of point 4 above, exceptions may include structural influences and changes in depositional systems tract, therefore fluvial style and relative sea level changes. In the Falher F, there may be a local structural influence, but the degree to which this structure can affect the Q:C ratio

is not analyzed here. With the current datasets in a relatively small area, the suggested channel type alone appears to be sufficient to delineate the changes along the palaeogeographic constraints.

4. In the interest of utilizing horizontal wells to drill into horizons with more constant drillability levels, it is recommended to drill along strike westward towards the minor trunk, or away from any of the fluvial feeders or deltaic positions (approximately T65 9W6 and T65 10W6) along strike towards the more strandplain locations. This way, intervals encountered would be from the similar depositional setting, parasequence, and less fluvially-influenced, thus similar Q:C ratio. Another suggestion is to place horizontal wells that are directed landward to the south, as the wells supposedly advance towards sandstone with lower ratio of quartz vs. chert thus avoiding or minimizing the drilling bit replacement.

In terms of the porosity and diagenetic history of the Falher F, the followings may be pointed out:

1. Early diagenesis cement in the Falher F include quartz overgrowth and kaolinite, whereas burial diagenesis cement includes the continuation of quartz overgrowth and kaolinite, followed by dolomite, ferroan dolomite, illite, calcite, and ferroan calcite in sequential order.
2. Malleable rock fragment pseudomatrix, quartz overgrowth, poikilotopic carbonate cement, and kaolinite cement are the most impactful agents to the porosity reduction of the Falher F chert arenite in the study area. However, other cement may be causing reservoir problems too, albeit more locally. For instance, extensive iron oxide coating and pore-filling illite in several samples may disturb the permeability, therefore creating microscale reservoir compartmentalization. Further laboratory analyses are required to attest to this interpretation.
3. The primary intergranular porosity is only preserved in petrofacies I and II (mature, rock fragment-poor chert arenite), whereas secondary porosity is found throughout petrofacies I to V. The latter is mostly attributed to

the dissolution of chert and rock fragment, which are most plentiful in petrofacies III to V (submature to mature, rock fragment-rich chert arenite). Microfractures are also common and predominantly occur at a microporosity-scale.

4. Albeit the lack of primary porosity, the Falher F chert arenite still preserves hydrocarbon storability potential that the secondary porosity is responsible for. In samples without visible pores under the microscope, micropores are very likely to be present as yielded by the core porosity values and SEM analysis.

The challenges present in the study intervals may therefore be managed by proper drilling strategies that consider the lateral and vertical distributions of the interpreted chert-influenced drillability fairway as well as the potential of substantial secondary microporosities within the Falher F tight sandstone.

CHAPTER 4: SUMMARY AND CONCLUSIONS

The following key points represent the results of the objectives stated in Chapter 1:

1. Based on the sedimentological and ichnological observations of 20 cores, the Falher F submember in the Wapiti area of northwestern Alberta consists of 13 lithofacies. These lithofacies can be further grouped into four facies associations: storm-dominated shoreface and distal deltaic complex (FA1), wave-dominated shoreface and proximal deltaic complex (FA2), brackish embayment (FA3), and coastal plain (FA4).
2. The general and complete lithologies of a typical Falher F succession consist of heterolithic, moderately burrowed sandy mudstone beds that transition into infrequently silty, hummocky cross-stratified to swaley cross-stratified lower very fine-grained sandstone at the base, indicating storm-dominated deposits and the equivalent distal delta front. They pass upwards into interbedded trough cross-stratified and planar-bedded fine-grained sandstone beds, which may be capped by a bimodal to unimodal chert conglomerate beds, suggesting wave-dominated shoreface or equivalent wave-dominated proximal delta front deposits. These marine successions are overlain by moderately burrowed sandy mudstone and interbedded mudstone and coal beds, implying depositions in brackish embayment and coastal plain complexes.
3. Both sedimentological and ichnological observations of the Falher F in the Wapiti area generally demonstrate similarities between the shoreface and the wave-dominated delta deposits. Discriminating between the two, thus, mainly relies upon the presence of a scoured, gravelly base associated with the carbonaceous-rich, poorly-sorted conglomerate bodies, suggesting the presence of a distributary channel or mouth bars, therefore the associated deltaic settings.
4. The Falher F in the Wapiti area is composed of four stratigraphic successions, which are parasequences F_P1 through F_P4. Each of these

successions consists of a combination of the previously mentioned 13 lithofacies. A single parasequence may be exclusively composed of either shoreface or deltaic deposits, or a combination of both.

5. Parasequences F_P1 through F_P3 are normal regressive deposits, therefore they are separated by interchangeable flooding surfaces and wave ravinement surfaces, termed here FS/WRS1 through FS/WRS2. Landward of the marine successions, these surfaces transition into flooding surfaces FS1 and FS2, respectively. Parasequence F_P4 consists of forced regressive deposits; therefore, the base is a regressive surface of marine erosion (RSME). Landward, it transitions into a subaerial unconformity (SU). Unlike the marine surfaces, SU generally does not have a distinctive remark on well logs. Therefore, their identification solely relies on core identifications where available.
6. The base of the Falher F is interpreted to be a maximum flooding surface (MFS), which separates the transgressive succession of the Falher G and prograding shoreface of the Falher F. The top of the Falher F in the study area records a nonmarine–nonmarine contact with the overlying Falher E coastal plain deposits. Therefore, delineating a reliable surface is challenging. The contact, however, is interpreted to be a flooding surface.
7. The distribution of various depositional environments of the Falher F in the Wapiti area can be illustrated using four paleogeographic maps, which each exhibit the extent of the progradation of the Falher F across F_P1 through F_P4 over time. These maps also serve as a depositional model, which reveals the resulting paleogeographic frameworks across four main stages of changes in sedimentation rate and relative sea level during the Falher F progradation in the study area.
8. Petrographic observations of the Falher F tight sandstone reveal that it consists exclusively of the chert arenite type. There are frequent changes in the composition of the detrital frameworks and the authigenic minerals. Changes in the ratio of detrital frameworks, with respect to chert content,

have been postulated to affect the varying degree of sandstone drillability, whereas changes in authigenic minerals significantly alter the porosity.

9. The variations in chert-influenced sandstone drillability within the Falher F chert arenite can be examined by comparing the normalized percentage of quartz (Q), chert (C), and rock fragments (RF) among samples. Generally, samples that are dominated by detrital chert clasts accumulated in the storm-dominated shoreface (FA2), whereas quartz-dominated samples are concentrated in the wave-dominated shoreface (FA1). Samples from the marginal marine (FA3) do not possess any general trends due to the complexity of the mixing of the wave, tidal, and fluvial energy.
10. The changes in depositional time from F_P2 to F_P3 do not seem to have significantly influenced the detrital compositions. This strengthens the interpretation that the sand-bearing and conglomerate-bearing parasequences F_P2 and F_P3, respectively, are both normal regressive (highstand systems tract) deposits. Therefore, the deposition of conglomerate intervals in the Falher F, which has been interpreted as due to a forced regressive origin in other Falher submembers, did not involve a relative fall in sea level.
11. The most remarkable distinction in detrital composition occurs between samples deposited in the western and eastern areas, which are associated with two separate conglomerate depocentres. Data points plotted from the western depocentre, regardless of the depositional environment and parasequence, tend to be spread out and are near a particular endmember in the ternary diagrams. In contrast, data points plotted from the eastern depocentre, regardless of the depositional environment and parasequence, frequently overlap each other and generally have no distinctive compositional differences. In the Falher F shoreface and wave-dominated delta setting, this is interpreted as indicating that there are two different fluvial feeder types, therefore the contrasting responses towards marine forces. The western sandstone is interpreted to have been transported via

a lower-energy secondary channel that branched out from the higher-energy primary channel in the east.

12. To perform horizontal drilling across uniformly drillable strata, it is proposed here that more penetrable lithologies may occur along the depositional strike across R10 to R11W6. These intervals are interpreted as being associated with a lower-energy minor trunk that branched out from the major fluvial feeder. To minimize replacements of the drilling bit, it is recommended here that the horizontal wells are placed landward (i.e. southward), along the strike towards the western depocentre, or along the strike in the direction away from the fluvial feeder or deltaic locations towards the strandplain, which approaches the shoreface sandstone that is mineralogically more drillable.
13. Compositional ratios aside, mineral and rock fragment suites of detrital framework grains in the eastern and western areas as well as in parasequences $F_{P}2$ and $F_{P}3$ have essentially identical properties. This strengthens the interpretation that the deposition of conglomerate bodies during parasequence $F_{P}3$ was not associated with changes in point sources from $F_{P}2$ to $F_{P}3$ over time, which would have required a forced regression.
14. Based on the petrographic observations, the Falher F chert arenite encompasses five petrofacies. These petrofacies have decreasing textural and compositional maturity, as well as a more complex diagenetic evolution. They are composed of mature, silica-cemented chert arenite (petrofacies I); mature, kaolinite- and silica-cemented chert arenite (petrofacies II); mature to submature, tightly compacted, illite-rich chert arenite (petrofacies III); mature to submature, dolomite-cemented chert arenite (petrofacies IV); and mature to submature, calcite- and dolomite-cemented chert arenite (petrofacies V).
15. The primary porosity of the Falher F chert arenite has been largely reduced by the interstitial cement and materials that were produced by mechanical and chemical changes. Extensive mechanical compaction

resulted in the abundance of an argillaceous pseudomatrix and intergranular chert welding. The chemical alteration was responsible for the precipitation of authigenic minerals in the remaining voids. From the most to the least frequently observed, the minerals are quartz overgrowth, dolomite, ferroan dolomite, kaolinite, iron oxide, illite, calcite, and ferroan calcite.

16. The Falher F retains its hydrocarbon storability potential primarily due to the secondary pores. Grain dissolution, cement dissolution, and microfractures are among the primary mechanisms that produce the secondary pores in the tight sandstone. These processes are considered to be ongoing following the pore-occluding mechanisms, such as cement precipitation and mechanical compaction; therefore, they provide spaces that the hydrocarbons can fill.
17. Observations of the textural relationships among various authigenic minerals in the Falher F suggest that the early diagenetic minerals include quartz overgrowths, chlorite, pyrite, and kaolinite, whereas the late diagenetic minerals are kaolinite, albite, dolomite, ferroan dolomite, calcite, ferroan calcite, and illite.

REFERENCES

Abbott, P.L. and Peterson, G.L. 1978. Effects of abrasion durability on conglomerate clast populations; examples from Cretaceous and Eocene conglomerates of the San Diego area, California. Journal of Sedimentary Research, v. 48, no. 1, p. 31–42.

Adani, N., Gingras, M.K. and Zonneveld, J.-P. 2018. Paleogeographic reconstruction of the Falher "F" and the implication to its chert-influenced durability fairway, Wapiti Field, Alberta. CSPG Core Conference 2018 Abstract, p. 41–45.

Aigner, T. 1985. Storm depositional systems: Dynamic stratigraphy in modern and ancient shallow-marine sequences. Lecture Notes in Earth Sciences, v. 3, Springer-Verlag, Berlin, 158 p.

Alberta Study Group, 1954. Lower Cretaceous of the Peace River Region. In: Western Canada Sedimentary Basin: A Symposium. L.M. Clark (ed.). American Association of Petroleum Geologists, Rutherford Memorial Volume, p. 268–278.

Ali, A., Abdalah, S. and Potter, D.K. 2012. Quantifying the Role of Grain Lining Hematite Cement in Controlling Permeability in a Relatively Tight Gas Sandstone Reservoir from the North Sea. SPE Reservoir Evaluation and Engineering, v. 15, no. 6, p. 618–623.

Armitage, I.A. 2002. Sedimentology, Ichnology, and High-resolution Allostratigraphy of the Falher "C" Member, Spirit River Formation, west-central Alberta, Canada. Unpublished MSc thesis, University of Alberta, Edmonton, Alberta, Canada, 178 p.

Armitage, I.A., Pemberton, S.G. and Moslow, T.F. 2004. Facies succession, stratigraphic occurrence, and paleogeographic context of conglomeratic shorelines within the Falher "C", Spirit River Formation, Deep Basin, west-central Alberta. Bulletin of Canadian Petroleum Geology, v. 52, no. 1, p. 39–56.

Armstrong, J. 1979. Regional considerations of the Elmworth Field and the Deep Basin: discussion. Bulletin of Canadian Petroleum Geology, v. 27, no. 4, p. 525–526.

Arnott, R.W.C. 1991. The Carrot Creek "K" Pool, Cardium Formation, Alberta: a conglomeratic reservoir related to a wave-reworked distributary mouth-bar complex. Bulletin of Canadian Petroleum Geology, v. 39, no. 1, p. 43–53.

Arnott, R.W.C. 1993. Sedimentological and stratigraphic model of the Falher "D" Pool, Lower Cretaceous, northwestern Alberta. Bulletin of Canadian Petroleum Geology, v. 41, p. 453–463.

Arnott, R.W.C. 1994. Falher "D" Pool, Lower Cretaceous, Northwestern Alberta – Sedimentological and Sequence Stratigraphic Framework. CSPG Mannville Core Conference, v. 11, no. 11, p. 25.

Arnott, R.W.C. 2003. The role of fluid- and sediment-gravity flow processes during deposition of deltaic conglomerates (Cardium Formation, Upper Cretaceous), west-central Alberta. Bulletin of Canadian Petroleum Geology, v. 51, no. 4, p. 426–436.

Bann, K.L. and Fawcett, M. 2016. The Wilrich Member, Alberta deep basin: An example of a topset-dominated delta deposited into a low-accommodation shallow sea. William C. Gussow Geoscience Conference 2016 Abstract, 5 p.

Bann, K.L. and Ross, D.J.K. 2014a. Facies analysis of the Lower Cretaceous Wilrich Member (lower Falher) of the Spirit River Formation. CSPG CSEG CWLS Conference 2014 Abstract, 5 p.

Bann, K.L. and Ross, D.J.K. 2014b. Sedimentology and ichnology of the Lower Cretaceous Wilrich Member (Lower Falher) of the Spirit River Formation. GeoConvention 2014 Abstract, 5 p.

Berner, R.A. 1984. Sedimentary pyrite formation: an update. Geochimica et cosmochimica Acta, v. 48, no. 4, p. 605–615.

Bhattacharya, J.P. and Giosan, L. 2003. Wave-influenced deltas: Geomorphological implications for facies reconstruction. Sedimentology, v. 50, no. 1, p. 187–210.

Bhattacharya, J.P. and Walker, R.G. 1992. Deltas. In: Facies Models: Response to Sea Level Change. R.G. Walker and N.P. James (eds.). Geological Association of Canada, p. 157–177.

Bjørlykke, K. 1983. Diagenetic reactions in sandstones. In: Sediment Diagenesis. A. Parker and B.W. Sellwood (eds.). NATO ASI Series, v. 115, D. Reidel Publishing Company, Dordrecht, Netherlands, p. 169–213.

Bjørlykke, K. and Egeberg, P.K. 1993. Quartz cementation in sedimentary basins. American Association of Petroleum Geologists Bulletin, v. 77, no. 9, p. 1538–1548.

Bjørlykke, K., Elverhøi, and Malm, A.O. 1979. Diagenesis in Mesozoic sandstones from Spitsbergen and the North Sea—a comparison. Geological Review, v. 68, no. 3, p. 1152–1171.

Blakey, D. 2016. Western Interior Seaway 99 Ma Albian/Cenomian [online]. Available from http://deeptimemaps.com/western-interior-seaway-thumbnails [accessed March 2017].

Blatt, H. 1979. Diagenetic processes in sandstones. Society of Economic Palaeontologists and Mineralogists Special Publication, no. 26, p. 141–157.

Blatt, H. and Christie, J.M. 1963. Undulatory extinction in quartz of igneous and metamorphic rocks and its significance in provenance studies of sedimentary rocks. Journal of Sedimentary Research, v. 33, no. 3, p. 559–579.

Bloch, S. 1994. Effect of Detrital Mineral Composition on Reservoir Quality. In: Reservoir Quality Assessment and Prediction in Clastic Rocks (SC30). M.D. Wilson (ed.). Society of Economic Palaeontologists and Mineralogists, p. 161–182.

Boyd, R., Dalrymple, R. and Zaitlin, B.A. 1992. Classification of clastic coastal depositional environments. Sedimentary Geology, v. 80, p. 139–150.

Bown, T.M. and Kraus, M.J. 1987. Integration of channel and floodplain suites, I. Developmental sequence and lateral relations of alluvial paleosols. Journal of Sedimentary Research, v. 57, no. 4, p. 587–601.

Burwash, R.A., McGregor, C.R. and Wilson, J.A. 1994. Precambrian Basement Beneath the Western Canada Sedimentary Basin. In: Geological Atlas of the Western Canada Sedimentary Basin. G.D. Mossop and I. Shetsen (comp.). Canadian Society of Petroleum Geologists and Alberta Research Council, p. 49–56.

Caddel, E.M. 2000. Sedimentology and Stratigraphy of the Falher C Member, Spirit River Formation, Northeastern British Columbia. Unpublished MSc Thesis, University of Calgary, Calgary, Alberta, Canada, 242 p.

Caddel, E.M. and Moslow, T.F. 2004. Outcrop sedimentology and stratal architecture of the Lower Albian Falher C sub-Member, Spirit River Formation, Bullmoose Mountain, northeastern British Columbia. Bulletin of Canadian Petroleum Geology, v. 52, no.1, p. 4–22.

Cant, D.J. 1983a. Spirit River Formation – A stratigraphic-diagenetic gas trap in the Alberta. American Association of Petroleum Geologists Bulletin, v. 67, p. 577–587.

Cant, D.J. 1983b. The Spirit River Formation, Deep Basin gas reservoir. Sedimentology of Selected Mesozoic Clastic Sequences: Corexp '83 in Conjunction with the Mesozoic of Middle North America, p. 3–10.

Cant, D.J. 1984. Development of shoreline-shelf sand bodies in a Cretaceous epeiric sea deposit. Journal of Sedimentary Petrology, v. 54, p. 541–556.

Cant, D.J. 1988. Regional structure and development of the Peace River Arch, Alberta: a Palaeozoic failed-rift system?. Bulletin of Canadian Petroleum Geology, v. 36, p. 284–295.

Cant, D.J. 1995. Sequence stratigraphic analysis of individual depositional successions: effects of marine/non-marine sediment partitioning and longitudinal sediment transport, Mannville Group, Alberta foreland basin, Canada. American Association of Petroleum Geologists Bulletin, v. 79, p. 749–762.

Carmichael, S.M.M. 1988. Linear estuarine conglomerate bodies formed during a mid-Albian marine transgression, “Upper Gates” Formation, Rocky Mountain Foothills of northeastern British Columbia. In: Sequences, Stratigraphy, Sedimentology: Surface and Subsurface. D.P. James and D.A. Leckie (eds.). Canadian Society of Petroleum Geologists, Memoir 15, p. 49–62.

Casas, J.E. 1996. Sedimentology, Facies Associations and Sequence Stratigraphy of Falher Divisions C and D, Lower Cretaceous Spirit River Formation, West-Central Alberta, Canada. Unpublished MSc thesis, McMaster University, Hamilton, Ontario, Canada, 231 p.

Casas, J.E. and Walker, R.G. 1997. Sedimentology and depositional history of Units C and D of the Falher Member, Spirit River Formation, west-central Alberta. Bulletin of Canadian Petroleum Geology, v. 45, no. 2, p. 218–238.

Catuneanu, O. 2006. Principles of sequence stratigraphy, 1st edition. Elsevier Science, 386 p.

Choquette, P.W. and Pray, L.C. 1970. Geologic nomenclature and classification of porosity in sedimentary carbonates. American Association of Petroleum Geologists Bulletin, v. 54, no. 2, p. 207–250.

Clifton, H.E. 2003. Supply, segregation, successions, and significance of shallow marine gravelly deposits. Bulletin of Canadian Petroleum Geology, v. 51, no. 4, p. 370–388.

Clifton, H.E. and Thompson, J.K. 1978. *Macaronichnus segregatis*: a feeding structure of shallow marine polychaetes. Journal of Sedimentary Petrology, v. 48, no. 4, p. 1293–1302.

Cochran, A. 1991. Compaction and porosity prediction in chert-rich sandstones and conglomerates. American Association of Petroleum Geologists Bulletin, v. 75, no. 3, p. 554.

Conolly, J.R. 1965. The occurrence of polycrystallinity and undulatory extinction in quartz in sandstones. Journal of Sedimentary Research, v. 35, no. 1, p. 116–135.

Crimes, T.P. 1975. The stratigraphical significance of trace fossils. In: The Study of Trace Fossils. R.W. Frey (ed.). Springer, New York, p. 109–130.

Curray, J.R., Emmel, F.J. and Crampton, P.J.S. 1969. Holocene history of a strand plain, lagoonal coast, Nayarit, Mexico. In: Memorias del Simposio Internacional de Lagunas Costeras. A.A. Castanares and F.B. Phleger (eds.). Universidad Nacional Autonoma, p. 63–100.

Dalrymple, R.W., Zaitlin, B.A. and Boyd, R. 1992. Estuarine facies models: conceptual basis and stratigraphic implications. Journal of Sedimentary Petrology, v. 62, p. 1130–1146.

Dapples, E.C. 1959. The behavior of silica in diagenesis. In: Silica in Sediments. H.A. Ireland (ed.). Society of Economic Palaeontologists and Mineralogists Special Publication, no. 7, p. 36–54.

Dapples, E.C., Krumbein, W.C. and Sloss, L.L. 1953. Petrographic and lithologic attributes of sandstones. Journal of Geology, v. 61, no. 4, p. 291–317.

Dashtgard, S.E. 2006. Sedimentology, Ichnology, and Stratigraphy of Modern Conglomeratic Depositional Environments. Unpublished PhD dissertation, University of Alberta, Edmonton, Canada, 223 p.

Davis, R.A. 1978. Beach and nearshore zone. In: Coastal Sedimentary Environments. R.A. Davis Jr. (ed.). Springer, New York, p. 237–285.

Davis, R.A. and FitzGerald, D.M. 2004. Beaches and coasts. Blackwell Science, Oxford, p. 432.

DesRoches, A.J. 2008. Integrated Ichnology, Sedimentology and Stratigraphy of the Lower Falher Member, Spirit River Formation, Northeastern British Columbia and Central Alberta. Unpublished MSc thesis, Simon Fraser University, Burnaby, British Columbia, Canada, 173 p.

DesRoches, A.J., Thompson, C.R. and MacEachern, J.A. 2007. Integrated Ichnology, Sedimentology and Stratigraphy of the Along-Strike Changes in Parasequences of the Lower Cretaceous Boreal Seaway, Central Alberta, Canada. CSPG CSEG Convention 2007 Abstract, 1 p.

DesRoches, A.J., Thompson, C.R, and MacEachern, J.A. 2008. Facies Criteria to Differentiate Between Wave-/Storm-Dominated Deltas and Strandplain

Shorefaces, Lower Cretaceous Falher Member, Spirit River Formation, Alberta, Canada. AAPG Annual Convention 2008 Abstract, 1 p.

Dickinson, W.R. 1970. Interpreting detrital modes of graywacke and arkose. Journal of Sedimentary Research, v. 40, no. 2, p. 695–707.

Dott, R.H. 1964. Wacke, graywacke and matrix; what approach to immature sandstone classification?. Journal of Sedimentary Research, v. 34, p. 625–632.

Dott, R.H. and Bourgeois, J. 1982. Hummocky stratification: significance of its variable bedding sequences. Geological Society of America Bulletin, v. 93, no. 8, p. 663–680.

Droser, M.L. and Bottjer, D.J. 1989. Ichnofabric of sandstones deposited in high-energy nearshore environments; measurement and utilization. Palaios, v. 4, no. 6, p. 598–604.

Duke, W.L., Arnott, R.W.C. and Cheel, R.J. 1991. Shelf sandstones and hummocky cross-stratification: new insights on a stormy debate. Geology, v. 19, p. 625–628.

Dumas, S. and Arnott, R.W.C. 2006. Origin of hummocky and swaley cross-stratification—The controlling influence of unidirectional current strength and aggradation rate. Geology, v. 34, no. 12, p. 1073–1076.

Ekdale, A.A., 1985. Paleoecology of the marine endobenthos. Palaeogeography, Palaeoclimatology, Palaeoecology, v. 50, no. 1, p. 63–81.

Ekdale, A.A., Bromley, R.G. and Pemberton, S.G. 1984. Ichnology: Trace Fossils in Sedimentology and Stratigraphy. Society of Economic Paleontologists and Mineralogists Short Course, v. 15, 317 p.

Fawcett, M.D. 2014. Reservoir parameters in the Wilrich Member of the Spirit River Formation. GeoConvention 2014 Abstract, 1 p.

Fockler, M. and McKenzie, B. 2016. Western Canada Resource Plays: The Phoenix Awaits. AAPG Annual Convention 2016 Abstract and Presentation, 61 p.

Folk, R.L. 1951. Stages of textural maturity in sedimentary rocks. Journal of Sedimentary Petrology, v. 21, p. 127–130.

Folk, R.L. 1954. Tile distinction between grain size and mineral composition in sedimentary rock nomenclature. Geology, v. 62, p. 344–359.

Folk, R.L. 1974. Petrology of sedimentary rocks. Hemphill Publishing Co., Austin, 170 p.

Frey, R.W. 1973. Concepts in the study of biogenic sedimentary structures. Journal of Sedimentary Research, v. 43, no. 1, p. 6–19.

Frey, R.W., Pemberton, S.G. and Saunders, T.D.A. 1990. Ichnofacies and bathymetry: a passive relationship. Journal of Paleontology, v. 64, p. 155–158.

Galloway, W.E. 1976. Sediments and stratigraphic framework of the Copper River fan-delta, Alaska. Journal of Sedimentary Research, v. 46, no. 3, p. 726–737.

Garzanti, E., Resentini, A., Andò, S., Vezzoli, G., Pereira, A. and Vermeesch, P. 2015. Physical controls on sand composition and relative durability of detrital minerals during ultra-long distance littoral and aeolian transport (Namibia and southern Angola). Sedimentology, v. 62, no. 4, p. 971–996.

Ghosh, S.K. 1991. Dissolution of silica in nature and its implications. Bulletin of Canadian Petroleum Geology, v. 39, p. 212.

Gingras, M.K., Bann, K.L., MacEachern, J.A., Waldron, J. and Pemberton, S.G. 2007. A conceptual framework for the application of trace fossils. In: Applied Ichnology. J.A. MacEachern, K.L. Bann, M.K. Gingras, S.G. Pemberton (eds.). Society of Economic Paleontologists and Mineralogists Short Course Notes, v. 52, p. 1–26.

Gingras, M.K., MacEachern, J.A. and Dashtgard, S.E. 2011. Process ichnology and the elucidation of physico-chemical stress. Sedimentary Geology, v. 237, no. 3–4, p. 115–134.

Gingras, M.K., MacEachern, J.A. Dashtgard, S.E. Zonneveld, J.-P. Schoengut, J., Ranger, M.J., and Pemberton, S.G. 2012. Estuaries. In: Trace Fossils as Indicators of Sedimentary Environments. D. Knaust and R.G. Bromley (eds.). Developments in Sedimentology, v. 64, p. 463–505.

Goldstein, R.H. and Rossi, C. 2002. Recrystallization in quartz overgrowths. Journal of Sedimentary Research, v. 72, no. 3, p. 432–440.

Hancock, J.M. and Kauffman, E.G. 1979. The Great Transgression of the Late Cretaceous. Journal of the Geological Society of London, v. 136, p. 125–186.

Hänninen, J., Vuorinen, I., Rajasilta, M. and Reid, P.C. 2015. Response of the Baltic and North Seas to river runoff from the Baltic watershed–physical and biological changes. Progress in Oceanography, v. 138, p. 91–104.

Harms, J.C., Southard, J.B., Spearing, D.R. and Walker, R.G. 1975. Depositional environments as interpreted from primary sedimentary structures and stratification sequences. Society for Sedimentary Geology (SEPM) Short Course, no. 2, 161 p.

Harrell, J. and Blatt, H. 1978. Polycrystallinity; effect on the durability of detrital quartz. Journal of Sedimentary Research, v. 48, no. 1, p. 25–30.

Harris, N.B. 2014. Falher and Cadomin diagenesis and implications for reservoir quality. GeoConvention 2014 Abstract, 2 p.

Hart, B.S. and Plint, A.G. 2003. Stratigraphy and sedimentology of shoreface and fluvial conglomerates: Insights from the Cardium Formation in NW Alberta and adjacent British Columbia. Bulletin of Canadian Petroleum Geology, v. 51, no. 4, p. 437–464.

Hayes, B.J. 2010. The Deep Basin Development Entity – Enhancing Exploitation of Alberta's Deep Basin Tight Gas Resource. GeoConvention 2010 Abstract, 3 p.

Hirschmiller, J.J. and Lemke, C.P. 2018. Estimating 'Gas Initially in Place' in the Spirit River Formation, and Relationships to Production and Economics – From Brazeau to Wapiti, Alberta. GeoConvention 2018 Abstract, 1 p.

Hobbs, T. W. 2003. Integrated Ichnological, Sedimentological and Sequence Stratigraphic Analysis of Along-Strike Variations in the Albian Upper Falher and Basal Notikewin Members, NW Alberta and NE British

Columbia, Canada. Unpublished MSc Thesis, Simon Fraser University, Burnaby, British Columbia, Canada, 423 p.

Hobbs, T. W. and MacEachern, J.A. 2002. Along-strike variations in the Falher A and basal Notikewin Members, Fort St. John Group of west-central Alberta and NE British Columbia: integrated ichnological-sedimentological models in a sequence stratigraphic framework. CSPG Annual Convention 2002 Abstract, 1 p.

Hobbs, T. W. and MacEachern, J.A. 2003. Integrated ichnological, sedimentological and sequence stratigraphic analysis of along-strike variations in the Albian Falher A Member, northwest Alberta and northeast British Columbia, Canada. AAPG Annual Meeting 2003 Abstract, 1 p.

Hoffman, T. 2008. Lateral Variability of Sedimentological and Ichnological Characteristics of the Falher "D" Member, West-Central Alberta, Canada. Unpublished MSc thesis, University of Alberta, Edmonton, Alberta, Canada, 253 p.

Holmden, C., Creaser, R.A. and Muehlenbachs, K. 1997. Paleosalinities in ancient brackish water systems determined by 87Sr/86Sr ratios in carbonate fossils: A case study from the Western Canada Sedimentary Basin. Geochimica et Cosmochimica Acta, v. 61, no. 10, p. 2105–2118.

Hower, J., Eslinger, E.V., Hower, M.E., and Perry, E.A. 1976. Mechanism of burial metamorphism of argillaceous sediment: 1. Mineralogical and chemical evidence. Geological Society of America Bulletin, v. 87, no. 5, p. 725–737.

Hsü, K.J. and Jenkyns, H.C. 1974. Pelagic Sediments: on Land and under the Sea. International Association of Sedimentologists Special Publication, v. 1, 447 p.

Hunter, R.E., Clifton, H.E. and Phillips, R.L. 1979. Depositional structures and processes in oblique bar-rip channel systems, southwestern Oregon. Journal of Sedimentary Petrology, v. 49, p. 711–726.

Jackson, P.C. 1984. Paleogeography of the Lower Cretaceous Mannville Group of Western Canada. In: Elmworth: Case study of a deep basin gas field. J.A. Masters (ed.). American Association of Petroleum Geologists, Memoir 38, p. 49–77.

Jenkyns, H.C. 1978. Pelagic environments. In: Sedimentary Environments and Facies. H.G. Reading (ed.). Blackwell Science, Oxford, p. 343–397.

Johnson, H.D. and Baldwin, C.T. 1996. Shallow clastic seas. In: Sedimentary Environments: Processes, Facies and Stratigraphy. H.G. Reading (ed.). Blackwell Science, Oxford, p. 232–280.

Kairo, S., Suttner, L.J., Dutta, P.K., Johnsson, M.J. and Basu, A. 1993. Variability in sandstone composition as a function of depositional environment in coarse-grained delta systems. In: Processes Controlling the Composition of Clastic Sediments. M.J. Johnson and A. Basu (eds.). Geological Society of America Special Paper, no. 284, p. 263–283.

Keller, W.D. 1978. Kaolinization of feldspar as displayed in scanning electron micrographs. Geology, v. 6, no. 3, p. 184–188.

Kirk, R.M. 1980. Mixed sand and gravel beaches: morphology, processes and sediments. Progress in Physical Geography, v. 4, p. 189–210.

Krassay, A.A. 1994. Storm features of siliciclastic shelf sedimentation in the mid-Cretaceous epeiric seaway of northern Australia. Sedimentary Geology, v. 89, no. 3–4, p. 241–264.

Kraus, M.J. 1999. Paleosols in clastic sedimentary rocks: their geologic applications. Earth-Science Reviews, v. 47, no. 1–2, p. 41–70.

Landers, R.H., Larese, R.E. and Bonnell, L.M. 2008. Toward more accurate quartz cement models: The importance of euhedral versus noneuhedral growth rates. American Association of Petroleum Geologists Bulletin, v. 92, no. 11, p. 1537–1563.

Lanson, B. and Velde, B. 1992. Decomposition of X-ray diffraction patterns; a convenient way to describe complex I/S diagenetic evolution. Clays and Clay Minerals, v. 40, no. 6, p. 629–643.

Larese, R.E. and Hall, D.L. 2003. Impact of interactive textural, compositional, and diagenetic controls on potential reservoir quality of low permeability sandstones. AAPG Annual Convention 2003 Abstract, 1 p.

Leckie, D.A. 1983. Sedimentology of the Moosebar and Gates Formations (Lower Cretaceous). Unpublished PhD dissertation, McMaster University, Hamilton, Ontario, Canada, 515 p.

Leckie, D.A. 1986a. Petrology and tectonic significance of Gates Formation (early Cretaceous) sediments in northeast British Columbia. Canadian Journal of Earth Sciences, v. 23, p. 129–141.

Leckie, D.A. 1986b. Rates, Controls, and Sand-Body Geometries of Transgressive-Regressive Cycles: Cretaceous Moosebar and Gates Formations, British Columbia. American Association of Petroleum Geologists Bulletin, v. 70, no. 5, p. 516–535.

Leckie, D.A., Fox, C. and Tamocai, C. 1989. Multiple paleosols of the late Albian Boulder Creek formation, British Columbia, Canada. Sedimentology, v. 36, no. 2, p. 307–323.

Leckie, D.A. and Smith, D.G. 1992. Regional setting, evolution, and depositional cycles of the western Canada foreland basin. In: Foreland basins and foldbelts. R.W. Macqueen and D.A. Leckie (eds.). American Association of Petroleum Geologists, Memoir 55, p. 9–46.

Leckie, D.A. and Walker, R.G. 1982. Storm- and Tide-Dominated Shorelines in Cretaceous Moosebar-Lower Gates Interval – Outcrop Equivalents of Deep Basin Gas Trap in Western Canada. American Association of Petroleum Geologists Bulletin, v. 66, no. 2, p. 138–157.

Macdonald, D.E., Langenberg, C.W. and Strobl, R.S. 1988. Cyclic marine sedimentation in the Lower Cretaceous Luscar Group and Spirit River Formation of the Alberta Foothills and Deep Basin. In: Sequences, Stratigraphy, Sedimentology: Surface and Subsurface. D.P. James and D.A. Leckie (eds.). Canadian Society of Petroleum Geologists, Memoir 15, p. 143–154.

MacEachern, J.A., Bann, K.L., Bhattacharya, J.P. and Howell, C.D. 2005. Ichnology of deltas: organism responses to the dynamic interplay of rivers, waves, storms and tides. In: River Deltas: Concepts, Models and Examples. J.P. Bhattacharya and L. Giosan (eds.). Society of Economic Palaeontologists and Mineralogists Special Publication, v. 83, p. 49–85.

MacEachern, J.A., Dashtgard, S.E., Knaust, D., Bann, K.L. and Pemberton, S.G. 2012. Sequence stratigraphy. In: Trace Fossils as Indicators of Sedimentary Environments. D. Knaust and R.G. Bromley, R.G. (eds.). Developments in Sedimentology, v. 64, p. 157–194.

MacEachern, J.A. and Gingras, M.K. 2007. Recognition of brackish-water trace-fossil suites in the Cretaceous interior seaway of Alberta, Canada. In: Sediment-Organism Interactions: A Multifaceted Ichnology. R.G. Bromley, L.A. Buatois, G.M. Mángano, J.F. Genise and R.N. Melchor (eds.). Society of Economic Palaeontologists and Mineralogists Special Publication, p. 149–193.

MacEachern, J.A. and Hobbs, T.W. 2004. The ichnological expression of marine and marginal marine conglomerates and conglomeratic intervals, Cretaceous Western Interior Seaway, Alberta and northeastern British Columbia. Bulletin of Canadian Petroleum Geology, v. 52, no. 1, p. 77–104.

MacEachern, J.A. and Pemberton, S.G. 1992. Ichnological aspects of Cretaceous shoreface successions and shoreface variability in the western interior seaway of North America. In: Application of Ichnology to Petroleum Exploration, A Core Workshop. S.G. Pemberton (ed.). Society of Economic Palaeontologists and Mineralogists Core Workshop, no. 17, p. 57-84.

MacEachern, J.A. and Pemberton, S.G. 1994. Ichnological character of incised valley fill systems from the Viking Formation of the Western Canada Sedimentary Basin, Alberta, Canada. In: Incised-Valley Systems: Origin and Sedimentary Sequences. R.W. Dalrymple, R. Boyd and B.A. Zaitlin (eds.), Society of Economic Palaeontologists and Mineralogists Special Publication, v. 51, p. 129–157.

MacEachern, J.A., Pemberton, S.G., Gingras, M.K., Bann, K.L. and Dafoe, L. T., 2007. Use of trace fossils in genetic stratigraphy. In: Trace Fossils. W. Miller III (ed.). Elsevier, Amsterdam, p. 105–128.

MacEachern, J.A., Saunders, T.D.A. and Pemberton, S.G. 1994. An Integrated Ichnological-Sedimentological Model for the Harmon-Cadotte Shoreface Succession, West-Central Alberta. Calgary: Western Canadian and International Expertise Exploration Update 1994 Abstract, 2 p.

Male, W.H. 1992. The Sedimentology of Ichnology of the Lower Cretaceous (Albian) Bluesky Formation in the Karr Area of West-Central Alberta. In: Application of Ichnology to Petroleum Exploration, A Core Workshop. S.G. Pemberton (ed.). Society of Economic Palaeontologists and Mineralogists Core Workshop, no. 17, p. 33–56.

Marinai, R.K. 1987. Petrography and diagenesis of the Ledge Sandstone Member of the Triassic Ivishak Formation. In: Petroleum geology of the northern part of the Arctic National Wildlife Refuge, northeastern Alaska. K.J. Bird and L.B. Magoon (eds.). U.S. Geological Survey Bulletin, v. 1778, p. 101–115.

Massari, F. and Parea, G.C. 1988. Progradational gravel beaches in a moderate- to high-energy microtidal marine environment. Sedimentology, v. 35, no. 6, p. 881–913.

Masters, J.A. 1978. Deep Basin gas trap, Western Canada: the container for Elmworth. CSPG Convention 1978 Abstract, p. 80–81.

Masters, J.A. 1979. Deep Basin Gas Trap, Western Canada. American Association of Petroleum Geologists Bulletin, v. 63, no. 2, p. 152–181.

Masters, J.A. 1984. Lower Cretaceous oil and gas in western Canada. In: Elmworth: Case study of a deep basin gas field. J.A. Masters (ed.). American Association of Petroleum Geologists, Memoir 38, p. 1–33.

Mattison, B.W. and Wall, J.H. 1993. Early Cretaceous foraminifera from the Middle and Upper Mannville and Lower Colorado subgroups in the Cold

Lake Oil Sands area of east-central Alberta: stratigraphic and paleoenvironmental implications. Canadian Journal of Earth Sciences, v. 30, p. 94–102.

McBride, E.F. 1963. A classification of common sandstones. Journal of Sedimentary Research, v. 33, no. 3, p. 664–669.

McBride, E.F. 1979. Importance of secondary porosity in sandstones to hydrocarbon exploration. American Association of Petroleum Geologists Bulletin, v. 63, no. 5, p. 834.

McBride, E.F. 1983. Sandstone Diagenesis: Principles Useful in Exploration. New Orleans Geological Society Short Course, 41 p.

McBride, E.F. 1985. Diagenetic processes that affect provenance determinations in sandstone. In: Provenance of Arenites. G.G. Zuffa (ed.). D. Reidel Publishing Company, Dordrecht, Netherlands, p. 95-113.

McBride, E.F. and Picard, M.D. 1987. Downstream changes in sand composition, roundness, and gravel size in a short-headed, high-gradient stream, northwestern Italy. Journal of Sedimentary Research, v. 57, no. 6, p. 1018–1026.

McLean, J.R. 1979. Regional considerations of the Elmworth Field and the Deep Basin. Bulletin of Canadian Petroleum Geology, v. 27, p. 53–62.

McLean, J.R. and Wall, J.H. 1981. The Early Cretaceous Moosebar Sea in Alberta. Bulletin of Canadian Petroleum Geology, v. 29, p. 334–377.

McLearn, F.H. 1944. Revision of the palaeogeography of the Lower Cretaceous of the Western Interior of Canada. Geological Survey of Canada, v. 44, no. 32, 11 p.

Mellon, G.B. 1967. Stratigraphy and petrology of the Lower Cretaceous Blairmore and Mannville groups, Alberta foothills and plains. Research Council of Alberta/Alberta Geological Survey Bulletin 21, 296 p.

Meloche, J.D. 2011. Valley Incision During Transgression: A Contrarian View of Structurally-Controlled Gravel Barriers in the WCSB. GeoConvention 2011 Abstract, 5 p.

Melvin, J. and Knight, A.1984. Lithofacies, diagenesis, and porosity of the Ivishak Formation, Prudhoe Bay area, Alaska. In: Clastic diagenesis. D.A. McDonald and R.C. Surdam (eds.). American Association of Petroleum Geologists, Memoir 37, p. 347–365.

Mensa-Wilmot, G., Calhoun, B. and Perrin, V.P. 1999. Formation drillability – definition, quantification and contributions to bit performance evaluation. SPE/IADC Middle East Drilling Technology Conference 1999, 8 p.

Mensa-Wilmot, G. and Fear, M.J. 2001. The Effects of Formation Hardness, Abrasiveness, Heterogeneity and Hole Size on PDC Bit Performance. SPE/IADC Drilling Conference 2001, 14 p.

Meyer, R. 2003. Depositional Controls on the Distribution of Ferroan Dolomite Cement in Virgelle Member (Eagle-Equivalent) Sandstones, Writing-on-Stone, Southern Alberta, Canada. AAPG Annual Meeting 2003 Abstract, 1 p.

Mitchum Jr., R.M. 1977. Seismic stratigraphy and global changes of sea level, part 11: glossary of terms used in seismic stratigraphy. In: Seismic Stratigraphy–Applications to Hydrocarbon Exploration. C. E. Payton (ed.). American Association of Petroleum Geologists, Memoir 26, p. 205–212.

Monger, J.W.H. 1989. Overview of Cordilleran geology. In: Western Canada Sedimentary Basin: A Case History. B.D. Ricketts (ed.). Canadian Society of Petroleum Geologists, p. 9–32.

Monger, J.W.H. 1999. Review of the Geology and Tectonics of the Canadian Cordillera. Short Course, British Columbia Geological Survey Branch, p. 72.

Monger, J.W.H. and Price, R. 2002. The Canadian Cordillera: Geology and Tectonic Evolution. CSEG Recorder, p. 17–36.

Morad, S., 1998. Carbonate cementation in sandstone: distribution patterns and geochemical evolution. International Association of Sedimentologists Special Publication, no. 26, p. 1–26.

Morad, S., Al-Ramadan, K., Ketzer, J.M. and De Ros, L.F. 2010. The impact of diagenesis on the heterogeneity of sandstone reservoirs: A review of the role of depositional facies and sequence stratigraphy. American Association of Petroleum Geologists Bulletin, v. 94, p. 1267–1309.

Moslow, T.F. and Ala, D. 2012. Reservoir Properties and Sedimentary Characteristics of the Falher G (i.e. Wilrich) Tight Gas Resource Play, Deep Basin, Alberta. GeoConvention 2012 Abstract, 2 p.

Moslow, T.F. and Zaitlin, B.A. 2008. Tight Gas Reservoirs of the Western Canada Deep Basin. AAPG Annual Convention 2008 Abstract, 1 p.

Moslow, T.F., Zaitlin, B.A. and Hildred, G. 2017. Variability in Spirit River (Wilrich-Falher) reservoir facies associations in the Deep Basin: sequence stratigraphy, accommodation space, reservoir quality and chemostratigraphy. CSPG Core Conference 2017 Abstract, p. 43–49.

Nemec, W. and Steel, R.J. 1984. Alluvial and coastal conglomerates: their significant features and some comments on gravelly mass-flow deposits. In: Sedimentology of Gravels and Conglomerates. E.H. Koster and R.J. Steel (eds.). Canadian Society of Petroleum Geologists, Memoir 10, p. 1–31.

Newitt, D.J. 2017. Integrated sedimentology, sequence stratigraphy, and reservoir characterization of the basal Spirit River Formation, west-central Alberta. Unpublished MSc thesis, University of Calgary, Calgary, Alberta, Canada, 106 p.

Newitt, D.J. and Pedersen, P.K. 2015. Depositional environments within the Wilrich member, Spirit River Formation – north central Alberta. GeoConvention 2015 Abstract, 2 p.

Newitt, D.J. and Pedersen, P.K. 2016. Contrasting Reservoir Properties for Albian Wilrich and Falher Shoreface Sandstones, Spirit River Formation, West-Central Alberta. GeoConvention 2016 Abstract, 1 p.

Nichols, G. 2009. Sedimentology and stratigraphy, 2nd edition. John Wiley & Sons, p. 419.

Nodwell, B. J. and Hart, B.S. 2006. Deeply-rooted palaeobathymetric control on the deposition of the Falher F conglomerate trend, Wapiti Field, Deep Basin, Alberta. Bulletin of Canadian Petroleum Geology, v. 54, no. 1, p. 1–21.

Olson, E., Rickabaugh, C. and Mason, C. 2008. Directional-Specific TCI Drill-Bit Design Features Allow for High Penetration Rates and Improved Durability in Tough Build Sections in Canadian Applications. CIPC/SPE Gas Technology Symposium 2008 Joint Conference, 10 p.

Pate, C. 1988. A comparison of isopach maps and total subsidence maps: implications for basin development and sandstone distribution during the lower Cretaceous in the deep basin area of Alberta and British Columbia. In: Sequences, Stratigraphy, Sedimentology: Surface and Subsurface. D.P. James and D.A. Leckie (eds.). Canadian Society of Petroleum Geologists, Memoir 15, p. 553–562.

Pattison, S.A. and Walker, R.G. 1994. Incision and filling of a lowstand valley; late Albian Viking Formation at Crystal, Alberta, Canada. Journal of Sedimentary Research, v. 64, no. 3b, p. 365–379.

Pemberton, S.G., Flach, D. and Mossop, G.D. 1982. Trace fossils from the Athabasca Oil Sands, Alberta, Canada. Science, v. 217, no. 4562, p. 825–827.

Pemberton, S.G., MacEachern, J.A., 1997. The ichnological signature of storm deposits: the use of trace fossils in event stratigraphy. In: Paleontological Event Horizons: Ecological and Evolutionary Implications. C.E. Brett (ed.). Columbia University Press, p. 73–109.

Pemberton, S.G., MacEachern, J.A. 2005. Significance of ichnofossils in applied stratigraphy. In: Applied Stratigraphy. E.A. Koutsoukos (ed.). Springer, Dordrecht, p. 281–302.

Pemberton, S.G., MacEachern, J.A., Dashtgard, S.E., Bann, K.L., Gingras, M.K., and Zonneveld, J.-P. 2012. Shorefaces. In: Trace Fossils as Indicators of Sedimentary Environments. D. Knaust and R.G. Bromley (eds.). Developments in Sedimentology, v. 64, p. 563–604.

Pemberton, S.G., MacEachern, J.A. and Frey, R.W. 1992. Trace fossil facies models: environmental and allostratigraphic significance. In: Facies Models: Response to Sea Level Change. R.G. Walker and N.P. James (eds.). Geological Association of Canada, p. 47–72.

Pemberton, S.G. and Wightman, D.M. 1992. Ichnological characteristics of brackish water deposits. In: Application of Ichnology to Petroleum Exploration, A Core Workshop. S.G. Pemberton (ed.). Society of Economic Palaeontologists and Mineralogists Core Workshop, no. 17, p. 141–167.

Pettijohn, F. J. 1949. Sedimentary rocks, 1st edition. Harper & Row, New York, 526 p.

Pettijohn, F. J. 1975. Sedimentary Rocks, 3rd edition. Harper & Row, New York, 628 p.

Pittman, E. D. and Larese, R.E. 1991. Compaction of lithic sands: experimental results and applications (1). American Association of Petroleum Geologists Bulletin, v. 75, no. 8, p. 1279–1299.

Plint, A.G. 2014. Mud dispersal across a Cretaceous prodelta: storm-generated, wave-enhanced sediment gravity flows inferred from mudstone microtexture and microfacies. Sedimentology, v. 61, no. 3, p. 609–647.

Plint, A.G. and Norris, B. 1991. Anatomy of a ramp margin sequence: facies successions, palaeogeography, and sediment dispersal patterns in the Muskiki and Marshybank formations, Alberta Foreland Basin. Bulletin of Canadian Petroleum Geology, v. 39, no. 1, p. 18–42.

Plint, A.G. and Walker, R.G. 1987. Cardium Formation 8. Facies and environments of the Cardium shoreline and coastal plain in the Kakwa Field and adjacent areas, northwestern Alberta. Bulletin of Canadian Petroleum Geology, v. 35, no. 1, p. 48–64.

Plummet, P.S. and Gostin, V.A. 1981. Shrinkage cracks: desiccation or synaeresis?. Journal of Sedimentary Petrology, v. 51, p. 1147–1156.

Porter, J.W., Price, R.A. and McCrossan, R.G. 1982. The Western Canadian Sedimentary Basin. Philosophical Transactions of the Royal Society of London Series A, v. 305, no. 1489, p. 169–192.

Posamentier, H.W. 2001. Lowstand alluvial bypass systems: incised vs. unincised. American Association of Petroleum Geologists Bulletin, v. 85, no. 10, p. 1771–1793.

Posamentier, H.W. and Allen, G. P. 1999. Siliciclastic sequence stratigraphy: concepts and applications. SEPM Concepts in Sedimentology and Paleontology, no. 7, p. 210.

Psuty, N.P. 1967. The geomorphology of beach ridges in Tabasco, Mexico. Unpublished PhD dissertation, Louisiana State University and Agricultural & Mechanical College, United States, 102 p.

Raychauduri, I., Brekke, H. G., Pemberton, S.G. and MacEachern, J.A. 1992. Depositional facies and trace fossils of a low energy shoreface succession, Albian Viking Formation, Chigwell Field, Alberta, Canada. In: Application of Ichnology to Petroleum Exploration, A Core Workshop. S.G. Pemberton (ed.). Society of Economic Palaeontologists and Mineralogists Core Workshop, no. 17, p. 319–338.

Raychauduri, I. and Pemberton, S.G. 1992. Ichnological and sedimentological characteristics of open marine to storm dominated restricted marine setting within the Viking/Bow Island formations, south-central Alberta. In: Application of Ichnology to Petroleum Exploration, A Core Workshop. S.G. Pemberton (ed.). Society of Economic Palaeontologists and Mineralogists Core Workshop, no. 17, p. 119–140.

Reading, H.C. and Collinson, J.D. 1996. Clastic Coast. In: Sedimentary Environments: Processes, Facies and Stratigraphy. H.G. Reading (ed.). Blackwell Science, Oxford, p. 154–231.

Reineck, H.E. and Wunderlich, F. 1968. Classification and origin of flaser and lenticular bedding. Sedimentology, v. 11, no. 1–2, p. 99–104.

Rodriguez, A.B., Hamilton, M.D. and Anderson, J.B. 2000. Facies and evolution of the modern Brazos Delta, Texas: wave versus flood influence. Journal of Sedimentary Research, v. 70, no. 2, p. 283–295.

Rouble, R.G. 1994. Sedimentology and Allostratigraphy of Falher Members A and B of the Lower Cretaceous Spirit River Formation, northwestern Alberta, Canada. Unpublished MSc thesis, McMaster University, Hamilton, Ontario, Canada, 199 p.

Rouble, R.G. and Walker, R. 1997. Sedimentology, high-resolution allostratigraphy, and key stratigraphic surfaces in Falher Members A and B, Spirit River Formation, West-Central Alberta. In: Petroleum Geology of the Cretaceous Mannville Group, Western Canada. S.G. Pemberton and D.P. James (eds.). Canadian Society of Petroleum Geologists, Memoir 18, 29 p.

Saunders, T.D.A. and Pemberton, S.G. 1990. On the palaeoecological significance of the trace fossil Macaronichnus. 13th International Sedimentological Congress 1990 Abstract, International Association of Sedimentologists, p. 416.

Schmidt, G.A. and Pemberton, S.G. 2004. Stratigraphy and paleogeography of a conglomeratic shoreline: The Notikewin Member of the Spirit River Formation in the Wapiti area of west-central Alberta. Bulletin of Canadian Petroleum Geology, v. 52, no. 1, p. 57–76.

Schmidt, V. and McDonald, D.A. 1979a. Diagenesis of Quartz Arenites. In: Secondary Reservoir Porosity in the Course of Sandstone Diagenesis. V. Schmidt and D.A. McDonald (eds.). American Association of Petroleum Geologists Education Course Note Series, no. 12, p. 77–97.

Schmidt, V. and McDonald, D.A. 1979b. The role of secondary porosity in the course of sandstone diagenesis. In: Aspects of Diagenesis. P.A. Scholle and P.R. Schlugger (eds.). Society of Economic Palaeontologists and Mineralogists Special Publication, no. 26, p. 175–207.

Schumm, S.A. 1993. River response to base level change: implications for sequence stratigraphy. Journal of Geology, v. 101, no. 2, p. 279–294.

Shanmugam, G. and Higgins, J.B. 1988. Porosity enhancement from chert dissolution beneath Neocomian unconformity: Ivishak formation, North Slope, Alaska. American Association of Petroleum Geologists Bulletin, v. 72, no. 5, p. 523–535.

Siever, R. 1962. Silica solubility, 0-200°C and the diagenesis of siliceous sediments. Journal of Geology, v. 70, p. 127–150.

Smith, R. 1984. Gas preserves and production performance of the Elmworth/Wapiti area of the Deep Basin. In: Elmworth: Case study of a deep basin gas field. J.A. Masters (ed.). American Association of Petroleum Geologists, Memoir 38, p. 153–172.

Smith, R., Zorn, C.E. and Sneider, R.M. 1984. The Palaeogeography of the Lower Cretaceous of Western Alberta and Northeastern British Columbian and Adjacent to the Deep Basin of the Elmworth Area. In: Elmworth: Case study of a deep basin gas field. J.A. Masters (ed.). American Association of Petroleum Geologists, Memoir 38, p. 79–114.

Stelck, C.R. 1975. Basement control of Cretaceous sand sequences in the western Canada. In: The Cretaceous systems in the western interior of North America. W.G.E. Caldwell (ed.). Geological Association of Canada Special Paper, no. 13, p. 427–440.

Stott, D.F. 1968. Lower Cretaceous Bullhead and Fort St. John Groups, between Smoky and Peace Rivers, Rocky Mountain Foothills, Alberta and British Columbia. Geological Survey of Canada, Bulletin 152, 279 p.

Stott, D.F. 1982. Lower Cretaceous Fort St. John Group and Upper Cretaceous Dunvegan Formation of the Foothills and Plains of Alberta, British Columbia, District of Mackenzie and Yukon Territory. Geological Survey of Canada, Bulletin 328, 124 p.

Stritch, R.A. and Schröder-Adams, C.J. 2000. Foraminiferal response to Albian relative sea-level changes in northwestern and central Alberta, Canada. Canadian Journal of Earth Sciences, v. 36, no. 10, p. 1617–1643.

Swift, D.J., Figueiredo Jr., A.G., Freeland, G.L. and Oertel, G.F. 1983. Hummocky cross-stratification and megaripples: a geological double standard?. Journal of Sedimentary Research, v. 53, no. 4, p. 125–1317.

Switzer, S.B., Holland, W.G., Christie, D.S., Graf, G.C., Hedinger, A.S., McAuley, R.J., Wierzbicki, R.A. and Packard, J.J. 1994. Devonian Woodbend–Winterburn strata of the Western Canadian Sedimentary Basin. In: Geological Atlas of the Western Canada Sedimentary Basin. G.D. Mossop and I. Shetsen (comp.). Canadian Society of Petroleum Geologists and Alberta Research Council, p. 165–202.

Tanner, P.W.G. 2003. Syneresis. In: Encyclopedia of Sediments and Sedimentary Rocks. G.V. Middleton (eds.). Kluwer Academic Publishers, Dordrecht, p. 718–720.

Tilley, B.J. and Longstaffe, F.J. 1989. Diagenesis and isotopic evolution of porewaters in the Alberta Deep Basin: the Falher Member and Cadomin Formation. Geochimica et Cosmochimica Acta, v. 53, no. 10, p. 2529–2546.

Ulmer-Scholle, D.S., Scholle, P.A., Schieber, J. and Raine, R.J. 2015. A color guide to the petrography of sandstones, siltstones, shales and associated rocks. American Association of Petroleum Geologists, Memoir 109, 494 p.

Usdowski, H.E. 1968. The formation of dolomite in sediments. In: Recent developments in carbonate sedimentology in Central Europe. G. Miller and G.M. Friedman (eds.). Springer-Verlag, Berlin, p. 21–32.

van Gelder, A., van den Berg, J.H., Cheng, G. and Xue, C. 1994. Overbank and channel fill deposits of the modern Yellow River delta. Sedimentary Geology, v. 90, no. 3–4, p. 293–305.

van Wagoner, J.C., Mitchum Jr., R.M., Campion, K.M. and Rahmanian, V.D. 1990. Siliciclastic sequence stratigraphy in well logs, cores and outcrops: concepts for high resolution correlation of time and facies. American Association of Petroleum Geologists Methods in Exploration Series, no. 7, 55 p.

VanSickle, S. R. 1995. Rock Type, Productivity and Reserves of the Falher F, Cutbank Area, Alberta. CSPG/CWLS 1995 Core Session Abstract, p. 277–297.

Vossler, S.M. and Pemberton, S.G. 1988. Ichnology of the Cardium Formation (Pembina oilfield): Implications for depositional and sequence stratigraphic interpretations. In: Sequences, Stratigraphy, Sedimentology: Surface and Subsurface. D.P. James and D.A. Leckie (eds.). Canadian Society of Petroleum Geologists, Memoir 15, p. 237–254.

Wadsworth, J., Boyd, R., Diessel, C. and Leckie, O. 2003. Stratigraphic style of coal and non-marine strata in a high accommodation setting: Falher Member and Gates Formation (Lower Cretaceous), western Canada. Bulletin of Canadian Petroleum Geology, v. 51, no. 3, p. 275–303.

Walker, T.R., Waugh, B. and Grone, A.J. 1978. Diagenesis in first-cycle desert alluvium of Cenozoic age, southwestern United States and northwestern Mexico. Geological Society of America Bulletin, v. 89, no. 1, p. 19–32.

Williams, G.D. and Stelck, C.R. 1975. Speculations on the Cretaceous palaeogeography of North America. In: The Cretaceous System in the Western Interior of North America. W.G.E. Caldwell (ed.). Geological Association of Canada Special Publication, no. 13, p. 1–20.

Worden, R.H. and Morad, S. 2003. Clay minerals in sandstones: controls on formation, distribution and evolution. In: Clay Mineral Cements in Sandstones. R.G. Worden and S. Morad (eds.). International Association of Sedimentologists Special Publication, no. 34, p. 3–41.

Wright, V. P. 1986. Paleosols: their recognition and interpretation. Blackwell Scientific, Oxford, 315 p.

Wright, V.P. 1992. Paleosol recognition: a guide to early diagenesis in terrestrial settings. In: Diagenesis, III. K.H. Wolf and G.H. Chilingarian (eds.). Developments in Sedimentology, v. 47, p. 591–619.

Wright, V.P. and Marriott, S.B. 1993. The sequence stratigraphy of fluvial depositional systems: the role of floodplain sediment storage. Sedimentary Geology, v. 86, p. 203–210.

Wyman, R.E., Holditch, S.A. and Randolph, R.L. 1980. Analyses of an Elmworth hydraulic fracture in Alberta. Journal of Petroleum Technology, v. 32, p. 1621–1630.

Yagishita, K. and Ohkubo, K. 2007. Relative durability of chert and rhyolite detritus in conglomerates and sandstones: with reference to the study of provenance geology. Terra Nova, no. 19, v. 3, p. 174–181.

Yin, S., Hu, Z., Ren, X., Wu, X., Chen, Y., Zheng, L. and Jiang, Z. 2016. Reservoir architecture patterns of sandy gravel braided distributary channel: A case study of Triassic Upper Karamay Formation, Xinjiang oilfield. Petroleum, v. 2, no. 2, p. 117–129.

Youn, S.H. 1981. Falher conglomerates and sandstones, Elmworth area: depositional environments and their significance on diagenetic processes. CSPG Annual Core and Field Sample Conference 1981, p. 38–42.

Young, S.W. 1976. Petrographic textures of detrital polycrystalline quartz as an aid to interpreting crystalline source rocks. Journal of Sedimentary Research, v. 46, no. 3, p. 595–603.

Zaitlin, B.A. and Moslow, T.F. 2006. A review of deep basin gas reservoirs of the Western Canada Sedimentary Basin. Mountain Geologist, v. 43, no. 3, p. 257-262.

Zonneveld, J.-P. and Moslow, T.F. 2004. Exploration potential of the Falher G shoreface conglomerate trend: evidence from outcrop. Bulletin of Canadian Petroleum Geology, v. 52, no. 1, p. 23–38.

Zonneveld, J.-P, Tisdale, D. and Legault, F. 2017. Analysis of contrasting adjacent tight sand reservoirs: the Falher F and Falher G (upper Wilrich) sandstone successions in the Kakwa region, Alberta. CSPG Core Conference 2017 Abstract, p. 50–53.

APPENDIX I: CORE LOGS

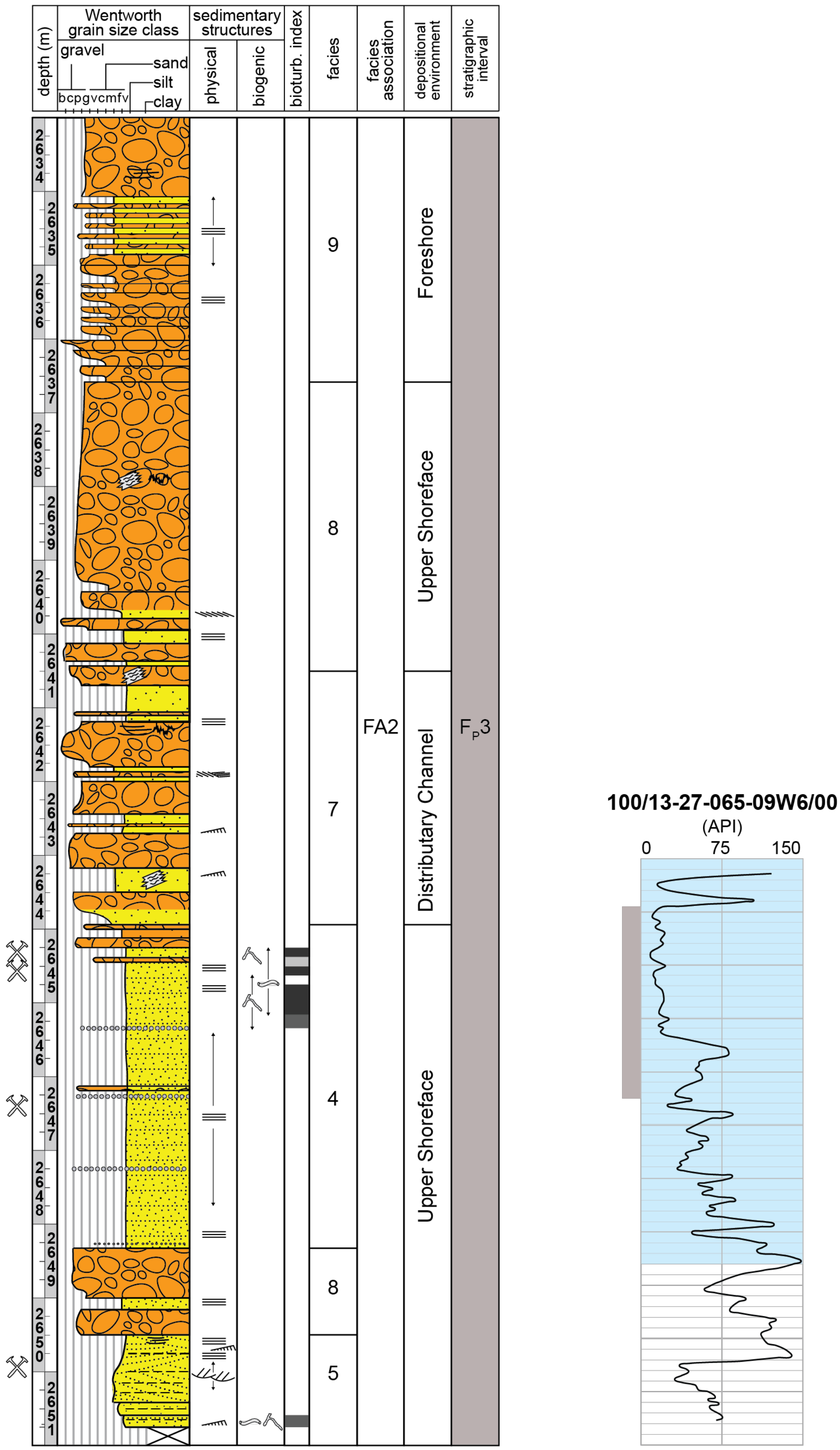
depth (m)
Wentworth grain size class
gravel
sand
silt
clay
b c p g vc c m f vf
sedimentary structures
physical
biogenic
bioturb. index
facies
facies association
depositional environment
stratigraphic interval
9
8
7
4
8
5
FA2
Foreshore
Upper Shoreface
Distributary Channel
Upper Shoreface
F_P3
100/13-27-065-09W6/00
(API)
0
75
150

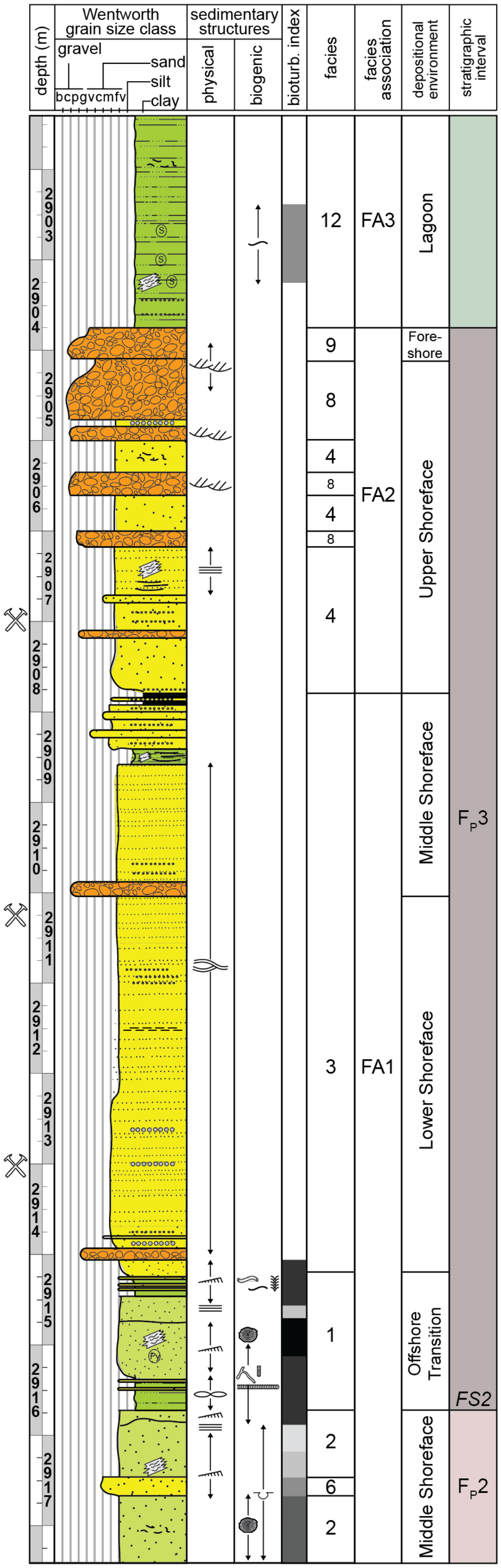
depth (m)
Wentworth grain size class
gravel
sand
silt
clay
b c p g v c m f v
sedimentary structures
physical
biogenic
bioturb. index
facies
facies association
depositional environment
stratigraphic interval
2903
2904
2905
2906
2907
2908
2909
2910
2911
2912
2913
2914
2915
2916
2917
12
9
8
4
8
4
8
4
3
1
2
6
2
FA3
FA2
FA1
Lagoon
Fore-shore
Upper Shoreface
Middle Shoreface
Lower Shoreface
Offshore Transition
Middle Shoreface
F$_P$3
FS2
F$_P$2


100/05-32-065-09W6/00
(API)
0
75
150

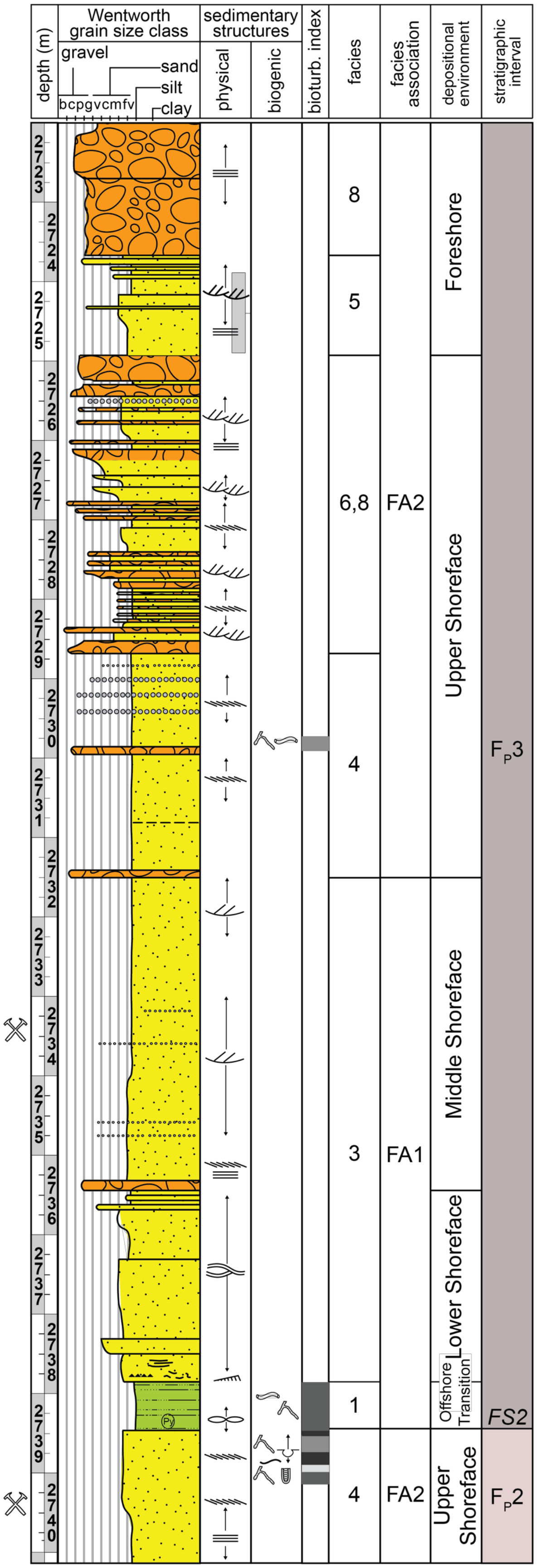
depth (m)
Wentworth grain size class
gravel
sand
silt
clay
b c p g vc m f vf
sedimentary structures
physical
biogenic
bioturb. index
facies
facies association
depositional environment
stratigraphic interval
2723
2724
2725
2726
2727
2728
2729
2730
2731
2732
2733
2734
2735
2736
2737
2738
2739
2740
8
5
6,8
4
3
1
4
FA2
FA1
FA2
Foreshore
Upper Shoreface
Middle Shoreface
Lower Shoreface
Offshore Transition
Upper Shoreface
F_P3
FS2
F_P2
Py


100/03-33-065-09W6/00
(API)
0
75
150

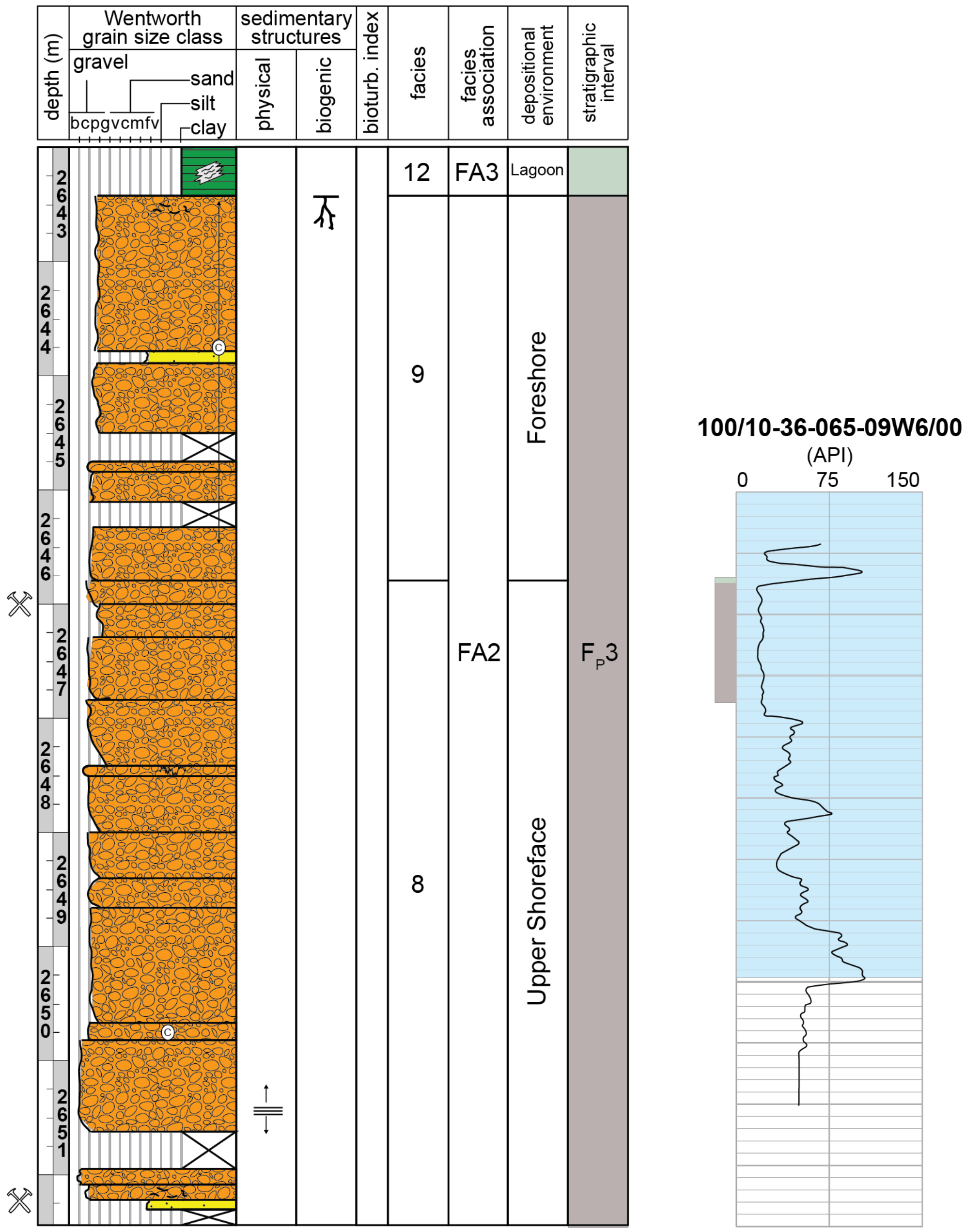
depth (m)
Wentworth grain size class
gravel
sand
silt
clay
bcpgvcmfv
sedimentary structures
physical
biogenic
bioturb. index
facies
facies association
depositional environment
stratigraphic interval
2643
2644
2645
2646
2647
2648
2649
2650
2651
12
FA3
Lagoon
9
Foreshore
8
FA2
Upper Shoreface
F P3
100/10-36-065-09W6/00
(API)
0
75
150

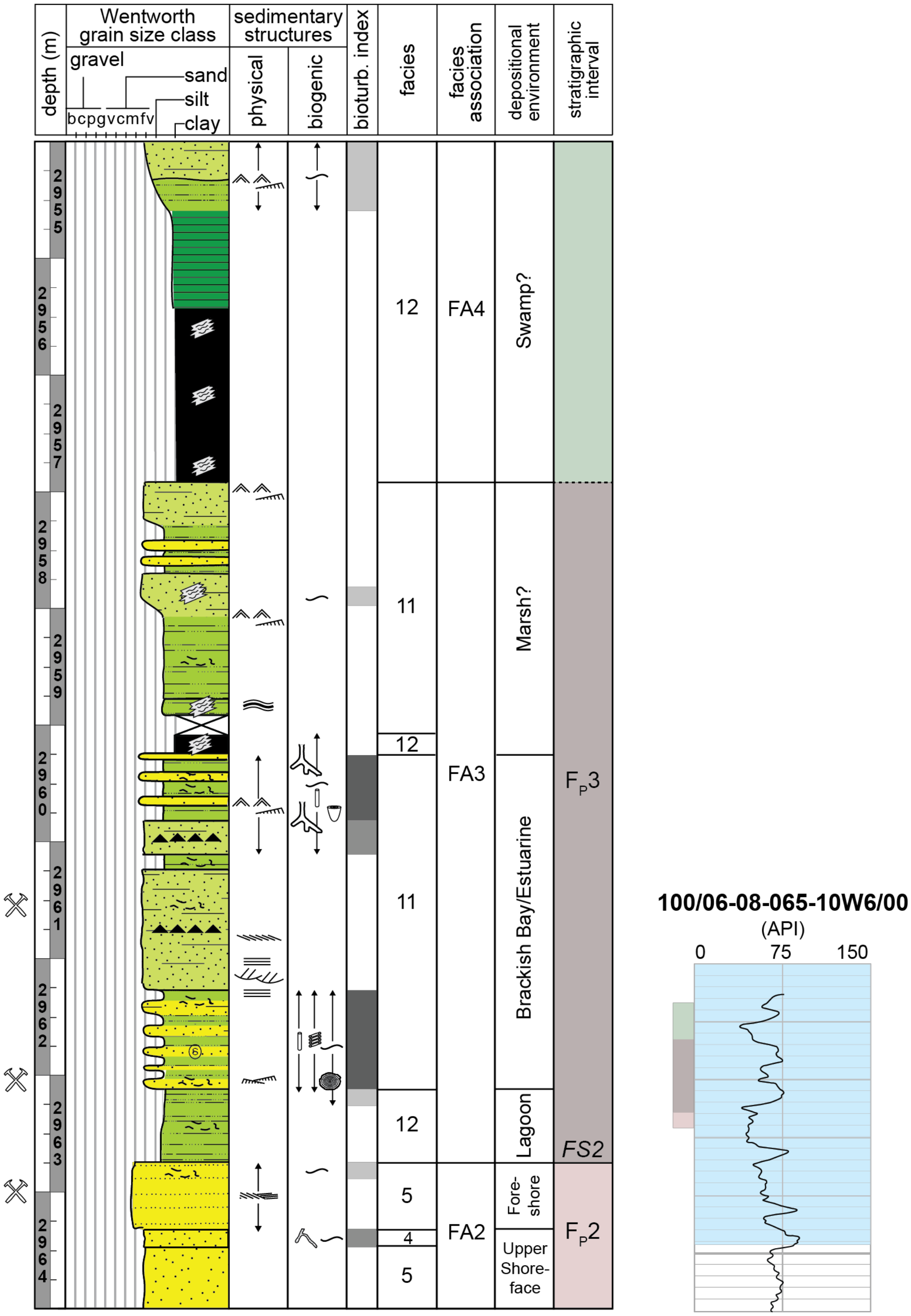
depth (m)
Wentworth grain size class
gravel
sand
silt
clay
b c p g v c m f v
sedimentary structures
physical
biogenic
bioturb. index
facies
facies association
depositional environment
stratigraphic interval
2955
2956
2957
2958
2959
2960
2961
2962
2963
2964
12
11
12
11
12
5
4
5
FA4
FA3
FA2
Swamp?
Marsh?
Brackish Bay/Estuarine
Lagoon
Fore-shore
Upper Shore-face
F P 3
FS2
F P 2
100/06-08-065-10W6/00
(API)
0
75
150

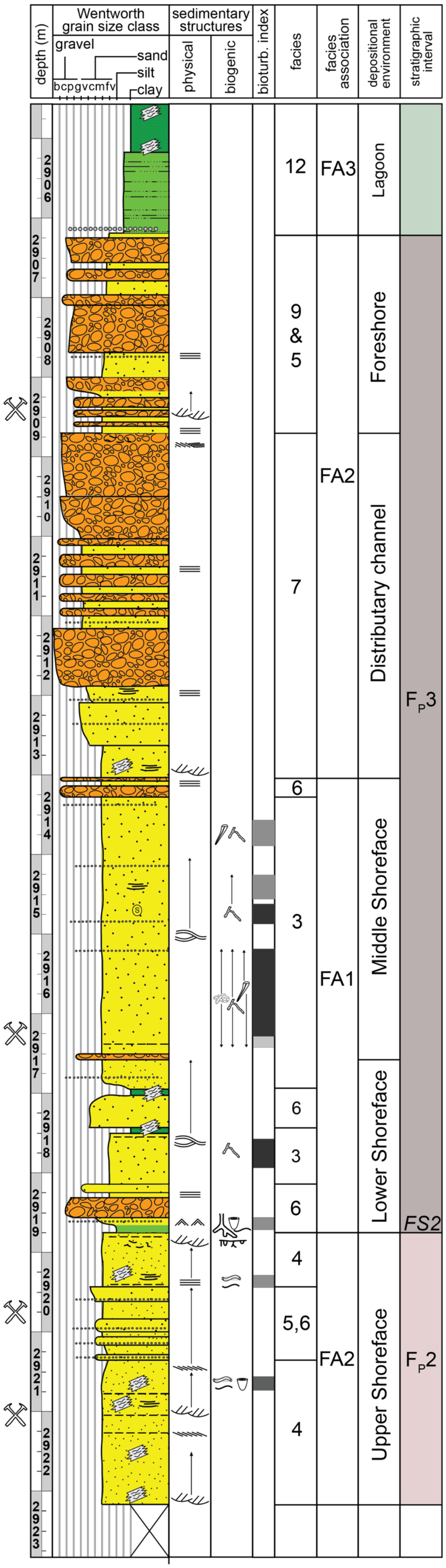
depth (m)
Wentworth grain size class
gravel
sand
silt
clay
bcpgvcmfv
sedimentary structures
physical
biogenic
bioturb. index
facies
facies association
depositional environment
stratigraphic interval
12
FA3
Lagoon
9 & 5
Foreshore
FA2
7
Distributary channel
6
3
Middle Shoreface
FA1
6
3
6
Lower Shoreface
FS2
4
5,6
FA2
4
Upper Shoreface
F_P3
F_P2
2906
2907
2908
2909
2910
2911
2912
2913
2914
2915
2916
2917
2918
2919
2920
2921
2922
2923

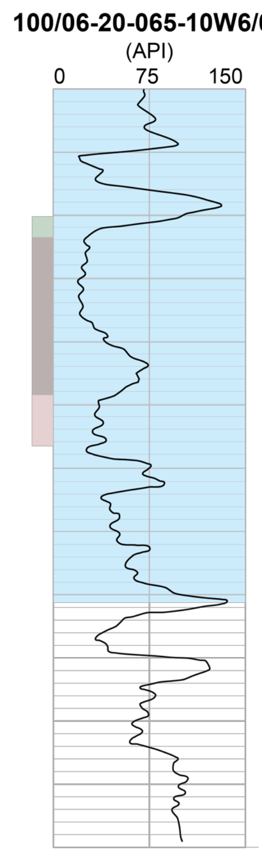
100/06-20-065-10W6/00
(API)
0
75
150

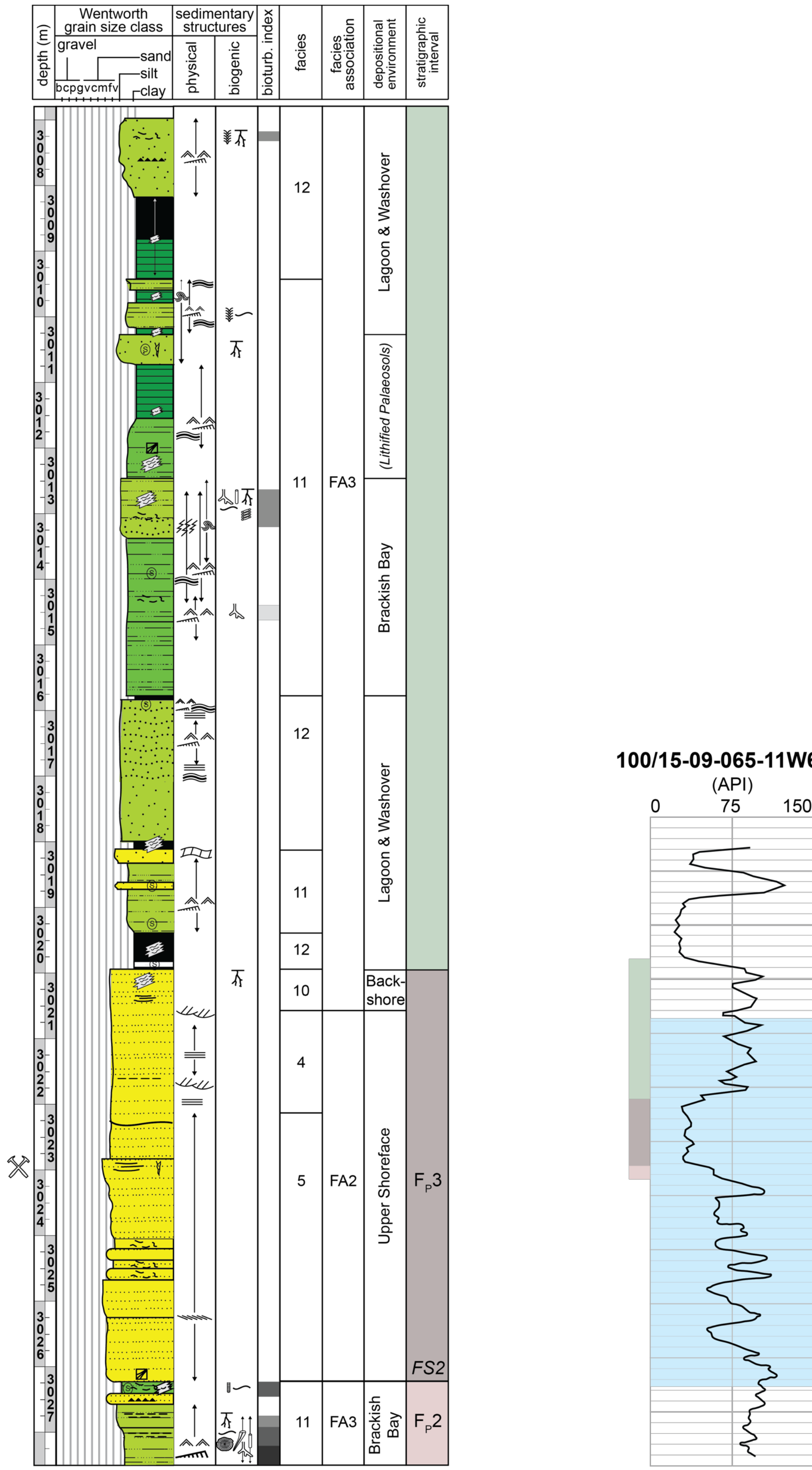

depth (m)
Wentworth grain size class
gravel
sand
silt
clay
b c p g vc c m f vf
sedimentary structures
physical
biogenic
bioturb. index
facies
facies association
depositional environment
stratigraphic interval
3008
3009
3010
3011
3012
3013
3014
3015
3016
3017
3018
3019
3020
3021
3022
3023
3024
3025
3026
3027
12
11
12
11
12
10
4
5
11
FA3
FA2
FA3
Lagoon & Washover
(Lithified Palaeosols)
Brackish Bay
Lagoon & Washover
Back-shore
Upper Shoreface
Brackish Bay
FP3
FS2
FP2
100/15-09-065-11W6/00
(API)
0
75
150

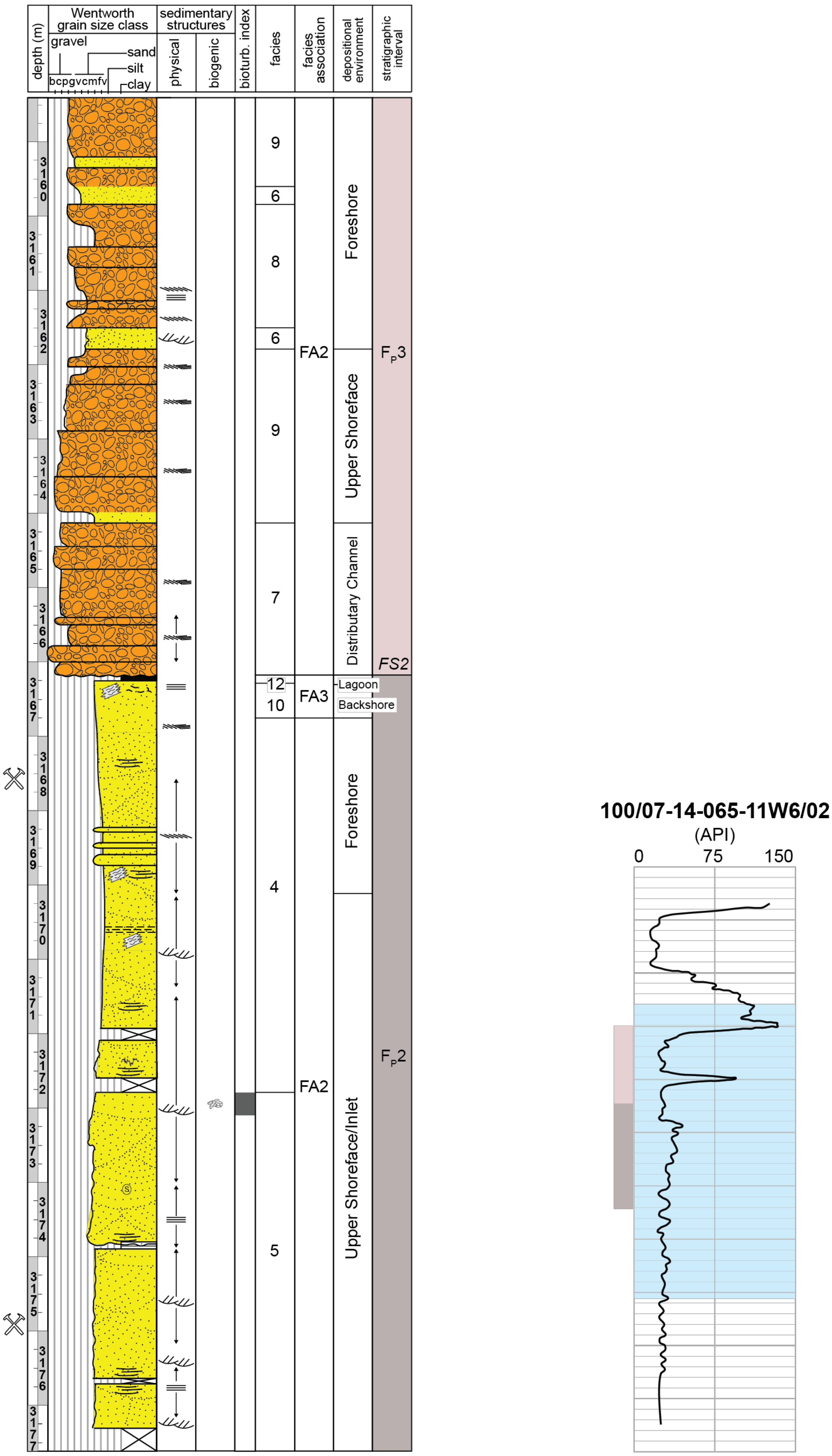

depth (m)
Wentworth grain size class
gravel
sand
silt
clay
b c p g vc c m f vf
sedimentary structures
physical
biogenic
bioturb. index
facies
facies association
depositional environment
stratigraphic interval
9
6
8
6
9
7
12
10
4
5
FA2
FA3
FA2
Foreshore
Upper Shoreface
Distributary Channel
Lagoon
Backshore
Foreshore
Upper Shoreface/Inlet
F_P3
FS2
F_P2
3160
3161
3162
3163
3164
3165
3166
3167
3168
3169
3170
3171
3172
3173
3174
3175
3176
3177
100/07-14-065-11W6/02
(API)
0
75
150

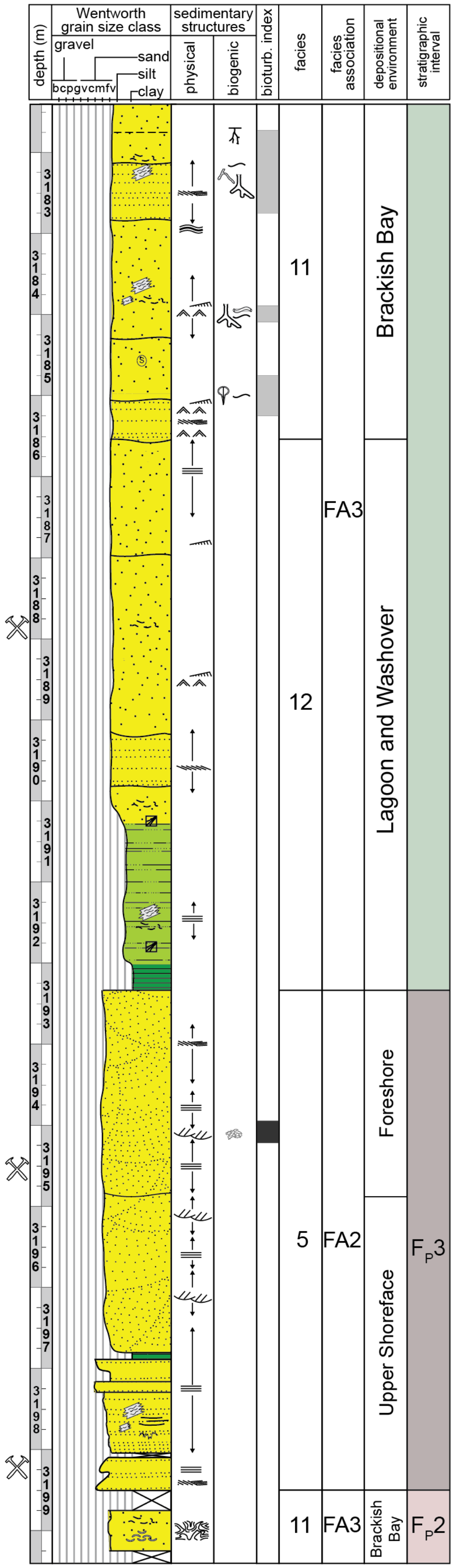
depth (m)
Wentworth grain size class
gravel
sand
silt
clay
bcpgvcmfv
sedimentary structures
physical
biogenic
bioturb. index
facies
facies association
depositional environment
stratigraphic interval
11
12
5
11
FA3
FA2
FA3
Brackish Bay
Lagoon and Washover
Foreshore
Upper Shoreface
Brackish Bay
F_P3
F_P2


100/07-16-065-11W6/02
(API)
0
75
150

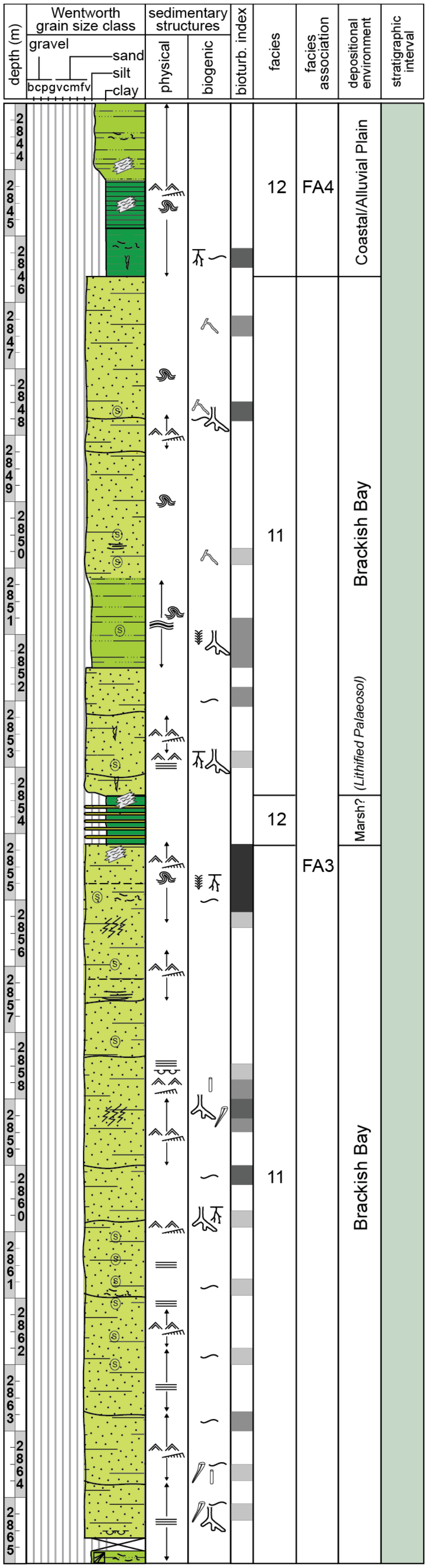
depth (m)
Wentworth grain size class
gravel
sand
silt
clay
bcpgvcmfv
sedimentary structures
physical
biogenic
bioturb. index
facies
facies association
depositional environment
stratigraphic interval
2844
2845
2846
2847
2848
2849
2850
2851
2852
2853
2854
2855
2856
2857
2858
2859
2860
2861
2862
2863
2864
2865
12
FA4
Coastal/Alluvial Plain
11
Brackish Bay
(Lithified Palaeosol)
12
Marsh?
FA3
11
Brackish Bay


100/03-20-065-11W6/00
(API)
0
75
150

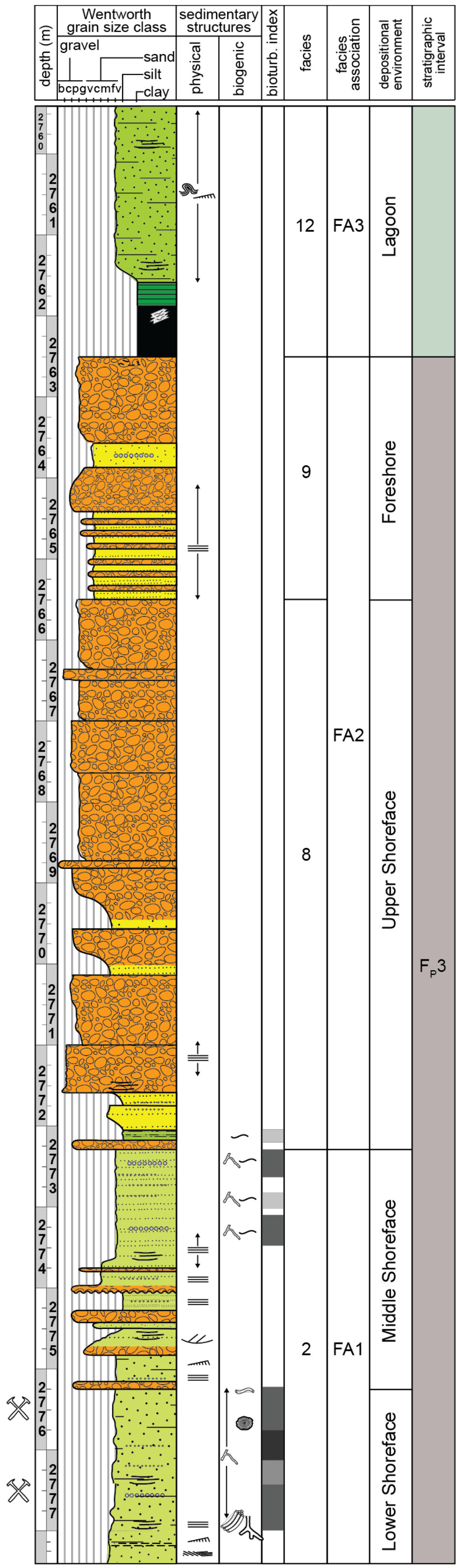

depth (m)
Wentworth grain size class
gravel
sand
silt
clay
bcpgvcmfv
sedimentary structures
physical
biogenic
bioturb. index
facies
facies association
depositional environment
stratigraphic interval
2760
2761
2762
2763
2764
2765
2766
2767
2768
2769
2770
2771
2772
2773
2774
2775
2776
2777
12
FA3
Lagoon
9
Foreshore
8
FA2
Upper Shoreface
2
FA1
Middle Shoreface
Lower Shoreface
F_P3

100/14-24-065-11W6/00
(API)
0
75
150

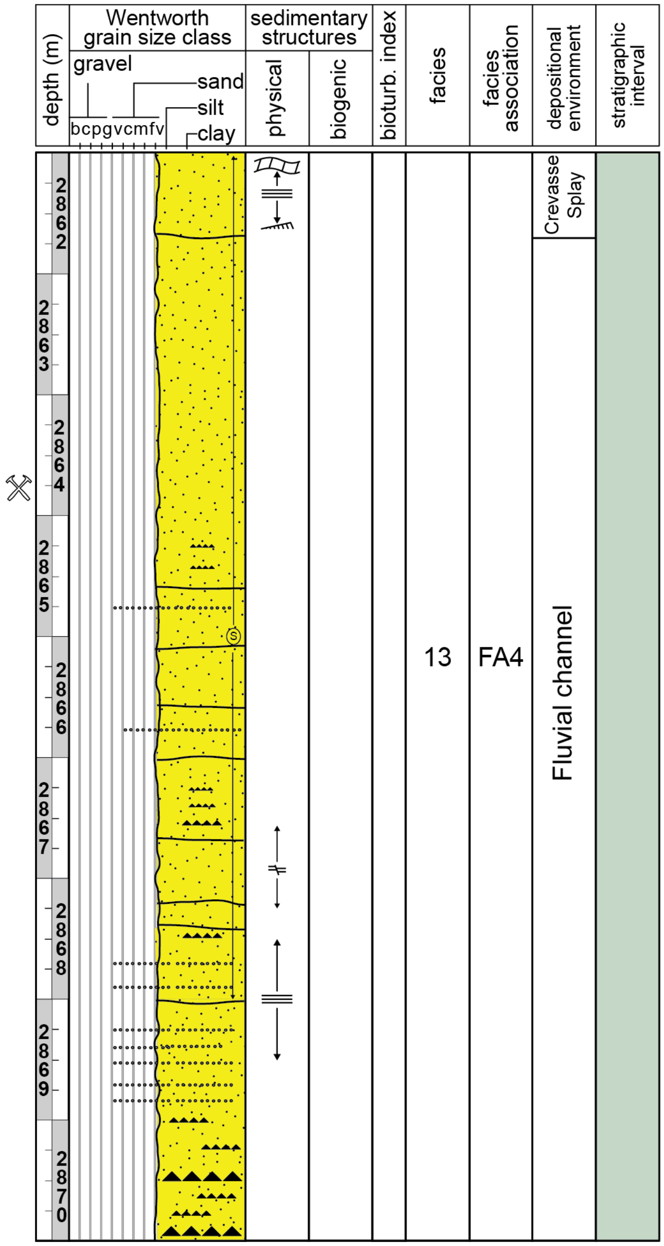
depth (m)
Wentworth grain size class
gravel
sand
silt
clay
bcpgvcmfv
sedimentary structures
physical
biogenic
bioturb. index
facies
facies association
depositional environment
stratigraphic interval
2862
2863
2864
2865
2866
2867
2868
2869
2870
Crevasse Splay
13
FA4
Fluvial channel

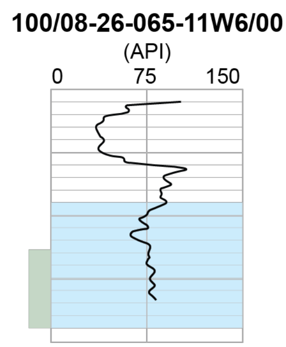
100/08-26-065-11W6/00
(API)
0
75
150

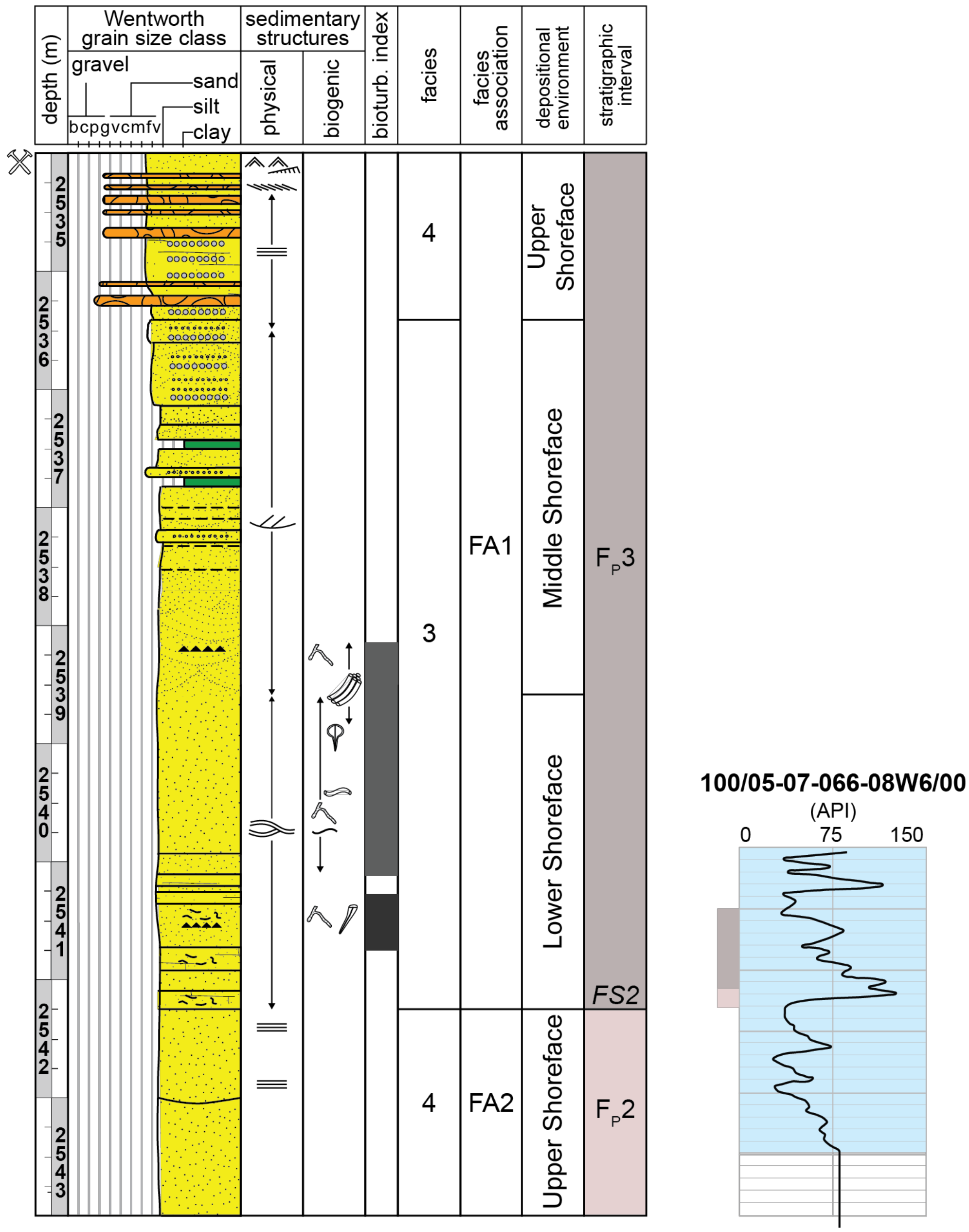
depth (m)
Wentworth grain size class
gravel
sand
silt
clay
b c p g v c m f v
sedimentary structures
physical
biogenic
bioturb. index
facies
facies association
depositional environment
stratigraphic interval
2535
2536
2537
2538
2539
2540
2541
2542
2543
4
3
4
FA1
FA2
Upper Shoreface
Middle Shoreface
Lower Shoreface
Upper Shoreface
F_P3
FS2
F_P2
100/05-07-066-08W6/00
(API)
0
75
150

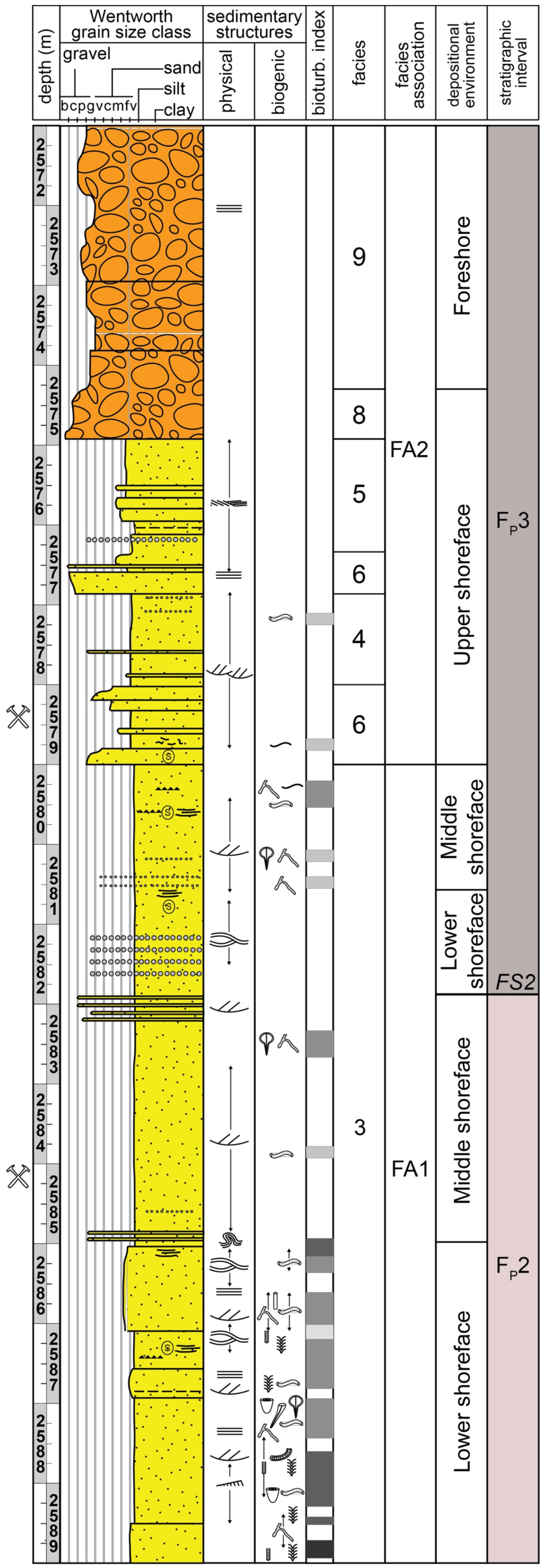
depth (m)
Wentworth grain size class
gravel
sand
silt
clay
bcpgvcmfv
sedimentary structures
physical
biogenic
bioturb. index
facies
facies association
depositional environment
stratigraphic interval
9
8
5
6
4
6
3
FA2
FA1
Foreshore
Upper shoreface
Middle shoreface
Lower shoreface
Middle shoreface
Lower shoreface
FP3
FS2
FP2

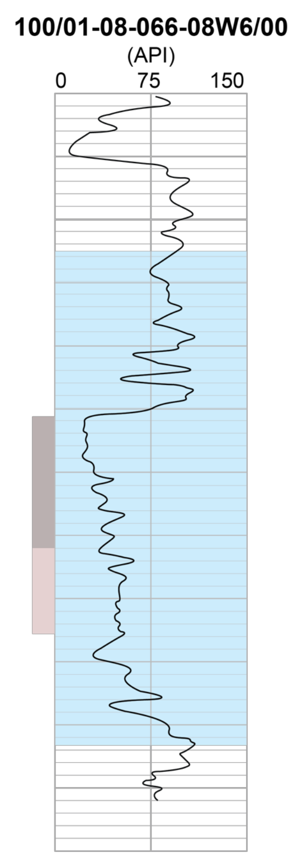
100/01-08-066-08W6/00
(API)
0
75
150

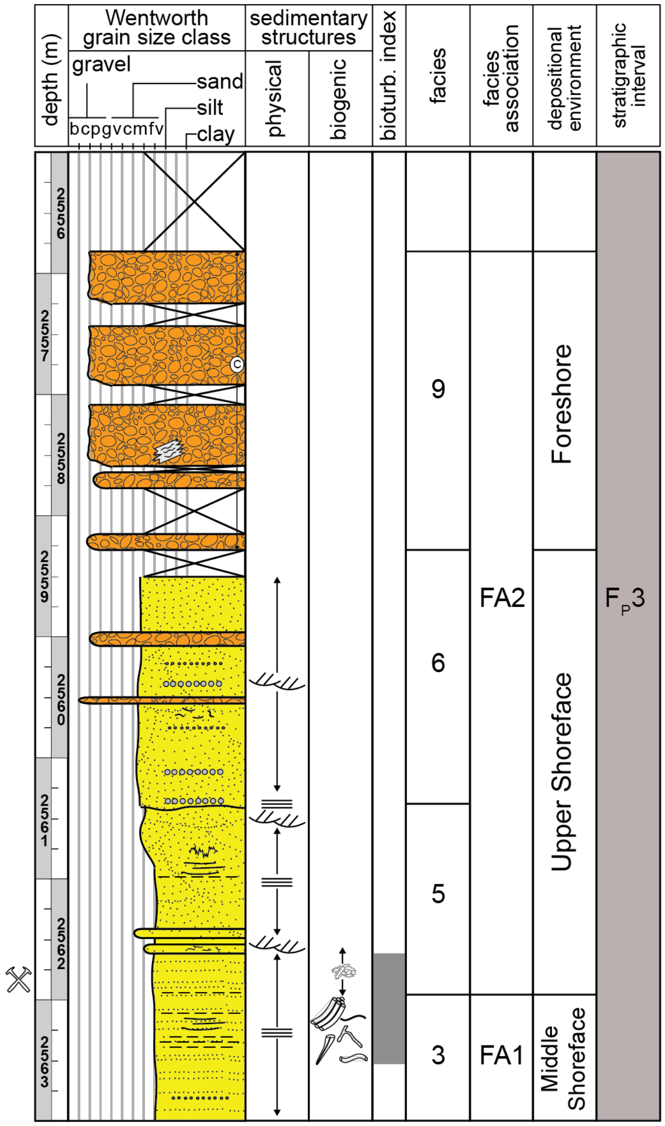
depth (m)
Wentworth grain size class
gravel
sand
silt
clay
bcpgvcmfv
sedimentary structures
physical
biogenic
bioturb. index
facies
facies association
depositional environment
stratigraphic interval
2556
2557
2558
2559
2560
2561
2562
2563
9
6
5
3
FA2
FA1
Foreshore
Upper Shoreface
Middle Shoreface
F_P3

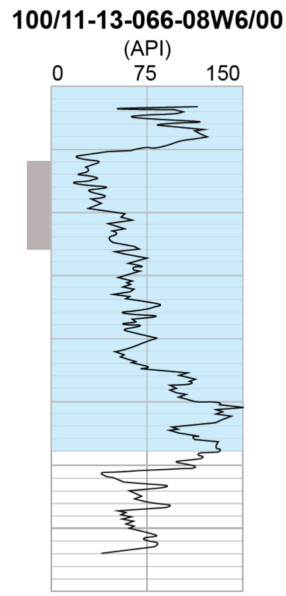
100/11-13-066-08W6/00
(API)
0
75
150

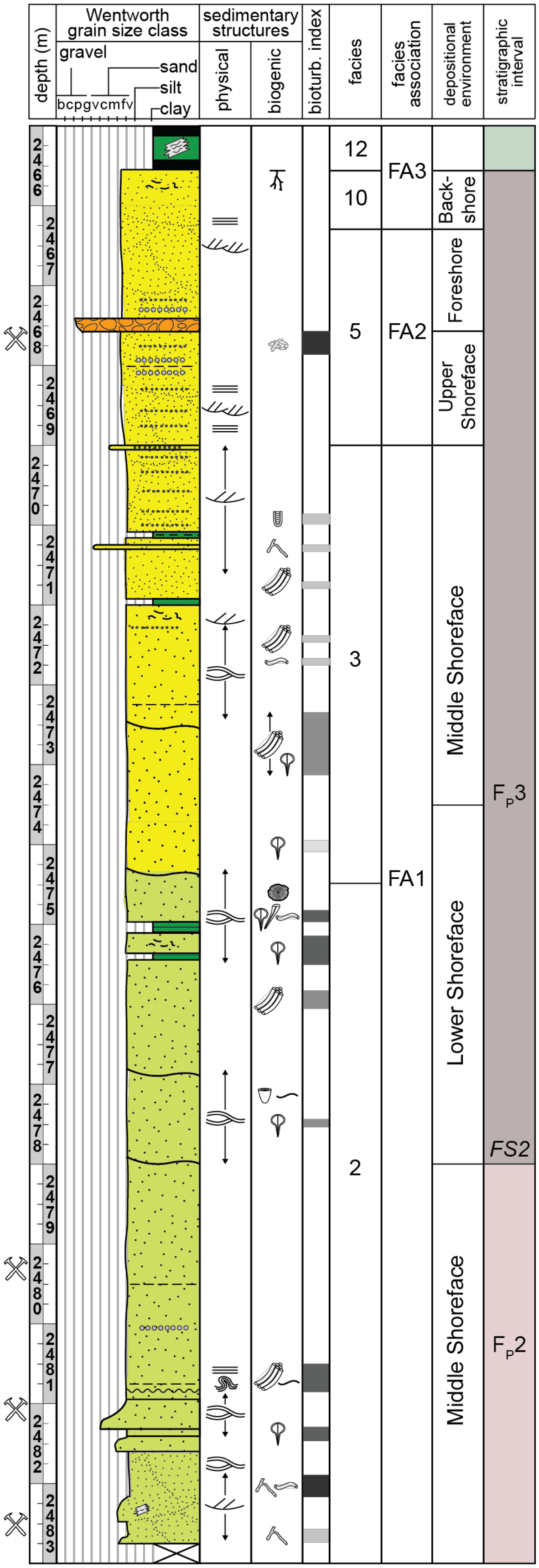
depth (m)
Wentworth grain size class
gravel
sand
silt
clay
b c p g vc m f vf
sedimentary structures
physical
biogenic
bioturb. index
facies
facies association
depositional environment
stratigraphic interval
2466
2467
2468
2469
2470
2471
2472
2473
2474
2475
2476
2477
2478
2479
2480
2481
2482
2483
12
10
5
3
2
FA3
FA2
FA1
Back-shore
Foreshore
Upper Shoreface
Middle Shoreface
Lower Shoreface
Middle Shoreface
F_P3
FS2
F_P2


100/03-18-066-08W6/00
(API)
0
75
150

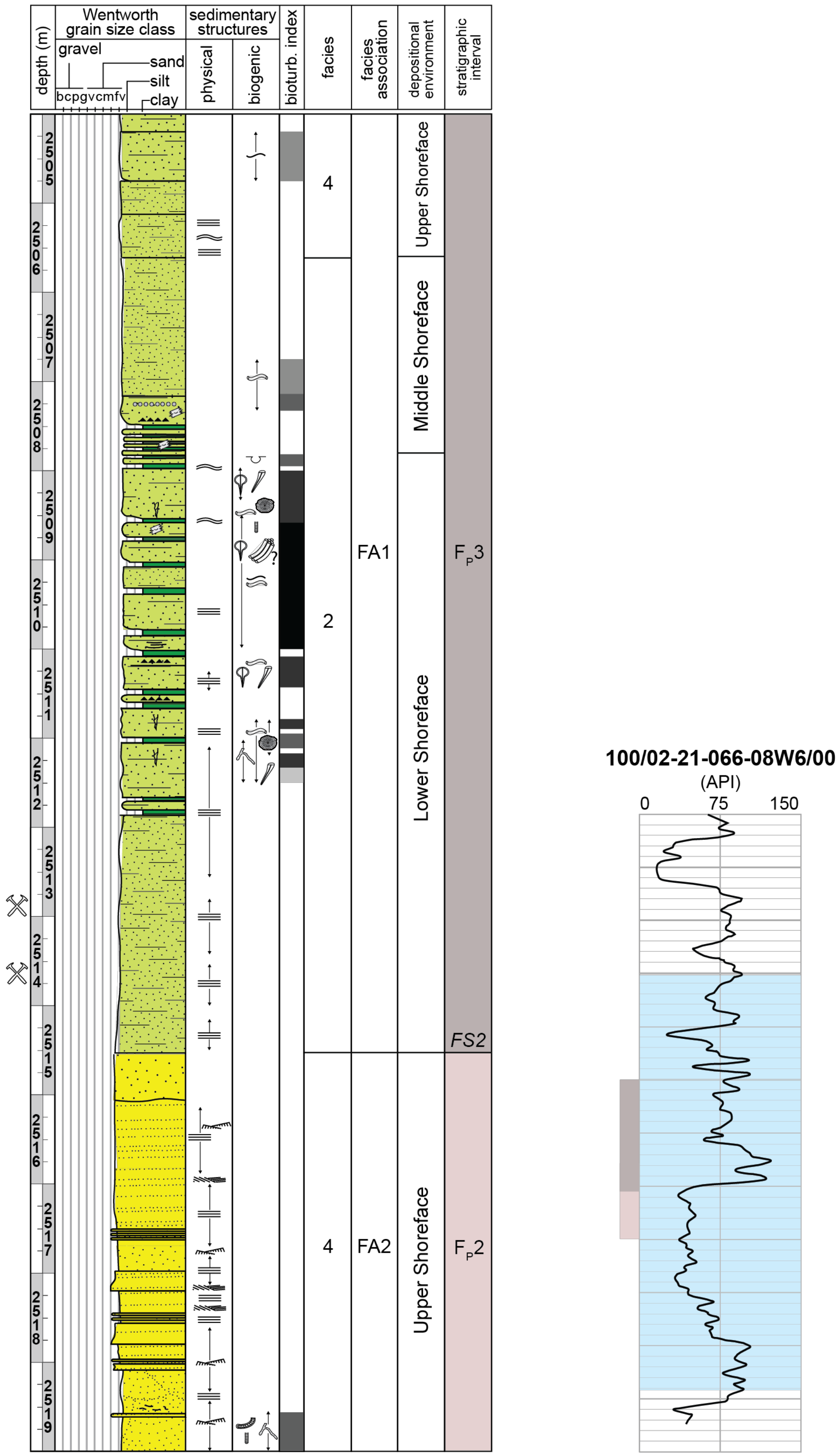
depth (m)
Wentworth grain size class
gravel
sand
silt
clay
bcpgvcmfv
sedimentary structures
physical
biogenic
bioturb. index
facies
facies association
depositional environment
stratigraphic interval
2505
2506
2507
2508
2509
2510
2511
2512
2513
2514
2515
2516
2517
2518
2519
4
2
4
FA1
FA2
Upper Shoreface
Middle Shoreface
Lower Shoreface
Upper Shoreface
F_P3
FS2
F_P2
100/02-21-066-08W6/00
(API)
0
75
150

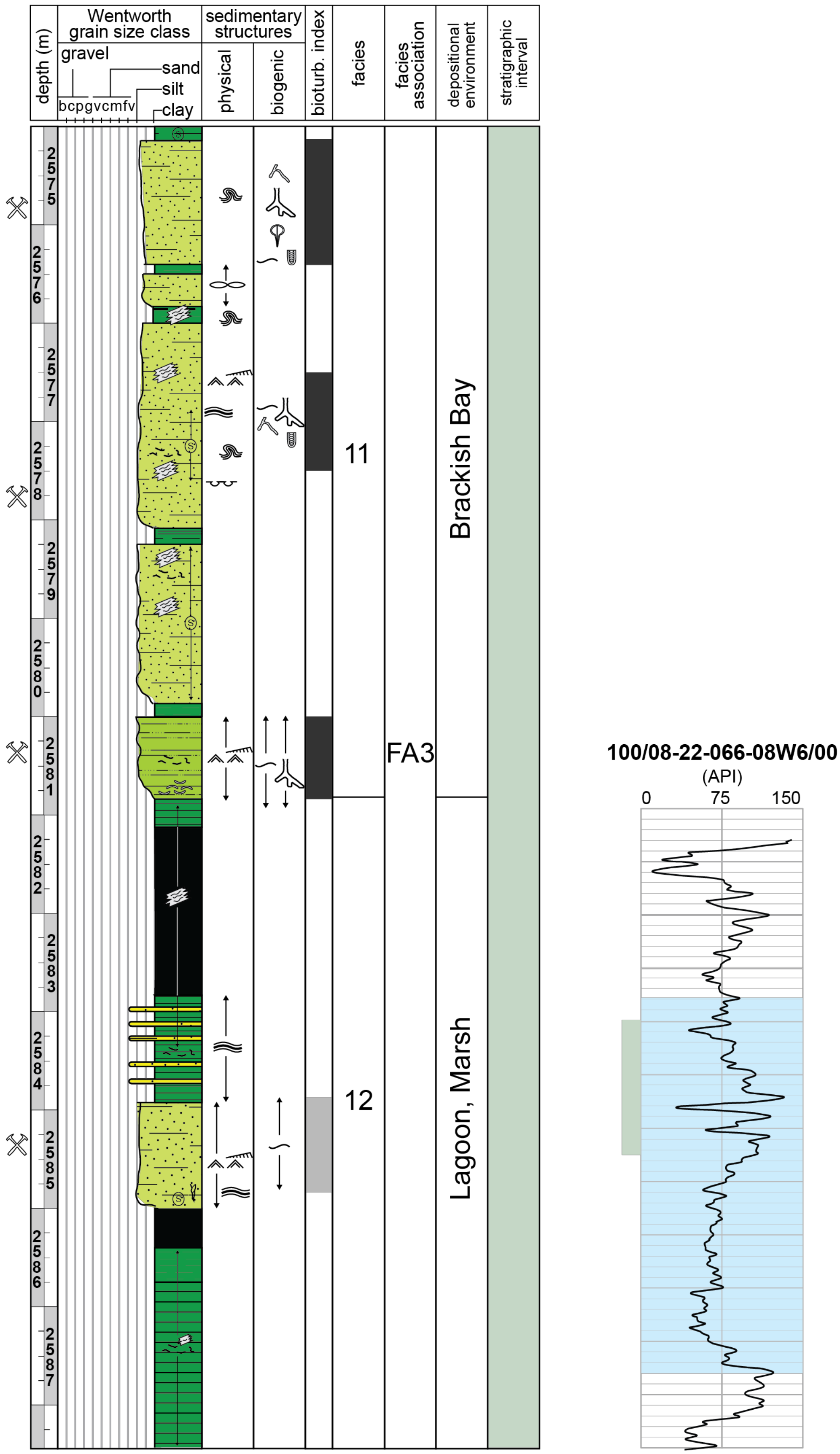

depth (m)
Wentworth grain size class
gravel
sand
silt
clay
bcpgvcmfv
sedimentary structures
physical
biogenic
bioturb. index
facies
facies association
depositional environment
stratigraphic interval
2575
2576
2577
2578
2579
2580
2581
2582
2583
2584
2585
2586
2587
11
12
FA3
Brackish Bay
Lagoon, Marsh
100/08-22-066-08W6/00
(API)
0
75
150

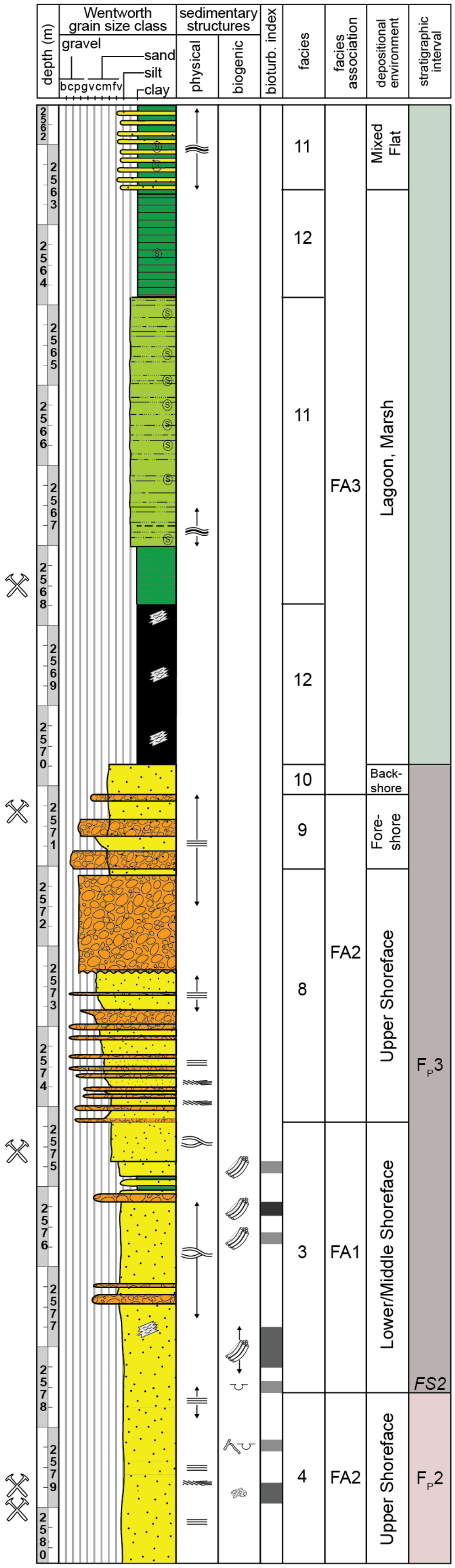
depth (m)
Wentworth grain size class
gravel
sand
silt
clay
b c p g v c m f v
sedimentary structures
physical
biogenic
bioturb. index
facies
facies association
depositional environment
stratigraphic interval
2562
2563
2564
2565
2566
2567
2568
2569
2570
2571
2572
2573
2574
2575
2576
2577
2578
2579
2580
11
12
11
12
10
9
8
3
4
FA3
FA2
FA1
FA2
Mixed Flat
Lagoon, Marsh
Back-shore
Fore-shore
Upper Shoreface
Lower/Middle Shoreface
Upper Shoreface
F_P3
FS2
F_P2


100/08-02-066-09W6/00
(API)
0
75
150

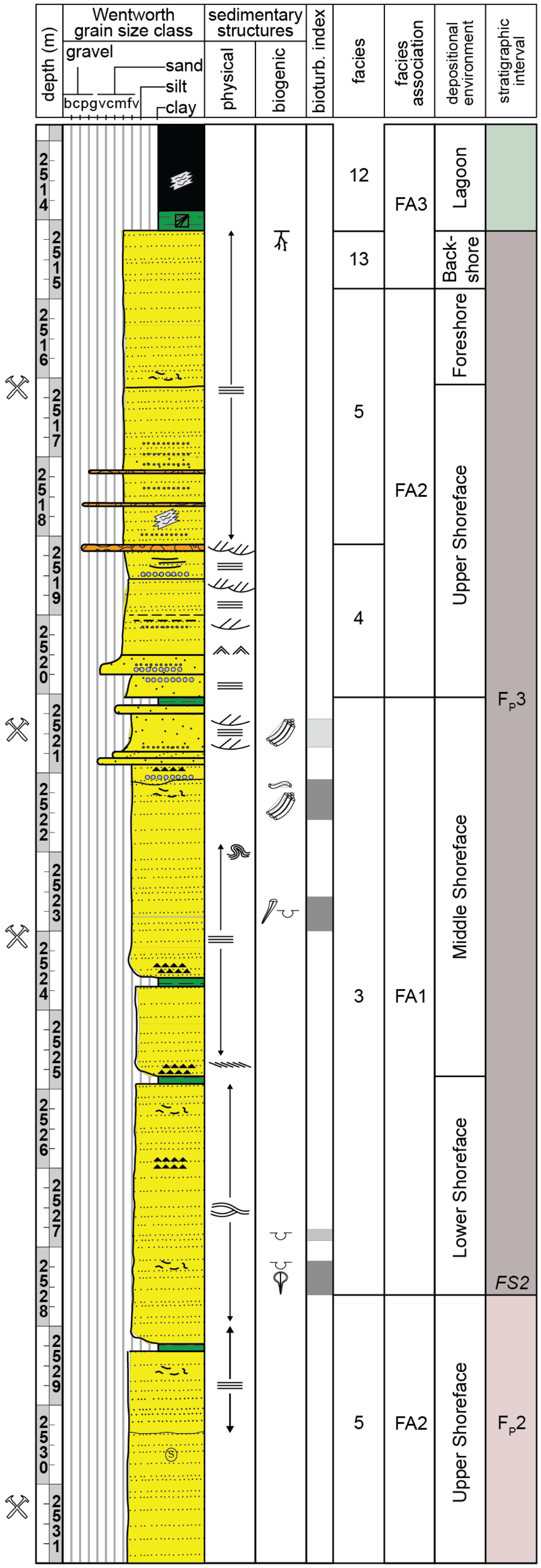
depth (m)
Wentworth grain size class
gravel
sand
silt
clay
bcpgvcmfv
sedimentary structures
physical
biogenic
bioturb. index
facies
facies association
depositional environment
stratigraphic interval
2514
2515
2516
2517
2518
2519
2520
2521
2522
2523
2524
2525
2526
2527
2528
2529
2530
2531
12
13
5
4
3
5
FA3
FA2
FA1
FA2
Lagoon
Back-shore
Foreshore
Upper Shoreface
Middle Shoreface
Lower Shoreface
Upper Shoreface
F_P3
FS2
F_P2

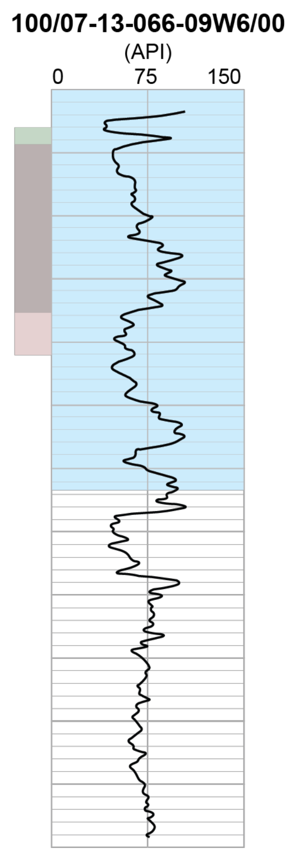
100/07-13-066-09W6/00
(API)
0
75
150

APPENDIX II: POINT COUNTING RESULTS

Well	Depth	Detrital Quartz		Chalcedony	Chert	Quartzite	Rock Fragments				Feldspars	Detrital Micas			Others	Authigenic Cement							Thin Section Porosity	Composition (raw)		
		Monocrystalline Quartz	Polycrystalline Quartz				Iron-stained RF	Metamorphic RF	Sedimentary RF	Dolomite		Biotite Mica	Muscovite Mica	Chlorite		Kaolinite	Illite/smectite	Chlorite	Dolomite	Fe-dolomite	Calcite & Fe-calcite	Iron Oxide		Q*	C*	RF*
Petrofacies I																										
1-8-66-8W6	2579.4	39.3	1.7		46.3		3.0		3.7						0.3							0.3	5.3	41.0	46.3	6.7
13-27-65-9W6	2650.8	35.3	6.0		34.7		6.7		7.0	7.0												1.0	2.3	41.3	34.7	20.7
3-18-66-8W6	2481.6	29.7	6.0		39.0		5.3	1.0	5.7	10.7			0.3									2.0	0.3	35.7	39.0	22.7
6-20-65-10W6	2920.7	27.0	7.7		33.0	1.3	9.7		10.3	4.3			0.3									3.3	3.0	34.7	34.3	24.3
																							Mean	**38.2**	**38.6**	**18.6**
Petrofacies II																										
10-36-65-9W6	2647.0	34.7	3.0		43.0	0.3	5.3		3.0							2.3							8.3	37.7	43.3	8.3
10-36-65-9W6	2652.3	33.3	5.3		34.7		14.7		0.7	0.3						4.0				0.3			6.7	38.7	34.7	15.7
11-13-66-8W6	2563.0	33.7	12.3		30.7	1.3	5.7		4.7	2.0	0.3		0.3			1.3			1.0	1.0		0.7	5.0	46.0	32.0	12.7
5-32-65-9W6	2911.3	32.3	10.3		21.3	0.3	3.3		6.7	2.0		0.3				4.7			4.3	0.7		1.3	12.3	42.7	21.7	12.0
6-20-65-10W6	2909.4	42.7	4.0		22.0	0.7	2.0		0.7			0.7				2.7	0.3		0.7	5.7		0.7	17.3	46.7	22.7	2.7
6-20-65-10W6	2922.0	33.0	5.0		32.3	1.0	9.3		5.0	0.3						3.3			1.3	1.7		2.7	5.0	38.0	33.3	14.7
6-8-65-10W6	2963.9	48.0	8.0		19.7	0.7	5.0		2.7						1.7	2.3						4.7	7.3	56.0	20.3	7.7
7-14-65-11W6	3168.3	47.0	4.0	0.3	8.3	1.0	5.3		7.7					0.7		8.3						9.7	7.7	51.3	9.3	13.0
7-14-65-11W6	3175.9	36.7	15.7		11.0	1.3	7.3		4.0	1.7						5.7			4.7	0.7		0.3	11.0	52.3	12.3	13.0
8-2-66-9W6	2571.0	34.7	8.0		36.3	3.0	6.7		0.7			0.7			0.3	4.0							5.7	42.7	39.3	7.3
8-2-66-9W6	2579.6	34.3	7.7		26.3		7.0	0.3	3.7	8.3		0.7	0.3		0.3	2.7				2.7		0.3	5.3	42.0	26.3	19.3
8-2-66-9W6	2579.8	32.7			34.0		7.3		5.0	5.0	0.3	0.3				3.0	0.7		0.7	5.7		3.3	2.0	32.7	34.0	17.7
																							Mean	**44.9**	**26.8**	**11.5**
Petrofacies III																										
3-18-66-8W6	2468.6	33.3	4.7		43.7		1.7	0.7	4.3		1.3	1.0	0.3				1.3		0.3	2.7		4.7		38.0	43.7	8.0
5-32-65-9W6	2908.1	12.3	16.0	0.3	36.0	1.3	11.3		15.3										0.7			4.0	2.7	28.7	37.3	26.7
5-7-66-8W6	2535.1	35.3	4.0		44.3	0.7	2.3	1.0	5.7			2.0					2.0		0.7	0.3		1.7		39.3	45.0	9.0
2-21-66-8W6	2513.8	31.0	5.3		41.3		2.0		11.3	2.0		1.0			0.3		0.7		0.3	1.3		3.3		36.3	41.3	15.3
8-22-66-8W6	2581.5	15.3	1.3		48.0	0.3	8.7	0.7	6.7	0.3	0.3		0.7	0.7	4.3		3.0			3.0		6.7		16.7	48.3	16.7
8-26-65-11W6	2884.7	23.7	2.0		42.3		2.7	0.3	11.0					0.7					0.7	6.0		10.7		25.7	42.3	14.0
																							Mean	**30.8**	**43.0**	**14.9**
Petrofacies IV																										
1-8-66-8W6	2585.2	17.7	3.3	0.3	23.7	0.7	5.0		7.3	15.3	0.3								1.0	24.7		0.3	0.3	21.3	24.3	28.0
13-27-65-9W6	2645.6	32.7	0.7		30.0		2.7	0.7	16.0	1.3	0.3	0.3			0.3		0.3		1.0	13.0		0.7		33.3	30.0	21.0
13-27-65-9W6	2646.0	22.3	0.7		27.0		2.7		7.7	9.7	0.3	1.0							1.0	26.7		1.0		23.0	27.0	20.3
13-27-65-9W6	2647.5	36.0	2.7		21.0	0.7	2.3	0.3	9.3	10.0		0.3	0.3	0.3	0.3				1.3	14.0		1.0		38.7	21.7	22.0
14-24-65-10W6	2776.5	28.7	6.7		32.3	0.3	3.7	1.3	1.0	13.0	1.0	3.0							4.7	1.3		2.0	1.0	35.3	32.7	20.0
14-24-65-10W6	2777.5	23.7	2.3		33.7		2.3		0.3	24.0	1.0	0.7					1.7		7.7	1.3		1.0	0.3	26.0	33.7	27.7

15-9-65-11W6	3024.0	32.7	6.3		32.0	0.7	4.3	1.0	4.7	1.0							1.3		2.0	12.3		1.7		39.0	32.7	11.0
2-21-66-8W6	2514.6	29.0	5.0		37.7		0.7	0.3	2.7	3.7		0.7					1.3		0.3	13.7		1.0	4.0	34.0	37.7	7.3
3-18-66-8W6	2480.4	21.3	7.0		35.3			0.7	3.7	3.3									5.7	15.3		1.0	6.7	28.3	35.3	7.7
3-18-66-8W6	2483.5	31.3	6.7		31.3		3.0	0.3	3.0	3.0			0.3				1.0		3.3	11.3		2.3	3.0	38.0	31.3	9.3
3-33-65-9W6	2740.4	36.3	0.3		31.0	1.7	8.7	0.3	5.7	2.0			0.7	1.0	1.0				6.3			2.3	2.7	36.7	32.7	16.7
3-33-65-9W6	2734.3	28.0	1.0		29.7		7.3		14.3	7.0	0.3	0.3			0.3		0.3		0.7	10.0		0.3	0.3	29.0	29.7	29.0
5-32-65-9W6	2914.1	25.7	17.0		27.7	0.3	2.7		5.0	13.0	0.7	1.0							2.0	0.3		1.7	3.0	42.7	28.0	21.3
6-20-65-10W6	2917.3	18.3	3.7		37.7	0.7	7.7	1.0	7.0	3.0	0.3	1.3	0.3				1.0		4.3	4.0		9.3	0.3	22.0	38.3	19.0
6-8-65-10W6	2963.3	25.0	2.0		9.7		9.0		20.0	7.7									9.3	10.7		6.7		27.0	9.7	36.7
7-16-65-11W6	3188.9	15.7	2.7	1.0	30.7	2.3	3.0	1.3	4.3	2.0	0.7				1.7		1.0		13.0	17.3		3.3		19.3	33.0	11.3
7-16-65-11W6	3195.5	19.7	10.3		40.3	0.3	8.3		4.3	2.0			0.3				2.0		6.0	4.0		1.7	0.7	30.0	40.7	14.7
7-16-65-11W6	3199.1	28.3	12.7		30.3	0.3	7.7	1.0	2.3	9.7			0.3						1.3	3.3		2.7		41.0	30.7	20.7
8-2-66-9W6	2568.5	22.3	0.7		25.3		5.0		3.7	1.3			1.7	0.3	0.3		4.0		6.3	22.0		7.0		23.0	25.3	10.0
																							Mean	**30.9**	**30.2**	**18.6**
Petrofacies V																										
6-8-65-10W6	2961.6	15.3	1.7		15.0		12.7		7.7	6.7					1.3				12.0	11.7	10.3	5.7		17.0	15.0	27.0
7-13-66-9W6	2517.5	34.7	8.0		29.0		8.7		2.3	1.3	1.0	3.3	0.7				0.7			1.7	5.7	0.7	2.3	42.7	29.0	13.3
7-13-66-9W6	2521.6	21.0	12.0		35.7	0.3	6.0		8.0		2.3	3.7					0.7	1.3	1.0	2.0	2.0	0.3	3.7	33.0	36.0	16.3
7-13-66-9W6	2524.1	25.3	11.3		36.7		2.7	0.3	4.0	3.7	0.3	2.0					4.0	0.7	3.0	4.3	1.0	0.3	0.3	36.7	36.7	11.0
7-13-66-9W6	2531.3	29.7	5.7		25.3		4.3		11.3	6.0		0.3				2.3			9.3	0.7		1.3	3.7	35.3	25.3	21.7
8-2-66-9W6	2575.8	34.0	5.0		36.3	0.7	3.3	1.0	6.7	1.0		3.3							1.7	2.0	1.0		4.0	39.0	37.0	12.0
8-22-66-8W6	2575.8	21.0	4.7		23.0	0.3	11.0	0.3	19.0	1.3					0.3				3.7	4.0	7.3	4.0		25.7	23.3	31.7
8-22-66-8W6	2578.7	25.3	1.7		15.7	0.3	5.3	0.3	14.0	1.7					4.7				9.7	13.7	6.3	1.3		27.0	16.0	21.3
8-22-66-8W6	2585.4	28.7	2.3		9.7		3.3		4.3	4.7				0.3	0.7		0.3	3.7	20.3	4.0	12.3	5.3		31.0	9.7	12.3
																							Mean	**31.9**	**25.3**	**18.5**

APPENDIX III: THIN SECTION DESCRIPTIONS

Well ID & sample depth : 100/13-27-065-09W6/00, 2645.6 m Stains: double carbonate
Petrofacies : petrofacies IV Parasequence: FP3
Depositional setting : upper shoreface Lithofacies: facies 4
Facies assocation : FA2 (wave-dominated shoreface)

monocr. quartz	polycr. quartz	mica: biotite	mica: muscovite	rock fragments: sedimentary*	rock fragments: metamorphic	rock fragments: others**	chert	quartzite	others	cements: Fe-dolomite	cements: dolomite	cements: iron oxide	cements: calcite	cements: illite/smectite	cements: chlorite	cements: kaolinite	matrix	porosity
98	2	-	-	54	2	8	90	-	2	39	3	2	-	1	-	-	-	-

Totals: #

quartz	biotite	muscovite	rock fragments	chert + quartzite	others	Fe-dolomite	dolomite	iron oxide	calcite	illite/smectite	chlorite	kaolinite	matrix	porosity
100	-	-	64	90	2	39	3	2	-	1	-	-	-	-

Totals: %

quartz	biotite	muscovite	rock fragments	chert + quartzite	others	Fe-dolomite	dolomite	iron oxide	calcite	illite/smectite	chlorite	kaolinite	matrix	porosity
33.34	-	-	21	90	-	-	-	-	-	-	-	-	-	-

Totals: % clasts

quartz	biotite	muscovite	rock fragments	chert + quartzite	others
33.34	-	-	21	30	-

% normalized: (mQ + pQ) (C + Qe) RF

Q 39 C 36 RF 25

Total count: 300 Total clasts: 254 Total Q+C+RF: 253

Grain Size : upper very fine sand, angular to subrounded

Texture: well-sorted, clast-supported, predominantly long and concavo-convex contacts

Description***:

Quartz grains may appear more angular due to the overgrowths, although generally subrounded.

Rare dolomite grains.

Very rare heavy minerals present, possibly zircon.

Palaeophycus traces are present with dark rims composed of reddish-brown to opaque cement, possibly iron-rich (hematite?/limonite?) or carbonaceous-rich matters.

Quartz overgrowths are abundant.

Rare quartz with dolomite rims, possibly replacing the initial, more unstable silica overgrowths.

Common Fe-dolomite replacements on dolomite grains, chert clasts, and rock fragments (not quantified).

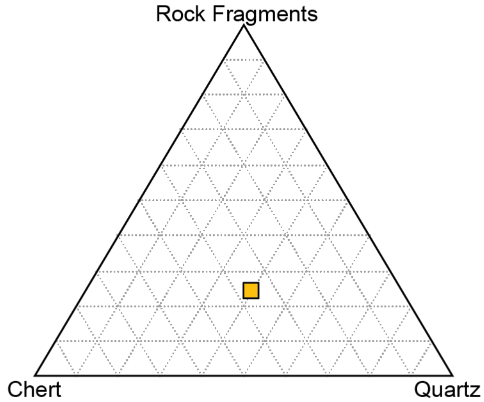

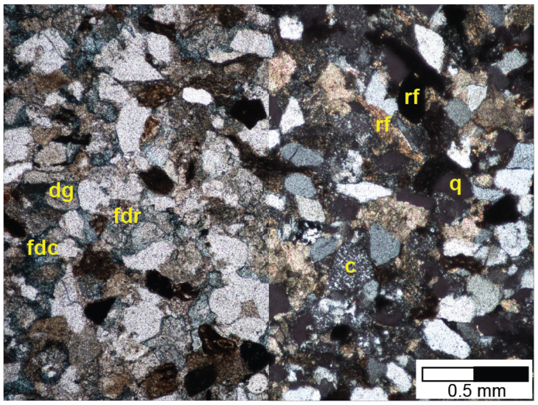

* = may include dolomite grains
** = iron-stained RF, volcanic RF, calcareous RF, and unidentified RF
*** = some very rarely occurring minerals may not be quantified on point counting results due to the automatic computer-generated crosshairs

Well ID & sample depth	: 100/13-27-065-09W6/00, 2646 m	Stains:	double carbonate
Petrofacies	: petrofacies IV	Parasequence:	Fp3
Depositional setting	: upper shoreface	Lithofacies:	facies 4
Facies assocation	: FA2 (wave-dominated shoreface)		

	monocr. quartz	polycr. quartz	biotite	mica: muscovite	rock fragments: sedimentary*	rock fragments: metamorphic	rock fragments: others**	chert	quartzite	others	cements: Fe-dolomite	cements: dolomite	cements: iron oxide	cements: calcite	cements: illite/smectite	cements: chlorite	cements: kaolinite	matrix	porosity
Count	67	2	3	-	52	-	9	81	-	-	80	3	3	-	-	-	-	-	-
Totals: #	69		3	-	61			81		-	-	-	-	-	-	-	-	-	-
Totals: %	23		1	-	20.33			27		-	-	-	-	-	-	-	-	-	-
Totals: % clasts	23		1	-	20.33			27		-									

% normalized: (mQ + pQ) (C + Qe) RF

Q	C	RF
33	28	29

Total count: 300 Total clasts: 214 Total Q+C+RF: 213

Grain Size : lower very fine to lower fine sand, subangular to subrounded

Texture: moderately-sorted, clast-supported, long and concavo-convex contacts

Description***:

Very rare feldspars.

Other grains include chalcedony.

Most sedimentary rock fragments are dolomite grains. Others are argillaceous and/or organic-rich rock fragments.

Fe-dolomite cement commonly occurs as pore-filling, poikilotopic cements up to 0.25 mm. Most commonly surrounding dolomite grains.

Dolomite rims appear on quartz and chert, possibly replacing the older, unstable silica overgrowths (see green arrows). Generally distinguishable with fine strands of illite coating the grains (see orange arrows), although may occasionally look very similar.

Common rock fragment pseudomatrix.

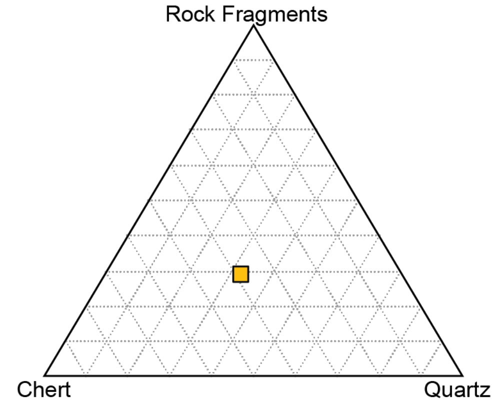

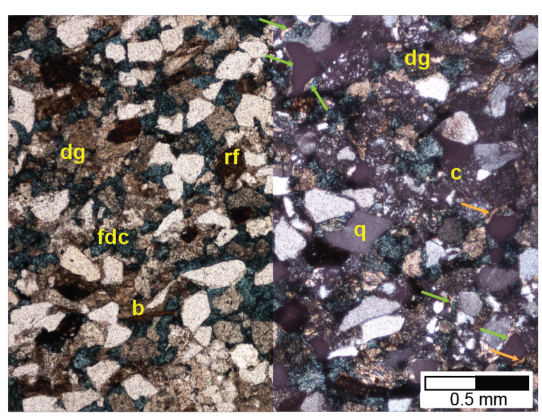

* = may include dolomite grains
** = iron-stained RF, volcanic RF, calcareous RF, and unidentified RF
*** = some very rarely occurring minerals may not be quantified on point counting results due to the automatic computer-generated crosshairs

Well ID & sample depth : 100/13-27-065-09W6/00, 2647.5 m Stains: double carbonate
Petrofacies : petrofacies IV Parasequence: FP3
Depositional setting : upper shoreface Lithofacies: facies 4
Facies assocation : FA2 (wave-dominated shoreface)

			mica		rock fragments					cements								
monocr. quartz	polycr. quartz	biotite	muscovite	sedimentary*	metamorphic	others**	chert	quartzite	others	Fe-dolomite	dolomite	iron oxide	calcite	illite/smectite	chlorite	kaolinite	matrix	porosity
108	8	1	1	58	1	7	63	2	2	42	4	3	-	-	-	-	-	16

Totals: #

116	1	1	66	65	0.67	14	1.33	1	-	-	-	-	-	5.33

Totals: %

38.67	0.33	0.33	21.67	21.67	0.67	14	1.33	1	-	-	-	-	-	5.33

Totals: % clasts

38.67	0.33	0.33	21.67	21.67	0.67

% normalized: (mQ + pQ) (C + Qe) RF

Q 47 C 26 RF 27

Total count: 300 Total clasts: 235 Total Q+C+RF: 229

Grain Size : lower fine sand, angular to rounded Texture: well-sorted, clast-supported, long and concavo-convex contacts

Description***:

Quartz grains predominantly appear to be subangular-angular due to pervasive syntaxial quartz overgrowths, but original shape is subrounded to rounded.

Metamorphic rock fragments (other than quartzite) are commonly schist as indicated by the internally-oriented clay minerals.

Very rare heavy minerals.

Abundant quartz overgrowths.

Rare dolomite rims on quartz grains, possibly replacing the initial, unstable silica overgrowths.

Fe-dolomite cements occur adjacent to dolomite grains. Predominantly as overgrowths/rims on dolomite grains, also common as poikilotopic cement up to 50 µm. Very rare Fe-dolomite also occurs as euhedral, rhombic inclusions within chert grains.

Rare grain-coating iron oxide, very thin (<20 µm).

Abundant microfractures although slightly difficult to observe, not quantified due to the extreme thinness, only visible under at least 40x magnification.

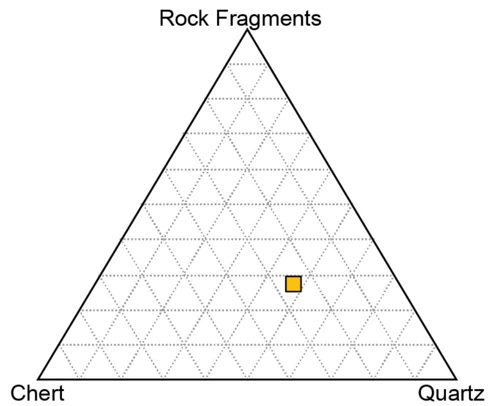

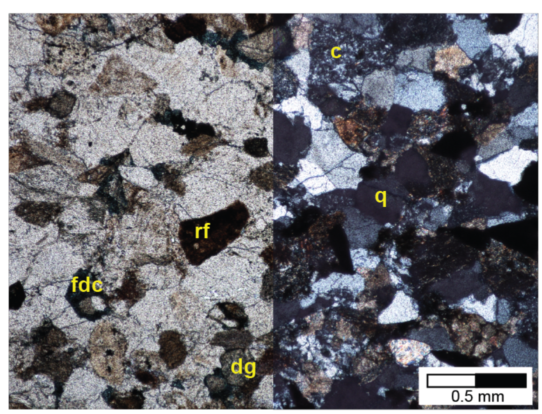

* = may include dolomite grains
** = iron-stained RF, volcanic RF, calcareous RF, and unidentified RF
*** = some very rarely occurring minerals may not be quantified on point counting results due to the automatic computer-generated crosshairs

Well ID & sample depth	: 100/13-27-065-09W6/00, 2650.8 m	Stains: double carbonate
Petrofacies	: petrofacies I	Parasequence: F$_P$3
Depositional setting	: upper shoreface	Lithofacies: facies 4
Facies assocation	: FA2 (wave-dominated shoreface)	

monocr. quartz	polycr. quartz	biotite	mica: muscovite	rock fragments: sedimentary*	rock fragments: metamorphic	rock fragments: others**	chert	quartzite	others	cements: Fe-dolomite	cements: dolomite	cements: iron oxide	cements: calcite	cements: illite/smectite	cements: chlorite	cements: kaolinite	matrix	porosity
106	18	-	-	42	-	20	104	-	-	-	-	3	-	-	-	-	-	7

Totals: #

quartz (monocr. + polycr.)	biotite	muscovite	rock fragments	chert + quartzite	others	Fe-dolomite	dolomite	iron oxide	calcite	illite/smectite	chlorite	kaolinite	matrix	porosity
126	-	-	62	104	-	-	-	3	-	-	-	-	-	7

Totals: %

quartz (monocr. + polycr.)	biotite	muscovite	rock fragments	chert + quartzite	others	Fe-dolomite	dolomite	iron oxide	calcite	illite/smectite	chlorite	kaolinite	matrix	porosity
41.33	-	-	20.67	34.67	-	-	-	1	-	-	-	-	-	2.33

Totals: % clasts

quartz (monocr. + polycr.)	biotite	muscovite	rock fragments	chert + quartzite	others
41.33	-	-	20.67	34.67	-

% normalized: (mQ + pQ) (C + Qe) RF

Q	C	RF
43	36	21

Total count: 300 Total clasts: 290 Total Q+C+RF: 290

Grain Size : upper fine sand, subangular to rounded

Texture: well-sorted, clast-supported, long and concavo-convex contacts

Description***:

Rounded grains are restricted to quartz.

Half of the quantified sedimentary rock fragments are dolomite grains.

Abundant quartz overgrowths.

Common iron oxide coatings but thin (<20 µm).

Other pore-filling cements are not observed.

Fe-dolomite only occurs as replacement minerals, particularly on chert and rock fragments, and euhedral, rhombic inclusions. Inclusions also include non-ferroan dolomite.

Rare primary intergranular porosity is preserved, generally <50 µm.

Most porosity is secondary, primarily due to extensive dissolution on chert and rock fragments. Microfractures are also pervasive, primarily along grain contacts.

Compared to other upper shoreface F$_P$3 samples in the same well, this sample has better porosity and “cleaner” composition.

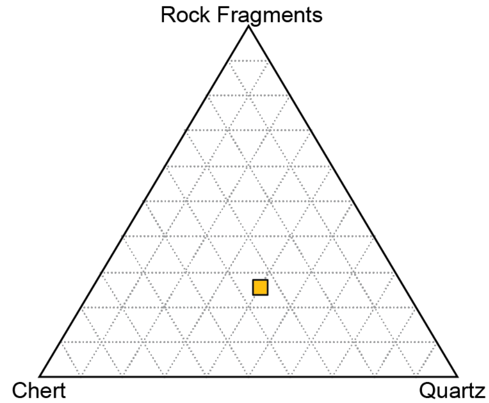

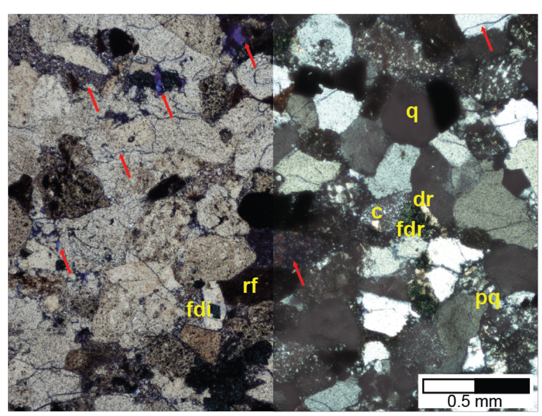

* = may include dolomite grains
** = iron-stained RF, volcanic RF, calcareous RF, and unidentified RF
*** = some very rarely occurring minerals may not be quantified on point counting results due to the automatic computer-generated crosshairs

Well ID & sample depth	: 100/05-32-065-09W6/00, 2908.1 m	Stains:	double carbonate
Petrofacies	: petrofacies III	Parasequence:	Fp3
Depositional setting	: upper shoreface	Lithofacies:	facies 4
Facies assocation	: FA2 (wave-dominated shoreface)		

			mica		rock fragments					cements								
monocr. quartz	polycr. quartz	biotite	muscovite	others**	sedimentary*	metamorphic	chert	quartzite	others	Fe-dolomite	dolomite	iron oxide	calcite	illite/smectite	chlorite	kaolinite	matrix	porosity
37	48	-	-	34	48	-	108	4	1	-	-	12	-	-	-	-	-	8
Totals: #																		
85		-	-	82			112		1	-	-	12	-	-	-	-	-	8
Totals: %																		
28.67		-	-	26.67			37.33		0.33	-	-	4	-	-	-	-	-	2.67
Totals: % clasts																		
28.67		-	-	26.67			37.33		0.33									

% normalized: (mQ + pQ) (C + Qe) RF

Q 31 C 40 RF 29

Total count: 300 Total clasts: 279 Total Q+C+RF: 278

Grain Size : upper very fine to upper fine sand, angular to rounded

Texture: well-sorted, clast-supported, long and concavo-convex contacts

Description***: Rounded grains are restricted to quartz.

Rare partially iron-stained chert, thus may be easily mistaken as other rock fragments.

Rare iron-stained detrital grains cut by drusy quartz veins, indicating iron-stained volcanic rock fragments, chert, or quartzite.

Other minerals include extremely rare chalcedony, feldspars, and dolomite grains.

Abundant interlocking syntaxial quartz overgrowths as the primary cement.

Common iron oxide stains, very patchy and sporadic, likely postdated significant burial compactions.

Common pseudomatrix (argillaceous and/or carbonaceous rock fragments, illitized chert) as another major intergranular components.

Rare authigenic chlorite as inclusions within quartz grains.

Authigenic dolomite only occurred as replacement minerals, not intergranular cements.

All pores have secondary origin, primarily from microfractures along grain contacts, quartz overgrowths, and across mineral grains. Infrequent dissolution on chert, rock fragments, and quartz overgrowths also occurred.

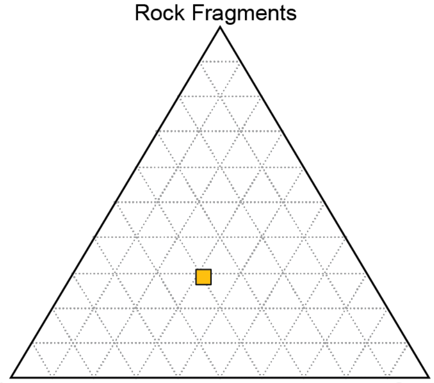

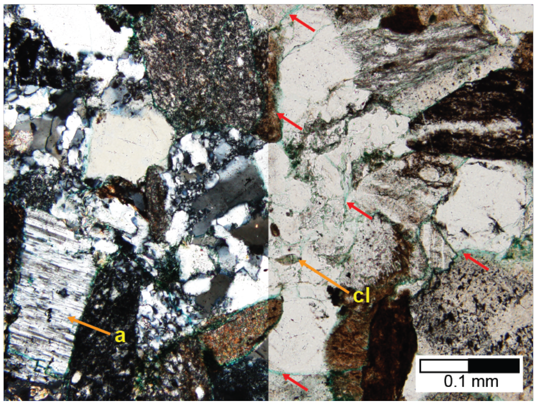

* = may include dolomite grains
** = iron-stained RF, volcanic RF, calcareous RF, and unidentified RF
*** = some very rarely occurring minerals may not be quantified on point counting results due to the automatic computer-generated crosshairs

Well ID & sample depth : 100/05-32-065-09W6/00, 2911.3 m Stains: double carbonate
Petrofacies : petrofacies II Parasequence: FP3
Depositional setting : upper shoreface Lithofacies: facies 3
Facies assocation : FA2 (wave-dominated shoreface)

monocr. quartz	polycr. quartz	biotite	muscovite (mica)	others** (mica)	sedimentary* (rock fragments)	metamorphic (rock fragments)	chert	quartzite	others	Fe-dolomite (cements)	dolomite (cements)	iron oxide (cements)	calcite (cements)	illite/smectite (cements)	chlorite (cements)	kaolinite (cements)	matrix	porosity
97	31	1	-	10	26	-	64	1	-	2	13	4	-	-	-	14	-	37

Totals: #

128	1	-	36	65	-	2	13	4	-	-	-	14	-	37

Totals: %

42.67	-	-	12	21.67	-	0.67	4.33	1.33	-	-	-	4.67	-	12.33

Totals: % clasts

42.67	-	-	12	21.67	-

% normalized: (mQ + pQ) (C + Qe) RF

Q	C	RF
56	28	16

Total count: 300 Total clasts: 230 Total Q+C+RF: 229

Grain Size : lower fine sand, subangular to rounded

Texture: well-sorted, clast-supported, long to concavo-convex contacts

Description***:

Rounded grains are restricted to quartz.

Abundant dolomite grains.

Other minerals include extremely rare chalcedony.

Abundant euhedral quartz overgrowths, predating other cements.

Abundant kaolinite cements within outsized pores, likely predating carbonate cements.

Abundant patchy dolomite cements, very sporadic.

Rare Fe-dolomite cements as rims on dolomite cements.

Rare pseudomatrix.

Rare iron oxide cements as coatings around grains or intergranular cement.

Pores are primarily from extensive dissolution of pseudomatrix (rock fragments), chert, ferromagnesian minerals, and/or quartz overgrowths. Intergranular secondary pores may appear to be similar to intergranular primary pores, but the presence of the remaining undissolved grains indicate the secondary origin.

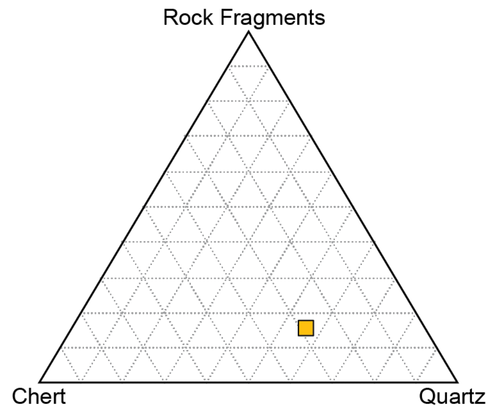

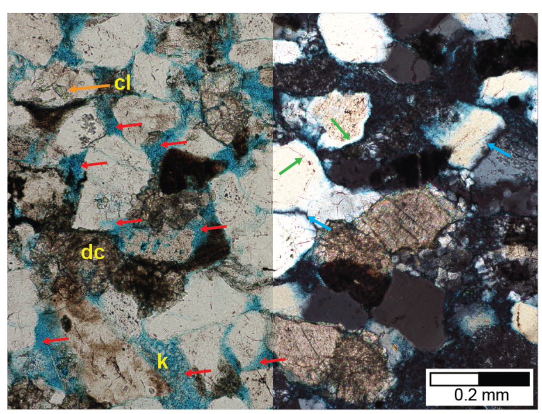

* = may include dolomite grains
** = iron-stained RF, volcanic RF, calcareous RF, and unidentified RF
*** = some very rarely occurring minerals may not be quantified on point counting results due to the automatic computer-generated crosshairs

Well ID & sample depth : 100/05-32-065-09W6/00, 2914.1 m Stains: double carbonate
Petrofacies : petrofacies IV Parasequence: FP3
Depositional setting : lower shoreface Lithofacies: facies 3
Facies assocation : FA1 (storm-dominated shoreface)

monocr. quartz	polycr. quartz	biotite	muscovite (mica)	others** (mica)	sedimentary* (rock fragments)	metamorphic (rock fragments)	chert	quartzite	others	Fe-dolomite (cements)	dolomite (cements)	iron oxide (cements)	calcite (cements)	illite/smectite (cements)	chlorite (cements)	kaolinite (cements)	matrix	porosity
77	51	3	-	8	56	-	83	1	-	1	6	5	-	-	-	-	-	9

Totals: #

quartz	biotite	muscovite	others + rock fragments	chert + quartzite	others	Fe-dolomite	dolomite	iron oxide	calcite	illite/smectite	chlorite	kaolinite	matrix	porosity
128	3	-	64	84	-	1	6	5	-	-	-	-	-	9

Totals: %

quartz	biotite	muscovite	others + rock fragments	chert + quartzite	others	Fe-dolomite	dolomite	iron oxide	calcite	illite/smectite	chlorite	kaolinite	matrix	porosity
42.67	1	-	21.34	28	-	0.33	2	1.67	-	-	-	-	-	3

Totals: % clasts

quartz	biotite	muscovite	others + rock fragments	chert + quartzite	others
42.67	1	-	21.34	28	-

% normalized: (mQ + pQ) (C + Qe) RF

Q	C	RF
46	31	23

Total count: 300 Total clasts: 279 Total Q+C+RF: 276

Grain Size : upper very fine sand, angular to subrounded

Texture: well-sorted, clast-supported, long to concavo-convex contacts

Description***:

Abundant dolomite grains.

Other minerals include extremely rare chalcedony.

Abundant interlocking syntaxial quartz overgrowths.

Rare Fe-dolomite cements, abundant dolomite cements. Dolomite commonly occurs as patchy intergranular cements, likely postdated significant burial compaction based on their limited and sporadic distribution. Dolomite cement may also occur as "overgrowths" surrounding the dolomite nuclei (see image). Fe-dolomite may surround the dolomite cements.

All pores are secondary type. Primarily from partial dissolution of chert, rock fragments (pseudomatrix), quartz overgrowths, or dolomite grains. Microfractures are also abundant along grain contacts and across mineral grains.

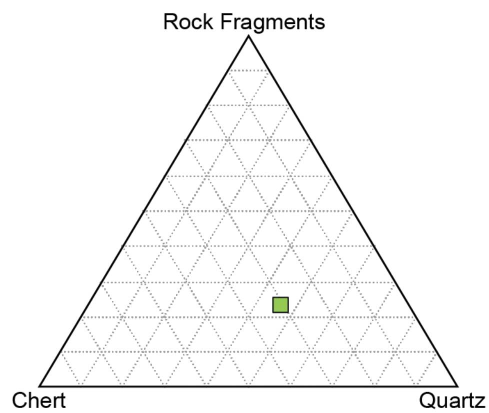

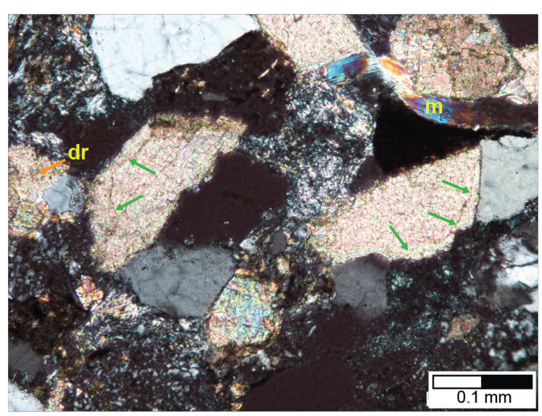

* = may include dolomite grains
** = iron-stained RF, volcanic RF, calcareous RF, and unidentified RF
*** = some very rarely occurring minerals may not be quantified on point counting results due to the automatic computer-generated crosshairs

Well ID & sample depth : 100/03-33-065-09W6/00, 2734.3 m — Stains: double carbonate

Petrofacies : petrofacies IV — Parasequence: Fp3

Depositional setting : middle shoreface — Lithofacies: facies 3

Facies assocation : FA1 (storm-dominated shoreface)

			mica		rock fragments					cements								
monocr. quartz	polycr. quartz	biotite	muscovite	others**	sedimentary*	metamorphic	chert	quartzite	others	Fe-dolomite	dolomite	iron oxide	calcite	illite/smectite	chlorite	kaolinite	matrix	porosity
84	3	1	-	22	65	-	89	-	1	30	2	1	-	1	-	-	-	1

Totals: #

87	1	-	87	89	1	30	2	1	-	1	-	-	-	1

Totals: %

29	0.33	-	29	29.67	0.33	10	0.67	0.33	-	0.33	-	-	-	0.33

Totals: % clasts

29	0.33	-	29	29.67	-

% normalized: (mQ + pQ) (C + Qe) RF

Q	C	RF
33	34	33

Total count: 300 Total clasts: 265 Total Q+C+RF: 263

Grain Size : upper very fine sand, angular to rounded

Texture: very well-sorted, clast-supported, long and concavo-convext contacts

Description***:

Quartz grains are rounded, although may look more angular due to the unclear boundaries of the quartz overgrowths.

Abundant rock fragment pseudomatrix.

Common dolomite grains.

Other minerals include feldspars.

Common quartz overgrowths.

Dolomite also occurs as replacement, predominantly on chert and rock fragments, rarely on quartz. Rare dolomite rims on quartz and chert grains, possibly as replacements of unstable silica phases.

Fe-dolomite predominantly occurs as poikilotopic cement up to 0.3 mm. May also appear as rims on patchy dolomite cements.

Illite is more common than what is quantified but difficult to point-count (mostly being offset by the computer-generated crosshairs due to its thinness). When observed, found as coatings on grains.

All pores have secondary origin due to dissolved rock fragments, chert, and dolomite grains as well as microfractures.

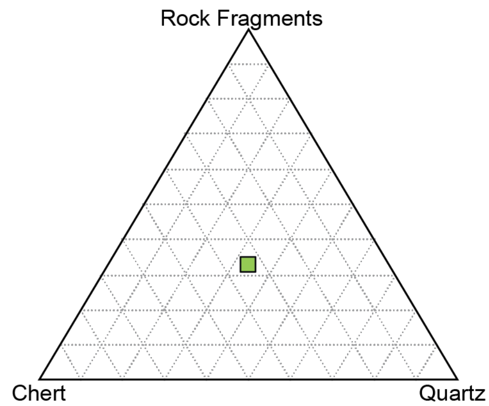

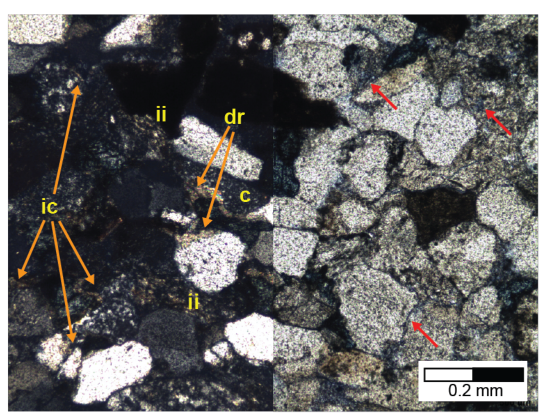

* = may include dolomite grains
** = iron-stained RF, volcanic RF, calcareous RF, and unidentified RF
*** = some very rarely occurring minerals may not be quantified on point counting results due to the automatic computer-generated crosshairs

Well ID & sample depth : 100/03-33-065-09W6/00, 2740.4 m Stains: double carbonate
Petrofacies : petrofacies IV Parasequence: Fp2
Depositional setting : upper shoreface Lithofacies: facies 4
Facies assocation : FA2 (wave-dominated shoreface)

	monocr. quartz	polycr. quartz	biotite (mica)	muscovite (mica)	others** (rock fragments)	sedimentary* (rock fragments)	metamorphic (rock fragments)	chert	quartzite	others	Fe-dolomite (cements)	dolomite (cements)	iron oxide (cements)	calcite (cements)	illite/smectite (cements)	chlorite (cements)	kaolinite (cements)	matrix	porosity
	109	1	-	-	25	23	1	93	5	6	-	19	7	-	-	-	-	-	8
Totals: #	110		-	-	49			98		6	-	19	7	-	-	-	-	-	8
Totals: %	36.67		-	-	16.67			32.67		-	-	-	-	-	-	-	-	-	-
Totals: % clasts	36.67		-	-	16.67			32.67		-									

% normalized: (mQ + pQ) (C + Qe) RF

Q 43 C 38 RF 19

Total count: 300 Total clasts: 266 Total Q+C+RF: 260

Grain Size : lower to upper very fine sand, angular to subrounded

Texture: well-sorted, clast-supported, predominantly long and concavo-convex contacts, minor sutured contacts

Description***:

Rare dolomite grains.

Common rock fragments as pseudomatrix.

Anomalously common volcanic rock fragments with well-defined feldspathic laths compared to other samples (here included in "unidentified rock fragments").

Other minerals include micas, authigenic glauconite.

Common quartz overgrowths.

Dolomite cements are very patchy, generally <0.2 mm.

Fe-dolomite cements only present as the outer rims of dolomite cements or grains.

All pores are secondary porosity. Predominantly as microfractures (commonly along grain contacts), rarely due to the dissolution of chert and rock fragments. Complete dissolution of clasts may result in similar appearance to primary intergranular porosity, but distinguishable by the presence of specks from remaining clasts around the dissolution boundaries.

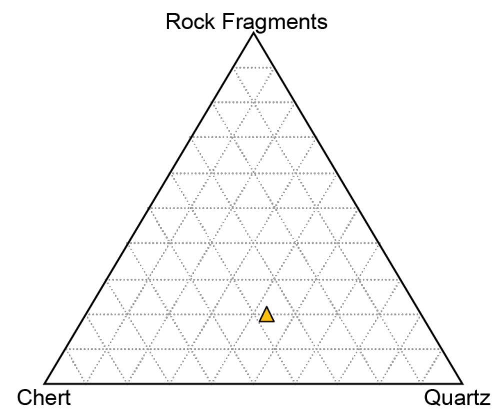

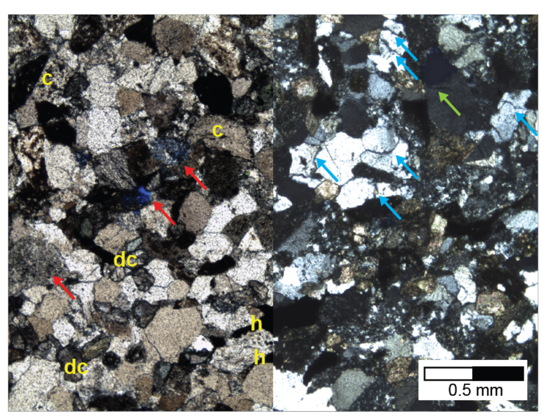

* = may include dolomite grains
** = iron-stained RF, volcanic RF, calcareous RF, and unidentified RF
*** = some very rarely occurring minerals may not be quantified on point counting results due to the automatic computer-generated crosshairs

Well ID & sample depth : 100/10-36-065-09W6/00, 2647 m   Stains: double carbonate

Petrofacies : petrofacies II   Parasequence: FP3

Depositional setting : foreshore   Lithofacies: facies 5

Facies assocation : FA2 (wave-dominated shoreface)

	monocr. quartz	polycr. quartz	biotite	muscovite (mica)	others** (mica)	sedimentary* (rock fragments)	metamorphic (rock fragments)	chert	quartzite	others	Fe-dolomite (cements)	dolomite (cements)	iron oxide (cements)	calcite (cements)	illite/smectite (cements)	chlorite (cements)	kaolinite (cements)	matrix	porosity
	104	9	-	-	16	9	-	129	1	-	-	-	-	-	-	-	7	-	25
Totals: #	113		-	-	25			130		-	-	-	-	-	-	-	7	-	25
Totals: %	37.67		-	-	8.33			43.33		-	-	-	-	-	-	-	2.33	-	8.33
Totals: % clasts	37.67		-	-	8.33			43.33		-									

% normalized: (mQ + pQ) (C + Qe) RF

Q 42 C 49 RF 9

Total count: 300   Total clasts: 268   Total Q+C+RF: 268

Grain Size : upper fine to lower medium sand, subangular to rounded

Texture: well-sorted, clast-supported, long to concavo-convex contacts.

Description***:

Rounded grains are restricted to quartz.

Other minerals include very rare biotite.

Abundant syntaxial quartz overgrowths.

Rare patchy dolomite cements. Common dolomite inclusions in quartz and chert.

Common chlorite inclusions in quartz.

All pores have secondary origin from extensive leaching of chert, rock fragment, and quartz grains/quartz overgrowths as well as infrequent microfractures.

Pores can be cement-free or occluded by kaolinite cement.

Typical "clean" sandstone that resembles the conglomerate beds.

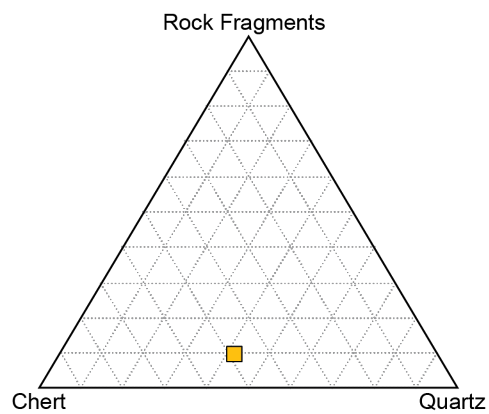

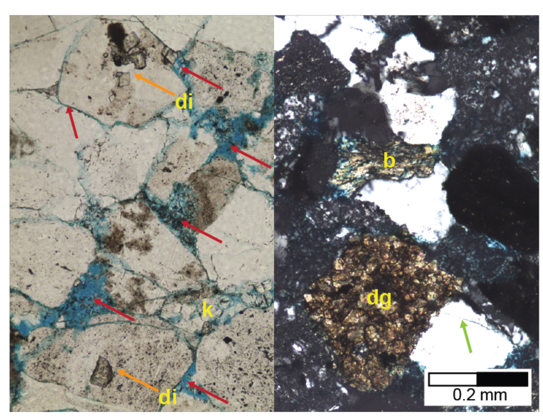

* = may include dolomite grains
** = iron-stained RF, volcanic RF, calcareous RF, and unidentified RF
*** = some very rarely occurring minerals may not be quantified on point counting results due to the automatic computer-generated crosshairs

Well ID & sample depth	: 100/10-36-065-09W6/00, 2652.3 m	Stains:	double carbonate
Petrofacies	: petrofacies II	Parasequence:	FP3
Depositional setting	: upper shoreface	Lithofacies:	facies 8
Facies assocation	: FA2 (wave-dominated shoreface)		

	monocr. quartz	polycr. quartz	biotite	mica: muscovite	mica: others**	rock fragments: sedimentary*	rock fragments: metamorphic	chert	quartzite	others	cements: Fe-dolomite	cements: dolomite	cements: iron oxide	cements: calcite	cements: illite/smectite	cements: chlorite	cements: kaolinite	matrix	porosity
	100	16	-	-	44	3	-	104	-	-	1	-	-	-	-	-	12	-	20
Totals: #	116		-	-	47			104		-	0.33	-	-	-	-	-	4	-	20
Totals: %	38.67		-	-	15.67			34.67		-	0.33	-	-	-	-	-	1.33	-	6.67
Totals: % clasts	38.67		-	-	15.67			34.67		-									

% normalized: (mQ + pQ) (C + Qe) RF

Q	C	RF
43	39	18

Total count: 300 Total clasts: 267 Total Q+C+RF: 267

Grain Size : lower to upper fine sand, angular to rounded

Texture: well-sorted, clast-supported, long and concavo-convex contacts

Description***:

Rounded grains are restricted to quartz.

Rare rock fragments with drusy quartz veins.

Abundant syntaxial quartz overgrowths.

Common chlorite and dolomite inclusions in quartz.

All pores have secondary origin from extensive leaching of chert, rock fragment, and quartz grains/quartz overgrowths as well as infrequent microfractures.

Pores can be cement-free or occluded by kaolinite cement.

Typical "clean" sandstone that resembles the conglomerate beds.

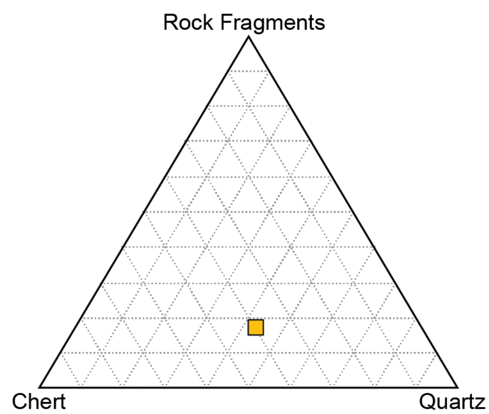

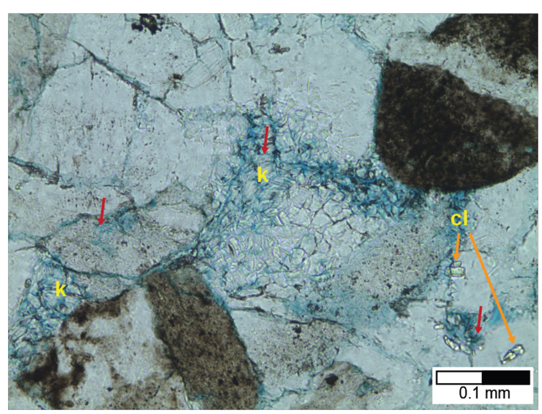

* = may include dolomite grains
** = iron-stained RF, volcanic RF, calcareous RF, and unidentified RF
*** = some very rarely occurring minerals may not be quantified on point counting results due to the automatic computer-generated crosshairs

Well ID & sample depth	: 100/06-08-065-11W6/00, 2961.6 m	Stains: double carbonate
Petrofacies	: petrofacies V	Parasequence: T
Depositional setting	: estuarine	Lithofacies: facies 11
Facies assocation	: FA3 (brackish embayment)	

	monocr. quartz	polycr. quartz	biotite	muscovite	others**	sedimentary*	metamorphic	chert	quartzite	others	Fe-dolomite	dolomite	iron oxide	calcite	illite/smectite	chlorite	kaolinite	matrix	porosity
Group			mica		rock fragments						cements								
Count	46	5	-	-	38	43	-	45	-	4	35	36	17	31	-	-	-	-	-
Totals: #	51		-	-	81			45		4	35	36	17	31	-	-	-	-	-
Totals: %	17		-	-	27			15		1.33	11.67	12	5.67	10.33	-	-	-	-	-
Totals: % clasts	17		-	-	27			15		1.33									

% normalized: (mQ + pQ) (C + Qe) RF

Q 29 C 25 RF 46

Total count: 300 Total clasts: 181 Total Q+C+RF: 177

Grain Size : upper very fine to upper fine sand, angular to rounded

Texture: poorly-sorted, matrix-supported, predominantly point and tangential contacts

Description***:

Rounded grains are restricted to quartz.

Abundant dolomite grains.

Abundant euhedral quartz overgrowths, possibly intervened with the formation of dolomite grains and grain-coating authigenic chlorite.

Common dolomite rims on quartz grains, possibly replacing the older, more unstable silica overgrowths.

Common calcite, dolomite, and Fe-dolomite as replacements on chert, rock fragments, and rarely quartz grains. When occur as replacements on pseudomatrix, they may appear similar with intergranular cements.

Common dedolomitization on dolomite grains.

Common authigenic chlorite as coatings on quartz overgrowths, possibly preventing silica cement to form further.

Very rare intergranular primary porosity. Common poorly-defined secondary porosity as microfractures.

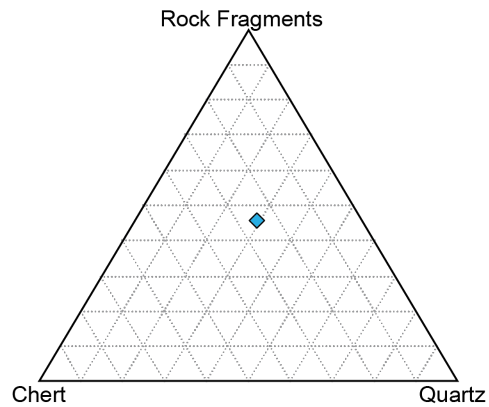

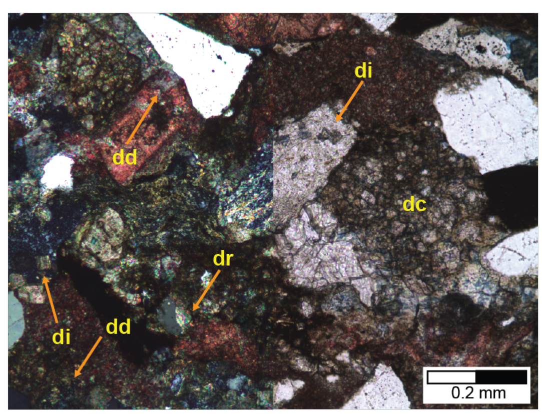

* = may include dolomite grains
** = iron-stained RF, volcanic RF, calcareous RF, and unidentified RF
*** = some very rarely occurring minerals may not be quantified on point counting results due to the automatic computer-generated crosshairs

Well ID & sample depth : 100/06-08-065-11W6/00, 2963.3 m Stains: double carbonate
Petrofacies : petrofacies IV Parasequence: T
Depositional setting : estuarine Lithofacies: facies 11
Facies assocation : FA3 (brackish embayment)

	monocr. quartz	polycr. quartz	mica: biotite	mica: muscovite	rock fragments: others**	rock fragments: sedimentary*	rock fragments: metamorphic	chert	quartzite	others	cements: Fe-dolomite	cements: dolomite	cements: iron oxide	cements: calcite	cements: illite/smectite	cements: chlorite	cements: kaolinite	matrix	porosity
	75	6	-	-	27	83	-	29	-	-	32	28	20	-	-	-	-	-	-
Totals: #	81		-	-	110			29		-	32	28	20	-	-	-	-	-	-
Totals: %	27		-	-	36.67			9.67		-	-	-	-	-	-	-	-	-	-
Totals: % clasts	27		-	-	36.67			9.67		-									

% normalized: (mQ + pQ) (C + Qe) RF

Q 37 C 13 RF 50

Total count: 300 Total clasts: 220 Total Q+C+RF: 220

Grain Size : upper very fine sand, angular to subangular

Texture: moderately-sorted, matrix-supported, point and tangential contacts

Description***:

Abundant dolomite grains.

Other minerals include chlorite.

Common euhedral quartz overgrowths.

Abundant poikilotopic iron oxide cements, up to 5 mm.

Abundant dolomite as replacements on chert and rock fragments as well as pore-occluding cements. Also common as rims on quartz grains.

Fe-dolomite cements generally occur as rims on dolomite cements and/or grains as well as replacements on dolomite grains.

Rare channel-type secondary porosity.

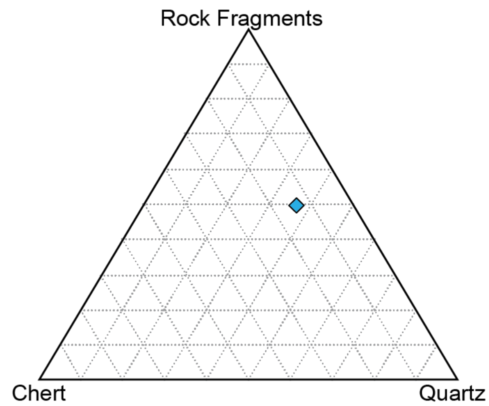

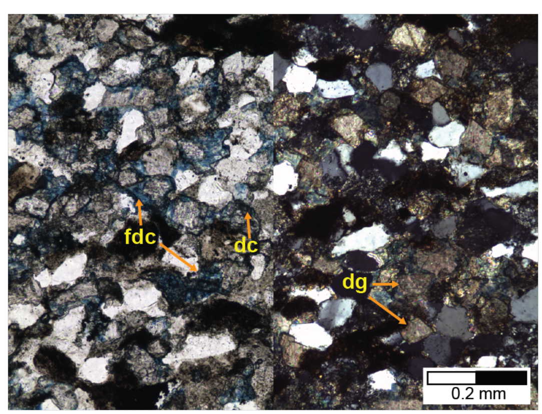

* = may include dolomite grains
** = iron-stained RF, volcanic RF, calcareous RF, and unidentified RF
*** = some very rarely occurring minerals may not be quantified on point counting results due to the automatic computer-generated crosshairs

Well ID & sample depth	: 100/06-08-065-11W6/00, 2963.9 m	Stains:	double carbonate
Petrofacies	: petrofacies II	Parasequence:	FP3
Depositional setting	: foreshore	Lithofacies:	facies 5
Facies assocation	: FA2 (wave-dominated shoreface)		

monocr. quartz	polycr. quartz	biotite (mica)	muscovite (mica)	others** (rock fragments)	sedimentary* (rock fragments)	metamorphic (rock fragments)	chert	quartzite	others	Fe-dolomite (cements)	dolomite (cements)	iron oxide (cements)	calcite (cements)	illite/smectite (cements)	chlorite (cements)	kaolinite (cements)	matrix	porosity
144	24	-	-	15	8	-	59	2	5	-	-	14	-	-	-	7	-	22
Totals: #																		
168		-	-	23			61		5	-	-	14	-	-	-	7	-	22
Totals: %																		
56		-	-	7.67			20.33		1.67	-	-	4.67	-	-	-	2.33	-	7.33
Totals: % clasts																		
56		-	-	7.67			20.33		1.67									

% normalized: (mQ + pQ) Q 20.34 (C + Qe) C 7.67 RF RF 66.67

Total count: 300 Total clasts: 257 Total Q+C+RF: 252

Grain Size : upper fine sand, subangular to rounded

Texture: very well-sorted, clast-supported, long and concavo-convex contacts.

Description***:

Rounded grains are restricted to quartz.

Abundant syntaxial quartz overgrowths.

Iron oxide commonly occurs as grain coatings, postdating quartz overgrowths.

Abundant siderite inclusions and common dolomite inclusions on chert. Commonly postdated chert dissolution. This southernmost sample in the study interval is the only sample with well-defined authigenic siderite, therefore may indicate that siderite is possibly more common southwards.

Very rare intergranular primary porosity. Abundant partial to complete leaching of pseudomatrix and chert, rarely on quartz.

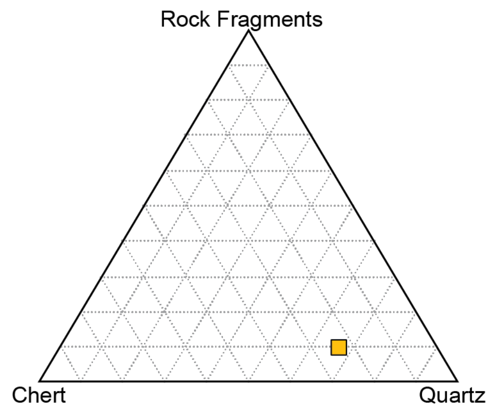

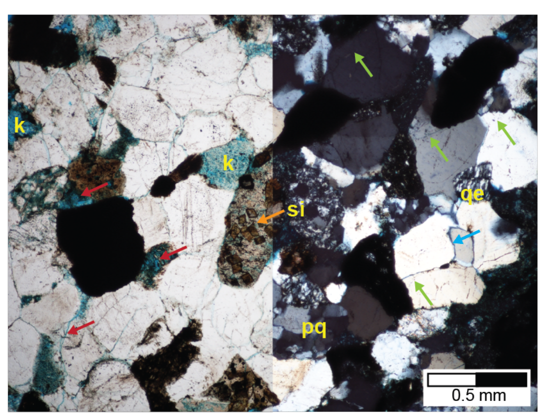

* = may include dolomite grains
** = iron-stained RF, volcanic RF, calcareous RF, and unidentified RF
*** = some very rarely occurring minerals may not be quantified on point counting results due to the automatic computer-generated crosshairs

Well ID & sample depth : 100/06-20-065-10W6/00, 2909.4 m Stains: double carbonate
Petrofacies : petrofacies II Parasequence: FP3
Depositional setting : foreshore Lithofacies: facies 5
Facies assocation : FA2 (wave-dominated shoreface)

monocr. quartz	polycr. quartz	biotite	muscovite	mica: others**	rock fragments: sedimentary*	rock fragments: metamorphic	chert	quartzite	others	cements: Fe-dolomite	cements: dolomite	cements: iron oxide	cements: calcite	cements: illite/smectite	cements: chlorite	cements: kaolinite	matrix	porosity
128	12	2	-	6	2	-	66	2	-	17	2	2	-	1	-	8	-	52

Totals: #

quartz	biotite	muscovite	mica & rock fragments	chert & quartzite	others	Fe-dolomite	dolomite	iron oxide	calcite	illite/smectite	chlorite	kaolinite	matrix	porosity
140	2	-	8	68	-	17	2	2	-	1	-	8	-	52

Totals: %

quartz	biotite	muscovite	mica & rock fragments	chert & quartzite	others	Fe-dolomite	dolomite	iron oxide	calcite	illite/smectite	chlorite	kaolinite	matrix	porosity
46.67	0.67	-	2.67	22.67	-	5.67	0.67	0.67	-	0.33	-	2.67	-	17.33

Totals: % clasts

quartz	biotite	muscovite	mica & rock fragments	chert & quartzite	others
46.67	0.67	-	2.67	22.67	-

% normalized: (mQ + pQ) (C + Qe) RF

Q 65 C 31 RF 4

Total count: 300 Total clasts: 218 Total Q+C+RF: 216

Grain Size : upper fine sand, subangular to rounded

Texture: well-sorted, clast-supported, point to long contacts due to abundant pores

Description***:

Rounded grains are restricted to quartz.

Rare pebbles are composed of chert and rock fragments.

Abundant euhedral to syntaxial quartz overgrowths, predated extensive dissolution.

Very rare, patchy Fe-dolomite cements postdated extensive dissolution.

Rare booklets of kaolinite cements postdated extensive dissolution.

Both primary and secondary pores are preserved. Most pores are, however, secondary, due to extensive complete dissolution of chert, rock fragments, and biotite. Larger pores have secondary origin, whereas primary intergranular pores are small-scale (see yellow vs. red arrows). Also common microfractures on grains. Abundant cement-free pores.

"Clean" and porous, similar to the conglomeratic beds.

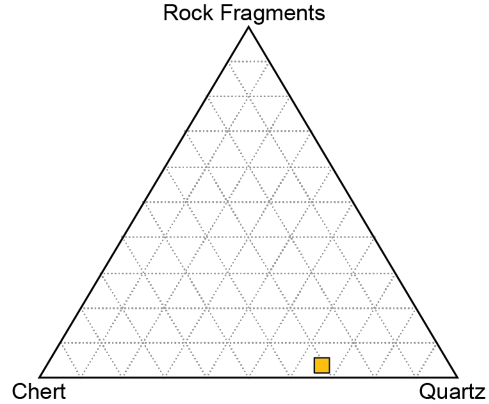

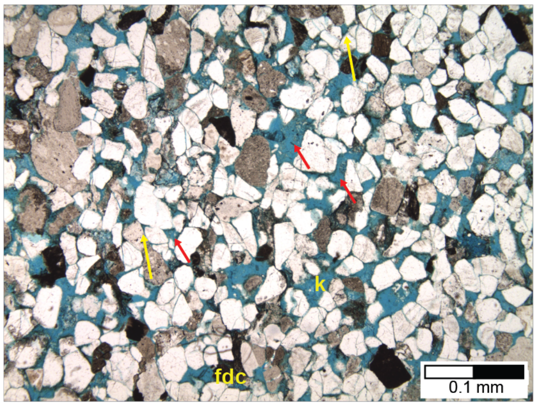

* = may include dolomite grains
** = iron-stained RF, volcanic RF, calcareous RF, and unidentified RF
*** = some very rarely occurring minerals may not be quantified on point counting results due to the automatic computer-generated crosshairs

Well ID & sample depth : 100/06-20-065-09W6/00, 2917.3 m Stains: double carbonate
Petrofacies : petrofacies III Parasequence: FP3
Depositional setting : middle shoreface Lithofacies: facies 3
Facies assocation : FA1 (storm-dominated shoreface)

	monocr. quartz	polycr. quartz	mica: biotite	mica: muscovite	rock fragments: others**	rock fragments: sedimentary*	rock fragments: metamorphic	chert	quartzite	others	cements: Fe-dolomite	cements: dolomite	cements: iron oxide	cements: calcite	cements: illite/smectite	cements: chlorite	cements: kaolinite	matrix	porosity
	55	11	4	1	23	30	3	113	2	1	12	13	28	-	3	-	-	-	1
Totals: #	66		4	1	56			115		1	12	13	28	-	3	-	-	-	1
Totals: %	22		1.33	0.33	18.67			38.33		0.33	4	4.33	9.33	-	1	-	-	-	0.33
Totals: % clasts	22		1.33	0.33	18.67			38.33		0.33									

% normalized: (mQ + pQ) (C + Qe) RF

Q	C	RF
28	48	24

Total count: 300 Total clasts: 243 Total Q+C+RF: 238

Grain Size : lower fine sand, angular to subrounded Texture: well-sorted, clast-supported, long and concavo-convex contacts

Description***:

Other minerals include chalcedony.

Abundant dolomite grains.

Abundant pseudomatrix. Chert with impurities may appear similar to pseudomatrix.

Abundant euhedral quartz overgrowths, predated other cements.

Rare drusy quartz veins/feature on chert.

Abundant, very thick hematite/limonite stains (reddish brown to opaque) and coatings, postdated other cements. Also occurs as thin laminae up to 1 μm wide and >10 μm long.

Authigenic dolomite and Fe-dolomite are always associated with the detrital dolomite. Postdated the quartz overgrowths.

Abundant illite coatings.

All pores have secondary origin; primarily due to partial leaching of chert, rock fragments, quartz overgrowths as well as microfractures <10 μm.

Rock Fragments

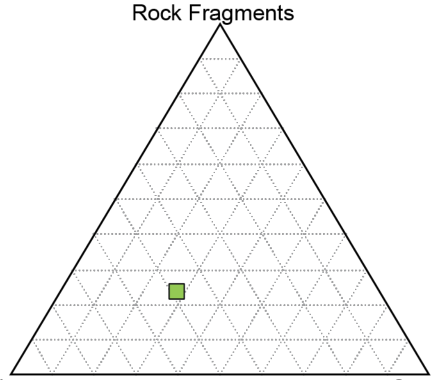

Chert Quartz

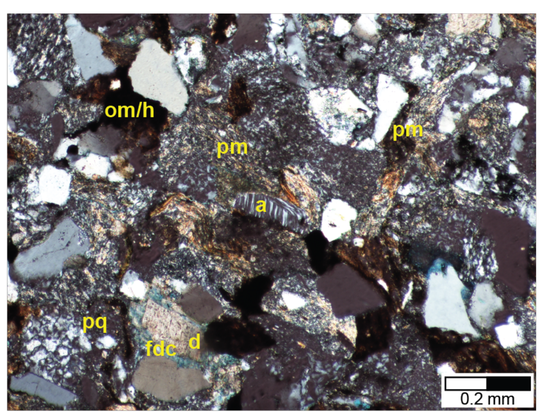

* = may include dolomite grains
** = iron-stained RF, volcanic RF, calcareous RF, and unidentified RF
*** = some very rarely occurring minerals may not be quantified on point counting results due to the automatic computer-generated crosshairs

Well ID & sample depth	: 100/06-20-065-09W6/00, 2920.7 m	Stains:	double carbonate
Petrofacies	: petrofacies I	Parasequence:	FP2
Depositional setting	: upper shoreface	Lithofacies:	facies 5
Facies assocation	: FA2 (wave-dominated shoreface)		

monocr. quartz	polycr. quartz	biotite (mica)	muscovite (mica)	others** (rock fragments)	sedimentary* (rock fragments)	metamorphic (rock fragments)	chert	quartzite	others	Fe-dolomite (cements)	dolomite (cements)	iron oxide (cements)	calcite (cements)	illite/smectite (cements)	chlorite (cements)	kaolinite (cements)	matrix	porosity
81	23	-	1	29	44	-	99	4	-	-	-	10	-	-	-	-	-	9

Totals: #

quartz	biotite	muscovite	rock fragments	chert + quartzite	others	Fe-dolomite	dolomite	iron oxide	calcite	illite/smectite	chlorite	kaolinite	matrix	porosity
104	-	1	73	103	-	-	-	10	-	-	-	-	-	9

Totals: %

quartz	biotite	muscovite	rock fragments	chert + quartzite	others	Fe-dolomite	dolomite	iron oxide	calcite	illite/smectite	chlorite	kaolinite	matrix	porosity
34.67	-	0.33	24.33	34.33	-	-	-	3.33	-	-	-	-	-	3

Totals: % clasts

quartz	biotite	muscovite	rock fragments	chert + quartzite	others
34.67	-	0.33	24.33	34.33	-

% normalized: (mQ + pQ) (C + Qe) RF

Q	C	RF
37	37	26

Total count: 300 Total clasts: 281 Total Q+C+RF: 280

Grain Size : lower to upper very fine sand, subangular to rounded grains

Texture: well-sorted, clast-supported, primarily long and concave-convex contacts, infrequently sutured

Description***:

Rounded grains are restricted to quartz.

Abundant dolomite grains.

Other minerals include very rare feldspars.

Common authigenic pyrite as dispersed opaque specks.

Abundant euhedral to syntaxial quartz overgrowths, predating all cements.

Abundant Fe-dolomite cements as dolomite grain coatings.

Common intermixed iron oxide and organic matters as grain coatings.

Very rare intergranular primary porosity preserved. Abundant secondary porosity from microfractures along rigid grain contacts as well as partial to complete chert and rock fragment dissolution, which may appear similar to primary porosity.

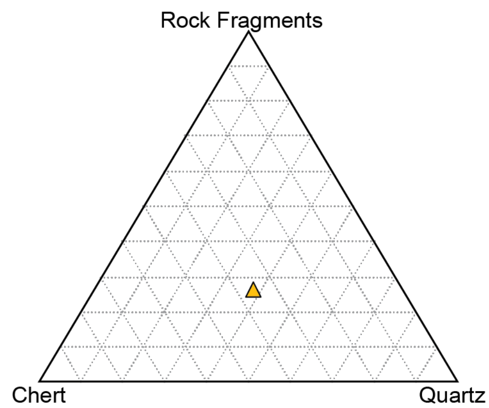

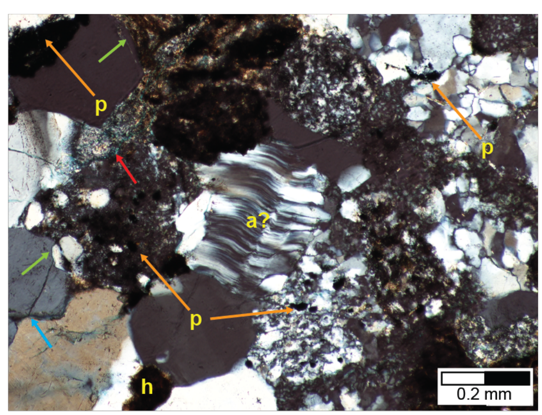

* = may include dolomite grains
** = iron-stained RF, volcanic RF, calcareous RF, and unidentified RF
*** = some very rarely occurring minerals may not be quantified on point counting results due to the automatic computer-generated crosshairs

Well ID & sample depth	: 100/06-20-065-11W6/00, 2922.0 m	Stains:	double carbonate
Petrofacies	: petrofacies II	Parasequence:	FP2
Depositional setting	: upper shoreface	Lithofacies:	facies 4
Facies assocation	: FA2 (wave-dominated shoreface)		

			mica		rock fragments					cements								
monocr. quartz	polycr. quartz	biotite	muscovite	others**	sedimentary*	metamorphic	chert	quartzite	others	Fe-dolomite	dolomite	iron oxide	calcite	illite/smectite	chlorite	kaolinite	matrix	porosity
99	15	-	-	28	16	-	97	3	-	5	4	8	-	-	-	10	-	15

Totals: #

114	-	-	44	100	-	5	4	8	-	-	-	10	-	15

Totals: %

38	-	-	14.67	33.33	-	1.67	1.33	2.33	-	-	-	3.33	-	5

Totals: % clasts

38	-	-	14.67	33.33	-

% normalized: (mQ + pQ) (C + Qe) RF

Q 44 C 39 RF 17

Total count: 300 Total clasts: 258 Total Q+C+RF: 258

Grain Size : upper fine sand, angular to rounded

Texture: well-sorted, clast-supported, predominantly long and concavo-convex contacts, common sutured contacts

Description***:

Rounded grains are restricted to quartz. Abundant quartz showing possible weathering, as indicated by extensive microfractures, iron stains, or very dusty appearance.

Common dolomite detrital grains.

Rare iron-stained rock fragments that are cut by drusy quartz veins, indicating possible authigenic origins of localized drusy quartz.

Other minerals include very rare heavy minerals.

Abundant syntaxial quartz overgrowths, predating all cements.

Abundant dolomite as replacements and rhombic inclusions, particularly on chert and rock fragments. Dolomite cement and Fe-dolomite rims are generally associated with dolomite grains. Distinguishable due to the rigid and blocky appearance of dolomite grains vs. patchy appearances of authigenic dolomite.

Rare intergranular primary porosity. Abundant secondary porosity from partial to complete dissolutions of chert, rock fragments, and possibly quartz as well as microfractures along grain contacts and across crystal planes.

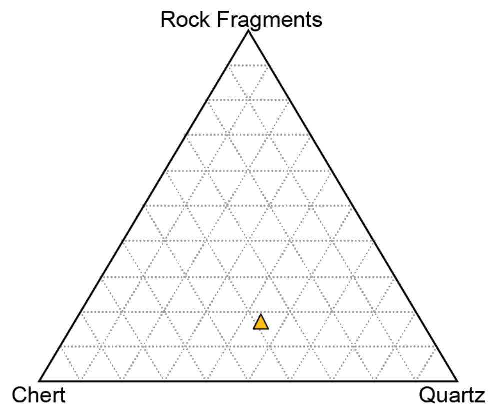

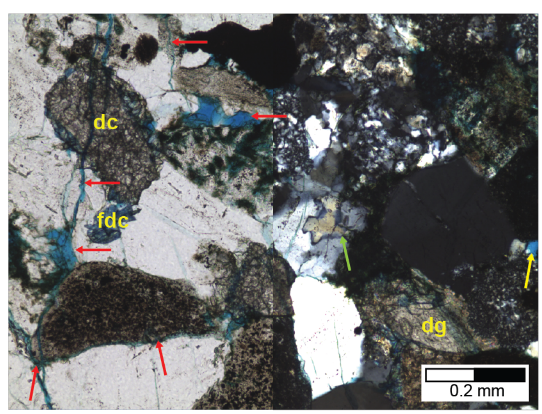

* = may include dolomite grains
** = iron-stained RF, volcanic RF, calcareous RF, and unidentified RF
*** = some very rarely occurring minerals may not be quantified on point counting results due to the automatic computer-generated crosshairs

Well ID & sample depth	: 100/15-09-065-11W6/00, 3024.0 m	Stains:	double carbonate
Petrofacies	: petrofacies IV	Parasequence:	Fp3
Depositional setting	: upper shoreface	Lithofacies:	facies 5
Facies assocation	: FA2 (wave-dominated shoreface)		

monocr. quartz	polycr. quartz	mica: biotite	mica: muscovite	rock fragments*: sedimentary*	rock fragments*: metamorphic	rock fragments*: others**	chert	quartzite	others	cements: Fe-dolomite	cements: dolomite	cements: iron oxide	cements: calcite	cements: illite/smectite	cements: chlorite	cements: kaolinite	matrix	porosity
98	19	-	-	17	-	13	96	2	-	37	6	-	-	4	-	-	-	5

Totals: #

quartz	biotite	muscovite	rock fragments	chert + quartzite	others	Fe-dolomite	dolomite	iron oxide	calcite	illite/smectite	chlorite	kaolinite	matrix	porosity
117	-	-	30	98	-	37	6	-	-	4	-	-	-	5

Totals: %

quartz	biotite	muscovite	rock fragments	chert + quartzite	others	Fe-dolomite	dolomite	iron oxide	calcite	illite/smectite	chlorite	kaolinite	matrix	porosity
39	-	-	11	32.67	-	12.33	2	-	-	1.33	-	-	-	1.67

Totals: % clasts

quartz	biotite	muscovite	rock fragments	chert + quartzite	others
39	-	-	11	32.67	-

% normalized: (mQ + pQ) (C + Qe) RF

Q	C	RF
47	40	13

Total count: 300 Total clasts: 248 Total Q+C+RF: 248

Grain Size : lower very fine to upper fine sand, subangular to rounded

Texture: well-sorted, clast-supported, primarily long and concavo-convex with frequent sutured contacts

Description***:

Rounded grains are restricted to quartz.

Common dolomite grains.

Most rock fragments occur as pseudomatrix.

Abundant quartz overgrowths.

Fe-dolomite generally occurs as replacements on dolomite grains and/or cements, as well as pseudomatrix. In the latter case it may appear as pore-occluding cements. Where occurs as intergranular cement, it is sporadically patchy.

Abundant intermixing of organic matter and iron oxide coatings, as thick as ~30 μm.

Bioturbation is possibly present as thin drapes (up to 0.3 mm thick, 3 mm long) composed of iron oxide and organic matter.

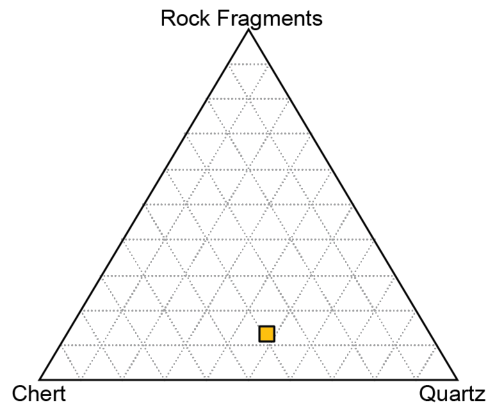

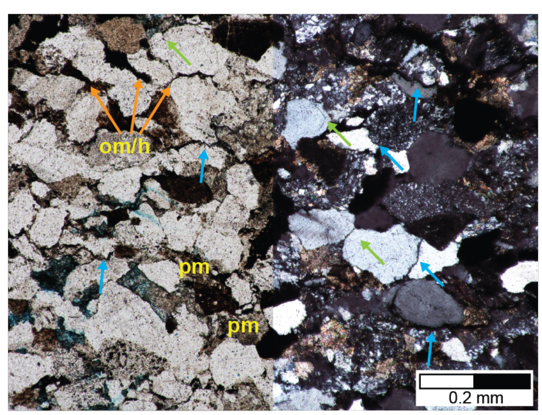

* = may include dolomite grains
** = iron-stained RF, volcanic RF, calcareous RF, and unidentified RF
*** = some very rarely occurring minerals may not be quantified on point counting results due to the automatic computer-generated crosshairs

Well ID & sample depth : 100/07-14-065-11W6/02, 3168.3 m Stains: double carbonate
Petrofacies : petrofacies II Parasequence: FP2
Depositional setting : foreshore Lithofacies: facies 4
Facies assocation : FA2 (wave-dominated shoreface)

			mica		rock fragments					cements								
monocr. quartz	polycr. quartz	biotite	muscovite	others**	sedimentary*	metamorphic	chert	quartzite	others	Fe-dolomite	dolomite	iron oxide	calcite	illite/smectite	chlorite	kaolinite	matrix	porosity
141	12	-	-	16	23	-	25	3	3	-	-	29	-	-	-	25	-	23

Totals: #

153	-	-	39	28	3	-	-	29	-	-	-	25	-	23

Totals: %

51.33	-	-	12.33	9.33	1	-	-	9.67	-	-	-	8.33	-	7.67

Totals: % clasts

51.33	-	-	12.33	9.33	1

% normalized: (mQ + pQ) (C + Qe) RF

Q	C	RF
70	13	17

Total count: 300 Total clasts: 223 Total Q+C+RF: 220

Grain Size : lower fine sand, subangular to rounded

Texture: well-sorted, clast-supported, long to concavo-convex contacts

Description***:

Rounded grains are restricted to quartz.

Other minerals include rare chlorite, chalcedony.

Rare pseudomatrix.

Abundant syntaxial to euhedral quartz overgrowths, predating all cements.

Abundant intermixed of organic matter and iron oxide as poikilotopic and grain-coating cements; iron oxide may have predated significant burial compaction and dissolution.

Common siderite inclusions, particularly in chert and dolomite grains.

Common pore-filling kaolinite cements.

Rare primary intergranular porosity. Abundant secondary porosity from partial to complete dissolution of chert, rock fragments, and possibly feldspars, may result in similar appearance with primary intergranular porosity.

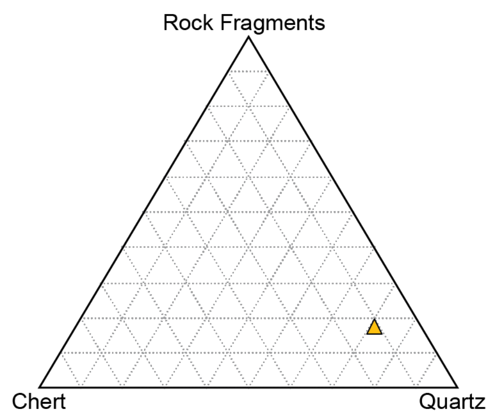

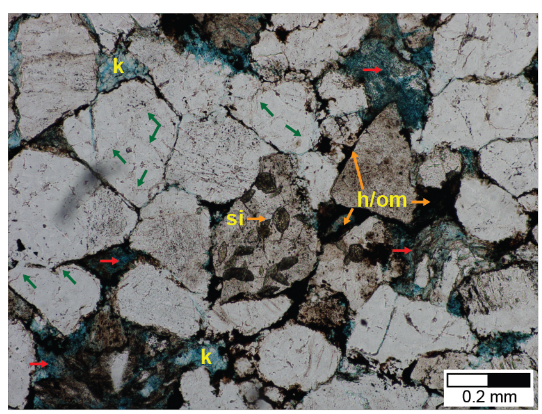

* = may include dolomite grains
** = iron-stained RF, volcanic RF, calcareous RF, and unidentified RF
*** = some very rarely occurring minerals may not be quantified on point counting results due to the automatic computer-generated crosshairs

Well ID & sample depth : 100/07-14-065-09W6/02, 3175.9 m   Stains: double carbonate
Petrofacies : petrofacies II   Parasequence: FP2
Depositional setting : upper shoreface   Lithofacies: facies 5
Facies assocation : FA2 (wave-dominated shoreface)

monocr. quartz	polycr. quartz	biotite	mica: muscovite	mica: others**	rock fragments: sedimentary*	rock fragments: metamorphic	chert	quartzite	others	cements: Fe-dolomite	cements: dolomite	cements: iron oxide	cements: calcite	cements: illite/smectite	cements: chlorite	cements: kaolinite	matrix	porosity
110	47	-	-	22	17	-	33	4	-	2	14	1	-	-	-	17	-	33

Totals: #

157	-	-	39	37	-	2	14	1	-	-	-	17	-	33

Totals: %

52.34	-	-	13	12.34	-	0.67	4.67	0.33	-	-	-	5.67	-	11

Totals: % clasts

52.34	-	-	13	12.34	-

% normalized: (mQ + pQ) (C + Qe) RF

Q 67 C 16 RF 17

Total count: 300   Total clasts: 233   Total Q+C+RF: 233

Grain Size : upper fine sand, angular to rounded   Texture: well-sorted, clast-supported, long to concavo-convex contacts

Description***:

Rounded grains are restricted to quartz.

Abundant syntaxial quartz overgrowths as the primary cement.

Common sporadic, patchy dolomite cement, rather localized, postdated the quartz overgrowths.

Abundant chlorite inclusions, rarely also as meshwork of pore-occluding cement.

Abundant pores due to partial to complete dissolution of chert, rock fragments, and quartz overgrowths; microfractures. Not all pores are occluded by kaolinite, cement-free pores are common.

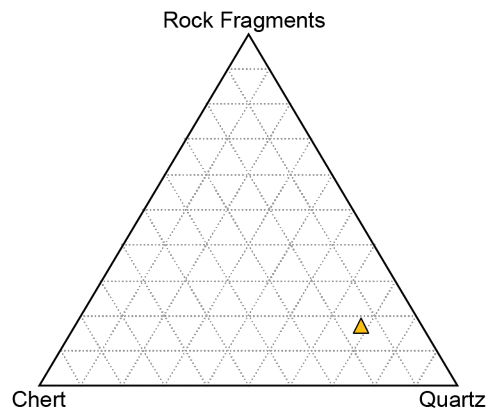

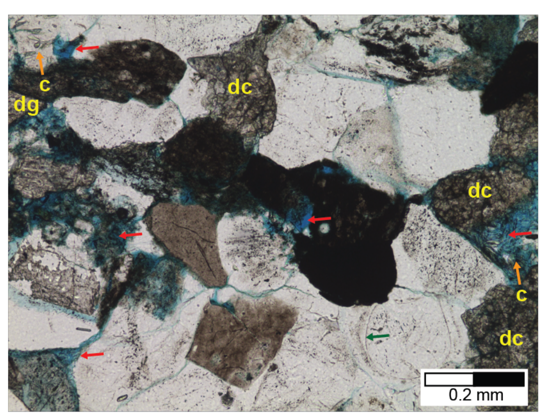

* = may include dolomite grains
** = iron-stained RF, volcanic RF, calcareous RF, and unidentified RF
*** = some very rarely occurring minerals may not be quantified on point counting results due to the automatic computer-generated crosshairs

Well ID & sample depth : 100/07-16-065-11W6/02, 3188.9 m Stains: double carbonate
Petrofacies : petrofacies IV Parasequence: T
Depositional setting : estuarine Lithofacies: facies 11
Facies assocation : FA3 (brackish embayment)

			mica		rock fragments					cements								
monocr. quartz	polycr. quartz	biotite	muscovite	others**	sedimentary*	metamorphic	chert	quartzite	others	Fe-dolomite	dolomite	iron oxide	calcite	illite/smectite	chlorite	kaolinite	matrix	porosity
47	8	-	-	9	19	4	92	7	10	52	39	10	-	3	-	-	-	-

Totals: #

55	-	-	32	99	10	52	39	10	-	3	-	-	-	-

Totals: %

19.34	-	-	11.34	33	3.33	17.33	13	3.33	-	1	-	-	-	-

Totals: % clasts

19.34	-	-	11.34	33	3.33

% normalized: (mQ + pQ) (C + Qe) RF

Q	C	RF
30	52	18

Total count: 300 Total clasts: 196 Total Q+C+RF: 186

Grain Size : upper very fine to upper fine sand, angular to subrounded

Texture: well-sorted, matrix-supported, tangential to long contacts

Description***:

Abundant dolomite grains.

Other minerals include chalcedony, feldspars, chlorite.

Common euhedral quartz overgrowths.

Abundant patchy to poikilotopic Fe-dolomite cement.

Abundant pseudomatrix.

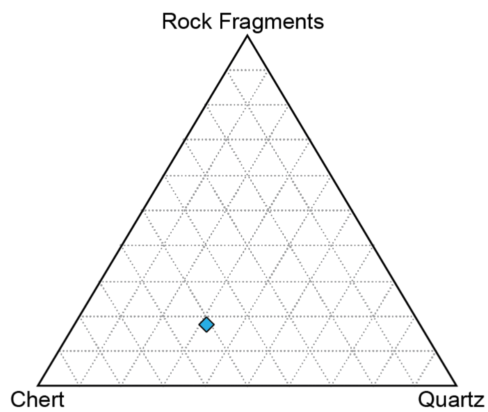

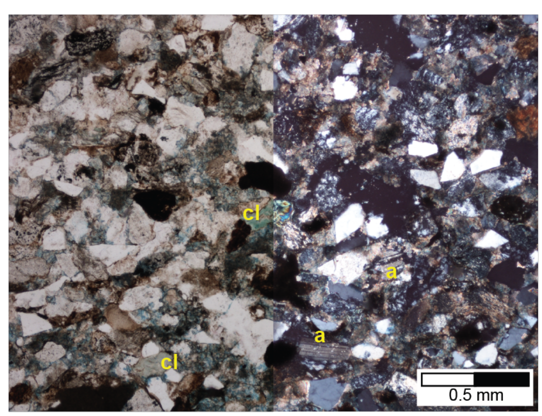

* = may include dolomite grains
** = iron-stained RF, volcanic RF, calcareous RF, and unidentified RF
*** = some very rarely occurring minerals may not be quantified on point counting results due to the automatic computer-generated crosshairs

Well ID & sample depth : 100/07-16-065-11W6/02, 3199.1 m Stains: double carbonate
Petrofacies : petrofacies IV Parasequence: FP3
Depositional setting : lower shoreface Lithofacies: facies 3
Facies assocation : FA1 (storm-dominated shoreface)

monocr. quartz	polycr. quartz	biotite	muscovite (mica)	others** (mica)	sedimentary* (rock fragments)	metamorphic (rock fragments)	chert	quartzite	others	Fe-dolomite (cements)	dolomite (cements)	iron oxide (cements)	calcite (cements)	illite/smectite (cements)	chlorite (cements)	kaolinite (cements)	matrix	porosity
85	38	-	1	23	36	3	91	1	-	10	4	8	-	-	-	-	-	-

Totals: #

123	-	1	62	92	-	10	4	8	-	-	-	-	-	-

Totals: %

41	-	0.33	20.67	30.67	-	3.33	1.33	2.33	-	-	-	-	-	-

Totals: % clasts

41	-	0.33	20.67	30.67	-

% normalized: (mQ + pQ) (C + Qe) RF

Q 44 C 34 RF 22

Total count: 300 Total clasts: 278 Total Q+C+RF: 277

Grain Size : upper very fine sand, angular to subrounded

Texture: well-sorted, clast-supported, long to concavo-convex contacts, frequently stylolitized

Description***:

Abundant dolomite grains.

Other minerals include heavy minerals (as inclusion).

Abundant pseudomatrix.

Abundant interlocking syntaxial quartz overgrowths.

Abundant patchy dolomite and Fe-dolomite cements.

Common pore-occluding iron oxide cements (not grain-coating).

Common specks of sporadic pyrite.

Common chlorite inclusions within quartz.

Secondary pores are limited to very small-scale microfractures along grain contacts.

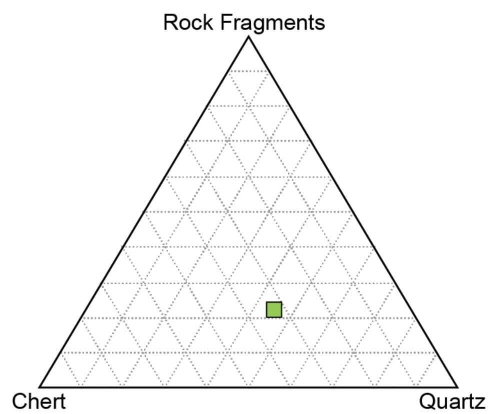

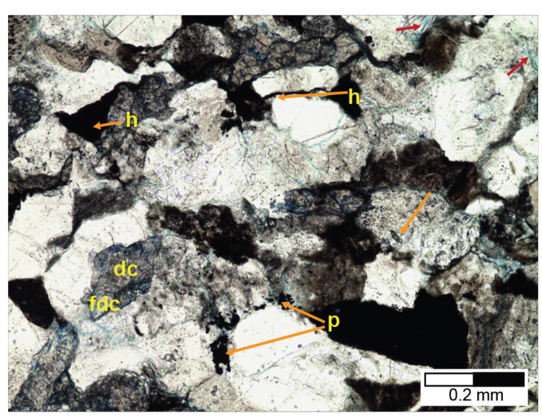

* = may include dolomite grains
** = iron-stained RF, volcanic RF, calcareous RF, and unidentified RF
*** = some very rarely occurring minerals may not be quantified on point counting results due to the automatic computer-generated crosshairs

Well ID & sample depth : 100/07-16-065-09W6/00, 3195.5 m Stains: double carbonate
Petrofacies : petrofacies IV Parasequence: FP3
Depositional setting : lower shoreface Lithofacies: facies 3
Facies assocation : FA1 (storm-dominated shoreface)

			mica		rock fragments						cements								
	monocr. quartz	polycr. quartz	biotite	muscovite	others**	sedimentary*	metamorphic	chert	quartzite	others	Fe-dolomite	dolomite	iron oxide	calcite	illite/smectite	chlorite	kaolinite	matrix	porosity
	59	31	-	1	25	19	-	121	1	-	12	18	5	-	6	-	-	-	2
Totals: #	90		-	1	44			122		-	12	18	5	-	6	-	-	-	2
Totals: %	30		-	0.33	14.67			40.67		-	4	6	1.67	-	2	-	-	-	0.67
Totals: % clasts	30		-	0.33	14.67			40.67		-									

% normalized: (mQ + pQ) (C + Qe) RF

Q 35 C 48 RF 17

Total count: 300 Total clasts: 257 Total Q+C+RF: 256

Grain Size : lower fine sand, angular to subrounded

Texture: moderately-sorted, clast-supported, long to concavo-convex contacts, rarely stylolitized

Description***:

Common dolomite grains.

Other minerals include feldspars.

Abundant syntaxial, interlocking quartz overgrowths.

Abundant pseudomatrix, some are dissolved.

Abundant patchy dolomite and Fe-dolomite cements. Also common as inclusions in quartz and chert.

Common grain-coating authigenic chlorite.

Pores may be cement-free or partially to completely occluded by kaolinite.

Abundant secondary pores due to partial to complete dissolution of various grains and pseudomatrix as well as cements, thus dissolution postdated the authigenic minerals at least partially.

Microfractures are common.

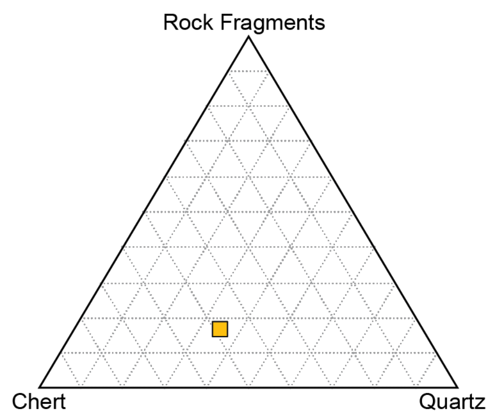

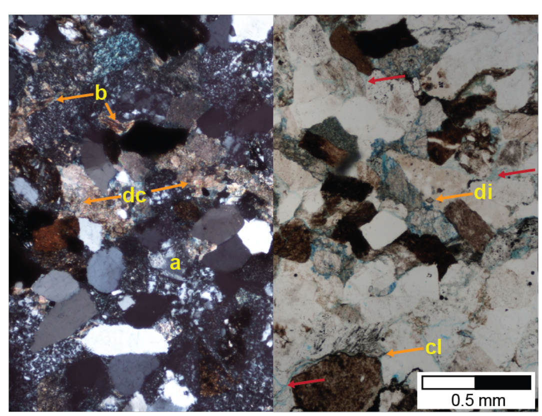

* = may include dolomite grains
** = iron-stained RF, volcanic RF, calcareous RF, and unidentified RF
*** = some very rarely occurring minerals may not be quantified on point counting results due to the automatic computer-generated crosshairs

Well ID & sample depth : 100/14-24-065-10W6/00, 2776.5 m Stains: double carbonate
Petrofacies : petrofacies IV Parasequence: FP2
Depositional setting : lower shoreface Lithofacies: facies 3
Facies assocation : FA1 (storm-dominated shoreface)

monocr. quartz	polycr. quartz	biotite	muscovite (mica)	others** (mica)	sedimentary* (rock fragments)	metamorphic (rock fragments)	chert	quartzite	others	Fe-dolomite (cements)	dolomite (cements)	iron oxide (cements)	calcite (cements)	illite/smectite (cements)	chlorite (cements)	kaolinite (cements)	matrix	porosity
86	20	9	-	11	45	4	97	1	-	4	14	6	-	-	-	-	-	3

Totals: #

quartz	biotite	mica	rock fragments	chert + quartzite	others	Fe-dolomite	dolomite	iron oxide	calcite	illite/smectite	chlorite	kaolinite	matrix	porosity
106	9	-	60	98	-	4	14	6	-	-	-	-	-	3

Totals: %

quartz	biotite	mica	rock fragments	chert + quartzite	others	Fe-dolomite	dolomite	iron oxide	calcite	illite/smectite	chlorite	kaolinite	matrix	porosity
35.33	9	-	20	32.66	-	1.33	4.67	2	-	-	-	-	-	1

Totals: % clasts

quartz	biotite	mica	rock fragments	chert + quartzite	others
35.33	9	-	20	32.66	-

% normalized: (mQ + pQ) (C + Qe) RF

Q 40 C 37 RF 23

Total count: 300 Total clasts: 273 Total Q+C+RF: 273

Grain Size : upper very fine sand, angular to subrounded

Texture: well-sorted, clast-supported, long and concavo-convex contacts

Description***:

Abundant dolomite grains.

Other minerals include feldspars.

Abundant interlocking quartz overgrowths.

Common Fe-dolomite cements as rims of dolomite grains/cements.

Abundant specks of pyrite.

Rare iron oxide cements along grain contacts.

Secondary pores are primarily from microfractures along grain contacts, less commonly from dissolution of chert, rock fragment, and/or quartz grains. Within secondary intergranular pores, kaolinite is commonly present.

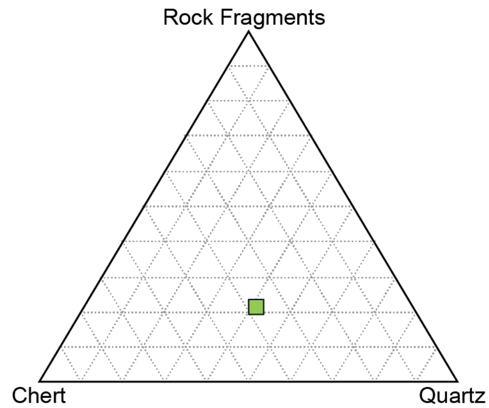

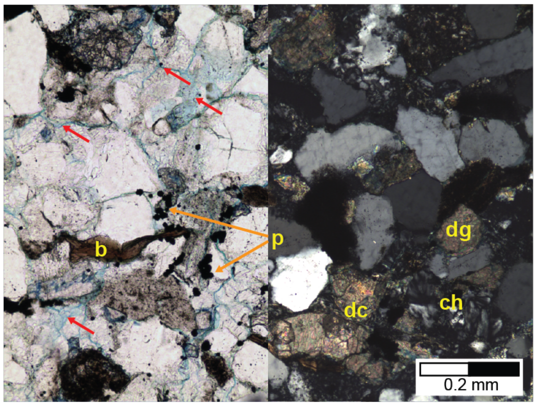

* = may include dolomite grains
** = iron-stained RF, volcanic RF, calcareous RF, and unidentified RF
*** = some very rarely occurring minerals may not be quantified on point counting results due to the automatic computer-generated crosshairs

Well ID & sample depth : 100/14-24-065-10W6/00, 2777.5 m Stains: double carbonate
Petrofacies : petrofacies IV Parasequence: Fp2
Depositional setting : lower shoreface Lithofacies: facies 3
Facies assocation : FA1 (storm-dominated shoreface)

		mica			rock fragments					cements								
monocr. quartz	polycr. quartz	biotite	muscovite	others**	sedimentary*	metamorphic	chert	quartzite	others	Fe-dolomite	dolomite	iron oxide	calcite	illite/smectite	chlorite	kaolinite	matrix	porosity
71	7	2	-	7	76	-	101	-	-	5	23	3	-	5	-	-	-	1

Totals: #

78	2	-	83	101	-	5	23	3	-	5	-	-	-	1

Totals: %

26	0.67	-	27.67	33.67	-	1.67	7.67	1	-	1.67	-	-	-	0.33

Totals: % clasts

26	0.67	-	27.67	33.67	-

% normalized: (mQ + pQ) (C + Qe) RF

Q 30 C 38 RF 32

Total count: 300 Total clasts: 263 Total Q+C+RF: 261

Grain Size : upper very fine sand, angular to subrounded

Texture: well-sorted, clast-supported, long and concavo-convex contacts

Description***:

Abundant dolomite grains.

Other minerals include very rare feldspars and chalcedony.

Abundant interlocking quartz overgrowths.

Abundant Fe-dolomite cement as rims of dolomite grains/cements.

Common specks of pyrite.

Common grain-coating authigenic chlorite.

Rare grain-coating illite.

Secondary pores are primarily from microfractures along grain contacts.

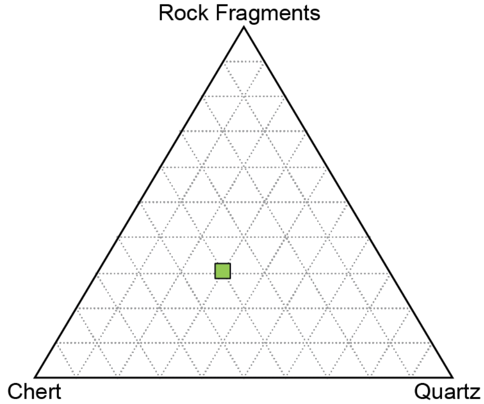

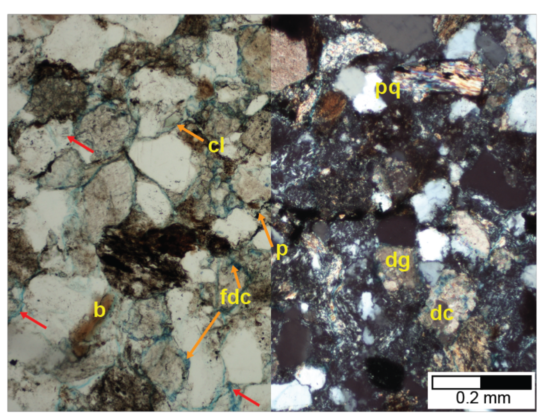

* = may include dolomite grains
** = iron-stained RF, volcanic RF, calcareous RF, and unidentified RF
*** = some very rarely occurring minerals may not be quantified on point counting results due to the automatic computer-generated crosshairs

Well ID & sample depth : 100/08-26-065-11W6/00, 2884.7 m Stains: double carbonate
Petrofacies : petrofacies III Parasequence: T
Depositional setting : fluvial channel Lithofacies: facies 13
Facies assocation : FA4 (coastal plain)

monocr. quartz	polycr. quartz	biotite (mica)	muscovite (mica)	others** (rock fragments)	sedimentary* (rock fragments)	metamorphic (rock fragments)	chert	quartzite	others	Fe-dolomite (cements)	dolomite (cements)	iron oxide (cements)	calcite (cements)	illite/smectite (cements)	chlorite (cements)	kaolinite (cements)	matrix	porosity
71	6	-	-	8	33	1	127	-	2	18	2	32	-	-	-	-	-	-

Totals: #

quartz	biotite	muscovite	rock fragments	chert + quartzite	others	Fe-dolomite	dolomite	iron oxide	calcite	illite/smectite	chlorite	kaolinite	matrix	porosity
77	-	-	42	127	2	18	2	32	-	-	-	-	-	-

Totals: %

quartz	biotite	muscovite	rock fragments	chert + quartzite	others	Fe-dolomite	dolomite	iron oxide	calcite	illite/smectite	chlorite	kaolinite	matrix	porosity
25.67	-	-	13.99	42.33	0.67	6	0.67	10.67	-	-	-	-	-	-

Totals: % clasts

quartz	biotite	muscovite	rock fragments	chert + quartzite	others
25.67	-	-	13.99	42.33	0.67

% normalized: (mQ + pQ) (C + Qe) RF

Q 31 C 52 RF 17

Total count: 300 Total clasts: 246 Total Q+C+RF: 244

Grain Size : lower to upper very fine sand, angular to subangular

Texture: well-sorted, clast-supported, long and concavo-convex contacts

Description***:

Other minerals include sporadic albite, biotite, muscovite.

Abundant shale pseudomatrix up to 1 mm.

Common euhedral to syntaxial quartz overgrowths.

Common dolomite and Fe-dolomite as replacements.

Abundant iron oxide and organic matter coatings up to 50 μm thick.

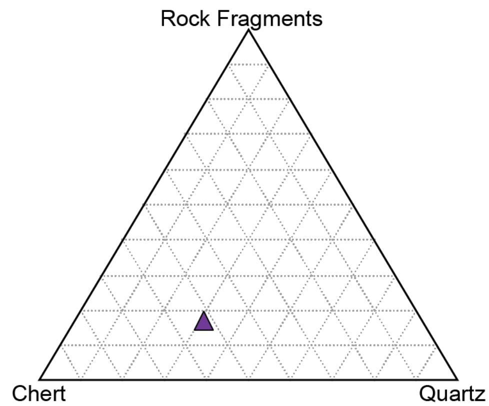

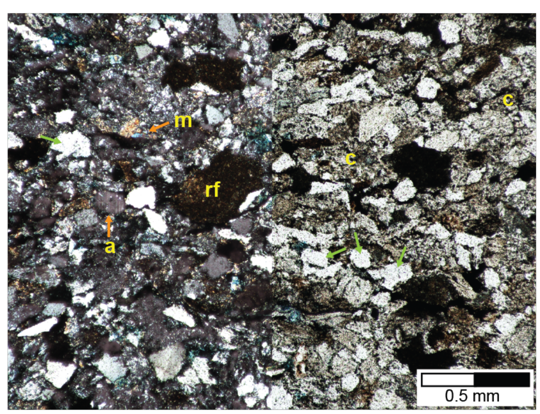

* = may include dolomite grains
** = iron-stained RF, volcanic RF, calcareous RF, and unidentified RF
*** = some very rarely occurring minerals may not be quantified on point counting results due to the automatic computer-generated crosshairs

Well ID & sample depth	: 100/05-07-066-08W6/00, 2535.1 m	Stains: double carbonate
Petrofacies	: petrofacies III	Parasequence: FP3
Depositional setting	: upper shoreface	Lithofacies: facies 4
Facies assocation	: FA2 (wave-dominated shoreface)	

	monocr. quartz	polycr. quartz	biotite	muscovite (mica)	others** (mica)	sedimentary* (rock fragments)	metamorphic (rock fragments)	chert	quartzite	others	Fe-dolomite (cements)	dolomite (cements)	iron oxide (cements)	calcite (cements)	illite/smectite (cements)	chlorite (cements)	kaolinite (cements)	matrix	porosity
	106	12	6	-	7	17	3	133	2	-	1	2	5	-	6	-	-	-	-
Totals: #	118		6	-	27			135		-	1	2	5	-	6	-	-	-	-
Totals: %	39.33		2	-	9			45		-	0.33	0.67	1.67	-	2	-	-	-	-
Totals: % clasts	39.33		2	-	9			45		-									

% normalized: (mQ + pQ) (C + Qe) RF

Q 42 C 48 RF 10

Total count: 300 Total clasts: 286 Total Q+C+RF: 280

Grain Size : upper very fine to upper fine sand, angular to rounded

Texture: moderately-sorted, clast-supported, concavo-convex and long contacts

Description***:

Rounded grains are restricted to quartz.

Tends to be micaceous with generally splayed and kinked biotite.

Common euhedral quartz overgrowths.

Abundant pseudomatrix. Chert with impurities may act as pseudomatrix too.

Abundant grain-coating illite, mostly postdating quartz overgrowths.

Common grain-coating organic matter and iron oxide cement, postdating quartz overgrowths.

All pores have secondary origin; primarily from microfractures <5 μm wide along grain contacts of quartz-to-quartz, chert-to-chert, and quartz-to-chert, rarely from partial dissolution of chert.

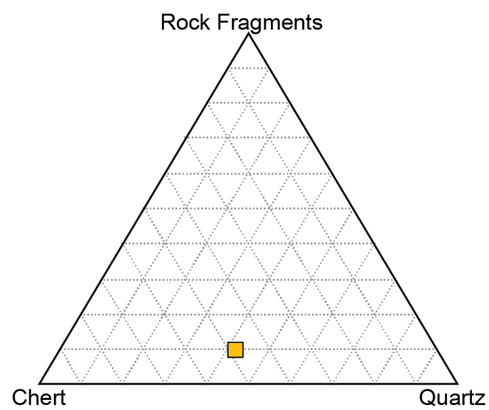

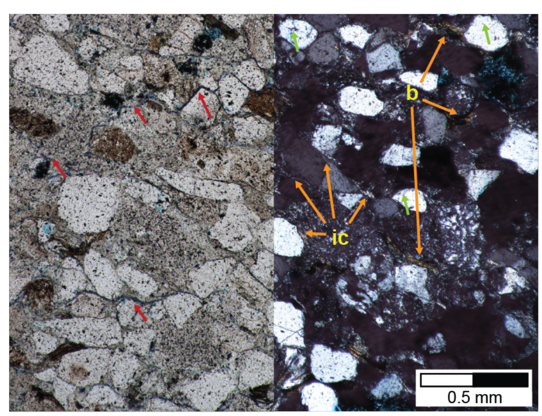

* = may include dolomite grains
** = iron-stained RF, volcanic RF, calcareous RF, and unidentified RF
*** = some very rarely occurring minerals may not be quantified on point counting results due to the automatic computer-generated crosshairs

Well ID & sample depth	: 100/01-08-066-08W6/00, 2579.4 m	Stains:	double carbonate
Petrofacies	: petrofacies I	Parasequence:	FP3
Depositional setting	: upper shoreface	Lithofacies:	facies 6
Facies assocation	: FA2 (wave-dominated shoreface)		

monocr. quartz	polycr. quartz	mica: biotite	mica: muscovite	rock fragments: sedimentary*	rock fragments: metamorphic	rock fragments: others**	chert	quartzite	others	cements: Fe-dolomite	cements: dolomite	cements: iron oxide	cements: calcite	cements: illite/smectite	cements: chlorite	cements: kaolinite	matrix	porosity
118	5	-	-	11	-	9	139	-	1	-	-	1	-	-	-	-	-	16

Totals: #

quartz	biotite	muscovite	rock fragments	chert	others	Fe-dolomite	dolomite	iron oxide	calcite	illite/smectite	chlorite	kaolinite	matrix	porosity
123	-	-	20	139	1	-	-	1	-	-	-	-	-	16

Totals: %

quartz	biotite	muscovite	rock fragments	chert	others	Fe-dolomite	dolomite	iron oxide	calcite	illite/smectite	chlorite	kaolinite	matrix	porosity
41.01	-	-	6.67	46.33	0.33	-	-	0.33	-	-	-	-	-	5.33

Totals: % clasts

quartz	biotite	muscovite	rock fragments	chert	others
41.01	-	-	6.67	46.33	0.33

% normalized: (mQ + pQ) (C + Qe) RF

Q	C	RF
44	49	7

Total count: 300 Total clasts: 283 Total Q+C+RF: 282

Grain Size : Upper fine to upper medium sand, subangular to rounded

Texture: Well-sorted, clast-supported, predominantly long and concavo-convex contacts, rarely sutured.

Description***:

Rounded grains are restricted to quartz.

Other minerals include extremely rare heavy minerals.

Abundant interlocking, syntaxial quartz overgrowth.

Common Fe-dolomite replacement on chert.

Rare grain-coating iron oxide. In dissolved grains, coatings either follow the original grain shape or follow the irregular dissolved boundaries, indicating that dissolution was probably before and after Fe-oxide cement had formed. Tightly compacted grains/clasts are either separated by iron oxide coatings or coatings-free, indicating that iron oxide cement was probably precipitated before, during, and after mechanical compaction.

Abundant secondary pores (dissolved chert and rock fragments, microfractures along grain contacts and across the grains); rare primary porosity.

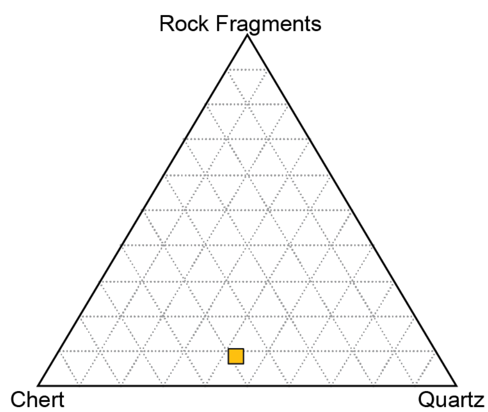

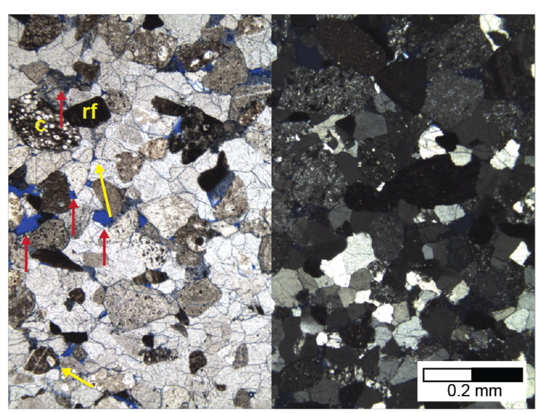

* = may include dolomite grains
** = iron-stained RF, volcanic RF, calcareous RF, and unidentified RF
*** = some very rarely occurring minerals may not be quantified on point counting results due to the automatic computer-generated crosshairs

Well ID & sample depth : 100/01-08-066-08W6/00, 2585.2 m Stains: double carbonate
Petrofacies : petrofacies IV Parasequence: FP2
Depositional setting : middle shoreface Lithofacies: facies 2
Facies assocation : FA1 (storm-dominated shoreface)

			mica		rock fragments					cements								
monocr. quartz	polycr. quartz	biotite	muscovite	sedimentary*	metamorphic	others**	chert	quartzite	others	Fe-dolomite	dolomite	iron oxide	calcite	illite/smectite	chlorite	kaolinite	matrix	porosity
53	10	-	-	68	-	15	71	2	2	74	3	1	-	-	-	-	-	1
Totals: #																		
63		-	-	83			73		2	74	-	1	-	-	-	-	-	1
Totals: %																		
21.34		-	-	28			24.34		0.67	24.67	-	0.33	-	-	-	-	-	0.33
Totals: % clasts																		
21.34		-	-	28			24.34		0.67									

% normalized: (mQ + pQ) (C + Qe) RF

Q 29 C 33 RF 38

Total count: 300 Total clasts: 224 Total Q+C+RF: 219

Grain Size : Lower to upper very fine sand, angular to subrounded

Texture: Moderately-sorted, open framework, predominantly tangential to point contacts.

Description***:

Rare chert clasts with drusy quartz veins.

Abundant dolomite grains.

Other minerals include very rare feldspars, chalcedony, albite, biotite, muscovite, chlorite (unclear as detrital grains or authigenic).

Common euhedral quartz overgrowths.

Abundant poikilotopic, intergranular-filling Fe-dolomite cement, possibly anomalously early compared to other samples.

Common dolomite "overgrowths" on quartz and chert grains, possibly replacing earlier unstable silica cement. Common dolomite replacement on chert and albite.

Most intergranular volume is filled by Fe-dolomite cement.

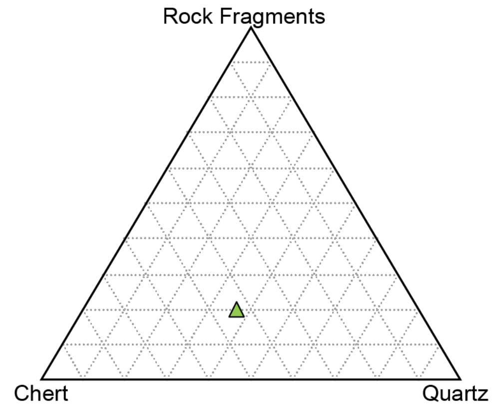

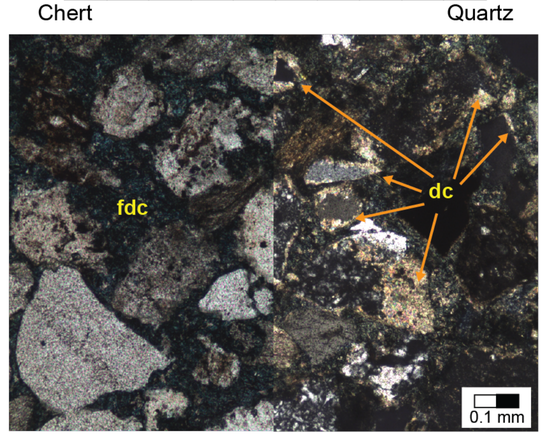

* = may include dolomite grains
** = iron-stained RF, volcanic RF, calcareous RF, and unidentified RF
*** = some very rarely occurring minerals may not be quantified on point counting results due to the automatic computer-generated crosshairs

Well ID & sample depth : 100/11-13-066-08W6/00, 2563 m   Stains: double carbonate
Petrofacies : petrofacies II   Parasequence: FP3
Depositional setting : upper shoreface   Lithofacies: facies 5
Facies assocation : FA2 (wave-dominated shoreface)

		mica			rock fragments					cements								
monocr. quartz	polycr. quartz	biotite	muscovite	others**	sedimentary*	metamorphic	chert	quartzite	others	Fe-dolomite	dolomite	iron oxide	calcite	illite/smectite	chlorite	kaolinite	matrix	porosity
101	37	-	1	17	20	-	92	4	1	3	3	2	-	-	-	4	-	15

Totals: #

138	-	1	37	96	1	3	3	2	-	-	-	4	-	15

Totals: %

46	-	0.33	12.66	32	0.33	1	1	0.67	-	-	-	1.33	-	5

Totals: % clasts

46	-	0.33	12.66	32	0.33

% normalized: (mQ + pQ) (C + Qe) RF

Q 51 C 35 RF 14

Total count: 300   Total clasts: 273   Total Q+C+RF: 271

Grain Size : lower fine sand, angular to subrounded

Texture: well-sorted, clast-supported, long to concavo-convex with common sutured contacts.

Description***:

Abundant dolomite grains.

Other minerals include feldspars.

Abundant pseudomatrix.

Abundant interlocking syntaxial quartz overgrowths.

Common dolomite and Fe-dolomite patchy cements. Likely post-dated kaolinite cements due to the incorporation of some kaolinite cements into dolomite cements.

Rare grain-coating authigenic illite.

All pores have secondary origin; from partial to complete dissolution of chert, rock fragments (pseudomatrix), quartz overgrowths and microfractures along grain contacts. Pores may be cement-free but generally occluded with kaolinite or dolomite.

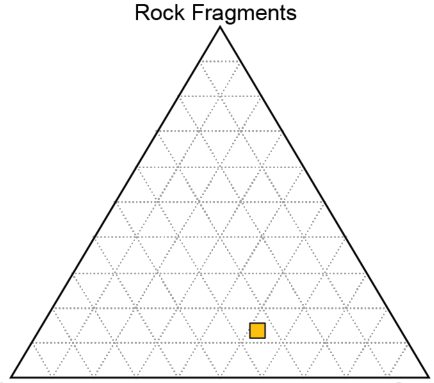

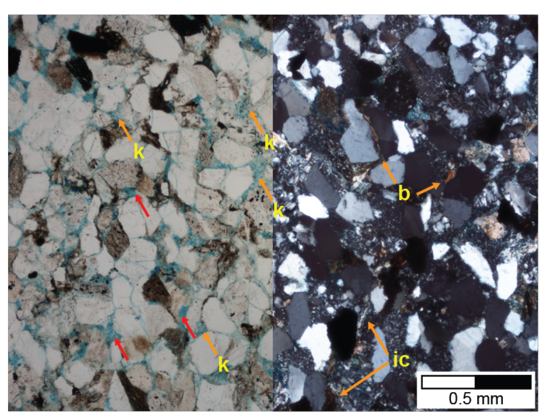

* = may include dolomite grains
** = iron-stained RF, volcanic RF, calcareous RF, and unidentified RF
*** = some very rarely occurring minerals may not be quantified on point counting results due to the automatic computer-generated crosshairs

Well ID & sample depth	: 100/03-18-066-08W6/00, 2468.6 m	Stains:	double carbonate
Petrofacies	: petrofacies III	Parasequence:	FP3
Depositional setting	: upper shoreface	Lithofacies:	facies 5
Facies assocation	: FA2 (wave-dominated shoreface)		

		mica		rock fragments						cements								
monocr. quartz	polycr. quartz	biotite	muscovite	sedimentary*	metamorphic	others**	chert	quartzite	others	Fe-dolomite	dolomite	iron oxide	calcite	illite/smectite	chlorite	kaolinite	matrix	porosity
100	14	3	1	13	2	5	131	-	4	8	1	14	-	4	-	-	-	-
Totals: #																		
115		3	1	20			131		4	8	1	4.67	-	4	-	-	-	-
Totals: %																		
38		1	0.33	8			43.67		1.33	2.67	0.33	4.67	-	1.33	-	-	-	-
Totals: % clasts																		
38		-	-	8			43.67		1.33									

% normalized: (mQ + pQ) (C + Qe) RF

Q 42 C 49 RF 9

Total count: 300 Total clasts: 287 Total Q+C+RF: 283

Grain Size : lower fine sand, subangular to subrounded

Texture: well-sorted, clast-supported, long to concavo-convex contacts

Description***:

Other minerals include feldspars that are relatively more abundant than other samples (although still rare), rare biotite, muscovite.

Rock fragments primarily occur as pseudomatrix. Pseudomatrix also includes common illitized chert squeezed among fresher detrital chert.

Common euhedral quartz overgrowths.

Intermixing of iron oxide cement and organic matter is present outside the quartz overgrowth, in the secondary pores, and between compacted grains, indicating the formation that may have postdated the other diagenetic events. Relatively thick compared to other samples (up to 40 μm).

Fe-dolomite commonly occurs as replacement on chert, rock fragments, albite, and infrequently biotite; and rarely as pore-filling cement, indicating the formation that may have postdated significant mechanical compaction.

In general, compositionally more immature than other upper shoreface sandstone samples in the study interval.

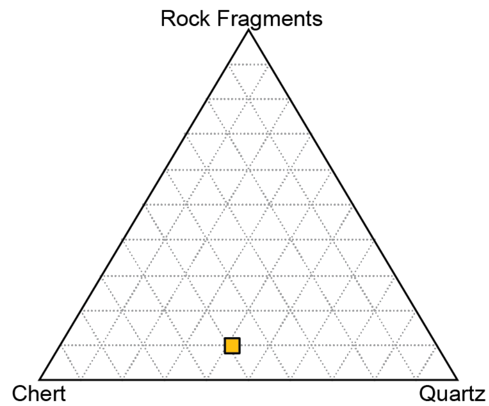

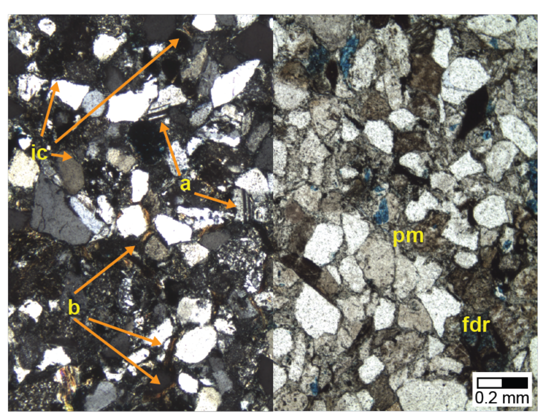

* = may include dolomite grains
** = iron-stained RF, volcanic RF, calcareous RF, and unidentified RF
*** = some very rarely occurring minerals may not be quantified on point counting results due to the automatic computer-generated crosshairs

Well ID & sample depth : 100/03-18-066-08W6/00, 2480.4 m Stains: double carbonate
Petrofacies : petrofacies IV Parasequence: FP2
Depositional setting : middle shoreface Lithofacies: facies 2
Facies assocation : FA1 (storm-dominated shoreface)

		mica		rock fragments						cements								
monocr. quartz	polycr. quartz	biotite	muscovite	sedimentary*	metamorphic	others**	chert	quartzite	others	Fe-dolomite	dolomite	iron oxide	calcite	illite/smectite	chlorite	kaolinite	matrix	porosity
64	21	-	-	21	2	-	106	-	-	46	17	3	-	-	-	-	-	20

Totals: #

monocr. + polycr. quartz	biotite	muscovite	rock fragments	chert + quartzite	others	Fe-dolomite	dolomite	iron oxide	calcite	illite/smectite	chlorite	kaolinite	matrix	porosity
85	-	-	23	106	-	46	17	3	-	-	-	-	-	20

Totals: %

monocr. + polycr. quartz	biotite	muscovite	rock fragments	chert + quartzite	others	Fe-dolomite	dolomite	iron oxide	calcite	illite/smectite	chlorite	kaolinite	matrix	porosity
28.33	-	-	7.67	35.33	-	-	-	-	-	-	-	-	-	-

Totals: % clasts

monocr. + polycr. quartz	biotite	muscovite	rock fragments	chert + quartzite	others
28.33	-	-	7.67	35.33	-

% normalized: (mQ + pQ) (C + Qe) RF

Q	C	RF
40	49	11

Total count: 300 Total clasts: 217 Total Q+C+RF: 217

Grain Size : upper very fine to upper fine sand, subangular to subrounded

Texture: moderately-sorted, clast-supported, long and concavo-convex contacts with common sutured contacts

Description***: Micaceous, predominantly of biotite. Biotite frequently "coats" grains, distinguishable with illite coatings despite the similar high birefringence.

Abundant dolomite grains.

Common rock fragments as pseudomatrix.

Chert rarely possesses overgrowths (dusty quartz?), distinguishable due to the dustier appearance of the nuclei.

Common quartz overgrowths.

Common dolomite overlapping quartz overgrowths, indicating its late formation as compared to quartz overgrowths.

Common dolomite and Fe-dolomite as replacements on chert and/or rock fragments.

Dolomite cement is present within the secondary pores, indicating that dolomite precipitation still occurs during and after dissolution. Also infrequently observed as thin coatings between quartz overgrowths and their nuclei (see image).

Common illite as grain coatings. Common intermixed of iron oxide and organic matter as grain coatings (up to 30 μm).

All pores have secondary origin; due to the dissolution of predominantly chert, rock fragments (particularly those behaving as pseudomatrix), and less frequently dolomite cement, as well as microfractures. A transition from a thin bed with abundant pores to a thin bed with no visible porosity is observed in thin section.

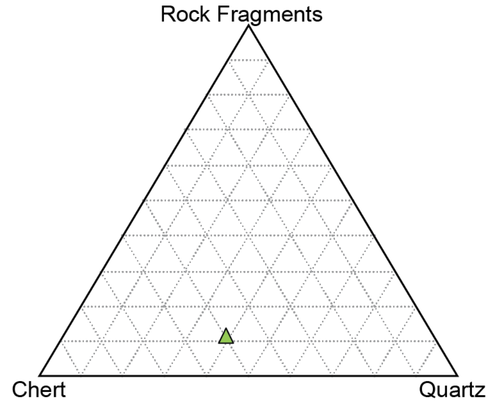

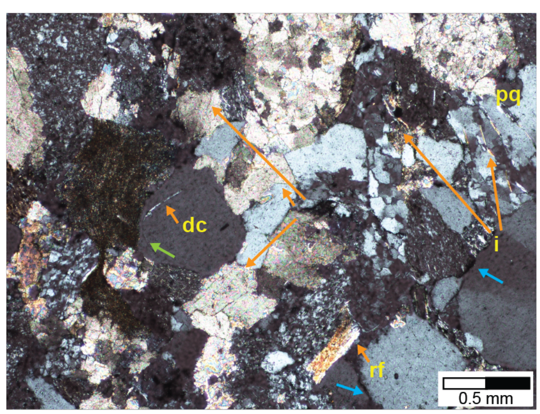

* = may include dolomite grains
** = iron-stained RF, volcanic RF, calcareous RF, and unidentified RF
*** = some very rarely occurring minerals may not be quantified on point counting results due to the automatic computer-generated crosshairs

Well ID & sample depth	: 100/03-18-066-08W6/00, 2481.6 m	Stains:	double carbonate
Petrofacies	: petrofacies I	Parasequence:	FP2
Depositional setting	: middle shoreface	Lithofacies:	facies 2
Facies assocation	: FA1 (storm-dominated shoreface)		

monocr. quartz	polycr. quartz	biotite	mica: muscovite	rock fragments: sedimentary*	rock fragments: metamorphic	rock fragments: others**	chert	quartzite	others	cements: Fe-dolomite	cements: dolomite	cements: iron oxide	cements: calcite	cements: illite/smectite	cements: chlorite	cements: kaolinite	matrix	porosity
89	18	-	1	49	3	16	117	-	-	-	-	6	-	-	-	-	-	1
Totals: #																		
107		-	1	68			117		-	-	-	6	-	-	-	-	-	1
Totals: %																		
107		-	1	68			117		-	-	-	6	-	-	-	-	-	1
Totals: % clasts																		
35.67		-	0.33	22.67			39		-									

% normalized: (mQ + pQ) (C + Qe) RF

Q	C	RF
37	40	23

Total count: 300 Total clasts: 293 Total Q+C+RF: 292

Grain Size : upper very fine to upper fine sand, subangular to subrounded

Texture: well-sorted, clast-supported, predominantly with long and concavo-convex contacts but sutured contacts are common.

Description*:** The lack of vacuoles/dusty rims between quartz overgrowths and their nuclei make it difficult to determine the shape of quartz grains. Generally, the vacuoles/dusty rims only partially encircle the nuclei, therefore the mere presence of quartz overgrowths can be recognized but the extent is unknown.

Very rare chert clasts with polycrystalline quartz veins.

Abundant dolomite grains.

Abundant quartz overgrowths.

Common iron oxide coatings, possibly mixed with organic matter.

Common dolomite and Fe-dolomite as replacements and euhedral rhombic inclusions. May appear similar to pore-occluding intergranular cements, but their relationship with the affected chert and/or rock fragments denote their replacement origin.

All pores have secondary origin; from predominantly dissolution of chert and rock fragments, and rarely microfractures. These are however very small-scale and not always readily visible.

The limited visible porosity indicates significant mechanical compaction as also shown by the common presence of pressure solution.

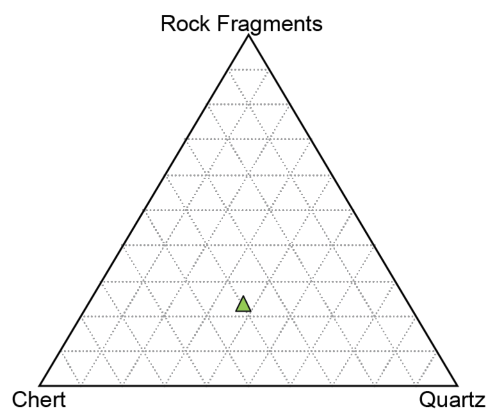

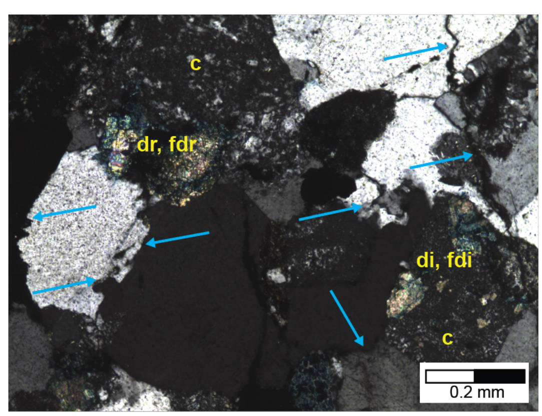

* = may include dolomite grains
** = iron-stained RF, volcanic RF, calcareous RF, and unidentified RF
*** = some very rarely occurring minerals may not be quantified on point counting results due to the automatic computer-generated crosshairs

Well ID & sample depth	: 100/03-18-066-08W6/00, 2483.5 m	Stains:	double carbonate
Petrofacies	: petrofacies IV	Parasequence:	FP2
Depositional setting	: middle shoreface	Lithofacies:	facies 2
Facies assocation	: FA1 (storm-dominated shoreface)		

			mica		rock fragments						cements								
	monocr. quartz	polycr. quartz	biotite	muscovite	sedimentary*	metamorphic	others**	chert	quartzite	others	Fe-dolomite	dolomite	iron oxide	calcite	illite/smectite	chlorite	kaolinite	matrix	porosity
	94	20	-	1	18	1	9	94	-	-	34	10	7	-	3	-	-	-	9
Totals: #	114		-	1	28			94		-	34	10	7	-	3	-	-	-	9
Totals: %	38.01		-	0.33	9.33			31.34		-	11.33	3.33	2.33	-	1	-	-	-	3
Totals: % clasts	38.01		-	0.33	9.33			31.34		-									

% normalized: (mQ + pQ) (C + Qe) RF

Q 48 C 40 RF 12

Total count: 300 Total clasts: 237 Total Q+C+RF: 236

Grain Size : upper very fine to upper fine sand, angular to subangular

Texture: moderately-sorted, clast-supported, long and concavo-convex contacts

Description***:

The extreme lack of vacuoles between quartz grains and their overgrowths make it difficult to distinguish the actual shape of quartz grains.

Abundant dolomite grains.

Common pseudomatrix from argillaceous and carbonaceous rock fragments as well as highly illitized chert.

Other minerals include biotite, muscovite, chlorite, chalcedony.

Rare volcanic rock fragments with well-defined feldspathic lithics.

Abundant quartz overgrowths.

Fe-dolomite primarily occurs as rims on dolomite detrital grains.

All pores have secondary origin; from dissolution of chert and rock fragments, also rarely of quartz overgrowths.

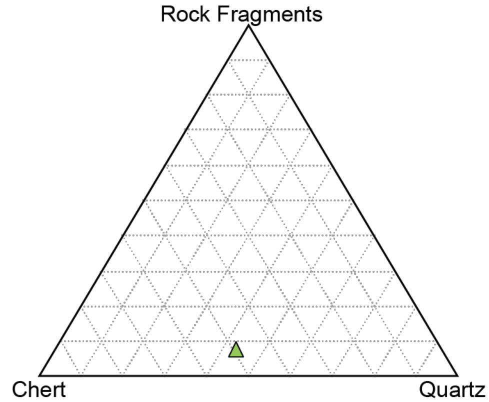

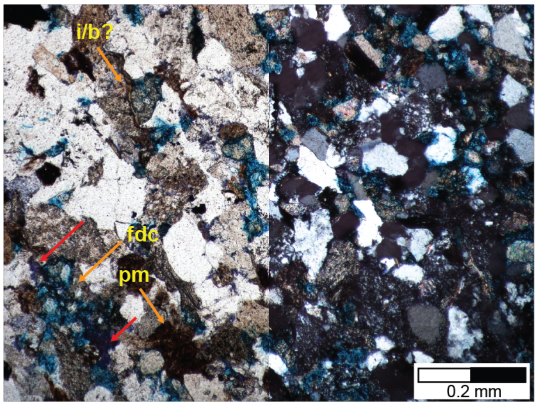

* = may include dolomite grains
** = iron-stained RF, volcanic RF, calcareous RF, and unidentified RF
*** = some very rarely occurring minerals may not be quantified on point counting results due to the automatic computer-generated crosshairs

Well ID & sample depth	: 100/02-21-066-08W6/00, 2513.8 m	Stains: double carbonate
Petrofacies	: petrofacies III	Parasequence: Fp3
Depositional setting	: lower shoreface	Lithofacies: facies 2
Facies assocation	: FA1 (storm-dominated shoreface)	

			mica		rock fragments					cements								
monocr. quartz	polycr. quartz	biotite	muscovite	others**	sedimentary*	metamorphic	chert	quartzite	others	Fe-dolomite	dolomite	iron oxide	calcite	illite/smectite	chlorite	kaolinite	matrix	porosity
93	16	3	-	6	40	-	124	-	1	4	1	10	-	2	-	-	-	-
Totals: #																		
109		3	-	46			124		1	4	1	10	-	2	-	-	-	-
Totals: %																		
36.34		1	-	15.33			41.34		0.33	1.33	0.33	3.33	-	0.67	-	-	-	-
Totals: % clasts																		
36.34		1	-	15.33			41.34		0.33									

% normalized: (mQ + pQ) (C + Qe) RF

Q 39 C 44 RF 17

Total count: 300 Total clasts: 282 Total Q+C+RF: 278

Grain Size : upper very fine to lower fine sand, subangular to subrounded

Texture: well-sorted, clast-supported, long and concavo-convex contacts

Description***:

Abundant dolomite grains.

Other minerals include very rare chlorite, glauconite, albite, and extremely rare heavy minerals.

Abundant pseudomatrix.

Abundant euhedral quartz overgrowths.

Abundant iron oxide and organic matter coatings that are aither present or absent between tightly compacted grains, indicating formation of iron oxide before, during, and after significant mechanical compaction. Also frequently incorporated into the dolomite replacement, indicating the formation prior to the precipitation of authigenic dolomite.

Common Fe-dolomite predominantly occurs as replacement on feldspars and dolomite grains, not as intergranular cement, indicating a formation after significant burial compaction.

Common grain-coating illite.

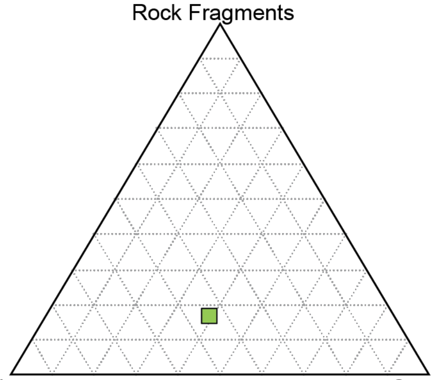

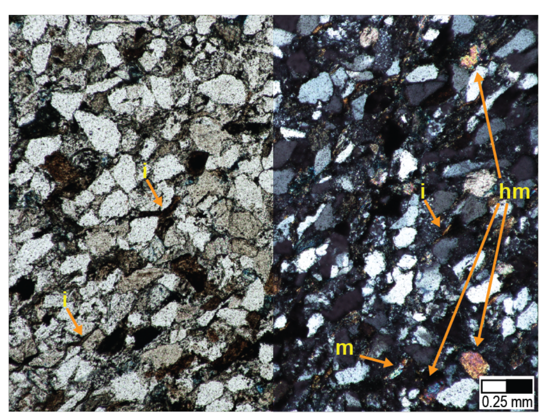

* = may include dolomite grains
** = iron-stained RF, volcanic RF, calcareous RF, and unidentified RF
*** = some very rarely occurring minerals may not be quantified on point counting results due to the automatic computer-generated crosshairs

Well ID & sample depth : 100/02-21-066-08W6/00, 2514.6 m   Stains: double carbonate
Petrofacies : petrofacies IV   Parasequence: FP3
Depositional setting : lower shoreface   Lithofacies: facies 3
Facies assocation : FA1 (storm-dominated shoreface)

monocr. quartz	polycr. quartz	biotite	mica: muscovite	mica: others**	rock fragments: sedimentary*	rock fragments: metamorphic	chert	quartzite	others	cements: Fe-dolomite	cements: dolomite	cements: iron oxide	cements: calcite	cements: illite/smectite	cements: chlorite	cements: kaolinite	matrix	porosity
87	15	2	-	2	19	1	113	-	-	41	1	3	-	4	-	-	-	12

Totals: #

quartz	biotite	muscovite	mica others + rock fragments	chert	others	Fe-dolomite	dolomite	iron oxide	calcite	illite/smectite	chlorite	kaolinite	matrix	porosity
102	2	-	23	113	-	41	1	3	-	4	-	-	-	12

Totals: %

quartz	biotite	muscovite	mica others + rock fragments	chert	others	Fe-dolomite	dolomite	iron oxide	calcite	illite/smectite	chlorite	kaolinite	matrix	porosity
34	0.67	-	7.34	37.66	-	13.67	0.33	1	-	1.33	-	-	-	4

Totals: % clasts

quartz	biotite	muscovite	mica others + rock fragments	chert	others
34	0.67	-	7.34	37.66	-

% normalized: (mQ + pQ) (C + Qe) RF

Q 43 C 48 RF 9

Total count: 300   Total clasts: 239   Total Q+C+RF: 237

Grain Size : upper very fine to lower fine sand, subangular to subrounded

Texture: well-sorted, clast-supported, long and concavo-convex contacts

Description***:

Abundant dolomite grains.

Other minerals include very rare albite.

Abundant argillaceous rock fragments and schist acting as pseudomatrix.

Abundant syntaxial quartz overgrowths.

Abundant iron oxide and organic matter as grain coatings.

Fe-dolomite cement generally replaced earlier dolomite cement, therefore it is more abundant than the non-ferroan dolomite.

Also occurs as replacement on chert, rock fragments, and albite.

Abundant illite/smectite, generally compacted between grains.

Rare authigenic chlorite as inclusions in albite.

Pores are predominantly due to partially dissolved dolomite grains, chert, and rock fragments.

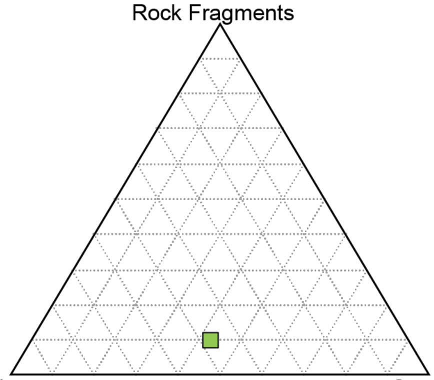

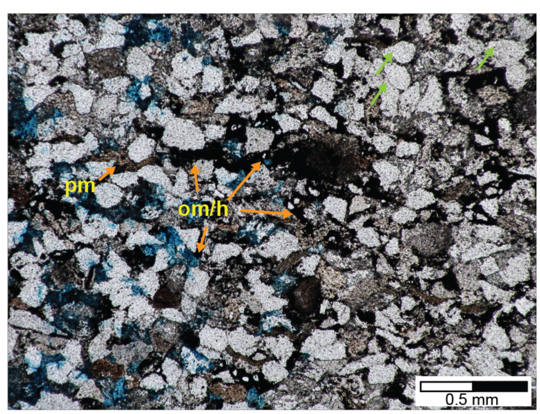

* = may include dolomite grains
** = iron-stained RF, volcanic RF, calcareous RF, and unidentified RF
*** = some very rarely occurring minerals may not be quantified on point counting results due to the automatic computer-generated crosshairs

Well ID & sample depth : 100/08-22-66-08W6/00, 2575.8 m — Stains: double carbonate
Petrofacies : petrofacies V — Parasequence: T
Depositional setting : estuarine — Lithofacies: facies 11
Facies assocation : FA3 (brackish embayment)

		mica		rock fragments						cements								
monocr. quartz	polycr. quartz	biotite	muscovite	others**	sedimentary*	metamorphic	chert	quartzite	others	Fe-dolomite	dolomite	iron oxide	calcite	illite/smectite	chlorite	kaolinite	matrix	porosity
63	14	-	-	33	61	1	69	1	1	12	11	12	22	-	-	-	-	-

Totals: #

77	-	-	95	70	1	12	11	12	22	-	-	-	-	-

Totals: %

25.67	-	-	31.67	23.33	-	-	-	-	-	-	-	-	-	-

Totals: % clasts

25.67	-	-	31.67	23.33	-

% normalized: (mQ + pQ) (C + Qe) RF

Q 32 C 29 RF 39

Total count: 300 — Total clasts: 242 — Total Q+C+RF: 241

Grain Size : upper fine sand, angular to rounded

Texture: poorly-sorted, matrix-supported, long and con-cavo-convex contacts

Description***:

Rounded grains are restricted to quartz.

Abundant dolomite and calcite grains.

Other minerals include muscovite, chlorite, feldspars.

Abundant euhedral quartz overgrowths, predating all cements.

Rare chert with drusy quartz overgrowths.

Common dedolomitization, thus at least a proportion of authigenic calcite postdated authigenic dolomite. However, at least a proportion of authigenic Fe-dolomite also postdated calcite (see white arrows).

All carbonate cements are patchy to poikilotopic.

Rare secondary pores occur as cement dissolution.

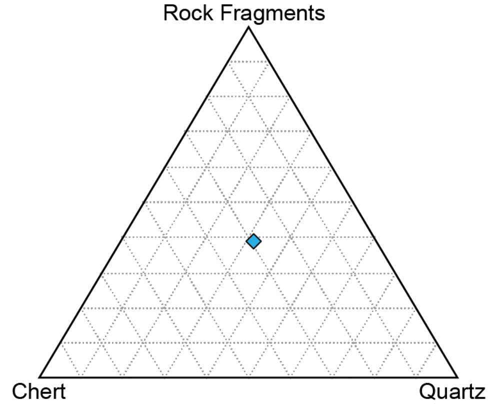

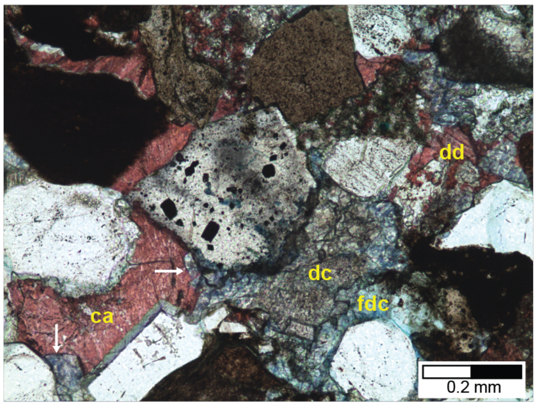

* = may include dolomite grains
** = iron-stained RF, volcanic RF, calcareous RF, and unidentified RF
*** = some very rarely occurring minerals may not be quantified on point counting results due to the automatic computer-generated crosshairs

Well ID & sample depth	: 100/08-22-066-08W6/00, 2578.7 m	Stains:	double carbonate
Petrofacies	: petrofacies V	Parasequence:	T
Depositional setting	: estuarine	Lithofacies:	facies 11
Facies assocation	: FA3 (brackish embayment)		

			mica		rock fragments					cements								
monocr. quartz	polycr. quartz	biotite	muscovite	others**	sedimentary*	metamorphic	chert	quartzite	others	Fe-dolomite	dolomite	iron oxide	calcite	illite/smectite	chlorite	kaolinite	matrix	porosity
76	5	-	-	16	47	1	47	1	14	41	29	4	19	-	-	-	-	-
Totals: #																		
81		-	-	64			48		14	41	29	4	19	-	-	-	-	-
Totals: %																		
27		-	-	21.33			16		-	-	-	-	-	-	-	-	-	-
Totals: % clasts																		
27		-	-	21.33			16		-									

% normalized: (mQ + pQ) (C + Qe) RF

Q 42 C 25 RF 33

Total count: 300 Total clasts: 207 Total Q+C+RF: 193

Grain Size : lower very fine to lower fine sand, angular to rounded

Texture: poorly-sorted, matrix-supported, point and tangential contacts

Description***:

Rounded grains are restricted to quartz.

Abundant dolomite and calcite grains.

Other minerals include muscovite, chlorite.

Abundant euhedral quartz overgrowths, predating all cements.

Common dedolomitization, thus at least a few calcite postdated dolomite.

Very rare Fe-calcite cements, generally mixed with the calcite cements without well-defined separation.

All carbonate cements are patchy to poikilotopic.

Rare secondary pores occur as cement dissolution.

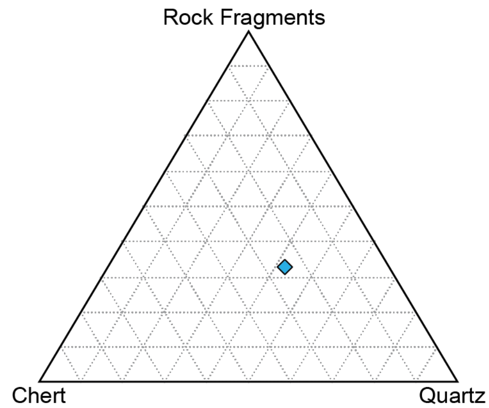

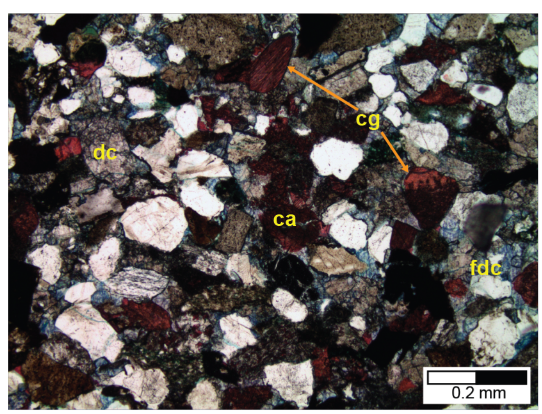

* = may include dolomite grains
** = iron-stained RF, volcanic RF, calcareous RF, and unidentified RF
*** = some very rarely occurring minerals may not be quantified on point counting results due to the automatic computer-generated crosshairs

Well ID & sample depth : 100/08-22-066-08W6/00, 2581.5 m Stains: double carbonate
Petrofacies : petrofacies III Parasequence: T
Depositional setting : estuarine Lithofacies: facies 11
Facies assocation : FA3 (brackish embayment)

monocr. quartz	polycr. quartz	biotite	muscovite (mica)	others** (mica)	sedimentary* (rock fragments)	metamorphic (rock fragments)	chert	quartzite	others	Fe-dolomite (cements)	dolomite (cements)	iron oxide (cements)	calcite (cements)	illite/smectite (cements)	chlorite (cements)	kaolinite (cements)	matrix	porosity
46	4	-	2	26	21	2	144	1	15	9	-	20	-	9	-	-	-	-

Totals: #

quartz	biotite	muscovite	others + rock fragments	chert + quartzite	others	Fe-dolomite	dolomite	iron oxide	calcite	illite/smectite	chlorite	kaolinite	matrix	porosity
50	-	2	50	145	15	9	-	20	-	9	-	-	-	-

Totals: %

quartz	biotite	muscovite	others + rock fragments	chert + quartzite	others	Fe-dolomite	dolomite	iron oxide	calcite	illite/smectite	chlorite	kaolinite	matrix	porosity
16.67	-	0.67	16.67	48.33	5	3	-	6.67	-	3	-	-	-	-

Totals: % clasts

quartz	biotite	muscovite	others + rock fragments	chert + quartzite	others
16.67	-	0.67	16.67	48.33	5

% normalized: (mQ + pQ) (C + Qe) RF

Q	C	RF
20	60	20

Total count: 300 Total clasts: 262 Total Q+C+RF: 245

Grain Size : lower fine sand, angular to subrounded

Texture: well-sorted, clast-supported, long and concavo-convex contacts

Description***:

Abundant dolomite and calcite grains.

Other minerals include chlorite, biotite, glauconite, feldspars.

Abundant pseudomatrix.

Abundant syntaxial quartz overgrowths.

Authigenic calcite occurs as replacement on chert, rock fragment, feldspars, and quartz, not as intergranular cement.

Rare secondary pores from dissolution of dolomite grains.

Possible bioturbation (see image) where iron oxide-free chert with Fe-dolomite inclusion is surrounded by possibly intermixing of organic matter and iron oxide cement.

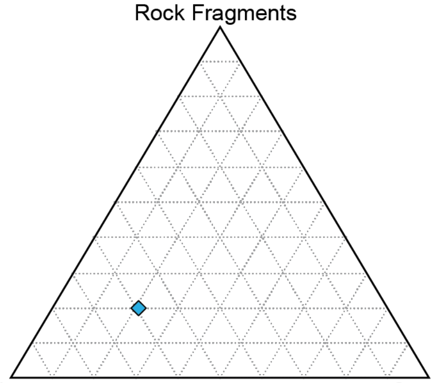

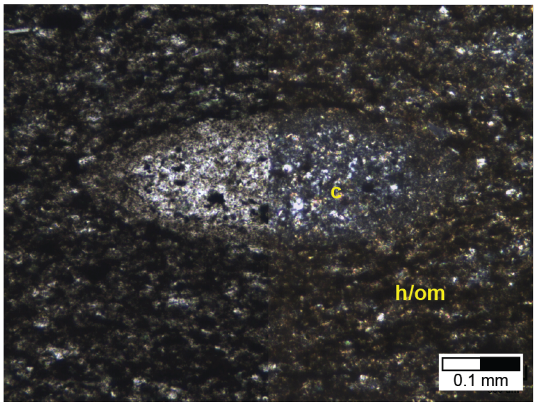

* = may include dolomite grains
** = iron-stained RF, volcanic RF, calcareous RF, and unidentified RF
*** = some very rarely occurring minerals may not be quantified on point counting results due to the automatic computer-generated crosshairs

Well ID & sample depth	: 100/08-22-066-08W5/00, 2585.4 m	Stains:	double carbonate
Petrofacies	: petrofacies V	Parasequence:	T
Depositional setting	: estuarine	Lithofacies:	facies 11
Facies assocation	: FA3 (brackish embayment)		

			mica		rock fragments					cements								
monocr. quartz	polycr. quartz	biotite	muscovite	others**	sedimentary*	metamorphic	chert	quartzite	others	Fe-dolomite	dolomite	iron oxide	calcite	illite/smectite	chlorite	kaolinite	matrix	porosity
86	7	-	-	10	27	-	29	-	3	12	61	16	37	1	11	-	-	-

Totals: #

93	-	-	37	29	3	12	61	16	37	1	11	-	-	-

Totals: %

31	-	-	12.33	9.67	1	4	20.33	5.33	12.33	0.33	3.67	-	-	-

Totals: % clasts

31	-	-	12.33	9.67	-

% normalized: (mQ + pQ) (C + Qe) RF

Q	C	RF
58	18	23

Total count: 300 Total clasts: 162 Total Q+C+RF: 159

Grain Size : lower to upper very fine sand, subangular to subrounded

Texture: moderately-sorted, matrix-supported, long to concavo-convex contacts

Description***:

Abundant dolomite and calcite grains.

Other minerals include micas, glauconite, feldspars.

Abundant pseudomatrix.

Abundant syntaxial quartz overgrowths.

Authigenic calcite occurs as replacement on chert, rock fragment, feldspars, and quartz, not as intergranular cement.

Common rhombohedral dolomite as inclusions.

Rare secondary pores from dissolution of dolomite grains.

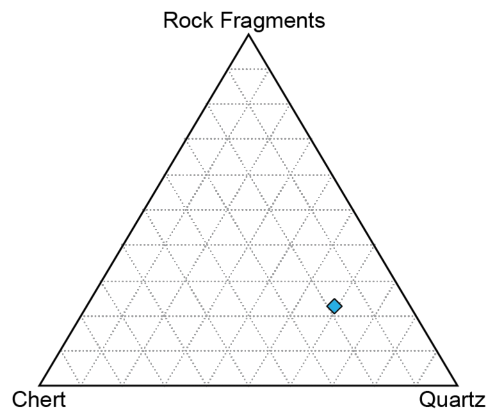

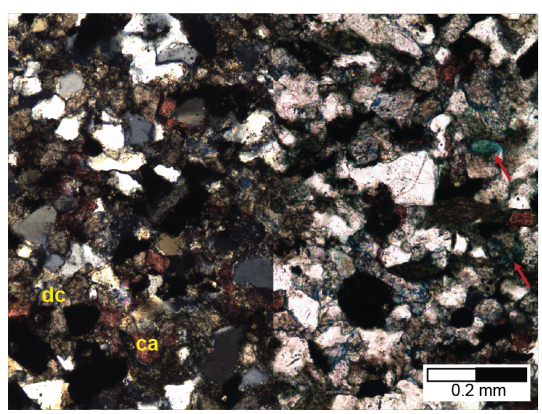

* = may include dolomite grains
** = iron-stained RF, volcanic RF, calcareous RF, and unidentified RF
*** = some very rarely occurring minerals may not be quantified on point counting results due to the automatic computer-generated crosshairs

Well ID & sample depth : 100/08-02-066-09W6/00, 2568.5 m Stains: double carbonate
Petrofacies : petrofacies IV Parasequence: T
Depositional setting : estuarine Lithofacies: facies 11
Facies assocation : FA3 (brackish embayment)

	monocr. quartz	polycr. quartz	biotite	mica: muscovite	rock fragments*: sedimentary*	rock fragments*: metamorphic	rock fragments*: others**	chert	quartzite	others	cements: Fe-dolomite	cements: dolomite	cements: iron oxide	cements: calcite	cements: illite/smectite	cements: chlorite	cements: kaolinite	matrix	porosity
Count	67	2	-	5	15	-	15	76	-	1	66	19	21	-	12	-	-	-	-
Totals: #	69		-	5	30			76		1	66	19	21	-	12	-	-	-	-
Totals: %	23		-	5	10			25.33		1	66	19	21	-	12	-	-	-	-
Totals: % clasts	23		-	1.67	10			25.33		0.33									

% normalized: (mQ + pQ) (C + Qe) RF

Q 39 C 44 RF 17

Total count: 300 Total clasts: 182 Total Q+C+RF: 176

Grain Size : lower very fine sand, angular to subrounded

Texture: moderately-sorted, clast-supported, long and concavo-convex contacts

Description***:

Abundant dolomite grains.

Rock fragments predominantly occur as pseudomatrix. Common illitized chert occurs as pseudomatrix as well (calculated as RF).

Other minerals include albite, glauconite.

Common quartz overgrowths.

Fe-dolomite occurs as pore-filling, poikilotopic cements.

Dolomite rims commonly occur as overgrowths on quartz grains.

Possibly preserved bioturbation as thin drapes of reddish brown to opaque-coloured materials, possibly composed of intermixed iron oxide and organic matter.

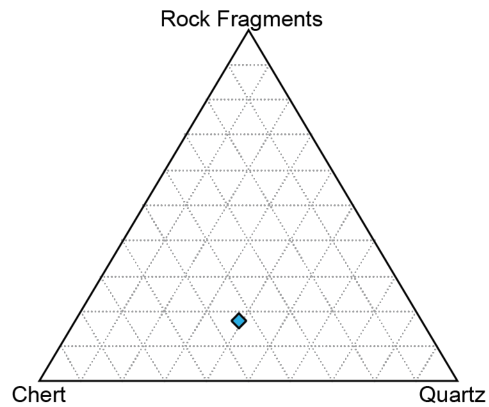

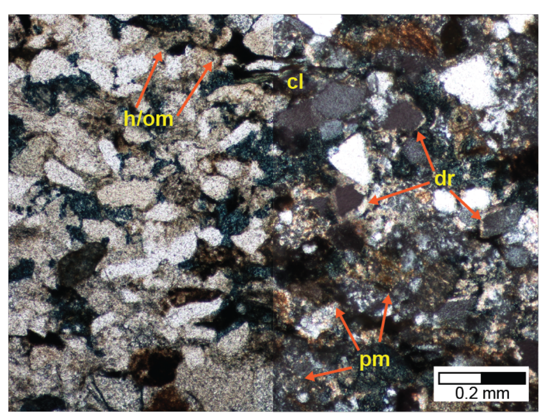

* = may include dolomite grains
** = iron-stained RF, volcanic RF, calcareous RF, and unidentified RF
*** = some very rarely occurring minerals may not be quantified on point counting results due to the automatic computer-generated crosshairs

Well ID & sample depth : 100/08-02-066-09W6/00, 2571 m Stains: double carbonate
Petrofacies : petrofacies II Parasequence: FP3
Depositional setting : foreshore Lithofacies: facies 5
Facies assocation : FA2 (wave-dominated shoreface)

			mica		rock fragments					cements								
monocr. quartz	polycr. quartz	biotite	muscovite	others**	sedimentary*	metamorphic	chert	quartzite	others	Fe-dolomite	dolomite	iron oxide	calcite	illite/smectite	chlorite	kaolinite	matrix	porosity
104	24	2	-	20	2	-	109	9	1	-	-	-	-	-	-	12	-	17

Totals: #

128	2	-	22	118	1	-	-	-	-	-	-	12	-	17

Totals: %

42.67	0.67	-	7.34	39.33	0.33	-	-	-	-	-	-	4	-	5.67

Totals: % clasts

42.67	0.67	-	7.34	39.33	0.33

% normalized: (mQ + pQ) (C + Qe) RF

Q 48 C 44 RF 8

Total count: 300 Total clasts: 271 Total Q+C+RF: 268

Grain Size : upper fine sand, subrounded to rounded

Texture: well-sorted, clast-supported, long and conca-vo-convex contacts

Description***:

Other minerals include extremely rare heavy minerals.

Abundant interlocking syntaxial quartz overgrowths, some are partially dissolved.

Abundant booklets of kaolinite within secondary pores.

Possible rare chalcedony(?) cements within outsized pores.

Rare Fe-dolomite inclusions within rock fragments and chert.

Very rare primary porosity. Most pores are secondary, due to extensive dissolution of quartz, chert, and rock fragments as well as well-defined microfractures. Generally, pores are occluded by kaolinite cements. Very rare cement-free pores.

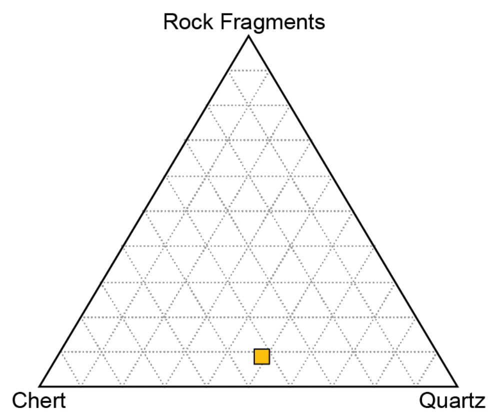

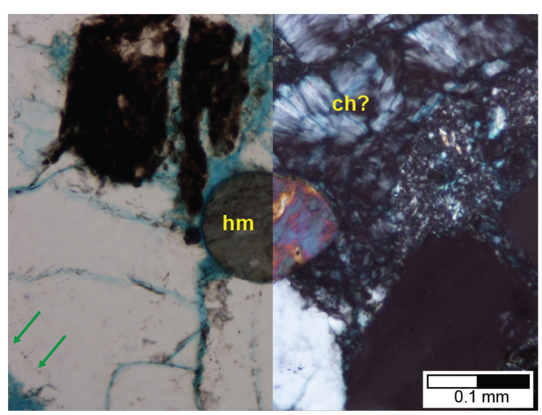

* = may include dolomite grains
** = iron-stained RF, volcanic RF, calcareous RF, and unidentified RF
*** = some very rarely occurring minerals may not be quantified on point counting results due to the automatic computer-generated crosshairs

Well ID & sample depth : 100/08-02-066-09W6/00, 2575.8 m
Stains: double carbonate
Petrofacies : petrofacies V
Parasequence: F_P3
Depositional setting : lower shoreface
Lithofacies: facies 3
Facies assocation : FA1 (storm-dominated shoreface)

			mica		rock fragments						cements								
	monocr. quartz	polycr. quartz	biotite	muscovite	others**	sedimentary*	metamorphic	chert	quartzite	others	Fe-dolomite	dolomite	iron oxide	calcite	illite/smectite	chlorite	kaolinite	matrix	porosity
	102	15	10	-	10	23	3	109	2	-	6	5	-	3	-	-	-	-	12
Totals: #	117		10	-	36			111		-	6	5	-	3	-	-	-	-	12
Totals: %	39		3.33	-	12			37		-	2	1.67	-	1	-	-	-	-	4
Totals: % clasts	39		3.33	-	12			37		-									

% normalized: (mQ + pQ) (C + Qe) RF

Q 44 C 42 RF 14

Total count: 300 Total clasts: 274 Total Q+C+RF: 264

Grain Size : upper very fine to lower fine sand, angular to subrounded

Texture: well-sorted, clast-supported, long to concavo-convex contacts

Description***:

Very rare dolomite grains.

Other minerals include extremely rare heavy minerals.

Abundant interlocking quartz overgrowths.

Rare other intergranular cements. Primary intergranular components are quartz overgrowths and pseudomatrix.

Rare dedolomitization on dolomite grains.

Porosity is restricted to secondary type, mainly from well-defined microfractures along competent grain contacts (quartz-quartz, quartz-chert, or chert-chert) and across grains. Dissolution is less common.

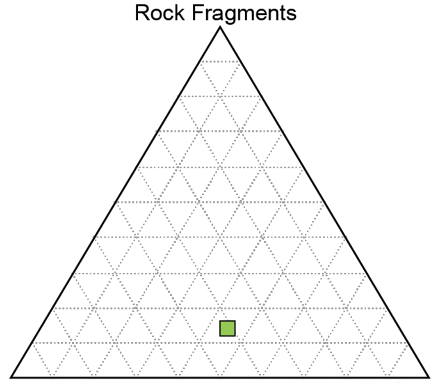

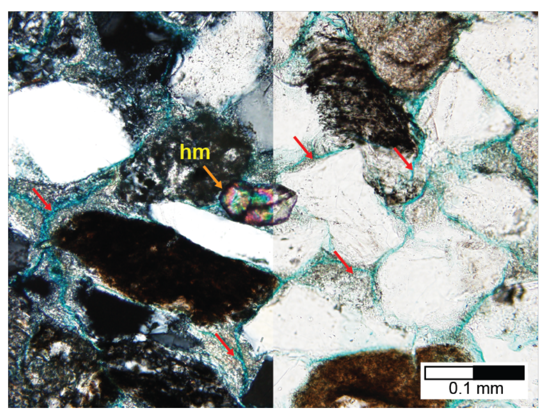

* = may include dolomite grains
** = iron-stained RF, volcanic RF, calcareous RF, and unidentified RF
*** = some very rarely occurring minerals may not be quantified on point counting results due to the automatic computer-generated crosshairs

Well ID & sample depth : 100/08-02-066-09W6/00, 2579.6 m Stains: double carbonate
Petrofacies : petrofacies II Parasequence: FP2
Depositional setting : upper shoreface Lithofacies: facies 4
Facies assocation : FA2 (wave-dominated shoreface)

monocr. quartz	polycr. quartz	biotite (mica)	muscovite (mica)	others**	sedimentary* (rock fragments)	metamorphic (rock fragments)	chert	quartzite	others	Fe-dolomite (cements)	dolomite (cements)	iron oxide (cements)	calcite (cements)	illite/smectite (cements)	chlorite (cements)	kaolinite (cements)	matrix	porosity
103	23	2	1	21	36	1	79	-	1	8	-	1	-	-	-	-	-	16

Totals: #

126	2	1	58	79	1	8	-	1	-	-	-	-	-	16

Totals: %

42	0.67	0.33	19.33	26.34	0.33	2.67	-	0.33	-	-	-	-	-	5.33

Totals: % clasts

42	0.67	0.33	19.33	26.34	0.33

% normalized: (mQ + pQ) (C + Qe) RF

Q 48 C 30 RF 22

Total count: 300 Total clasts: 275 Total Q+C+RF: 271

Grain Size : upper very fine to upper fine sand, angular to subrounded

Texture: moderately-sorted, clast-supported, long to concavo-convex contacts

Description*** :

Abundant dolomite grains.

Abundant syntaxial to euhedral quartz overgrowths, predating all cements.

Rare pseudomatrix, possibly has been largely dissolved.

Pores are generally filled by kaolinite, but may be cement-free as well. Kaolinite likely predated dolomite and Fe-dolomite.

Common Fe-dolomite cements as rims on dolomite grains and patchy dolomite cements, likely formed during and after dissolution, postdating siginificant burial compaction.

Common authigenic chlorite as inclusions.

Localized iron oxide coatings and drapes up to 50 μm thick.

Abundant secondary intergranular pores from complete dissolution of various grains and pseudomatrix (e.g. chert, rock fragments, possibly quartz overgrowths). May appear similar to primary intergranular pores, but can be distinguished by recognizing the remaining specks of grains within the pores.

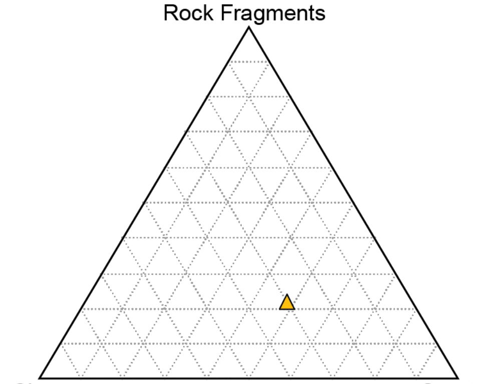

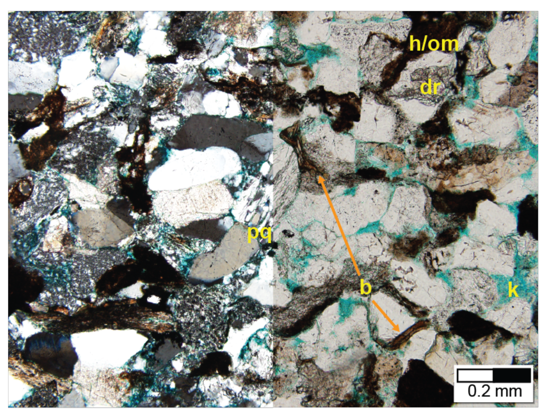

* = may include dolomite grains
** = iron-stained RF, volcanic RF, calcareous RF, and unidentified RF
*** = some very rarely occurring minerals may not be quantified on point counting results due to the automatic computer-generated crosshairs

Well ID & sample depth : 100/08-02-066-09W6/00, 2579.8 m — Stains: double carbonate

Petrofacies : petrofacies IV — Parasequence: FP2

Depositional setting : upper shoreface — Lithofacies: facies 4

Facies assocation : FA2 (wave-dominated shoreface)

monocr. quartz	polycr. quartz	biotite	muscovite	sedimentary*	metamorphic	others**	chert	quartzite	others	Fe-dolomite	dolomite	iron oxide	calcite	illite/smectite	chlorite	kaolinite	matrix	porosity
98	-	1	-	30	-	22	102	-	1	17	2	10	-	2	-	-	-	15

(mica: biotite, muscovite; rock fragments: sedimentary*, metamorphic, others**; cements: Fe-dolomite through kaolinite)

Totals: #

quartz	mica		rock fragments	chert	others	Fe-dolomite	dolomite	iron oxide	calcite	illite/smectite	chlorite	kaolinite	matrix	porosity
98	1	-	52	102	1	17	2	10	-	2	-	-	-	15

Totals: %

quartz	mica		rock fragments	chert	others	Fe-dolomite	dolomite	iron oxide	calcite	illite/smectite	chlorite	kaolinite	matrix	porosity
32.66	0.33	-	17.67	34	-	5.67	0.67	3.33	-	0.67	-	-	-	5

Totals: % clasts

quartz	mica		rock fragments	chert	others
32.66	0.33	-	17.67	34	-

% normalized: (mQ + pQ) (C + Qe) RF

Q 39 C 40 RF 21

Total count: 300 Total clasts: 254 Total Q+C+RF: 252

Grain Size : lower very fine to lower fine sand, subangular to rounded

Texture: well-sorted, clast-supported, predominantly long and concavo-convex contacts, rarely sutured contacts

Description***:

Rounded grains are restricted to quartz.

Abundant dolomite grains.

Common rock fragments and chert with abundant illite inclusions as pseudomatrix.

Other minerals include chlorite, muscovite, albite, heavy minerals (possibly zircon), glauconite. Micas are generally splayed.

Common quartz overgrowths.

Common illite as grain-coating cements or compacted minerals between pseudomatrix. May appear similar to thin, elongated dolomite replacement due to the birefringence.

Fe-dolomite cements predominantly occur as rims on dolomite grains and/or cements. Rarely as pore-filling, poikilotopic, or patchy cements.

All porosities are secondary. Predominantly occurs as partially dissolved chert and rock fragments as well as microfractures along grain contacts. Also rarely as dissolved dolomite cements.

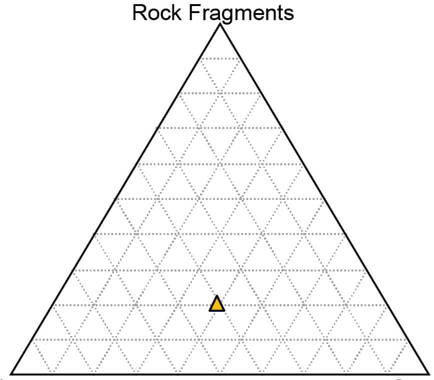

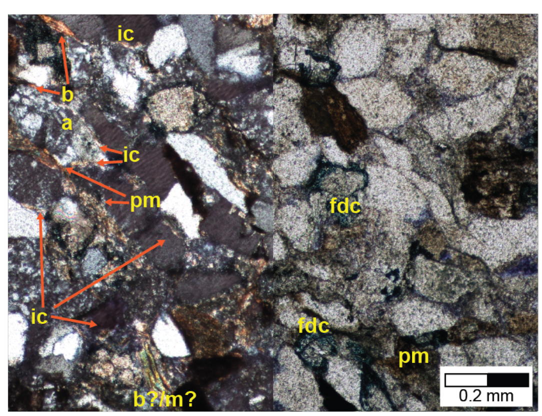

* = may include dolomite grains
** = iron-stained RF, volcanic RF, calcareous RF, and unidentified RF
*** = some very rarely occurring minerals may not be quantified on point counting results due to the automatic computer-generated crosshairs

Well ID & sample depth : 100/07-13-066-09W6/00, 2517.5 m Stains: double carbonate
Petrofacies : petrofacies V Parasequence: FP2
Depositional setting : upper shoreface Lithofacies: facies 5
Facies assocation : FA2 (wave-dominated shoreface)

	monocr. quartz	polycr. quartz	biotite (mica)	muscovite (mica)	others**	sedimentary* (rock fragments)	metamorphic (rock fragments)	chert	quartzite	others	Fe-dolomite (cements)	dolomite (cements)	iron oxide (cements)	calcite (cements)	illite/smectite (cements)	chlorite (cements)	kaolinite (cements)	matrix	porosity
Count	104	24	10	2	26	11	-	87	-	3	5	-	2	17	2	-	-	-	7
Totals: #	128		10	2	37			87		3	5	-	2	17	2	-	-	-	7
Totals: %	42.67		3.33	0.67	7			29		1	1.67	-	0.67	5.67	0.67	-	-	-	2.33
Totals: % clasts	42.67		3.33	0.67	7			29		1									

% normalized: (mQ + pQ) (C + Qe) RF

Q 50 C 34 RF 16

Total count: 300 Total clasts: 267 Total Q+C+RF: 252

Grain Size : lower fine sand, angular to rounded

Texture: well-sorted, clast-supported, predominantly point to tangential contacts, rarely long and concavo-convex

Description***:

Rounded grains are restricted to quartz.

Abundant dolomite grains, and partially to almost completely calcitized (dedolomitized) dolomite grains.

Rare iron-stained rock fragments with drusy quartz veins.

Other minerals include chlorite, feldspars.

Abundant syntaxial quartz overgrowths, predated other intergranular cements.

Common pseudomatrix.

Common Fe-dolomite as replacements on dolomite grains.

Rare Fe-calcite, commonly intermixed with calcite cements or replacements.

Abundant secondary pores from microfractures, channels, and partial to complete dissolution of chert, rock fragments, quartz, and various cements or replacement minerals. Most pores likely postdated other authigenic cements.

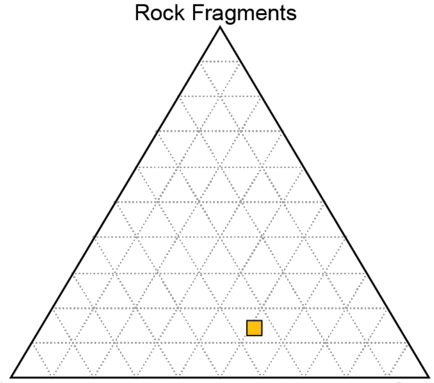

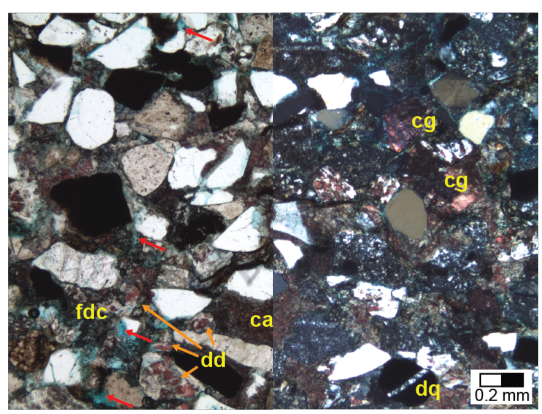

* = may include dolomite grains
** = iron-stained RF, volcanic RF, calcareous RF, and unidentified RF
*** = some very rarely occurring minerals may not be quantified on point counting results due to the automatic computer-generated crosshairs

Well ID & sample depth	: 100/07-13-066-09W6/00, 2521.6 m	Stains: double carbonate
Petrofacies	: petrofacies V	Parasequence: FP2
Depositional setting	: middle shoreface	Lithofacies: facies 3
Facies assocation	: FA1 (storm-dominated shoreface)	

			mica		rock fragments					cements								
monocr. quartz	polycr. quartz	biotite	muscovite	others**	sedimentary*	metamorphic	chert	quartzite	others	Fe-dolomite	dolomite	iron oxide	calcite	illite/smectite	chlorite	kaolinite	matrix	porosity
63	36	11	-	18	24	-	107	1	11	6	3	1	6	2	-	-	-	7
Totals: #																		
99		11	-	42			108		11	6	3	1	6	2	-	-	-	7
Totals: %																		
33		3.67	-	16.33			36		3.67	2	1	0.33	2	0.67	-	-	-	2.33
Totals: % clasts																		
33		3.67	-	16.33			36		3.67									

% normalized: (mQ + pQ) (C + Qe) RF

Q	C	RF
39	42	19

Total count: 300 Total clasts: 275 Total Q+C+RF: 253

Grain Size : upper very fine sand, angular to subrounded

Texture: moderately-sorted, clast-supported, long and concavo-convex contacts

Description***:

Abundant dolomite grains.

Micaceous due to abundant biotite.

Common calcite grains. However, some are likely authigenic/d-edolomitized.

Abundant pseudomatrix.

Other grains include very rare feldspars.

Abundant euhedral to syntaxial quartz overgrowths, predating all cements.

Common calcite as replacement minerals, less common as inter-granular cements.

Common secondary pores as microfractures and dissolution of chert, rock fragments, biotite, and feldspars.

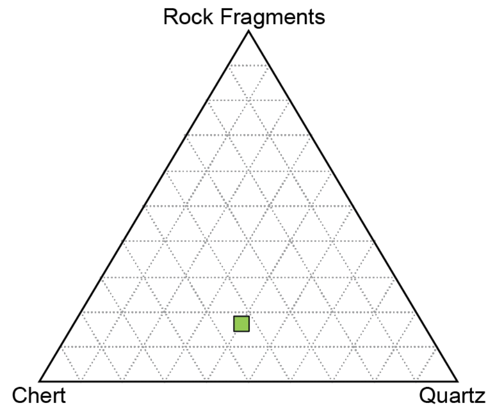

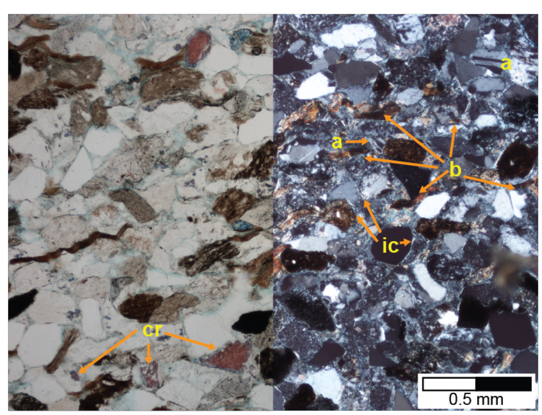

* = may include dolomite grains
** = iron-stained RF, volcanic RF, calcareous RF, and unidentified RF
*** = some very rarely occurring minerals may not be quantified on point counting results due to the automatic computer-generated crosshairs

Well ID & sample depth : 100/07-13-066-09W6/00, 2524.1 m Stains: double carbonate
Petrofacies : petrofacies V Parasequence: FP3
Depositional setting : middle shoreface Lithofacies: facies 3
Facies assocation : FA1 (storm-dominated shoreface)

monocr. quartz	polycr. quartz	biotite	muscovite (mica)	others** (mica)	sedimentary* (rock fragments)	metamorphic (rock fragments)	chert	quartzite	others	Fe-dolomite (cements)	dolomite (cements)	iron oxide (cements)	calcite (cements)	illite/smectite (cements)	chlorite (cements)	kaolinite (cements)	matrix	porosity
76	34	6	-	8	23	1	110	-	1	13	9	1	3	12	2	-	-	1

Totals: #

110	6	-	32	110	1	13	9	1	3	12	2	-	-	1

Totals: %

36.67	2	-	11	36.67	0.33	4.33	3	0.33	1	4	0.67	-	-	0.33

Totals: % clasts

36.67	2	-	11	36.67	0.33

% normalized: (mQ + pQ) (C + Qe) RF

Q 43 C 43 RF 14

Total count: 300 Total clasts: 259 Total Q+C+RF: 252

Grain Size : lower fine sand, angular to subangular

Texture: moderately-sorted, clast-supported, long to concavo-convex contacts

Description***:

Micaceous.

Other minerals include very rare feldspars.

Abundant dolomite grains, common calcite grains.

Common euhedral quartz overgrowths, rarely syntaxial.

Abundant pseudomatrix.

Abundant chlorite inclusions (<20 µm) within quartz and feldspars.

Calcite is more common as replacement minerals on dolomite, feldspar, and rarely quartz.

Common patchy dolomite and Fe-dolomite cement, likely postdated significant mechanical compactions.

Abundant grain-coating thin strands of illite, likely predated significant mechanical compactions.

Common dedolomitization.

Secondary pores are sourced from partial dissolution of grains and clasts as well as thin microfractures along grain contacts of competent grains (quartz and chert).

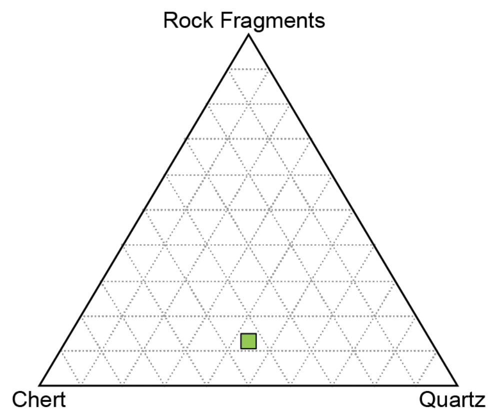

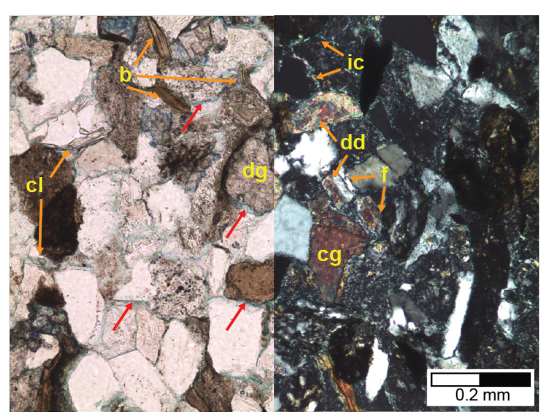

* = may include dolomite grains
** = iron-stained RF, volcanic RF, calcareous RF, and unidentified RF
*** = some very rarely occurring minerals may not be quantified on point counting results due to the automatic computer-generated crosshairs

Well ID & sample depth	: 100/07-13-066-09W6/00, 2531.3 m	Stains:	double carbonate
Petrofacies	: petrofacies II	Parasequence:	FP2
Depositional setting	: upper shoreface	Lithofacies:	facies 5
Facies assocation	: FA2 (wave-dominated shoreface)		

				mica		rock fragments				cements								
monocr. quartz	polycr. quartz	biotite	muscovite	others**	sedimentary*	metamorphic	chert	quartzite	others	Fe-dolomite	dolomite	iron oxide	calcite	illite/smectite	chlorite	kaolinite	matrix	porosity
89	17	1	-	13	52	-	76	-	-	17	13	-	-	-	-	7	-	11

Totals: #

106	1	-	65	76	-	17	13	-	-	-	-	7	-	11

Totals: %

35.34	0.33	-	21.67	25.33	-	5.67	4.33	-	-	-	-	2.33	-	3.67

Totals: % clasts

35.34	0.33	-	21.67	25.33	-

% normalized: (mQ + pQ) (C + Qe) RF

Q 43 C 31 RF 26

Total count: 300 Total clasts: 252 Total Q+C+RF: 251

Grain Size : upper very fine to upper fine sand, pebbly, angular to rounded

Texture: poorly-sorted, matrix-supported, point to tangential contacts with frequent long contacts

Description***:

Rounded grains are restricted to upper fine sand-sized quartz. Generally, the coarser the grains, the more rounded the quartz is.

Pebbles are primarily chert with very rare rock fragments.

Abundant dolomite grains.

Abundant euhedral quartz overgrowths, predating other cements.

Abundant patchy to poikilotopic dolomite and Fe-dolomite cements. Also common as inclusions in chert and rock fragments.

Dolomite cements likely postdated kaolinite cements.

Rare pseudomatrix.

Common authigenic chlorite as inclusion in quartz.

Abundant secondary pores from complete dissolution of cements and clasts/grains (chert, rock fragments, dolomite). Common channel-type pores. Pores may be filled with kaolinite or cement-free.

Not typically similar to other upper shoreface samples based on its sorting and framework.

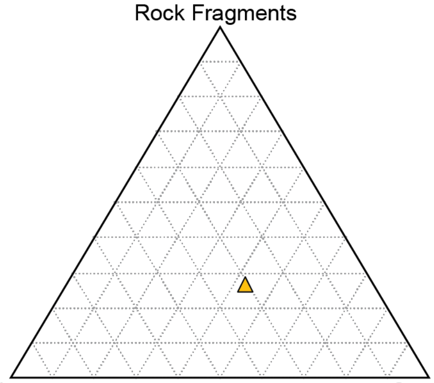

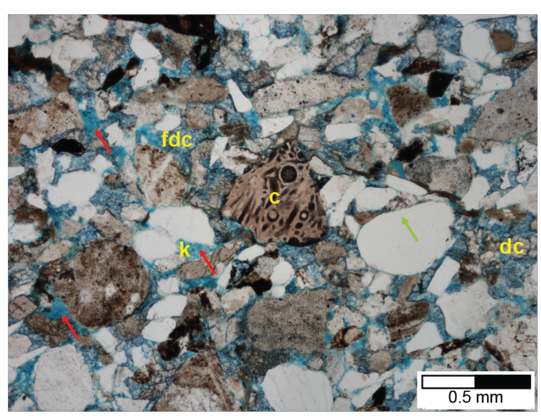

* = may include dolomite grains
** = iron-stained RF, volcanic RF, calcareous RF, and unidentified RF
*** = some very rarely occurring minerals may not be quantified on point counting results due to the automatic computer-generated crosshairs

APPENDIX IV: CORE ANALYSES

(compiled from GeoScout public database, accessed on June 29, 2018)

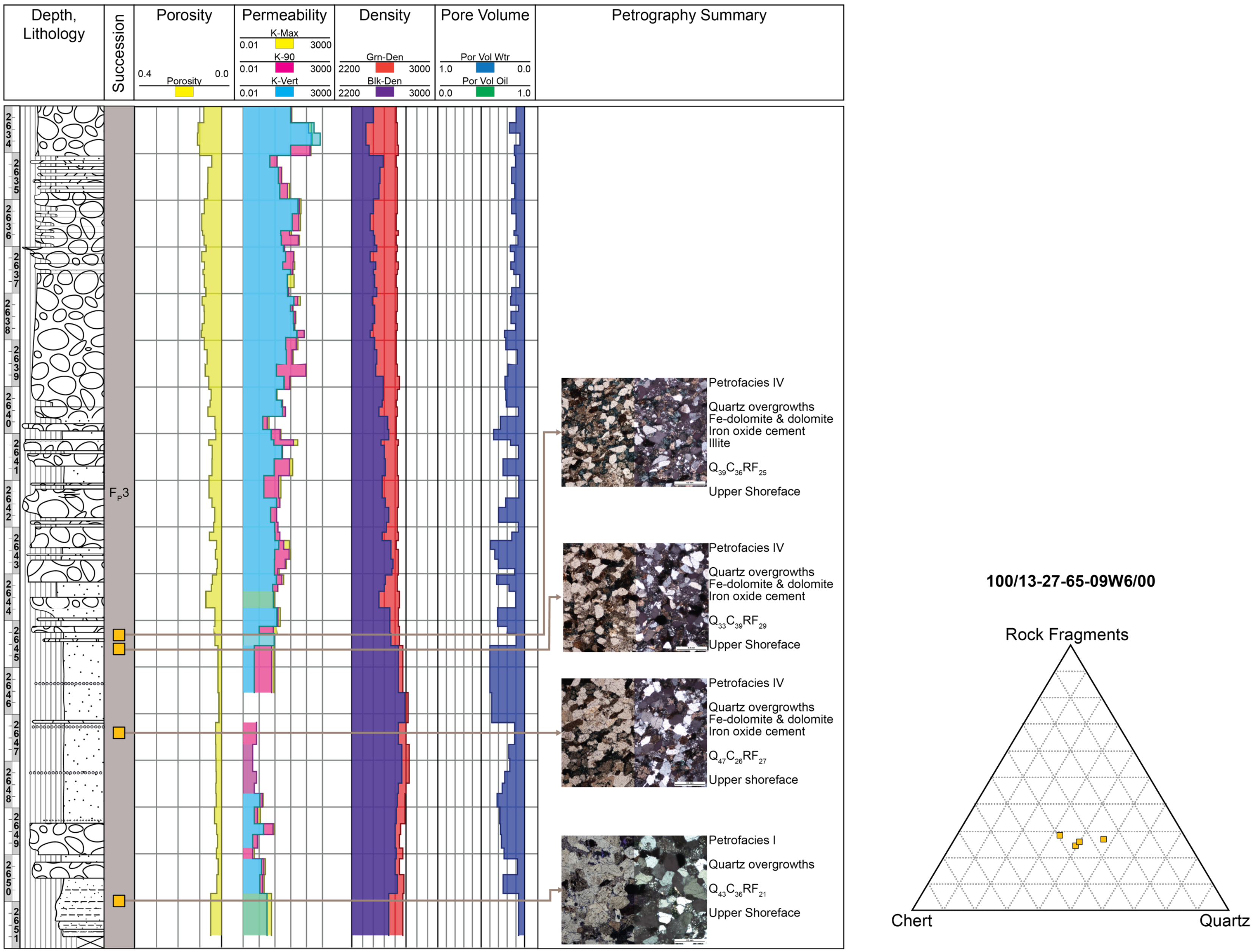
Depth, Lithology
Succession
Porosity
0.4 Porosity 0.0
Permeability
K-Max 0.01 3000
K-90 0.01 3000
K-Vert 0.01 3000
Density
Grn-Den 2200 3000
Blk-Den 2200 3000
Pore Volume
Por Vol Wtr 1.0 0.0
Por Vol Oil 0.0 1.0
Petrography Summary
2634
2635
2636
2637
2638
2639
2640
2641
2642
2643
2644
2645
2646
2647
2648
2649
2650
2651
F_P3
Petrofacies IV
Quartz overgrowths
Fe-dolomite & dolomite
Iron oxide cement
Illite
$Q_{39}C_{36}RF_{25}$
Upper Shoreface
Petrofacies IV
Quartz overgrowths
Fe-dolomite & dolomite
Iron oxide cement
$Q_{33}C_{39}RF_{29}$
Upper Shoreface
Petrofacies IV
Quartz overgrowths
Fe-dolomite & dolomite
Iron oxide cement
$Q_{47}C_{26}RF_{27}$
Upper shoreface
Petrofacies I
Quartz overgrowths
$Q_{43}C_{36}RF_{21}$
Upper Shoreface
100/13-27-65-09W6/00
Rock Fragments
Chert
Quartz

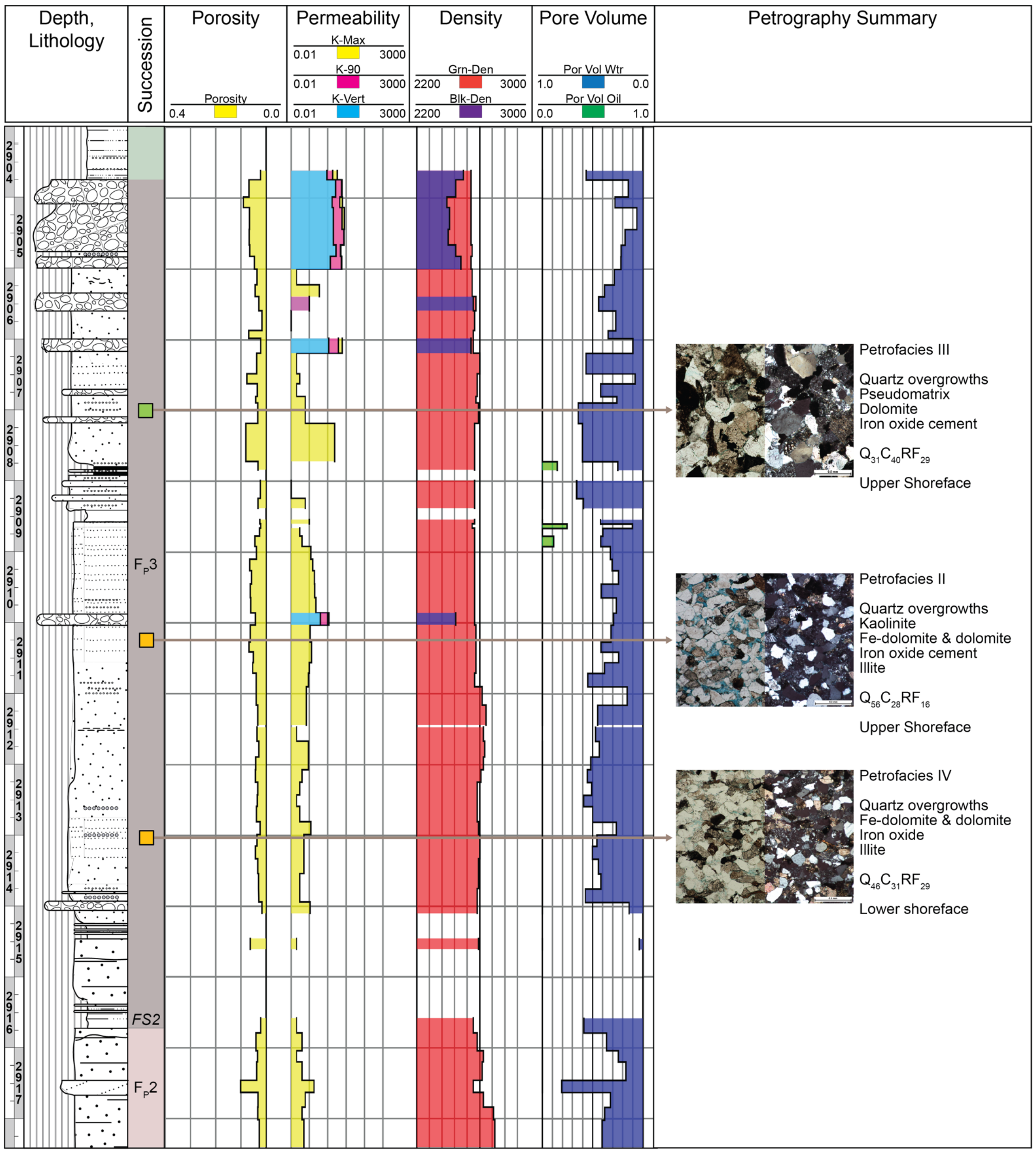
Depth, Lithology
Succession
Porosity
Porosity
0.4 0.0
Permeability
K-Max
0.01 3000
K-90
0.01 3000
K-Vert
0.01 3000
Density
Grn-Den
2200 3000
Blk-Den
2200 3000
Pore Volume
Por Vol Wtr
1.0 0.0
Por Vol Oil
0.0 1.0
Petrography Summary
2904
2905
2906
2907
2908
2909
2910
2911
2912
2913
2914
2915
2916
2917
FP3
FS2
FP2
Petrofacies III
Quartz overgrowths
Pseudomatrix
Dolomite
Iron oxide cement
Q31C40RF29
Upper Shoreface
Petrofacies II
Quartz overgrowths
Kaolinite
Fe-dolomite & dolomite
Iron oxide cement
Illite
Q56C28RF16
Upper Shoreface
Petrofacies IV
Quartz overgrowths
Fe-dolomite & dolomite
Iron oxide
Illite
Q46C31RF29
Lower shoreface

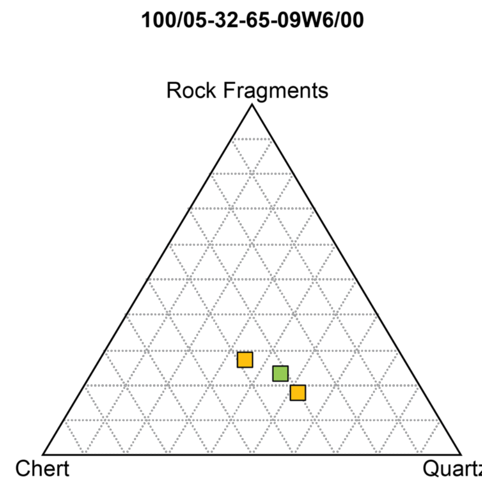
100/05-32-65-09W6/00
Rock Fragments
Chert
Quartz

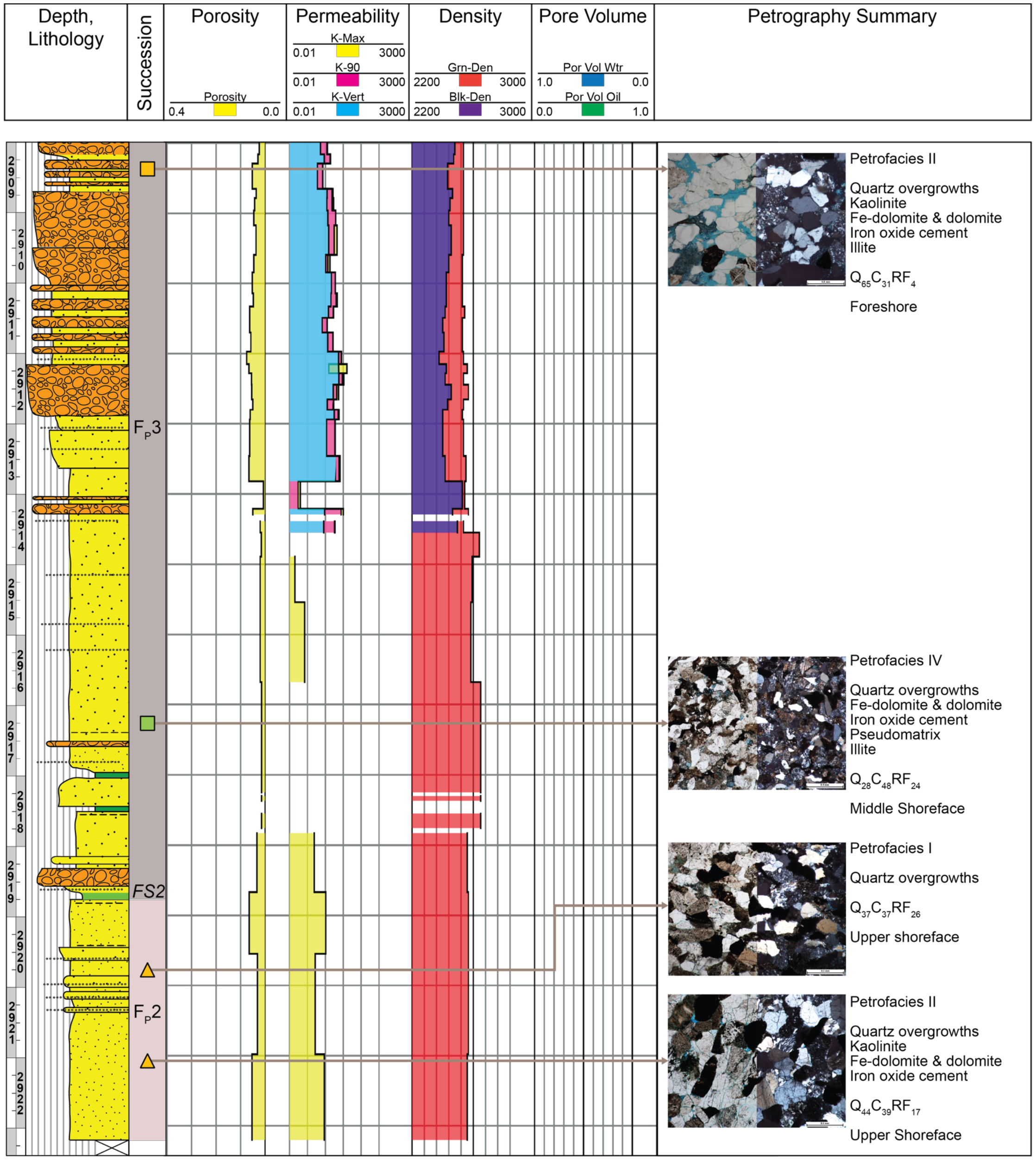
Depth, Lithology
Succession
Porosity
Permeability
Density
Pore Volume
Petrography Summary
K-Max
0.01 3000
K-90
0.01 3000
K-Vert
0.01 3000
Porosity
0.4 0.0
Grn-Den
2200 3000
Blk-Den
2200 3000
Por Vol Wtr
1.0 0.0
Por Vol Oil
0.0 1.0
2909
2910
2911
2912
2913
2914
2915
2916
2917
2918
2919
2920
2921
2922
F_P3
FS2
F_P2
Petrofacies II
Quartz overgrowths
Kaolinite
Fe-dolomite & dolomite
Iron oxide cement
Illite
$Q_{65}C_{31}RF_4$
Foreshore
Petrofacies IV
Quartz overgrowths
Fe-dolomite & dolomite
Iron oxide cement
Pseudomatrix
Illite
$Q_{28}C_{48}RF_{24}$
Middle Shoreface
Petrofacies I
Quartz overgrowths
$Q_{37}C_{37}RF_{26}$
Upper shoreface
Petrofacies II
Quartz overgrowths
Kaolinite
Fe-dolomite & dolomite
Iron oxide cement
$Q_{44}C_{39}RF_{17}$
Upper Shoreface

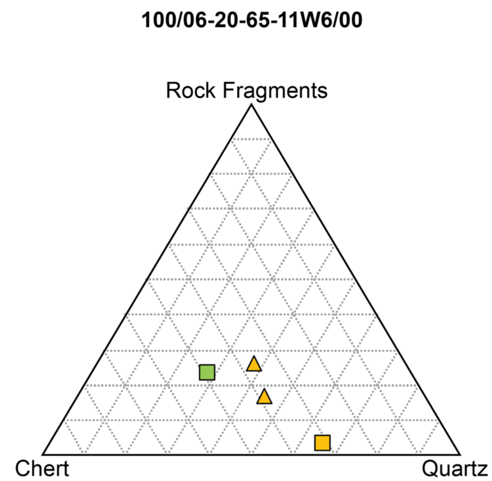
100/06-20-65-11W6/00
Rock Fragments
Chert
Quartz

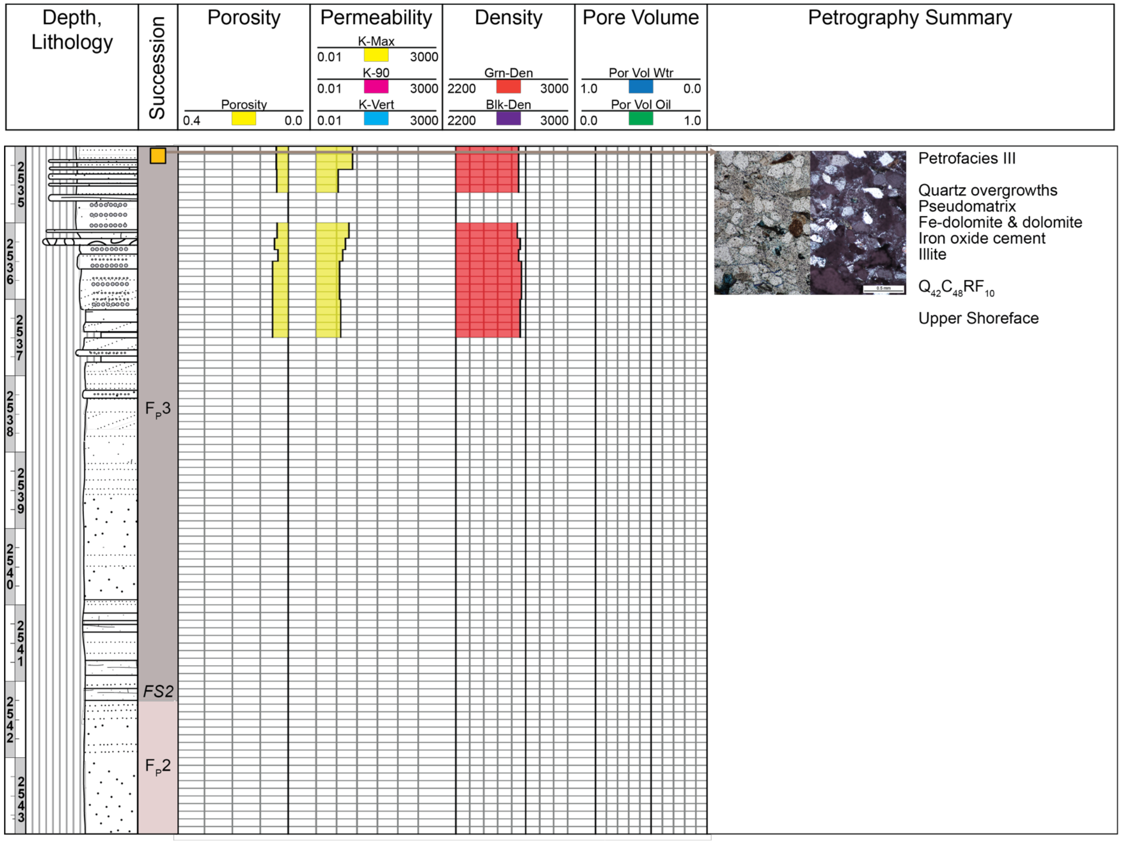

100/05-07-66-08W6/00

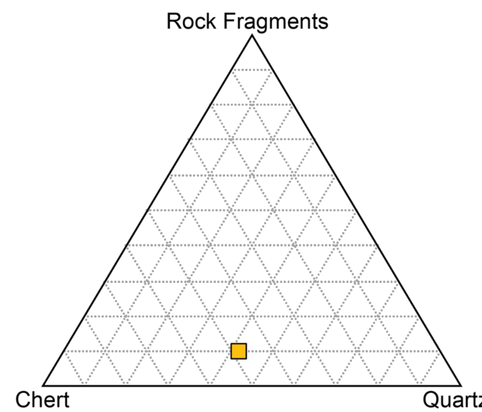

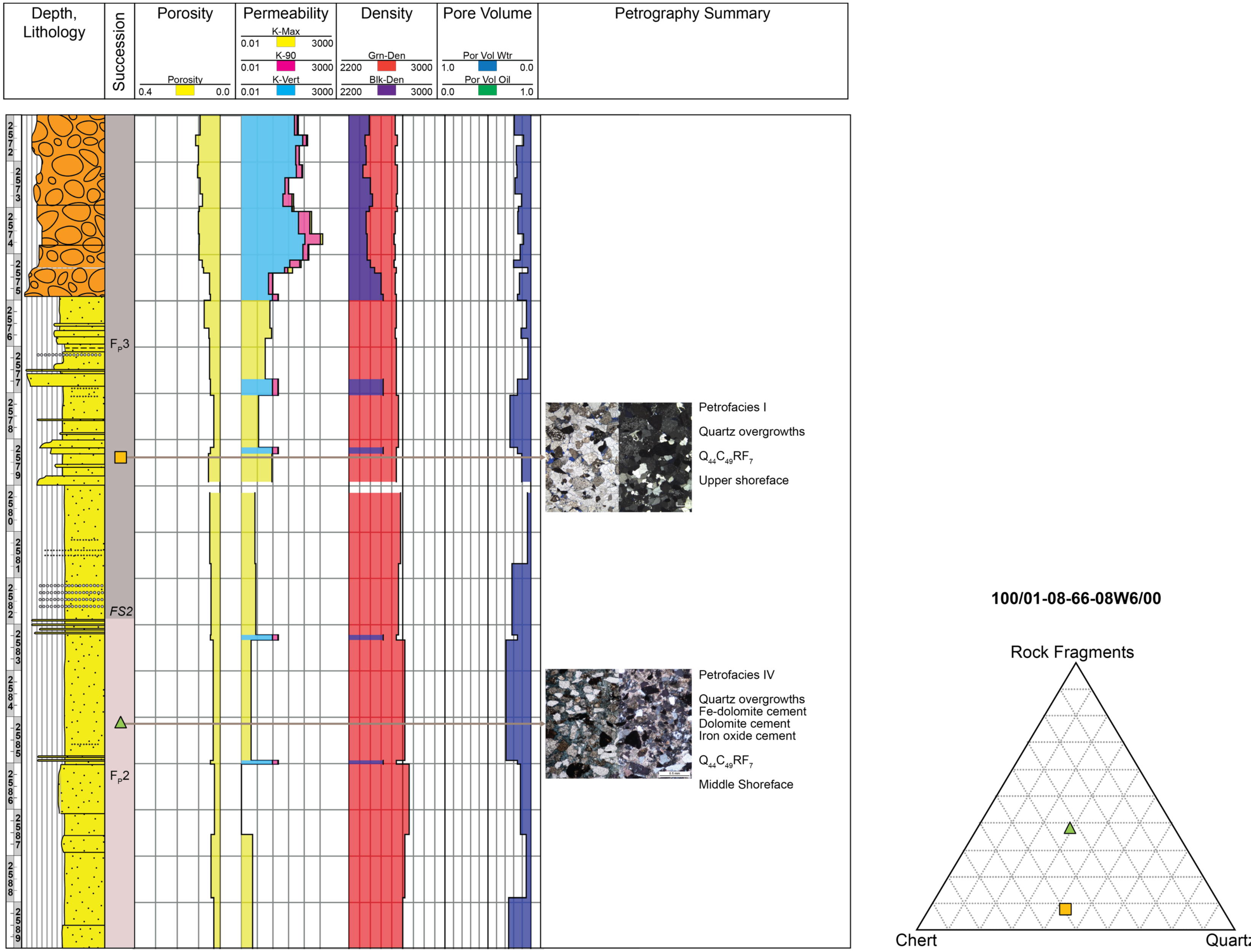
Depth, Lithology
Succession
Porosity
Porosity
0.4
0.0
Permeability
K-Max
0.01
3000
K-90
0.01
3000
K-Vert
0.01
3000
Density
Grn-Den
2200
3000
Blk-Den
2200
3000
Pore Volume
Por Vol Wtr
1.0
0.0
Por Vol Oil
0.0
1.0
Petrography Summary
2572
2573
2574
2575
2576
2577
2578
2579
2580
2581
2582
2583
2584
2585
2586
2587
2588
2589
F_P3
FS2
F_P2
Petrofacies I
Quartz overgrowths
$Q_{44}C_{49}RF_7$
Upper shoreface
Petrofacies IV
Quartz overgrowths
Fe-dolomite cement
Dolomite cement
Iron oxide cement
$Q_{44}C_{49}RF_7$
Middle Shoreface
100/01-08-66-08W6/00
Rock Fragments
Chert
Quartz

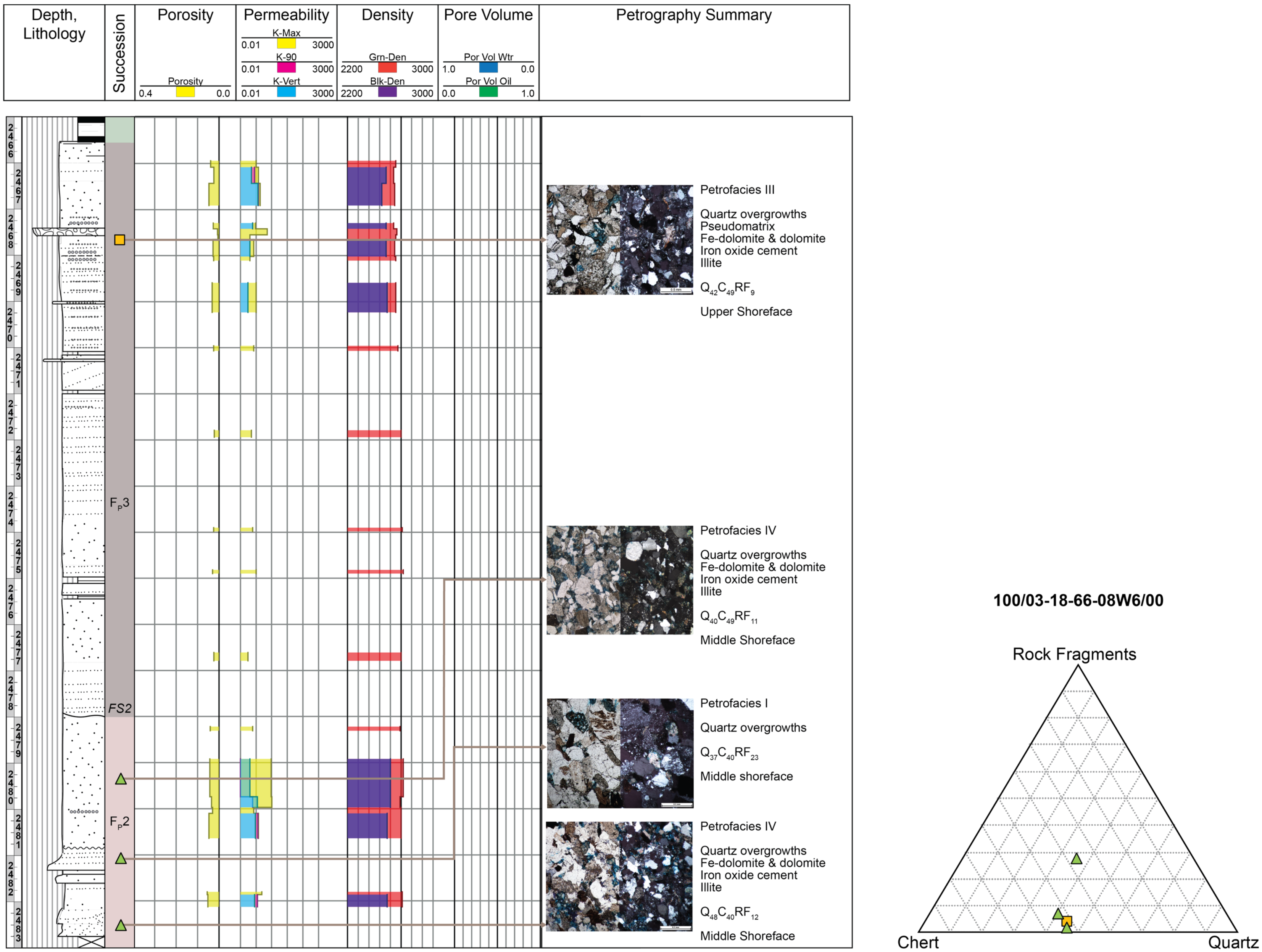

Depth, Lithology
Succession
Porosity
Porosity
0.4
0.0
Permeability
K-Max
0.01
3000
K-90
0.01
3000
K-Vert
0.01
3000
Density
Grn-Den
2200
3000
Blk-Den
2200
3000
Pore Volume
Por Vol Wtr
1.0
0.0
Por Vol Oil
0.0
1.0
Petrography Summary
2466
2467
2468
2469
2470
2471
2472
2473
2474
2475
2476
2477
2478
2479
2480
2481
2482
2483
F$_P$3
FS2
F$_P$2
Petrofacies III
Quartz overgrowths
Pseudomatrix
Fe-dolomite & dolomite
Iron oxide cement
Illite
$Q_{42}C_{49}RF_9$
Upper Shoreface
Petrofacies IV
Quartz overgrowths
Fe-dolomite & dolomite
Iron oxide cement
Illite
$Q_{40}C_{49}RF_{11}$
Middle Shoreface
Petrofacies I
Quartz overgrowths
$Q_{37}C_{40}RF_{23}$
Middle shoreface
Petrofacies IV
Quartz overgrowths
Fe-dolomite & dolomite
Iron oxide cement
Illite
$Q_{48}C_{40}RF_{12}$
Middle Shoreface
100/03-18-66-08W6/00
Rock Fragments
Chert
Quartz

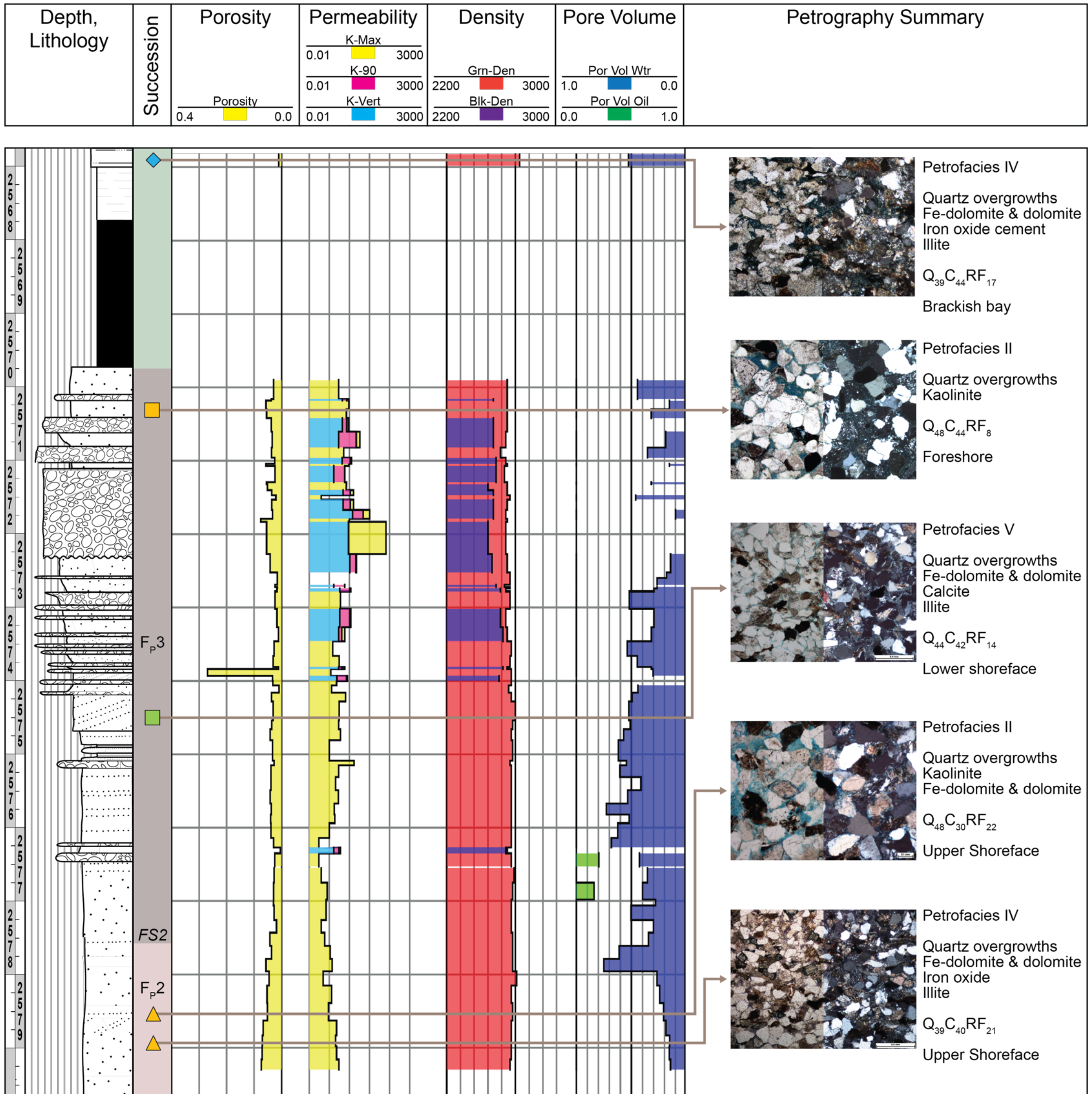
Depth, Lithology
Succession
Porosity
Porosity
0.4
0.0
Permeability
K-Max
0.01
3000
K-90
0.01
3000
K-Vert
0.01
3000
Density
Grn-Den
2200
3000
Blk-Den
2200
3000
Pore Volume
Por Vol Wtr
1.0
0.0
Por Vol Oil
0.0
1.0
Petrography Summary
2568
2569
2570
2571
2572
2573
2574
2575
2576
2577
2578
2579
F_P3
FS2
F_P2
Petrofacies IV
Quartz overgrowths
Fe-dolomite & dolomite
Iron oxide cement
Illite
$Q_{39}C_{44}RF_{17}$
Brackish bay
Petrofacies II
Quartz overgrowths
Kaolinite
$Q_{48}C_{44}RF_{8}$
Foreshore
Petrofacies V
Quartz overgrowths
Fe-dolomite & dolomite
Calcite
Illite
$Q_{44}C_{42}RF_{14}$
Lower shoreface
Petrofacies II
Quartz overgrowths
Kaolinite
Fe-dolomite & dolomite
$Q_{48}C_{30}RF_{22}$
Upper Shoreface
Petrofacies IV
Quartz overgrowths
Fe-dolomite & dolomite
Iron oxide
Illite
$Q_{39}C_{40}RF_{21}$
Upper Shoreface

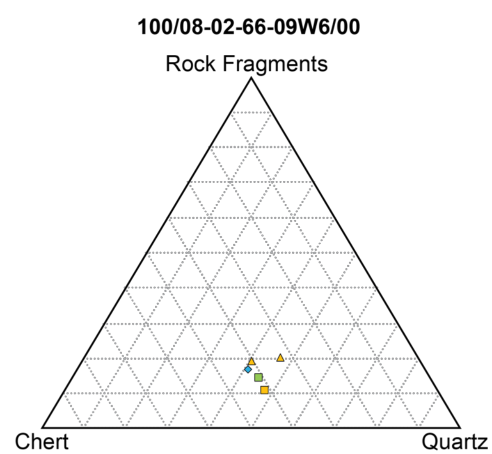
100/08-02-66-09W6/00
Rock Fragments
Chert
Quartz

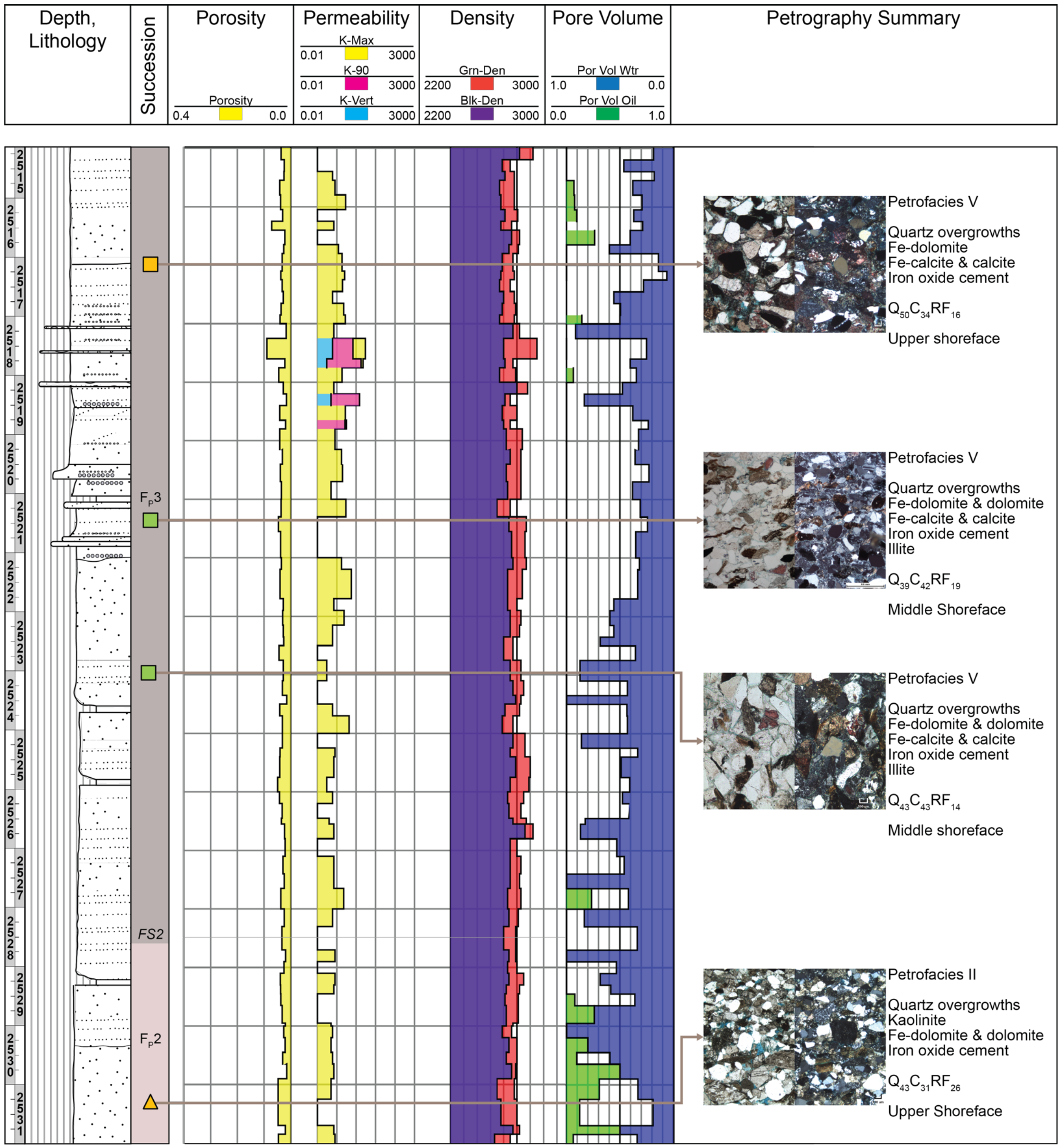
Depth, Lithology
Succession
Porosity
Porosity
0.4 0.0
Permeability
K-Max
0.01 3000
K-90
0.01 3000
K-Vert
0.01 3000
Density
Grn-Den
2200 3000
Blk-Den
2200 3000
Pore Volume
Por Vol Wtr
1.0 0.0
Por Vol Oil
0.0 1.0
Petrography Summary
2515
2516
2517
2518
2519
2520
2521
2522
2523
2524
2525
2526
2527
2528
2529
2530
2531
F_P3
FS2
F_P2
Petrofacies V
Quartz overgrowths
Fe-dolomite
Fe-calcite & calcite
Iron oxide cement
$Q_{50}C_{34}RF_{16}$
Upper shoreface
Petrofacies V
Quartz overgrowths
Fe-dolomite & dolomite
Fe-calcite & calcite
Iron oxide cement
Illite
$Q_{39}C_{42}RF_{19}$
Middle Shoreface
Petrofacies V
Quartz overgrowths
Fe-dolomite & dolomite
Fe-calcite & calcite
Iron oxide cement
Illite
$Q_{43}C_{43}RF_{14}$
Middle shoreface
Petrofacies II
Quartz overgrowths
Kaolinite
Fe-dolomite & dolomite
Iron oxide cement
$Q_{43}C_{31}RF_{26}$
Upper Shoreface

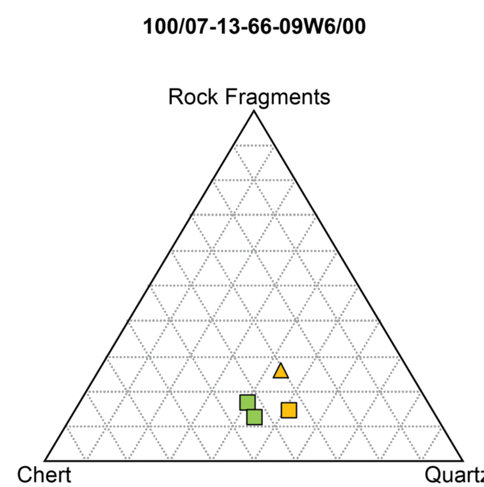
100/07-13-66-09W6/00
Rock Fragments
Chert
Quartz

APPENDIX V: X-RAY DIFFRACTION RESULTS

100/02-21-66-08W6/00 (2514.6) &
100/03-18-66-08W6/00 (2483.5)

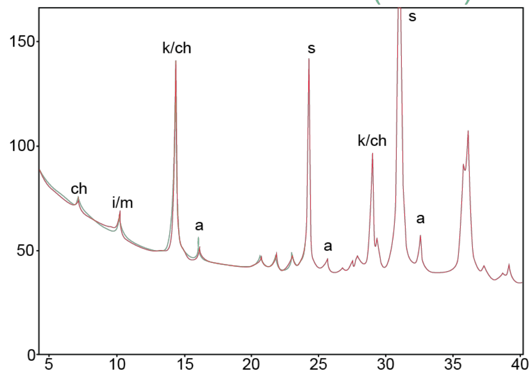

100/03-18-66-08W6/00 (2468.6)

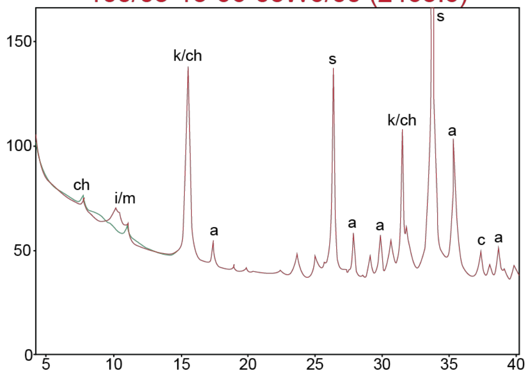

100/05-32-65-09W6/00 (2917.7)

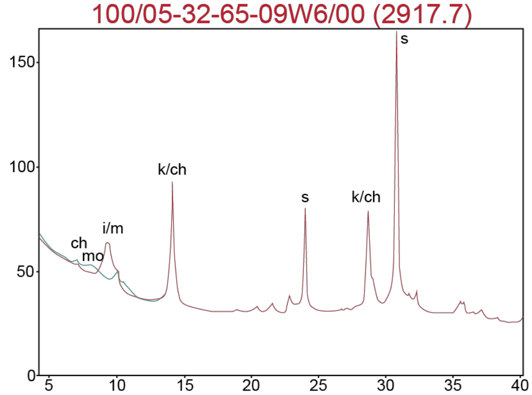

100/06-20-65-10W6/00 (2917.3)

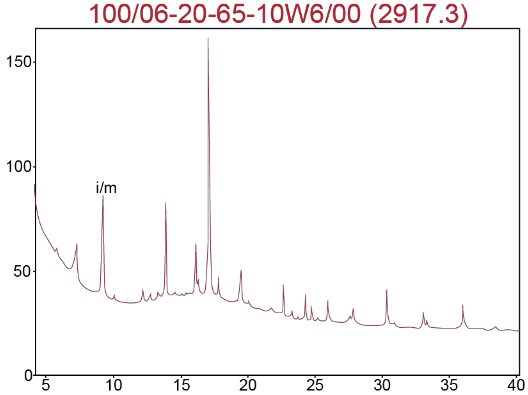

100/07-13-66-09W6 (2521.6)

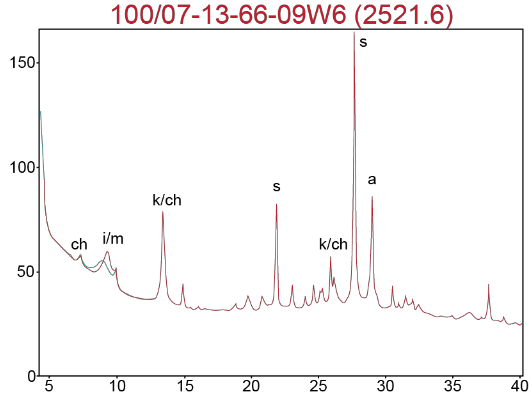

100/08-02-66-09W6 (2579.6)

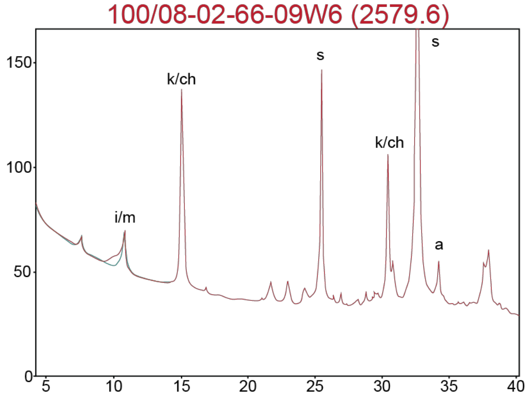

100/14-24-65-10W6/00 (2777.5)

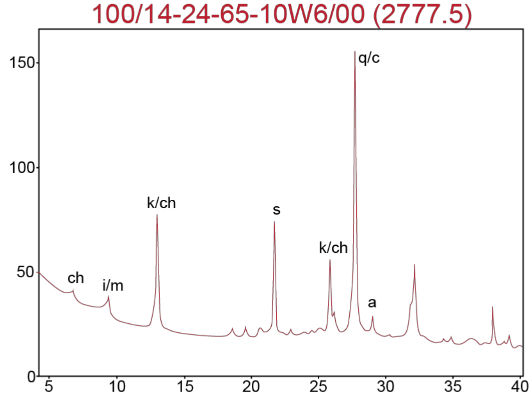

Abbreviations:

a	albite
ca	calcite
ch	chlorite
i	illite
k	kaolinite
m	micas
mo	montmorillonite
s	silica